Alternative splicing in *SCN1A*: Biophysical consequences for Na$_V$1.1 channels

Emily Fletcher

A thesis submitted to University College London for

the degree of Doctor of Philosophy

Department of Molecular Neuroscience

Institute of Neurology

Queen Square

London

WC1N 3BG

1

Declaration

I, Emily Fletcher, confirm that the work presented in this thesis is my original research work. Where contributions of others are involved, this has been clearly indicated in the thesis.

The copyright of this thesis rests with the author and no quotation from it or information derived from it may be published without the prior written consent of the author.

Acknowledgements

I would like to thank my supervisor Stephanie Schorge for her continued support, patience and kindness towards me during my PhD and also to Dimitri Kullmann for the opportunity to work in his excellent lab.

Most of all I'd like to thank my family for their unconditional support and love. To my Dad for reading this gobbledygook through, to my Mum for her pep talks, to Ashleigh and my grandparents for making me laugh and to Claire especially, you're a fantastic big sister. Thank you.

Lastly, I am truly grateful to have had opportunities for a good education. I am a very lucky person indeed.

It's a new dawn

It's a new day

It's a new life

For me

And I'm feeling good

Eunice Waymon, 1965

3

Abstract

Na$_V$1.1 is a voltage-gated sodium channel encoded by the gene *SCN1A*. Mutations in *SCN1A* cause dominantly inherited epilepsy syndromes in humans and Na$_V$1.1 is an important target of several anti-epileptic drugs (AEDs). A common polymorphism in this gene has been shown to alter the expression of two splice variants of the channel, Na$_V$1.1-5N (containing exon 5N) and Na$_V$1.1-5A (containing exon 5A). Although the splicing is highly conserved and the polymorphism that modifies it has been associated with altered AED dosage, the functional impact of the splicing on Na$_V$1.1 is unknown.

This project used whole cell voltage clamp of heterologously-expressed Na$_V$1.1-5A and 5N to compare the intrinsic properties of the splice variants, their modulation by AEDs, their interaction with a published epilepsy mutation (R1648H), their modulation by G-proteins and how they responded to co-expression of sodium channel β subunits.

The main finding was that, although when recorded at physiological temperatures the splice variants produced macroscopic currents that were similar for many parameters, they differed in the rate at which they recovered from inactivation, with Na$_V$1.1-5N recovering more rapidly than Na$_V$1.1-5A. This difference in recovery was conferred by a single amino acid substitution that is conserved in several sodium channels that are alternatively spliced at this site, and the difference was obscured in the presence of the common AED, phenytoin. Inclusion of the mutation R1648H also eradicated the difference by disproportionately slowing the recovery of Na$_V$1.1-5N. Although several other subtle

differences were seen, no consistent differences were found in interactions between the splice variants and G-proteins or β subunits. By converging on a single parameter, recovery from inactivation, the data presented here suggest this parameter is modulated by splicing, and may play a role in development and treatment of seizures.

Table of Contents

8

9

List of Tables

15

List of Figures

19

List of abbreviations

AED   Antiepileptic drug

AHP   Afterhyperpolarizations

AIS   Axon initial segments

ANOVA   Analysis of variance

ATP   Adenosine triphosphate

BAC   Bacterial artificial chromosome

BBB   Blood brain barrier

BFIC   Benign familial infantile convulsions

BHK   Baby Hamster Kidney fibroblasts

BSA   Bovine serum albumin

CAM   Cell Adhesion Molecules

cAMP   cyclic adenosine monophosphate

CFE   Cryptogenic focal epilepsy

CGE   Cryptogenic generalized epilepsy

CHO   Chinese Hamster Ovary Cells

CNS   Central nervous system

CsCl   Cesium chloride

CsF   Cesium fluoride

CsOH   Cesium hydroxide

CT   X-ray computed tomography

delPPP   Triple proline deletion

DMEM   Dulbecco's modified Eagle's medium

DMSO   Dimethyl sulphoxide

dNTP   Deoxynucleotide triphosphatases

DNA   Deoxyribonucleic acid

DTT   Dithiothreitol

EDTA   Ethylenediaminetetraacetic acid

EEG   Electroencephalogram

EMU   *N*-ethyl-*N*-nitrosourea

EPSP   Excitatory postsynaptic potentials

ER   Endoplasmic reticulum

FHM	Familial hemiplegic migraine
FS	Febrile seizures
FS+	Febrile seizures plus
GABA	Gamma-aminobutyric acid
GPCR	G-protein coupled receptor
GDP	Guanosine diphosphate
GEFS+	Genetic (formally Generalized) epilepsy with febrile seizures plus
GIRK	G-protein activated inwardly rectifying K+ channels
GRK	G-protein receptor kinase
GTCS	Generalized tonic-clonic seizures
GTP	Guanosine triphosphate
HBSS	Hank's Buffered Salt Solution
HCl	Hydrochloric acid
HEK 293	Human Embryonic Kidney Cells
HEPES	4-(2-hydroxyethyl)-1-piperazineethanesulfonic acid
IBE	International Bureau for Epilepsy

IC$_{50}$	Concentration that produces half maximal response inhibition
Ig	Immunoglobulin
ILAE	International League Against Epilepsy
IL-1β	Interleukin-1β
IS	Infantile spasms
INa$_P$	Persistent sodium current
INa$_T$	Transient sodium current
ICE-GTE	Intractable childhood epilepsy with generalized tonic-clonic seizures
IPSP	Inhibitory postsynaptic potentials
KCL	Potassium chloride
KMS	Potassium methyl sulphate
KOH	Potassium hydroxide
LB	Luria Bertani medium
LGS	Lennox-Gastaut syndrome
MLPA	Multiplex ligation-dependent probe amplification
mRNA	Messenger ribonucleic acid

MRI	Magnetic resonance imaging
NaCl	Sodium chloride
NaOH	Sodium hydroxide
Na_V	Voltage-gated sodium channel
NBQX	2,3-dihydroxy-6-nitro-7-sulfamoyl-benzo[f]quinoxaline-2,3-dione
NMDA	*N*-methyl-*D*-aspartate
NrCAM	Neuronal cell adhesion molecule
OMIM	Online Mendelian Inheritance in Man
PCR	Polymerase chain reaction
PBS	Phosphate-Buffered Saline
PE	Partial epilepsy
PEPD	Autosomal paroxysmal extreme pain disorder
PFA	Paraformaldehyde
PHT	Phenytoin
PIP_2	Phosphatidylinositol 4,5-bisphosphate
PS	Panayiotopoulos syndrome

PKA   Protein kinase A

PKC   Protein kinase C

PLCβ   Phospholipase C-beta

PNS   Peripheral nervous system

RMP   Resting membrane potential

RT   Room temperature

SC-RT-PCR   Single-cell-reverse transcription-polymerase chain reaction

SE   Status epilepticus

SEM   Standard error of the mean

SIGEI   Severe idiopathic generalized epilepsy of infancy

SIMFE   Severe infantile multifocal epilepsy

SMEI   Severe Myoclonic Epilepsy of Infancy

SMEB   Borderline Dravet syndrome

SNP   Single nucleotide polymorphisms

S.O.C   Super optimal broth (B was changed to C at a later date)

SPECT   Single photon emission computed tomography

TLE	Temporal lobe epilepsy
TRP	Transient receptor potential
tsA201 cells	HEK derivative cell line
UV	Ultraviolet
VGSC	Voltage-gated sodium channels
V_{50}	Voltage that produces half maximal activation/inactivation
WHO	World health organization

Chapter 1: Introduction

Overview of introduction

Ion channels are pore-forming proteins that permit the movement of ions across cell membranes and are involved in a wide range of physiological roles. Voltage-gated sodium channels (VGSCs) are responsible for generating and propagating action potentials in electrically excitable cells (Catterall 1995). Genes encoding ion channels, including VGSCs, undergo extensive alternative splicing (Blencowe 2006). *SCN1A*, the gene that encodes the α subunit of the VGSC designated $Na_V1.1$ is alternatively spliced at exon 5. *SCN1A* contains two copies of exon 5, denoted 5N and 5A. The two alternative splice variants encode channels that differ near one of the segments of the ion channel thought to be important for voltage-sensing. Sodium channels are tightly regulated, consequently even subtle effects of alternative splicing on channel gating may have important consequences for neuronal behaviour. Through $Na_V1.1$, this project focuses on the interaction between three broad fields: Biophysics and structure of VGSCs; the contribution of VGSCs to development and treatment of epilepsy, and the impact of alternative splicing on channel behaviour. In order to provide background for each of these broad themes, the introduction will be in four parts:

Part 1 reviews what is known about VGSCs, with an emphasis on explaining what outstanding questions this work sets out to resolve.

Part 2 gives a history of the study and treatment of epilepsy, focusing on the role of sodium channels as a drug target and a possible aggravating cause.

Part 3 provides a brief introduction to alternative splicing, but focuses on the problem of attributing specific functions to highly-conserved but nearly identical variants of proteins and channels.

Part 4 is an overview of the factors that are known to modulate sodium channels which were probed in this report, including: G-proteins, temperature, and intracellular ions.

Aim of study

There were several aims to this thesis: both practical and biological. The basic goal was to functionally characterize transiently transfected $Na_V1.1$-5A and $Na_V1.1$-5N channels in HEK 293 cells using whole-cell patch clamp. Ideally experiments would have been conducted in neuronal model and not a heterologous cell line. Within the limits of using HEK 293 cells there was a continuous aim to implement accurate biological conditions. This is reflected in using different intracellular anions and performing experiments at physiological temperatures. Using molecular biology and electrophysiological techniques different neuronal models were also contemplated.

Once the methodological aims were fulfilled one endeavour was to investigate the potential impact of $Na_V1.1$ splicing on the development and treatment of epilepsy. In parallel, a broader aim, to examine channel modulation by auxiliary β subunits and G-proteins, was undertaken using the methods previously mentioned.

1.1.1 Original characterization and cloning of VGSCs

The first VGSC was purified from rat brain in the early 1980s (Hartshorne & Catterall, 1981; Hartshorne & Catterall, 1984; Messner & Catterall, 1985). Early on, VGSCs were shown to comprise a hetero-oligomeric polypeptide comprising a functional channel-forming α unit (Goldin *et al.,* 1986) associated with one or more modulatory β subunits: a non-covalently attached β1 subunit and a disulphide-linked β2 subunit. More recently, three other human β subunit isoforms have been cloned which will be discussed later (section 1.1.9). The α subunits of VGSCs are encoded by a family of ten similar genes (Goldin 2001; Table 1.1). Generally the type of VGSC, designated $Na_V1.x$ (where $x = 1$ to 9) is specified by the α subunits (encoded by SCNnA, $n = 1 – 5$, or $8 – 11$). The presence of β subunits is implicit in the channel protein complex but usually not designated. The variations between the α subunits result in distinct currents. When modulated by combinations of β subunits and the resulting VGSCs confer specific physiological properties relevant to the tissue in which they are expressed (Goldin 2001). This importance of narrow control of VGSC properties is highlighted by diseases termed 'channelopathies'. These can be caused by mutations in individual VGSC genes that mainly affect the organ where the α subunit is most important (Kullmann 2002). In fact, given the paucity of specific toxins or pharmacological labels, much of what is known about the functional roles of the different VGSCs has come from characterization of the distinct channelopathies caused by mutations in the different VGSC genes.

Table 1.1: Na$_V$ channels CNS, Central nervous system; IC$_{50}$ half maximal inhibitory concentration; OMIM Online Mendelian Inheritance in Man; PNS, Peripheral nervous system; TTX, Tetrodotoxin; STX, Saxitoxin; V$_a$, half maximal conductance (Catterall *et al.,*2005; Chahine *et al.,*2005; Noda 2006; Brakenbury & Isom, 2008).

Channel	Gene name	Chromosomal location	Full length amino acid size	Tissue localization	TTX/STX(IC$_{50}$)	V$_a$ (mV)	Associated human pathophysiology	OMIM number
Na$_V$1.1	*SCN1A*	2q24.3	2009	CNS, PNS, heart	10 nM	-33	Epilepsy, migraine, autism	182389
Na$_V$1.2	*SCN2A*	2q2a23-24	2005	CNS	10 nM	-24	Epilepsy	182390
Na$_V$1.3	*SCN3A*	2q24	1951	CNS, heart	~15 nM	-23 to -26	Epilepsy	182391
Na$_V$1.4	*SCN4A*	17q23-25	1836	Skeletal muscle	~25 nM	-26 to -30	Hyperkalemic periodic paralysis, paramyotonia congenita	603967
Na$_V$1.5	*SCN5A*	3p21	2016	Heart, CNS	~6 μM	-27	Long QT syndrome, Brugada syndrome, progressive heart block, idiopathic ventricular fibrillation, congenital sick sinus syndrome, dilated cardiomyopathy	600163
Na$_V$1.6	*SCN8A*	12q13	1980	CNS, PNS, heart, glia, nodes of Ranvier	~6 nM	-17 to -40	Mental retardation, pancerebellar atrophy, and ataxia	600702
Na$_V$1.7	*SCN9A*	2q24	1977	PNS, Schwann cells	~25 nM	-31 to -45	Primary Erythermalgia, Channelopathy-Associated Insensitivity to Pain, Paroxysmal Extreme Pain Disorder, Epilepsy	603415
Na$_V$1.8	*SCN10A*	3p22-24	1957	PNS	>100 μM	-16 to -21	Undetermined	604427
Na$_V$1.9	*SCN11A*	3p21-24	1792	PNS	1 μM	-47 to -60	Undetermined	604385
Na$_x$	*SCN6A/7A*	2q21-23	1682	Heart, uterus, glia, PNS smooth muscle	<1 μM	Voltage, salt sensitive	Undetermined	182392

Table 1.2 Na$_V$ β subunits (Catterall *et al.,*2005; Chahine *et al.,*2005; Noda 2006; Brakenbury & Isom, 2008 abbreviations same as Table 1.1)

Channel	Gene name	Chromosomal location	Full length amino acid size	Tissue localization	TTX/STX(IC$_{50}$)	V$_a$ (mV)	Associated human pathophysiology	OMIM number
β1	*SCN1B*	19q13	218	Heart, skeletal muscle, CNS, glial cells, PNS	-	-	Epilepsy, Brugada syndrome, cardiac conduction defect, cancer	600235
β2	*SCN2B*	11q22	186	CNS, PNS	-	-	Altered pain response, seizure susceptibility, Multiple Sclerosis	601327
β3	*SCN3B*	11q23.3	215	CNS, adrenal gland, kidney, PNS	-	-	Brugada syndrome, Cancer	608214
β4	*SCN4B*	11q23	228	Heart, skeletal muscle,	-	-	Long QT syndrome, Huntington's disease	608256

1.1.2 Na$_V$1.1

Mutations within *SCN1A* cause central nervous system (CNS) channelopathies ranging from febrile convulsions and epilepsy to migraine (Dichgans *et al.,* 2005; Ragsdale 2008). *SCN1A* is located on human chromosome 2q24.3 (Escayg *et al.,* 2000) and encodes a large (223 kDa) protein. Original immunohistological work indicated that Na$_V$1.1 was primarily localized to the somata and dendrites of neurons within broad brain regions including the brainstem, substantia, cerebellum and hippocampus (Westernbroek *et al.,* 1992; Gong *et al.,* 1999). One of the challenges of localizing Na$_V$1.1 is the high identity between VGSC subunits. Functional work in a *SCN1A* knockout mouse model indicated that Na$_V$1.1 was predominant in inhibitory interneurons although no immunohistochemical paper had indicated this localization (Westernbroek *et al.,* 1992; Gong *et al.,* 1999; Yu *et al.,* 2006). In response to the data from the mouse model, and in spite of significant early work looking at the distribution of these channels, a subsequent immunohistochemical and *in situ* study re-assessed the localization of Na$_V$1.1 with a view to determining whether the channels were predominantly interneuronal. Ogiwara and colleagues (2007) demonstrated that Na$_V$1.1 was expressed in rat caudal brain regions, namely the thalamus, superior colliculus, inferior colliculus, pons, medulla, deep cerebellar nuclei and spinal cord. Expression signals were less intense in the hippocampus, cerebral cortex, and cerebellum. The authors verified their immunohistochemistry by using three distinct Na$_V$1.1 antibodies and comparing expression to brain slices of Na$_V$1.1 null mice (Ogiwara *et al.,* 2007). Further inspection corroborated the functional data from the knockout mice and showed that Na$_V$1.1 was localized to the axon initial segments (AISs), axons and somata of

36

Parvalbumin-positive interneurons in the immature neocortex and hippocampus (Ogiwara *et al.* 2007).

Within cerebellar white matter, the corpus callosum and fimbria Ogiwara and colleagues identified Na$_V$1.1 channels in the nodes of Ranvier. A later immunocytochemistry study supported these findings in the cerebellum but in not the latter two brain regions (Duflocq *et al.*, 2008). Na$_V$1.1 was also identified in *both* the nodes of Ranvier and AIS of neurons within similar mouse brain regions described by Ogiwara *et al.* (2007). These inconsistencies highlight the continuing difficulties in accurate Na$_V$1.1 immunostaining. However, Na$_V$1.1 expression was comparable in both studies (Ogiwara *et al., 2007*; Duflocq *et al.,* 2008). In the spinal cord Duflocq *et al.* (2008) identified three populations of nodes: Na$_V$1.1 predominant, Na$_V$1.6 predominant or those expressing a mixed population of both channels. Within Na$_V$1.1 specific nodes, a higher concentration of channels were clustered near the soma. Unlike Na$_V$1.6 specific nodes, channels were more evenly distributed throughout the AIS. In the third, 'mixed' node population, Na$_V$1.6 expression complemented Na$_V$1.1 localization whereby Na$_V$1.6 channels were more highly expressed in the distal AIS Duflocq *et al.* (2008). This regional localization implicates Na$_V$1.1 in action potential generation and propagation in GABAergic interneurons perhaps with specific firing properties that are dependant on VGSC background (Duflocq *et al.,* 2008).

1.1.3 Structure of VGSC α subunits

The α subunits of VGSCs have a highly conserved structure that is organized into four homologous domains (I – IV) that are connected by cytoplasmic linkers. Each domain

37

contains six transmembrane segments (S1 to S6; Figure 1.1 A). The C and N termini are intracellular. The S4 segments act as the voltage sensors and a membrane-associated loop between segments S5 and S6 in each domain determines ion conductance and acts as the selectivity filter (Guy and Seetharamulu, 1986). The tertiary structure of sodium channels remains ambiguous. X-ray crystallography of potassium channels imply that some segments are within the membrane and cryo-electron microscopy studies by Sato and colleagues (2001) suggest that the channel is bell-shaped and vertically traversed by a cross-shaped pore that allows the permeation of Na^+ ions (Figure 1.1 B). Many studies have linked the different regions of the α subunits to the VGSC functions that underlie action potentials. Different regions of the peptide, even in some cases individual amino acids, have been shown to contribute to gating, permeation and inactivation of the channels.
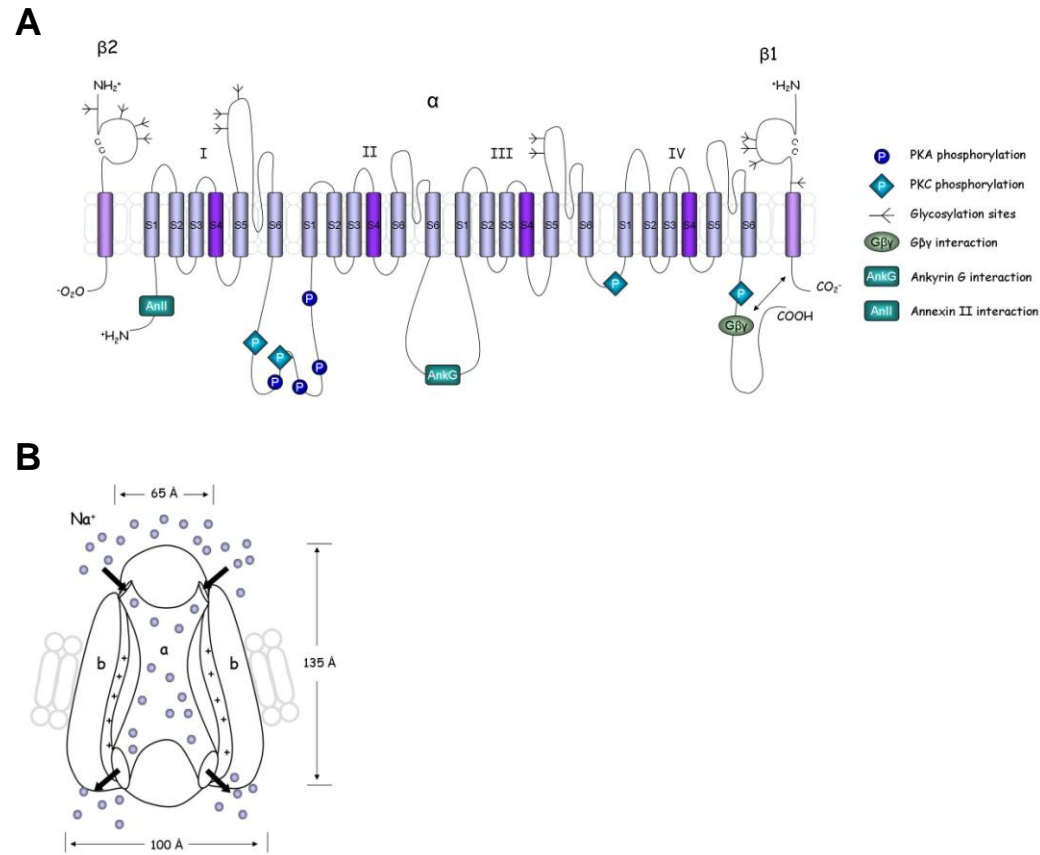
Figure 1.1: Putative topology and three dimensional structure of a VGSC. *A*. The membrane topology of the α and β subunits. *B.* The proposed three dimensional structure of a VGSC. Sodium ion channels are postulated to enter and exit via four holes located on the extracellular and intracellular faces respectively. Two smaller peripheral channels that run parallel either side to the main pore are hypothesized to create a hydrophilic environment important for voltage sensing. PKC, Protein kinase C; PKA, protein kinase A. Picture and text redrawn from Cusdin *et al.,* 2008; Sato *et al.,* 2001 and www.wikipedia.com

1.1.4 Structural elements underlying channel gating

At the onset of an action potential sodium channels move from a closed to an open, conducting state. VGSCs are activated, or 'gated', by membrane depolarization. The most recognized model of how they detect and respond to membrane depolarization is the sliding helix model. According to this model, within the voltage sensing S4 helices, there are positive arginine or lysine residues at every third position that lie between hydrophobic/non-polar residues and respond to changes in voltage across the membrane (Hille 2001). At rest, ion pairs formed between these charged residues and with neighbouring segments lock in the S4 segment. A depolarisation of the membrane potential causes each S4 segment to 'screw' outwards in the extracellular direction through an aqueous environment called the 'canaliculus' (Sands *et al.,* 2005). The motion causes the cationic residues to move from a 'water pocket facing position' to a more external position (Sands *et al.,* 2005). This movement is thought to generate a conformational change of the S5 helices within the channel pore to shift it from a closed to an open state where its ion conductance is zero or maximal, respectively.

1.1.5 Structural elements underlying channel permeation

Tetrodoxin (TTX) is a sodium channel blocker that binds to and occludes the outer pore of most neuronal VGSCs. Mutagenesis studies investigating which specific amino acids bind to TTX revealed that the S5-S6 linker of each domain contributed to the pore, which consisted of inner (DEKA) and outer (EEDD) negatively charged rings of amino acids (Catterall 2005; Noda *et al.,* 1989; Terlau *et al.,* 1991). Mutations within the inner ring

were shown to alter single-channel conductance and ion-selectivity (Pusch *et al.* 1991; Heinemann *et al.,* 1992b).

1.1.6 Inactivation of VGSCs

There are several VGSC inactivation states divided into fast and slow categories. The fast mode of inactivation, which is better understood than slow inactivation, occurs briefly (<1 msec) after channel opening, and blocks Na^+ ions permeating through the pore. At repolarising potentials, channels remain in a refractory, inactivated state, inhibiting ion flux until their recovery at hyperpolarised resting membrane levels. Fast inactivation occurs via a 'hinged lid' mechanism. The cytoplasmic linker between domains III and IV contains an inactivation particle consisting of three adjacent amino acids: isoleucine, phenylalanine and methionine. In the inactivated state this triad, presented via the reminder of the rigid loop, acts as a latch that docks within the intracellular pore through hydrophobic interactions (West *et al.,* 1992). Several amino acids lining the mouth of the pore form the receptor for the inactivation gate and the whole complex is stabilized by the proximal part of the c-terminus (Lerche *et al.,* 1997; McPhee *et al.,* 1998; Motoike *et al.,* 2004; Smith & Goldin, 1997; Figure 1.2). The time course of inactivation helps to regulate the frequency at which neurons can fire. Fast inactivation is voltage-dependent and triggered by the movement of the voltage sensor during channel activation. The voltage sensor in the fourth domain plays a pivotal role in this process (Chen *et al.,* 1996).

Slow inactivation of VGSCs is less understood and remains ill defined in the literature (Ulbricht 2005). 'Slowly' inactivating currents can take seconds to shut down (Taddese &

Bean 2002; Ptak *et al.,* 2005). 'Non-inactivating' describes currents that do not inactivate on any time scale. For the purpose of this report these two types of current will be considered distinct. The mechanism behind and structural basis of 'slowly' inactivating currents are not fully understood, but are thought to involve different structural components to those for fast inactivation. Slow inactivation does not occur in conditions which can induce transient current inactivation (Clay 2003) and in heterologous systems expressing brain sodium channels prolonged or repetitive depolarisations are used to reveal slow inactivation (Toib *et al.,* 1998). It is hypothesized that during this type of inactivation the pore undergoes a conformational change, which may restrict ion flow (Ong *et al.,* 2000; Struyk & Cannon 2002).
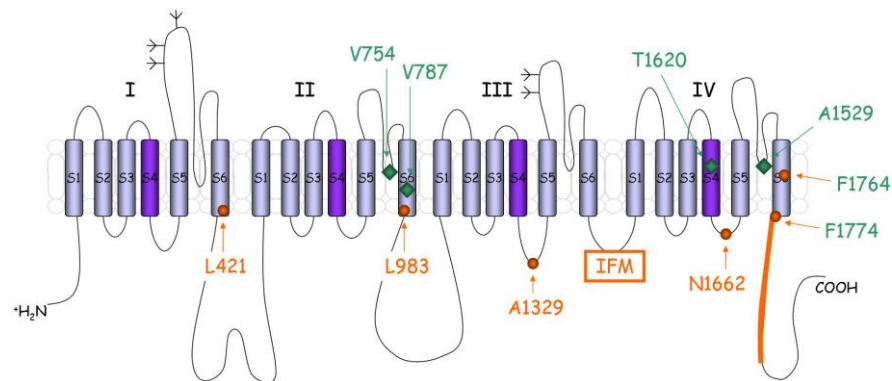
Figure 1.2: Amino acids involved in VGSC inactivation The residues that interact with the isoleucine, phenylalanine, methionine (IFM) motif in fast inactivation are shown as orange circles. Residues thought to be involved in slow inactivation are shown as green diamonds (Redrawn from Goldin 2003).

1.1.7 The Persistent Sodium Current

A 'non-inactivating' or 'persistent' sodium current (INa$_P$; Figure 1.3) is present in almost all mammalian neurons and it is likely to be an intrinsic component of transient sodium

currents (Bean 2007). Of the different types of sodium current, the basis of $I\text{Na}_p$ is least understood, but several mechanisms have been proposed, including: increased pore open-time, change in activation/inactivation voltage dependence, any of which may be associated with altered channel phosphorylation (Stafstrom 2007). Although $I\text{Na}_P$ only accounts for 1-3% of the peak inward sodium current, it can substantially alter the firing characteristics of healthy brain cells (Cummins *et al.,* 1994; Fan *et al.,* 1994; Wu *et al.,* 2005; Zeng *et al.,* 2005). For example, in many neurons, the dominant form of $I\text{Na}_P$ has approximately a 10 mV more negative activation threshold than the transient sodium current (Alzheimer *et al.,* 1993). In some preparations $I\text{Na}_P$ was observed to activate at very hyperpolarized potentials, between -85 and – 90 mV (Huang & Trussell, 2008). $I\text{Na}_p$ activation at more negative potentials allows the non-inactivating current to amplify dendritic excitatory postsynaptic potentials (EPSPs) as well as subthreshold stimulations at the AIS and proximal axon (Astman *et al.,* 2006; Schwindt & Crill, 1995). On hyperpolarisation $I\text{Na}_P$ is partly inactivated resulting in a large decrease of inward sodium current which is comparable to an increase in outward current (Vervaeke *et al.,* 2006). In this way afterhyperpolarizations (AHP) are augmented and it is postulated that this causes transiently-gated sodium channels to recover from fast inactivation more rapidly, which can lead to increased spike frequency (Vervaeke *et al.,* 2006). Additionally, persistent current influences the 'intrinsic electrical properties of neurons' (Vervaeke *et al.,* 2006), and can drive membrane potential oscillations (Jahnsen & Llinas 1984a; Agrawal *et al.,* 2001).
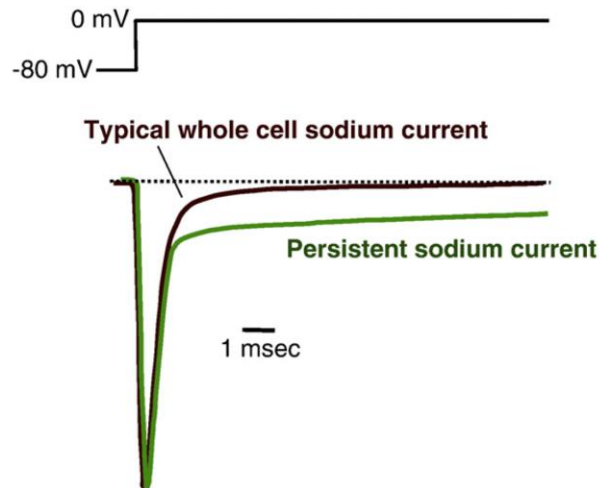
Figure 1.3: The persistent sodium current Superimposition of typical whole cell sodium current (black trace) and sodium current with an abnormally large persistent component (green trace). Taken from Ragsdale 2008.

Not all persistent currents are generated equally, and for electrophysiologists the definition of INa$_p$ is somewhat blurred. For example, INa$_p$ recorded from heterologously expressed VGSCs, including Na$_V$1.1, and cultured neurons have been reported to activate between -60 to +20 mV (Ptak *et al.,* 2005; Aman *et al.,* 2009). The window current predicted to peak at -50 mV (Crill 1996) describes the overlap of the transient sodium current activation and inactivation curves; wherein a proportion of sodium channels continue to open while others begin to inactivate (Crill 1996), in this window currents would be expected to 'persist' during longer voltage-steps. In fact, the commonly used Horn-Vandenberg-Bezanilla INa gating model predicts a sustained current at voltages positive to − 60 mV, which some argue may account for *in vitro* 'persistent' currents (Horn & Vandenberg 1984; Vandenberg & Bezanilla 1991; Clay 2003). However, Sun and colleagues (2007)

demonstrated that Na$_V$1.3 macroscopic currents recorded from transfected HEK cells demonstrated significant INa$_P$ that was not carried by the window current, suggesting a different mechanism may underlie this current. Unfortunately, until a drug that specifically blocks INa$_P$ is found, the mechanistic discrepancies of slow inactivation, non-inactivating and persistent currents are unlikely to be resolved.

1.1.8 Persistent sodium currents in disease

The characteristics of persistent currents enhance abnormal biophysical mechanisms, mainly by generating increased neuronal excitability (Kohling 2002). It also thought to have functional importance for epileptogenesis, that is, the development to the state of epilepsy (Scharfman 2007). The mechanisms of epileptogenesis are complicated and often paradoxical. However, a fundamental principle is an imbalance between excitation and inhibition (McCormick & Contreras, 2001). Seizures are thought to arise from the simultaneous occurrence of high-frequency firing, often referred to as 'hyperexcitability', and with the 'hypersynchronization of neuronal populations' (Bromfield *et al.,* 2006). There are physiological controls of hyperexcitability, but as highlighted by persistent current, there are also factors that can promote increased neuronal firing. When preventative mechanisms against excessive activity break down or mechanisms that facilitate excitation are over activated, pathological activity arises (Scharfman 2007).

A relatively small increase (~2%) in INa$_P$ would change spike initiation and promote repetitive firing (Kuo *et al.,* 2006). In seizure-prone areas including the hippocampus, entorhinal cortex and neocortex INa$_P$ has been shown to amplify remote dendritic signals.

(Schwindt *et al.,* 1993; Lipowsky *et al.,* 1996; Magistretti *et al.,* 1999; Köhling, 2002). This boosts current flow along neuronal dendrites to higher levels to that attained by solitary stimulations and therefore, contributes to pathological firing (Köhling, 2002). Likewise, the neuronal networks to which these cells belong can be paced by INa$_P$ regulated oscillations promoting epileptogenesis (Köhling, 2002). More specifically, INa$_P$ is able to maintain the characteristic tonic discharging of layer III entorhinal neurons via spike AHP amplification. In temporal lobe epilepsy, these cells deteriorate rapidly because of their high activity levels. This disrupts neuronal rhythmicity and exacerbates abnormal firing (Dickson *et al.,* 1997). Burst discharges are speculated to initiate irregular synchronous excitations (Köhling, 2002) and *in vitro* studies suggest that this activity is dependent on INa$_P$ (Franceschetti *et al.,* 1995). In some epilepsy models persistent currents have been shown to underlie epilepform activity, namely, paroxysmal depolarization shifts (Segal *et al.,* 1994; Bromfield *et al.,* 2003). However, without specific antagonists the contribution of persistent sodium currents is difficult to disentangle from the contributions of transient currents.

1.1.9 A select overview of proteins that interact with VGSCs

After translation, nascent VGSCs interact with a variety of proteins (Figure 1.4) that are involved in their trafficking and maturation into functional channels (Shao *et al.,* 2009). For example, ankyrins are scaffolding proteins that bind to the second intracellular loop of neuronal VGSCs and cluster channels at the nodes of Ranvier (Garrido *et al.,* 2003; Jenkins & Bennett 2003: Duflocq *et al.,* 2008). In contrast, the adaptor protein papin binds to discrete domains within the same region as ankryin and is involved in retention and

46

internalization of VGSCs (Shao *et al.,* 2009).   Protein kinases (PK) are enzymes that control protein activity by adding phosphate groups to serine, threonine, or tyrosine residues (Lodish *et al.,* 2000). Isoforms of PKA and PKC differentiately modulate the trafficking and biophysical properties of VGSCs. Phosphorylation of $Na_V1.1$ and $Na_V1.7$ by PKA reduces sodium currents and through a similar mechanism, PKC attenuates $Na_V1.2$ and $Na_V1.5$ currents (Bartschat & Rhodes 1995; Carr *et al.,* 2003; Tateyama *et al.,* 2003; Chen *et al.,* 2006). However, kinases have been reported to increase currents of other members of the VGSC family (Brackenbury & Djamgoz 2006). This may result from indirect kinase-protein interactions with A-kinase anchoring proteins (AKAP), which are involved in ion channel trafficking (Tibbs *et al.,* 1998; Shao *et al.,* 2009). Calmodulin, a calcium-binding protein, binds to motifs within the c-terminal tails of skeletal and neuronal VGSCs and has been shown to alter gating in a calcium-dependant manner (Herzog *et al.,* 2003). Targeted degradation of $Na_V1.1$ and other VGSCs is likely to be mediated by a member of the ubiquitin family, Nedd4-2, which also binds to domains within the c-terminal tail of these channels (Fotia *et al.,* 2004).
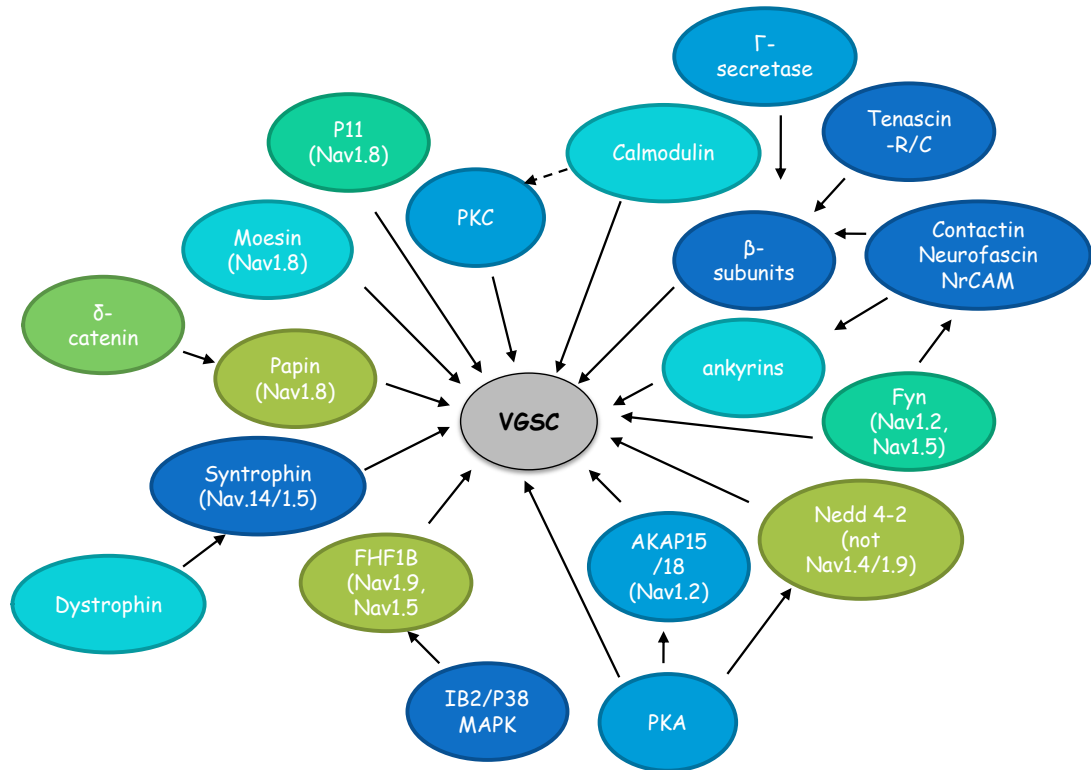
Figure 1.4 Schematic of protein interactions with VGSCs. Calmodulin hinders PKC action by binding to its substrates (dashed arrow). p11, Calcium binding protein; fyn, tyrosine kinase protooncogene; FHF1B, fibroblast growth factor; Nedd 4-2, ubiquitin ligase; AKAP15/18, Protein kinase; MAPK, Mitogen activated protein kinase. Redrawn from Shao *et al.* 2009.

1.1.10 Accessory β subunits

The α subunit is sufficient for channel function, pharmacology, and appears to determine channel distribution, consequently the channel name $Na_V1.n$ is linked only to the identity of the α subunit, but combinations of β subunit isoforms affect the expression level, voltage dependence and gating kinetics of the channels and are essential for proper channel function (Isom 2001). However, β subunits may not always be present. During early development VGSC α subunits are not bound to β subunits (Scheinmann *et al.,* 1989). Moreover, β1 (Ellerkmann *et al.,* 2003), β2 (Gastaldi *et al.,* 1998) and β3 (Gorter *et al.,*

48

2006) are transiently down regulated in experimental models of epilepsy and/or epilepsy. It is not currently known what the consequences of β subunit downregulation are for VGSC function, or whether different VGSC types are differentially modulated by assembly with different β subunit partners.

There are five human β subunit isoforms reported and based on sequence similarity these are separated into two groups: β1, β1b, β3 and β2, β4 (Morgan *et al.,* 2000; Qu *et al.,* 2001; Yu *et al.,* 2003). The two groups associate with the α subunit differently: β1, β1b and β3 attach through non-covalent bonds while β2 and β4 link with the extracellular domain via disulphide bonds. *In vivo,* the expression of β subunits frequently overlaps but it is complementary in some regions. The α subunit associates with one β1, β1b or β3 together with one β2 or β4 (Morgan *et al.,* 2000; Yu *et al.,* 2003). All β subunits are single transmembrane domain proteins. Their extracellular amino-terminus contains a single immunoglobulin (Ig) domain and it is within this region that the β1 subunit is thought to interact with extracellular protrusions between S5-S6 of domains I and IV in skeletal and brain α subunits (Makita *et al.,* 1996). The short intracellular c-terminal also interacts with α subunits. The impact of the β subunits on channel kinetics is highly dependent on cell background (Isom 2001). The detailed overview below focuses on the findings with the most-investigated β1 subunit, and only summarises recent findings concerning the other β subunits.

1.1.11 β1

Early patch-clamping studies investigating the effect of these auxiliary subunits on channel kinetics centred on $Na_V1.2$. $Na_V1.1$ recombinant channels were initially too difficult to engineer (Alekov *et al.,* 2001). Subsequent investigations have demonstrated that the two VGSC homologs undergo similar modulation. Initial electrophysiological studies were carried out using *Xenopus* oocytes. One advantageous feature of these cells is their low expression levels of endogenous multimeric channels (Avanzini *et al.,* 2007). In this expression system the VGSC α subunit, when expressed on its own, displayed a 'slow gating mode'. Co-expression of β1 induced a faster gating mode, that is, the rates of channel activation and inactivation were increased. Moreover β1 increased peak sodium currents and produced a hyperpolarizing shift in the voltage dependence of inactivation (Isom *et al.,* 1992; Patton *et al.,* 1994). A decade later, similar effects were observed from recordings with rat $Na_V1.1$ (Spampanato *et al.,* 2001; 2003). However, a comparable $Na_V1.2$ study using CHO cells indicated that when expressed alone in these cells the α subunit did not have the 'slow gating mode' seen in oocytes; it activated and inactivated quickly. Northern blot analysis confirmed that there were no endogenous β subunits in these cells. Further experiments indicated that co-expression with β1 increased α subunit expression levels and the voltage dependence of inactivation was shifted to more negative potentials (Isom *et al.,* 1995). Conversely, when these experiments were repeated in HEK 293 cells the voltage dependence of activation and inactivation were shifted to more positive potentials. It is clear that within different cell lines β1 and the α subunit can have different interactions, possibly due to distinctive posttranslational modifications or

interactions with cell-specific endogenous proteins giving rise to different channel properties (Toib *et al.,*1998; Qu *et al.,*2001; Meadows *et al.,* 2002; Xu *et al.,* 2007).

What is the true modulatory effect of β1? This remains unclear but further insights are given by mutations within its Ig loop and from animal knockout studies. The integrity of the tertiary structure of the Ig loop of β1 is dependent on a disulphide bridge between cysteines 40 and 121. A change in the second cysteine to a neutral amino acid (C121W) in human *SCN1B* was the first mutation identified as causing a childhood febrile epilepsy syndrome (Wallace *et al.,* 1998). Three further mutations located in this domain have been identified and result in the same phenotype (Scheffer *et al.,* 2007). Electrophysiological studies in mammalian cells, investigating the functional effects of C121W, suggest that the alterations in VGSC function are subtle. For instance, the frequency-dependent rundown of $Na_V1.2$ and $Na_V1.3$ channels was reduced (Meadows *et al.,* 2003). The authors hypothesized that external disruption like fever, together with these slight functional changes, may be sufficient to break down normal channel regulation. A second amino acid of β1, R85, is a hotspot with two alternative mutations: R85C and R85H. Although no functional investigations have revealed the effects of these mutations, this amino acid lies close to modulatory glycosylation sites and therefore may alter channel glycosylation, which may alter channel gating.

An investigation by Chen and colleagues (2004) demonstrated that homozygous knockout β1 mice are ataxic, suffer spontaneous seizures, slow growth and die within three weeks of birth. These mice displayed disrupted axo-glial junctions, which were thought to contribute

to their axonal slowed conduction in the CNS and suggested the β1 isoform is essential for the structural integrity and functioning of myelinated axons. Surprisingly, and in contrast to the heterologous expression data, the absence of β1 in a mixed population of hippocampal neurons did not change sodium current activation or inactivation.

1.1.12 β1B

β1 and its splice variant β1B share an identical extracellular domain encoded by exons 1-3. β1B contains a novel c-terminal that is encoded by the part incorporation of intron 3 before an in-frame stop codon (Qin *et al.,* 2003). Electrophysiological studies in oocytes demonstrated that the human β1B subunit increased peak sodium current when co-expressed with $Na_V1.2$ but channel gating was not significantly changed. The investigators suggested that this increase may be due to several factors including an increase of the open probability of the channel (Qin *et al.,* 2003). What this study does highlight is that the c-terminal is important in either channel conductance or trafficking but further studies in neuronal models are needed to clarify its precise modulatory nature.

1.1.13 β2

Electrophysiological studies in HEK 293 cells and β2 null mice suggest this subunit can cause a positive shift in the voltage dependence of inactivation and increases CNS sodium current amplitude (Qu *et al.,* 2001; Chen *et al.,* 2002). The latter is thought to reflect β2 increasing the density of α subunits at the cell surface. To date no mutations in the β2 subunit gene are known to give rise to epilepsy (Ito *et al.,* 2006). Additionally, β2 knockout mice develop normally but demonstrate an increased susceptibility to pilocarpine-induced

seizures suggesting these subunits may play a role in suppressing seizures (Chen *et al.,* 2002).

1.1.14 β3

β3 and β1 share a high sequence similarity in their extracellular domains (Stevens *et al.,* 2001). Due to their similar functional effects and expression patterns it is generally accepted that these two subunits complement each other *in vivo* (Morgan *et al.,* 2000; Stevens *et al.,* 2001; Qu *et al.,* 2001). However, mutagenesis studies showed that the differential phosphorylation of an intracellular serine residue present in β3 but not β1 altered $Na_V1.2$ voltage dependency of inactivation and recovery from inactivation (Merrick *et al.,* 2010). Moreover, a recent electrophysiological study of β3 null mice demonstrated that these rodents had aberrant heart conduction properties but no abnormal neurological phenotype was reported (Hakim *et al.,* 2010), suggesting that β1 may play a more prominent role in the CNS.

1.1.15 β4

To date, no functional data on β4 knockout mice have been published. The first functional investigations into β4 suggested its effects were not unique, for instance, co-expression of $Na_V1.2$ and β4 in HEK 293 cells resulted in a negative shift in the voltage dependence of activation (Yu *et al.,* 2003). In similar conditions a comparable effect was observed for $Na_V1.1$ channels (Akam *et al.,* 2009). However, a later study by Grieco *et al.* (2005) revealed that the cytoplasmic tail of the β4 was the molecular basis of resurgent sodium currents in Purkinje neurons. In these cells, $Na_V1.6$ channels undergo normal gating

kinetics but on repolarisation, as the channels recover from inactivation, a smaller transient inward current is recorded that quickly deactivates. The β4 intracellular tail has an unusual row of positive charged amino acids along with hydrophobic residues that could convey the correct properties of a pore 'blocker', that is, it would be voltage dependent and may unbind slowly enough at more negative potentials to produce the kinetics demonstrated by the resurgent current (Bean 2005). Therefore, modulation by β4 may have important consequences in controlling repetitive firing in the nervous system. This may be channel-specific, cell-specific or both as this β4 modulation was not reproduced in HEK cells expressing $Na_V1.1$ channels (Akam *et al.,* 2009). Akam *et al.* demonstrated that β4 promoted $Na_V1.1$ derived persistent currents, which were masked by co-expression β1 subunits. Chimeric and mutagenesis experiments showed that the extracellular domain of β1 subunits regulated $Na_V1.1$ *I*Na_P and suggests that β1 and β4 may have opposing effects on the gating and kinetics of $Na_V1.1$ (Akam *et al.,* 2009).

1.1.16 Proposed alternative functions of β subunits

Evidence suggests that β subunits are involved in modulating the trafficking of VGSC α subunits to the surface membrane. In embryonic rat neurons β2 subunits retrieved neuronal α subunits from intracellular pools and inserted channels into the membrane (Schmidt *et al.,* 1985). This effect is observed in multiple cell types; even down to *Xenopus* oocytes where it was shown that the microvillus surface areas of these cells were significantly increased upon co-injection with $rNa_V1.2$ and β2 compared to oocytes injected with only α or both α and β1 subunits (Isom *et al.,* 1995b). The authors surmised that this resulted from increased α subunit cell surface expression through αβ2 interactions (Isom *et al.,* 1995b). More

54

recently, Rusconi and colleagues (2007) demonstrated that all four β subunits partially rescued a trafficking-defective $Na_V1.1$ GEFS+ mutant α subunit expressed in HEK cells. In these experiments, the β1 subunits exerted the greatest affect. Mutagenesis studies have demonstrated that both extra- and intracellular regions of β1 are important for increased mutant α subunit cell-surface expression (Rusconi *et al.,* 2007). This auxiliary subunit may play a non-redundant role in $Na_V1.1$ trafficking because the function of one folding-defective $Na_V1.1$ channel was only restored by β1 (Rusconi *et al.,* 2009). β subunits are also involved in trafficking of PNS VGSCs. For instance, the first intracellular loop of $Na_V1.8$ contains the endoplasmic reticulum (ER) retention motif RRR (Zhang *et al.,* 2008). Both $Na_V1.1$ and $Na_V1.5$ channels have similar motifs in the same region. Using cell-surface biotinylation and immunoblotting techniques Zhang and colleagues (2008) showed that c-terminal tail of β3 masked the retention motif within heterologously expressed $Na_V1.8$ channels. This allowed the primary subunits to be trafficked to the cell surface, an effect not observed with co-expression of homologous β1 subunits.

The extracellular immunoglobulin (Ig) domains of β subunits are structurally homologous to the cell adhesion molecules (CAMs) contactin (β2, β4; Isom *et al.,* 1995a) and myelin Po (β1, β3; McComerick *et al.,* 1998; Morgan *et al.,* 2000). Through this domain β1 subunits interact with several adhesion molecules, including tenascin-R and neuronal cell adhesion molecules (NrCAMs), and play a role in neuronal migration and pathfinding (Srinivasan *et al.,* 1998). BACE, the protease that produces β-amyloid, cleaves the extracellular domain of β subunits (Kim *et al.,* 2007; Miyazaki *et al.,* 2007). The soluble Ig fragments produced by this cleavage modulate cell adhesion and migration (Brackenbury & Isom 2008). β1 subunit

55

Ig domains interact homophilically, and, with the receptor protein tyrosine phosphatase, β subunits recruit ankyrin proteins to their intracellular tails (McEwen *et al.,* 2004). Ankyrin binds to the cytoskeleton, enabling VGSC localization to the nodes of Ranvier for example, or in the absence of α subunits, mediates neurite extension at the growth cone (Malhotra *et al.,* 2002; Brackenbury *et al.,* 2008). β subunits have numerous binding partners that are involved in regulating similar cellular processes. The various types of dysfunction associated with loss of VGSC β subunits suggests they are vital to CNS development and maintenance and are not simply auxiliary to α subunits (Brackenbury & Isom 2008).

Although their modulatory effects in the literature are contradictory, β subunits can substantially affect the behaviour of different α subunits. One purpose of this study is to determine whether channels containing exon 5N (Na_V1.1-5N) interact with different combinations of β subunits in the same manner as those containing exon 5A (Na_V1.1-5A).

1.2.1 A selected overview of the historical and social impact of inherited epilepsies

'Epilepsy' is derived from the Greek word *epilambanein,* which means 'to seize' or 'to attack' (Gross 1992). Amongst the bizarre etiologies and treatments reported through more than a millennium of history, one idea has remained consistent: that epilepsy is inheritable. Around 400 B.C. this was first recorded in a Hippocratic text *The Sacred Disease*, later noted by renaissance physicians and robustly documented in the modern age (Gross 1992). Unfortunately, people affected with epilepsies, both genetic and symptomatic, did and continue to face discrimination. Early 20th century eugenicists in New Jersey, USA, considered affected families as an 'epileptic menace' and argued the disorder predisposed

patients to commit 'brutal crimes' (Hermann 2010). Villages were designed to detain 'epileptics' who were involuntary sterilized under a law created in 1911. This was revoked two years later for humanitarian reasons (Hermann 2010). Decades later, Shoffner *et al.,* (1990) were the first to identify a mutation in mitochondrial DNA that caused a generalized epilepsy (see Table 1.2). Within the last 20 years hundreds of epilepsy causing mutations in the human genome, including in VGSC genes, have been identified. Yet despite advances in the understanding and treatment of this disorder, today in some countries in Asia epilepsy is a lawful reason to stop or annul marriages (WHO 2010). Laws that prevented people with epilepsy marrying in the UK and USA were abolished in the 1970s and 80s (WHO 2010). In this context of isolationism, it is ironic that so much of our understanding of the brain is derived from studies of epileptic patients. Indeed, modern research, including this investigation of *SCN1A*, attempts to interpret how genetics change the presentation, progression and treatment of epilepsy. This may also further our understanding of healthy brain function, but it would be impossible without the involvement of families with inherited forms of epilepsy.

1.2.2 Classification of seizures

Today stigma about people with epilepsy still remains and may harm their employment opportunities, health or life insurance and ability to gain access to a driving license (WHO, 2010). Clinicians are cautious of these socio-economical impacts and distinguish between individuals have experienced a single epileptic seizure and patients suffering from epilepsy (Fisher *et al.,* 2005). In 2005, The International League Against Epilepsy (ILAE) and the International Bureau for Epilepsy (IBE) defined epileptic seizures as: *"A transient*

57

occurrence of signs and/or symptoms due to abnormal excessive or synchronous neuronal activity in the brain" (Fisher *et al.,* 2005). The mode of onset of seizures is widely categorized as *Generalized* or *Focal* (Berg *et al.,* 2010) and the categories are detailed in Table 1.2. Definitions in the recent consensus report by the ILAE's Commission on Classification and Terminology (Berg *et al.,* 2010) of each seizure sub-type relevant to this study are described later in the text. Broadly, generalized seizures initiate in either cortical or subcortical regions and quickly spread throughout bilateral networks (Berg *et al.,* 2010). Generalised seizures do not repeatedly localize to the same region (Berg *et al.,* 2010). Focal seizures are identified as more consistent in their origin and propagation between ictal events. Seizures are more likely to start in a subcortical region within one hemisphere, either in a distinct or broad area and in general propagate within the same cerebral half but can spread to the contralateral side (Berg *et al.,* 2010).

Table 1.3: ILAE classification of seizures (Berg *et al.*, 2010)

I	Generalized seizures
	Tonic-clonic (in any combination)
	Absence
	Typical
	Atypical
	Absence with special features:
	Myoclonic absence
	Eyelid myoclonia
	Myoclonic
	Myoclonic
	Myoclonic atonic
	Myoclonic tonic
	Clonic
	Tonic
	Atonic
II	**Focal seizures**
III	**Unknown**
	Epileptic spasms

1.2.3 Epilepsy syndromes

The ILAE and IBE define epilepsy as *"a disorder of the brain characterized by an enduring predisposition to generate epileptic seizures and by the neurobiological, cognitive, psychological, and social consequences of this condition. The definition of epilepsy requires the occurrence of at least one epileptic seizure"* (Fisher *et al.*, 2005). In Europe, the prevalence of epilepsy in 2004 was 4.3–7.8 per 1,000 but the proportion contributed by genetic disease was unknown (Pugliatti *et al.,* 2007). A dramatic change in epilepsy classification has occurred in the past year, reflecting the evolving nature of understanding of this disorder. Therefore these descriptions may not match with previous idiopathic, symptomatic and cryptogenic categories familiar to the reader (Berg *et al.,* 2010). Syndromes are often characterized by seizure presentation, age of onset,

electroencephalogram (EEG) findings, various hallmarks from Magnetic Resonance Imaging (MRI) or X-ray computed tomography (CT) scans and genetics (Brodie & French, 2000). Epilepsy is now grouped and defined into the following categories (ILAE and IBE, Berg *et al.,* 2010):

1. **Genetic:** genetic aberrations are known to be the primary cause of seizures proved by "diagnostic tests" and the seizures are the "core symptom of the disorder" (ILAE and IBE, Berg *et al.,* 2010).

2. **Structural/metabolic:** "there is a distinct other structural or metabolic condition or disease that has been demonstrated to be associated with a substantially increased risk of developing epilepsy" (ILAE and IBE, Berg *et al.,* 2010). Examples of structural conditions are given as: "Stroke, trauma and infection". The authors also recognize that metabolic conditions may have a genetic origin, but seizures result from a secondary effect caused by the primary disorder. For example, genetic mutations that hinder cortical development, thereby provoking seizures, would be categorized as structural/metabolic rather than genetic (ILAE and IBE, Berg *et al.,* 2010).

3. **Unknown cause:** the etiology is unidentified (ILAE and IBE, Berg *et al.,* 2010).

1.2.4 Diagnosis of epilepsy

It is thought that 50 % of epilepsies result from genetic abnormalities (Pal *et al.,* 2010) in either single or multiple autosomal, X-linked or mitochondrial genes (Stafstrom 2009).

Before a genetic evaluation is made of a patient with epilepsy, initial assessments are carried out (Pal *et al.,* 2010). These include reviewing patient's medical records, their family medical history, EEG and imaging assessments. If genetic causality is suspected, genomic DNA can be obtained from patient blood, muscle or skin (Pal *et al.,* 2010). There are several genetic analysis methods available to the investigator. As previously mentioned, before genetic markers were developed, family, or more specifically, twin studies provided information into the genetic causes of epilepsy and these studies are still used today (Sugawara *et al.,* 2002). For example, twins are chosen from a family where affected members with epilepsy are suspected of harbouring a mutation. Investigators compare concordance or discordance, that is, the presence or absence of the same trait between monozygotic and dizygotic twins. The former are thought to share all their alleles while the latter only half. Alleles are alternative DNA sequences of a gene that are located at specific locations on particular chromosomes. It is considered, therefore, that discordance between monozygotic, not dizygotic twins is solely due to environmental factors. This was thought to allow the assessment of both genetic and environmental contributions to the development of epilepsy (Greenberg *et al.,* 2007). Today, genetic markers are favoured, however, as these studies make two false assumptions: that twins share exact environments and genetic and environmental factors are independent of one another (Greenberg *et al.,* 2007).

The chromosomal location, 2q21-q33, of *SCN1A* was first identified in 1999, by Baulac and colleagues using linkage analysis, an approach that takes advantage of recombination and is effective in family studies. Recombination is the process through which maternal and paternal chromosomes exchange DNA sequences during meiosis. The greater the distance

between two DNA sequences the more likely the exchange. Genetic markers, usually single nucleotide polymorphisms (SNPs), are at specific locations along chromosomes and can be mapped. By convention, a SNP is a variation of a single nucleotide that occurs in more than 1% of the population (in contrast to mutations which can also be single nucleotide variations, but occur in much less than 1% of the population). The more distant the marker is from the disease gene, the more likely that recombination will occur between the marker and the gene. However, if a marker is close to the disease gene it is less likely to recombine, often co-segregates, and is linked to the affected gene. These linked markers give an indication of the location of the disease gene. Although the location of *SCN1A* is now known, in 15 % of patients with these childhood epilepsy disorders the genetic origin is unknown, so this analysis remains useful (Escagy & Goldin, 2010).

A similar principle to that of linkage studies applies to association analyses that compare the frequencies of DNA variants, usually SNPs, among unrelated patient and control chromosomal DNA (Altshuler *et al.,* 2008). This allows the geneticist to determine if a marker or markers are 'associated' with an augmented risk of a disease, and thereby may help identify more than one disease gene (Altshuler *et al.,* 2008). These studies are possible because humans have limited genetic deviations throughout continental populations (Altshuler *et al.,* 2008). Association analysis can be used to directly identify candidate genes or expand linkage study data. Specific association studies involving *SCN1A* will be discussed in detail later.

Mutational analysis looks for specific mutations in candidate genes that have been identified by linkage and/or association studies. In earlier reports for example of *SCN1A,* standard Polymerase Chain Reaction (PCR) techniques, that use primers that hybridize to coding and non-coding regions of the gene were used to detect point mutations (Claes *et al.,* 2003; Wallace *et al.,* 2003; Nabbout *et al.,* 2003; Harkin 2007). Multiplex Ligation-dependent Probe Amplification (MLPA) is an adapted PCR technique developed in 2002 by Schouten and colleagues that can detect genomic rearrangements. Primers are designed to amplify a specific length of DNA. Primers are split into two oligonucleotides and forward probes are fluorescently labelled. If the two adjacent target sequences are present, the primers will anneal and during PCR a ligase enzyme will join the two probes together. The greater number of probe-DNA hybridizations and probe coupling indicates duplicated regions or increased gene copies. If a sequence is absent the probe will not contribute to the fluorescence intensity. The fluorescence from each amplicon from patient and control samples are detected and compared. The relative differences in the peaks of fluorescence between the two groups, indicates the presence and level of sequence duplications or deletions (Schouten *et al.,* 2002; Marini *et al.,* 2007; Wang *et al.,* 2008). Additionally, genomic deletions can be confirmed by fluorescent *in-situ* hybridization (Wang *et al.,* 2008).

1.2.5 SCN1A and epilepsy

Genetic tests have detected nearly 700 mutations in *SCN1A* that cause a range of infantile epileptic encephalopathies with varying phenotypic severities, for brevity only a few will be discussed (Mulley *et al.,* 2005; Harkin *et al.,* 2007, Table 1.3, Figure 1.5).

Phenotypically, the most acute syndrome is called Severe Myoclonic Epilepsy of Infancy (SMEI), which was first described by Dravet in 1978 and therefore, is also called Dravet Syndrome. At about 6 months children will have their first epileptic seizure, that maybe generalized or focal, which is triggered by fever or an increase in body temperature. Within their first year of life these seizures may continue monthly, precipitated by fever (Scheffer *et al.,* 2009). For the next three years children exhibit myoclonic (synchronized muscle jerks); complex partial (consciousness is changed or lost) and absence seizures (glazed staring with eye twitches) and may become ataxic. Their EEGs may be normal during this period and their seizures may not subside or may even be exacerbated on antiepileptic drug (AED) administration (Guerrini *et al.,* 1998). At around one year of age children can begin to regress intellectually, and into adulthood are likely to have severe intellectual disabilities (Jansen *et al.,* 2006). Post infancy, brain MRI scans may show slight cerebral atrophy. Another two syndromes have been classified that are variations on this phenotype, one being 'Borderline Dravet syndrome' (SMEB) which describes patients who may not exhibit myoclonic seizures or despite severe seizures may be cognitively normal as an adult. Another variation of SMEI is 'Intractable childhood epilepsy with generalized tonic-clonic seizures' (ICE-GTE) where children do not exhibit strict myoclonic, complex partial or absence seizures but generalized tonic-clonic seizures, namely, convulsions (GTCS). The latter presents as an initial tonic phase of stiffening of the skeletal muscles causing the child to fall and also lose consciousness. Subsequently, a clonic jerking of the extremities phase begins, which may involve drooling, strong jaw contractions or bladder or bowel incontinence.
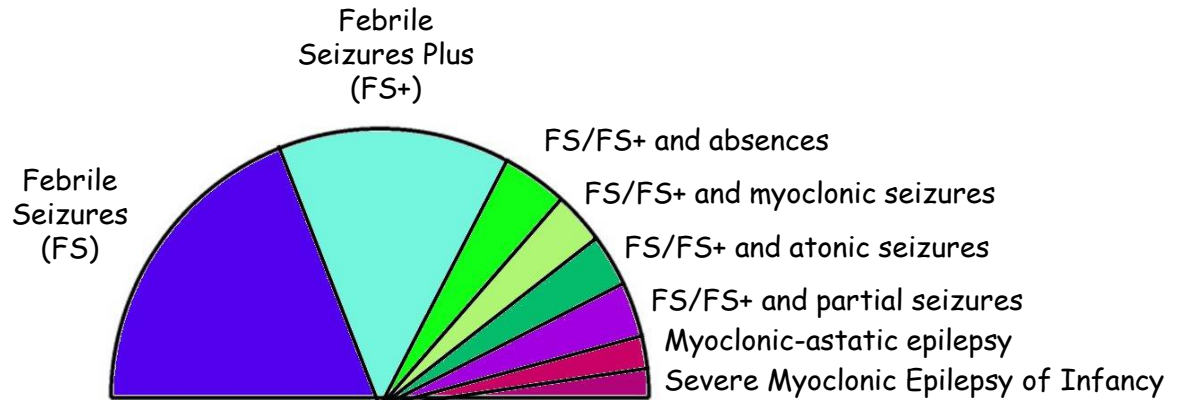
Figure 1.5 Spectrum of phenotypes associated with *SCN1A* abnormalities

A less severe phenotype is Myoclonic-astatic epilepsy (MAE, Figure 1.5). Two thirds of infants with this syndrome will develop afebrile GTCS and another third febrile seizures, between 1-5 years of age. Children will develop generalized seizures, including myoclonic, absence and atonic (spontaneous loss of postural tone and change or loss of consciousness) and can develop intellectual disabilities (Scheffer *et al.,* 2005).

Genetic (formally Generalized) epilepsy with febrile seizures plus (GEFS+) describes a milder sub-spectrum of familial epilepsy syndromes (Figure 1.5). The most frequent are Febrile seizures (FS). These are convulsions that occur in infants between the ages of 6 months to 6 years when their body temperatures rise above 38°C. The next most common sub-syndrome is Febrile seizures plus (FS+; Figure 1.5), where as well as febrile seizures, patients have afebrile GTCS. These may continue beyond 6 years of age after their febrile seizures have abated (Scheffer *et al.,* 2005). Both of these sub-syndromes can be associated with other seizure types depicted in Figure 1.5, but also with temporal lobe seizures that

65

can follow either FS or FS+ (Wallace *et al.,* 2002). Frontal lobe epilepsy has also been associated with one GEFS+ family (Baulac *et al.,* 1999).

1.2.6 GEFS+ is also caused by other ion channel related genes

Mutations in *SCN1A* account for the majority cases of GEFS+ epilepsy syndromes but aberrations in other genes also cause similar epilepsy syndromes (Reid *et al.,* 2009). These will be described using the OMIM categories, although the reader should note that for some there is little evidence. Because mutations in these other genes can produce phenocopies of GEFS+ mutations in *SCN1A* they may provide insight into the mechanism and pathways involved in developing the disease. GEFS+ is subdivided into genetic types denoted by a number, representing the chronological order of mutation identification in each disease gene (OMIM 604233). For GEFS+ Type 4 and 6 (OMIM 609800 & 612279 respectively) the specific syndrome -causing genes are unknown but the chromosomal loci have been mapped to Type 4: 2p24 and Type 6: 8p23-p21 (Audenaert *et al.,* 2005; Baulac *et al.,* 2008). The vast majority of epilepsy mutations, including those found in *SCN1A*, are inherited in a heterozygous manner, that is, only one allele is affected. Therefore, the mutation either causes a dominant effect or loss-of-function of the protein causing haploinsufficiency (Reid *et al.,* 2009).

1.2.7 GEFS+ type 1 SCN1B

A mutation in *SCN1B,* the gene that codes for β1 subunit was the first gene to be identified to cause GEFS+ (GEFS+ Type 1). It was discovered using linkage and PCR analysis of nearly 400 members of a Tasmanian family that had mixed phenotypes, including FS, FS+

66

and MAE (Wallace *et al.,* 1998). The mutation, C121W, disrupts a highly conserved cysteine residue thought to be essential for maintaining the tertiary structure of β1 extracellular loop. Subsequent missense and in-frame deletion mutations in the extracellular region have been indentified in other GEFS+ patients with heterogeneous phenotypes including R85C, R85H, I70_E74del and V138I (Wallace *et al.,*1998; Wallace *et al.,*2002; Audenaert *et al.,*2003; Scheffer *et al.,*2007; Orrico *et al.,*2009). This implies that the β1 extracellular domain is vital to healthy neuronal function. Electrophysiological reports into the effects of these mutations on VGSCs as discussed fully later earlier, these β1 mutations either altered channel slow inactivation or resulted in complete loss of β1 subunit function (Patino *et al.,* 2009). The importance of β1 extracellular loop is supported by a SMEI causing mutation, R125C, located within this region. It is the only known *homozygous recessive* GEFS+ mutation and results in loss of β1 function at the cell surface (Patino *et al.,* 2009). Moreover, the only identified mutation located outside β1 extracellular region, K208I, found within the transmembrane domain, caused a mild FS phenotype in an Italian patient (Orrico *et al.,* 2009).

1.2.8 GEFS+ type 3 GABRG2

The third gene found to cause GEFS+ (Type 3) was *GABRG2*, the gene that encodes the GABA$_A$ γ2 subunit. The GABA$_A$ is a multi-subunit channel complex of which α1β2γ2 is the most common in the brain. GABA$_A$ receptors are ligand-gated ion channels that outwardly conduct chloride, hyperpolarizing the membrane, and are involved in rapid synaptic that is *phasic,* inhibition. The γ2 subunit has four transmembrane domains: M1-M4. A missense mutation in the extracellular loop connecting M2-M3, K289M, was found

in a GEFS+ French pedigree (Baulac *et al.,* 2001). Similar to patients harbouring *SCN1A* and *SCN1B* mutations this family also demonstrated phenotypic heterozygosity ranging from mild FS to severe afebrile convulsions (Baulac *et al.,* 2001). Two-electrode voltage clamp studies of $\alpha1\beta2\gamma2_{K289M}$ channels expressed in *Xenopus* oocytes demonstrated a reduction in chloride conductance upon micromolar GABA application compared to wild-type channels (Baulac *et al.,* 2001). These data were the first to indicate that a dysfunction in inhibitory signalling may be the underlying cause of GEFS+. A reduction in I_{GABA} amplitude caused by $\gamma2_{K289M}$ was contradicted by later electrophysiological reports using fibroblasts and hippocampal neurons transfected with mutant channels (Bianchi *et al.,* 2002; Eugene *et al.,* 2007). These reports showed that $\alpha1\beta2\gamma2_{K289M}$ channels had faster deinactivation rates predicting a reduced duration of Inhibitory Postsynaptic Inhibitory Potentials (IPSPs) and in turn neuronal inhibition.

Subsequent *GABRG2* mutations have been identified and support this hypothesis. For example, Q351X was discovered in an Australian family whose members displayed the full spectrum of GEFS+ syndromes. Q351X introduces a stop codon within the cytoplasmic loop connecting M3 and M4 (Harkin *et al.,* 2002), truncating the subunit at M3. Immunofluorescence studies in HEK cells showed that $\alpha1\beta2\gamma2_{Q351X}$ channels were retained in the ER and failed to reach the cell membrane (Harkin *et al.,* 2002). In regions specific to $\alpha1\beta2\gamma2$, the authors surmised that this mutation would lead to a loss of neuronal inhibition by GABA.

Most thoroughly investigated is a third missense mutation in the N terminus of $\gamma 2$ mutation R43Q. Originally found in another large Australian pedigree, relatives were affected with a range of epilepsy syndromes including GEFS+ and SMEI, but also childhood absence and temporal lobe epilepsies (Wallace *et al.,* 2001a). Investigations in *Xenopus* oocytes and transfected fibroblasts revealed that $\gamma 2_{R43Q}$ reduced benzodiazepine sensitivity (Bianchi *et al.,* 2002; Bower *et al.,* 2002). Benzodiazepines bind to specific sites on $\gamma 2$ subunits and enhance chloride conductance (Kucken *et al.,* 2000). These drugs are often used to treat anxiety, but also are effective in preventing febrile seizures (Wallace *et al.,* 2001a). It is hypothesized that poorly understood endogenous benzodiazepine-like compounds, namely endozepines, can prevent fever-induced seizures (Wallace *et al.,* 2001a). $\alpha 1 \beta 2 \gamma 2_{R43Q}$ channels showed reduced I_{GABA} amplitudes (Bianchi *et al.,*2002) likely to result from abnormal subunit assembly and trafficking and in turn $GABA_A$ membrane expression (Sancar & Czajkowski, 2004). Mutagenesis studies performed by Hales and colleagues (2005) demonstrated that the R43 residue was essential for correct inter-subunit interface configurations and surmised that $\gamma 2_{R43Q}$ containing channels would lead to smaller IPSP amplitudes. Indeed, somatosensory cortical neurons from heterozygous knock-in mice harbouring the $\gamma 2_{R43Q}$ mutation had significantly diminished subunit expression and IPSP currents (Tan *et al.,* 2007). Surprisingly, this model recapitulates absence-seizures not GEFS+ phenotypes and suggests other factors, perhaps genetic, influence epileptic phenotypes in rodents; and also that impaired inhibition may be a common etiology for different epilepsy syndromes (Tan *et al.,* 2007). Chiu *et al.,* (2008) engineered an inducible mouse model that allowed $\gamma 2_{R43Q}$ expression to be switched on, within forebrain neurons, at

specific intervals during development. Their main finding was that mice induced at three weeks were more resistant to pharmacologically induced seizures compared with mice that expressed $\gamma2_{R43Q}$ from birth. The authors surmised that $GABA_A$ channel abnormalities early during development may affect neuronal network formation, structure and excitability determining seizure vulnerability in later life and could partly explain why *GABRG2* mutations are associated with childhood epilepsy syndromes (Chiu *et al.,* 2008).

1.2.9 GEFS+ Type 5 GABRD

A mutation in another $GABA_A$ subunit gene, *GABRD*, which encodes for the δ subunit is categorized into the fifth GEFS+ type. $GABA_A$ δ subunit containing receptors are located extra- or peri-synaptically (Reid *et al.,* 2009) and respond to diffuse, submicromolecular concentrations of GABA. Unlike $\gamma2$ proteins, δ subunits mediate *tonic* inhibition, which describes a sustained activation of $GABA_A$ receptors present in the extracellular space (Richerson 2004). Its function is not clear but it is thought to modulate neuronal coding and firing patterns (Hausser & Clark, 1997) and decrease amplitude and length of excitatory synaptic events, reducing the likelihood of firing (Feng *et al.,*2006). Dibbens *et al.* (2004) identified a mutation in the N-terminal, extracellular region of δ subunit, E177A, in only two members of a small GEFS+ family; therefore its link to epilepsy is disputed. Nonetheless immunoblotting and electrophysiological analyses of δ_{E177A} combined with physiological significant subunits $\alpha4$ and $\beta2$ in HEK cells, revealed the mutation reduced δ subunit cell surface expression and altered channel gating. For example, GABA-mediated $\alpha4\beta2\delta_{E177A}$ current amplitudes and desensitization were reduced and single channel analysis demonstrated that mean opening times of δ_{E177A} containing channels were significantly

decreased (Feng *et al.,* 2006). These data reiterate that an impairment of inhibition, either phasic or tonic, contributes to the varying epileptic phenotype of GEFS+ patients.

1.2.10 GEFS+ Type 7 SCN9A

The last GEFS+ category, Type 7, is associated with mutations in the sodium channel gene *SCN9A*. This codes for $Na_V1.7$ and as previously described is considered a 'peripheral' VGSC and is highly expressed in Dorsal Root Ganglion cells, sympathetic neurons, Schwann cells and neuroendocrine cells (Catterall *et al.,* 2005). Most mutations in *SCN9A* cause pain disorders including autosomal dominant primary erythermalgia (episodic burning pain in feet and lower legs initiated by exercise and warmth; OMIM 133020), autosomal paroxysmal extreme pain disorder (attacks of extreme pain in the rectal, ocular, and mandibular areas; PEPD; OMIM 167400) and autosomal recessive channelopathy associated insensitivity to pain (indifference to pain; OMIM 243000). A single-cell-reverse transcription-polymerase chain reaction (SC-RT-PCR) study confirmed that *SCN9A* is expressed in immature rat hippocampal pyramidal cells (Mechaly *et al.,* 2005). Singh *et al.* (2009) identified seven missense mutations distributed throughout the intra- and extracellular loops of $Na_V1.7$ in GEFS+ patients with either a Caucasian or Hispanic background. A large American family harboured a mutation located in the first intracellular loop, N641Y. Again, the members in this family demonstrated a broad range of GEFS+ syndromes including FS and MAE. To further understand the pathological mechanism of this mutation the authors engineered a $SCN9A^{N641Y}$ knock-in mouse model. Heterozygous and homozygous mice did not exhibit spontaneous seizures but demonstrate lowered electroconvulsive seizure thresholds (Singh *et al.,* 2009). The paper did not

analyze the biophysical properties of mutant channels in different cell backgrounds, and it remains undetermined whether GABAergic neurons up-regulate $Na_V1.7$ and directly modulate inhibitory signalling. The vulnerability of $SCN9A^{N641Y}$ mice to thermally-induced seizures was also not investigated. Additionally heterozygous missense mutations in similar regions of $Na_V1.7$ cause PEPD (Fertleman *et al.,* 2006), but the authors failed to address why these patients only had an epileptic and/or PEPD phenotype.
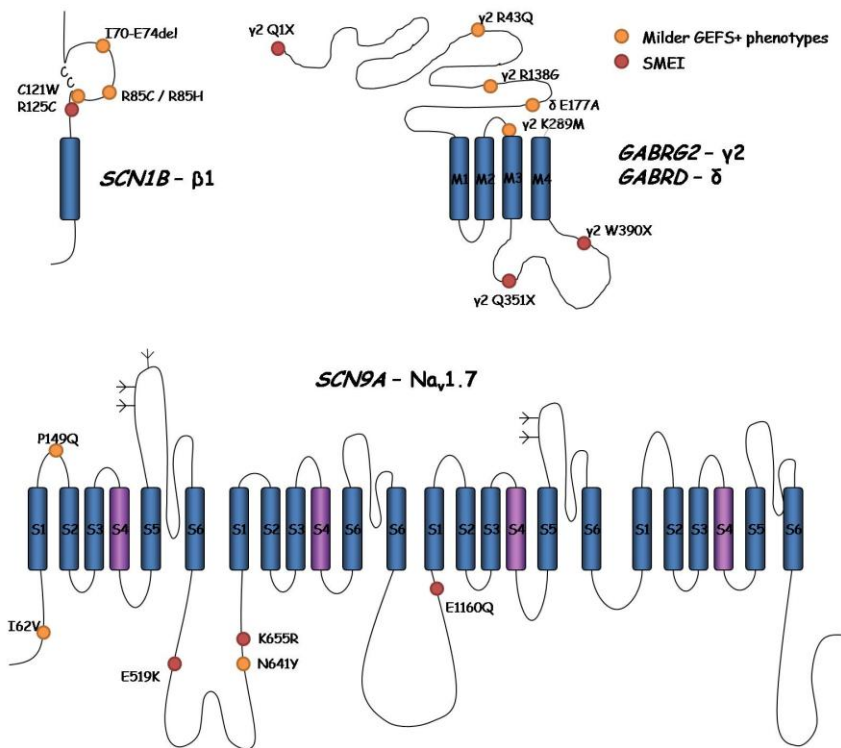
Figure 1.6 Mutations in VGSC β1, GABA$_A$ and Na$_V$1.7 genes that are associated with GEFS+. SMEI causing mutations are shown in red and milder phenotype causing mutations in yellow.

1.2.11 Unclassified GEFS+ genes

Two other genes have been linked to GEFS+ but have not been officially classified. A nonsense mutation in a third sodium channel gene *SCN2A* has been identified in only one

Japanese patient who suffered with febrile and afebrile seizures (Sugawara *et al.,* 2001). *SCN2A* codes for $Na_V1.2$ that is expressed in glutamatergic cells (Planells-Cases *et al.,* 2000) and suggests that disrupted excitability in these cells could also lead to hypersynchronized networks. However, currently most mutations in *SCN2A* lead to milder phenotypes of benign familial infantile convulsions (BFIC, OMIM 607745), and no other patient with GEFS+ like consequences of mutations in *SCN2A* has been described since 2001, suggesting this is a very rare cause of the disorder.

A second unclassified gene is the newly described triple proline deletion (delPPP) in the Hyperpolarisation-activated cyclic nucleotide-gated ion channel: *HCN2* found in 6 unrelated Australians with GEFS+ (Dibbens *et al.,* 2010). Half presented with FS and another half with MAE. Upon hyperpolarisation *HCN2* coded channels carry a 'funny' inward mixed cation, denoted I_f that slowly depolarizes the membrane to less negative potentials and is responsible for the creation of neuronal pacemaking potentials in the thalamus and cerebellum (Luthi & McCormick, 1998). Voltage-clamp experiments using *Xenopus* oocytes demonstrated that $HCN2_{delPPP}$ channels caused a small increase I_f that *in vivo* would cause a depolarization of the membrane (Dibbens *et al.,* 2010). I_f is also gated by cyclic adenosine monophosphate (cAMP) and increases the activity of these channels. The delPPP is close to the cAMP binding domain, but forskolin, an activator of cAMP, in *Xenopus* oocytes had no effect on I_f derived from this mutant (Dibbens *et al.,* 2010). *HCN2* is transcribed in both GABAergic and glutamatergic cells and an increase in depolarization may enhance inhibitory and excitatory signalling. Moreover, either an increase or a decrease in HCN channel function can result in hyperexcitability (Dibbens *et al.,* 2010).

Therefore, the pathological mechanism of this GEFS+ associated mutation remains undetermined.

1.2.12 Genotype phenotype relationships for mutations in SCN1A

Table 1.3 shows an overview of published *SCN1A* mutations up until July 2010 (University of Antwerp, http://www.molgen.ua.ac.be/SCN1A. Mutations/Statistics/Mutations.cfm). 90 % of genomic rearrangements mutations in the coding sequence of *SCN1A* cause SMEI and approximately 5 % of coding missense mutations cause GEFS+ (Type 2). 29 mutations throughout intronic regions of *SCN1A* are reported to cause more severe clinical presentations including SMEI (Claes *et al.,* 2001; Nabbout *et al.,* 2003; Mancardi *et al.,* 2006; Harkin *et al.,* 2007; Marini *et al.,* 2007). Less information is available about intronic mutations because it is uncommon for diagnostic laboratories to sequence non-coding regions (Catterall *et al.,* 2010). The literature assumes that *SCN1A* mutations that cause more severe phenotypes like SMEI result from Na$_V$1.1 loss of function. This theory is not unfounded: half of mutations truncate the beginning of the channel, hypothesized to cause aberrant channel trafficking, biophysical properties and interactions with other proteins: rendering Na$_V$1.1 non-functional (Catterall *et al.,* 2010; Escagy & Goldin, 2010) Additionally, *SCN1A* partial deletions and deletions have only been reported in SMEI patients (see Table 1.3). However, a recent case report of a GEFS+ Chinese patient harbouring a stop mutation in the first intracellular loop of Na$_V$1.1 questions this assumption (Yu *et al.,* 2006). The mutation in this adolescent had arisen *de novo,* that is, it was not inherited. This is also unusual for a GEFS+ causing mutation. Conversely, the majority of SMEI mutations are *de novo* and analysis of 44 Caucasian SMEI patients

revealed that three-quarters of non-inherited *SCN1A* mutations originated from the paternal chromosome (Heron *et al.,* 2010). The authors surmised this was caused by an increased rate of mitosis during spermatogenesis compared to oogenesis increasing the likelihood of replication errors (Heron *et al.,* 2010). A small percentage of SMEI mutations can also arise from somatic or germline mosaicism. This has reported in patients with Mediterranean, Roma/Gypsy and Japenese genetic backgrounds (Depienne *et al.,* 2006; Gennaro *et al.,* 2006; Morimoto *et al.,* 2006; Azmanov *et al.,* 2010). However, understanding the etiology of SMEI is complicated. In 2009 Marini and colleagues, using MLPA, described three SMEI patients with amplifications and/or duplications in *SCN1A*. The last exon, exon 26, was particularly affected: amplified (multiple copies) in one individual and duplicated (two copies) in another, suggesting that increased gene number copy is also pathogenic.

1.2.13 Other genes providing phenocopies of SCN1A mutations

PCDH19 codes for a subtype of protocadherins, which are the calcium dependent cell-cell adhesion molecules, and is expressed in the cortex and hippocampus (Dibbens *et al.,* 2008; Depienne *et al.,* 2009; Jamal *et al.,* 2010). In one report only female carriers heterozygous for mutations in this X-linked gene exhibit a SMEI-like epilepsy syndrome (Dibbens *et al.,* 2008). However, in a later study by Depienne *et al.* (2009) a male patient with a *deletion* of the gene also presented with the same phenotype. The authors surmised that epilepsy was caused by 'cellular interference'. Heterozygous females and males with a deletion of the gene within their sole X chromosome would have tissue mosaicism, that is, two populations of cells either mutant or wild-type that may interfere with cell-cell communication

(Depienne *et al.,* 2009). Males with mutations in *PCDH19* possess a homogeneous population of cells and therefore do not develop epilepsy (Depienne *et al.,* 2009).

.

Table 1.4 Overview of published *SCN1A* mutations CFE: cryptogenic focal epilepsy; CGE: cryptogenic generalized epilepsy; FHM: familial hemiplegic migraine; FS: febrile seizures; FS+: febrile seizures plus; GEFS+: generalized epilepsy with febrile seizures plus; ICEGTC: intractable childhood epilepsy with generalized tonic-clonic seizures; IS: infantile spasms; LGS: Lennox-Gastaut syndrome; MAE: myoclonic-astatic epilepsy; PE: partial epilepsy; PS: Panayiotopoulos syndrome; SIGEI: severe idiopathic generalized epilepsy of infancy; SIMFE: severe infantile multifocal epilepsy; SMEI: severe myoclonic epilepsy of infancy; SMEB: borderline SMEI; TLE: temporal lobe epilepsy. (Taken up to date on 23.07.10 from http://www.molgen.ua.ac.be/SCN1AMutations/Statistics/Mutations.cfm)

Epilepsy syndrome	Severe		Other	Mild		
	SMEI, SMEB, Dravet syndrome	ICEGTC, SIGEI, SIMFE, MAE, MAE&GEFS+	IS, LGS, CGE, CFE, SGE	GEFS+, FS+, PE&FS+, TLE&FS	FHM, PS	Total
Point Mutations						
translation initiation mutation	1					1
Splice donor mutation	41	1	1	1		44
Splice acceptor mutation	23					23
silent mutation	2					2
nonsense mutation	135					135
Missense mutation	246	14	9	28	7	304
in-frame deletion mutation	14					14
frameshift mutation	119	3	1	0		123
complex mutation	1	1				2
Total	**582**	**19**	**11**	**29**	**7**	**648**
Genomic rearrangments Translocation (rearrangements of regions between chromosomes)	1					1
partial/whole gene duplication mutation			1			1
partial/whole gene deletion mutation	42					42
partial/whole gene amplification mutation	3					3
Total	**46**	**0**	**1**	**0**	**0**	**47**
Total *SCN1A* mutations	**628**	**19**	**12**	**29**	**7**	**695**

1.2.14 Mouse models of SMEI

The following sections (1.2.14-1.2.19) will summarize the findings from studies involving rodent models of SMEI and GEFS+. Emphasis will be placed on the GEFS+ mutation investigated in this study, R1648H. These reports reveal the possible effects of a loss or predicted disruption of $Na_V1.1$ function would have on neuronal function and possible factors that may influence the epilepsy phenotype.

A breakthrough in understanding the pathological mechanisms of loss of $Na_V1.1$ function was achieved by a study by Yu and colleagues (2006) that investigated $Na_V1.1$ null mice. They disrupted the coding sequence of exon 26 in *SCN1A* in different strains of mice, preventing the expression of the channel *in vivo*, which was confirmed by southern blot analysis. The mice developed an ataxic and epileptic phenotype, in which the latter was dependent on genetic background in heterozygotes. For example, regardless of strain *SCN1A*$^{-/-}$ mice developed severe seizures on P9 and postnatally did not survive beyond two weeks, confirming that $Na_V1.1$ is essential for normal brain function. Heterozygous mice exhibited a delayed decline, had spontaneous seizures and sporadic deaths beginning after P21. Interestingly, in one mouse strain at postnatal week 12, approximately 80% mice died spontaneously post-seizure, compared to around 20%, in another strain at the same time point. These data were consistent with another $Na_V1.1$ null mouse model. Ogiwara *et al.* (2007) introduced a truncation mutation in the mouse *SCN1A* gene. R1407X has been identified in three unrelated SMEI patients (Ogiwara *et al.,* 2007) and causes a complete loss of $Na_V1.1$ function (Sugawara *et al.,* 2003). Ataxic *SCN1A*$^{RX/RX}$ mice developed spontaneous seizures at a similar developmental stage to the Yu *et al.* model. Again

78

heterozygotes suffered from spontaneous seizures approximately three weeks after birth and their lifespans were dependant on genetic background. These studies strongly indicate that genetic modifiers, discussed in detail later, may influence the phenotype of affected SMEI patients.

Later, Oakley *et al.* (2009) investigated whether age and elevated temperatures affected the epileptic presentation of the original *SCN1A* mutant mouse model. The strain in which the $SCN1A^{+/-}$ phenotype demonstrated greater penetrance was used to assess these factors. Seizures were induced by increasing core body temperature by a minimum of $1.5^{o}C$ in month-old heterozygous mice; their wild-type counterparts were unaffected. Furthermore, mutant mice at P20-P22 and P30-P46 were more susceptible to temperature-induced seizures, compared to younger, P17-18, heterozygous mice which remained resistant. At higher temperatures the former age-groups exhibited myoclonic seizures followed by generalized seizures that increased in duration, spike frequency, racine score and spike number in the older P30-P46 set (Oakley *et al.,* 2009). In addition, the temperature at which seizures were induced was dramatically reduced in the latter compared to P20-22 animals and spontaneous seizures were only observed in mice older than P32. Indeed, at physiological temperatures interictal EEG spike activity, indicative of spontaneous seizure susceptibility (Oakley *et al.,* 2009), was recorded in mice only more than a month old. This implies that at biological temperatures the more immature nervous systems of SMEI mice were better adapted to perturbations in neuronal excitability, and network vulnerabilities caused by *SCN1A* haploinsufficiency were only exposed at higher temperatures.

Electrophysiological findings in the original study indicate that these perturbations are likely to affect inhibitory signalling (Yu *et al.,* 2006).

Macroscopic currents from cultured hippocampal cells from *SCN1A*$^{-/-}$ and *SCN1A*$^{+/-}$ mice showed that a decrease in $Na_V1.1$ expression was correlated with a reduction in current density from GABAergic interneurons. Reduced sodium currents were not observed in excitatory pyramidal cells and $Na_V1.1$ channel gating was unaffected by cell type. These findings were corroborated in *SCN1A*^{RX} inhibitory cortical neurons (Ogiwara *et al.,* 2007). Kalme *et al.* (2007) using the Yu *et al.* mouse model demonstrated that peak, persistent and resurgent currents were reduced in inhibitory cerebellar purkinje neurons from $Na_V1.1$ null mice. Voltage dependencies of activation and inactivation were also unaltered in this cell type. Current clamp experiments demonstrated that the excitability of cortical, hippocampal and Purkinje inhibitory neurons was reduced in $Na_V1.1$ mutant mice (Yu *et al.,* 2006; Kalme *et al.,* 2007; Ogiwara *et al.,* 2007). For example, compared to healthy and *SCN1A*$^{+/-}$ neurons the number of action potentials of hippocampal and pyramidal GABAergic cells from homozygous mice was reduced over a broad range of current injections: $20 - 100$ pA. A comparable number of spikes were observed in wild-type and heterozygous hippocampal cells at low level depolarizing injections. However, at current pulses higher than 60 pA *SCN1A*$^{+/-}$ interneurons failed to maintain high frequency firing (Yu *et al.,* 2006), unlike *SCN1A*$^{+/-}$ pyramidal neurons that consistently fired at lower rates compared to wild-type interneurons (Kalme *et al.,* 2007). In both hippocampal and cerebellar cells of $Na_V1.1$ mutant mice the threshold potential was unchanged suggesting that $Na_V1.1$ is likely to play an essential role in establishing firing frequencies of inhibitory cells. This was emphasized

80

by analysis of P14 mutant mice; a compensatory upregulation of $Na_V1.3$ and an increase in $Na_V1.6$ activity were observed in hippocampal and Purkinje neurons respectively. The authors surmise that a feedback control system within neurons attempts counteract the decrease in cellular excitability, but is insufficient to establish normal neuronal firing rates (Yu *et al.,* 2006; Kalme *et al.,*2007).

1.2.15 Mouse models of GEFS+

There are fewer mutations described that are linked to GEFS+ than to SMEI, however, since some of these GEFS+ mutations have been identified in large pedigrees with variable penetrance and severity, there is extensive interest in investigating how the mutations alter neuronal behaviour, and what possible genetic backgrounds can modify this behaviour. To date, the most extensively studied mutation associated with GEFS+ is the R1648H mutation first described by Baulac *et al.* in 1999.

1.2.16 The original $Na_V1.1$-R1648H pedigree

GEFS+ mutations are distributed throughout the channel and thought to result in $Na_V1.1$ *dysfunction* and a milder GEFS+ phenotype (Ragsdale 2008). $Na_V1.1$-R1648H was one of the first identified missense mutations to cause GEFS+ (Figure 1.7; Baulac *et al.,* 1999; Escagy *et al.,* 2000). Analysis of four generations from a French family revealed that all affected members were heterozygous for the mutation. Moreover, the phenotypic variation between the relatives was striking. Some were mildly affected, for example patient II-1 at 60 years suffered from two spontaneous seizures without a previous history of epilepsy and was seizure free for a further 10 years (Baulac *et al.,*1999). Not all patients suffered with

febrile seizures at a young age, for instance patients II-1, II-2, II-3 and III-5. Others only suffered with febrile seizures but did not go on to develop generalized epilepsy, for example patient III-8 suffered with numerous febrile seizures only until the age of 7. Two siblings had particularly severe phenotypes, patients IV-5 and 6. Both exhibited febrile seizures that continued into late childhood/early adulthood as general tonic clonic seizures. There was also a huge variation in patient AED treatment, which is depicted in Figure 1.7. Unfortunately the authors did not specify which drugs were used for treatment. Nonetheless a wide variability in treatment efficacy is apparent. Some members of the family from different generations were successfully treated with AEDs, others controlled their seizures with mono- or polytherapy, and one patient, IV-5, was pharmacoresistent. Why are there large deviations R1648H patient phenotypes and drug treatment? As previously described this paradigm is not unique to this *SCN1A* mutation. In the past ten years extensive electrophysiological research into $Na_V1.1$-R1648H has tried to answer these questions.
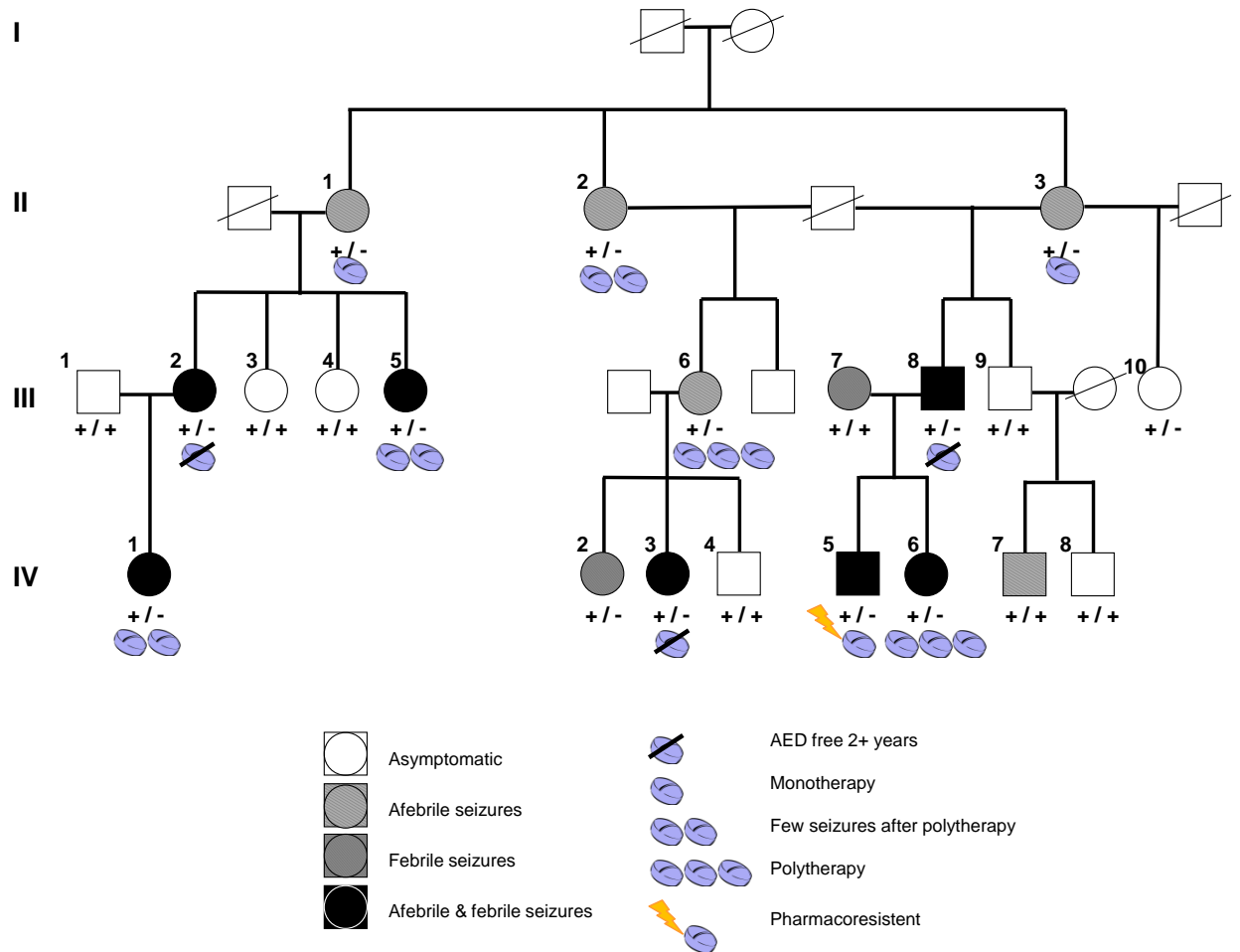
Figure 1.7 Partial pedigree of a French family with R1648H mutation. Family members are all heterozygous for the mutation but exhibit varied phenotypes and respond differently to AEDS.

1.2.17 Functional consequences of R1648H in Na$_V$1.1 channels expressed in heterologous cells

The consequences of this mutation are strikingly different depending on the cell background. The first functional characterisation of Na$_V$1.1-R1648H channels was performed in *Xenopus* oocytes using the rat ortholog of Na$_V$1.1. This study found that in the absence of β subunits R1648H increased channel recovery from inactivation and decreased

frequency dependence of inactivation, predicting an increased neuronal excitability (Spampanato *et al.,* 2001). However, it is not clear that these effects will be conserved in the human ortholog of $Na_V1.1$ expressed in cells of human origin.

In tsA201 cells (a cell line derived from the HEK line) a different gain of function effect was observed: an increase in persistent current. The authors co-expressed the human $Na_V1.1$-R1648H with β1 and β2 and argued that their conditions revealed more accurate functional defects responsible for GEFS+ compared to the seminal study in oocytes (Lossin *et al.,* 2002). Although the cell background is more similar to neurons the presence of β subunits may have masked some effects of this mutation. In humans it is unknown when during development β subunits are associated with α subunits. This is particularly relevant for $Na_V1.1$-R1648H as 10 of 14 affected members of the R1648H family had childhood, or developmentally regulated seizures (Baulac *et al.,* 1999). A second complication to assuming the β subunits are constitutively incorporated in all VGSCs is that in experimental epilepsy and/or following seizures β1, β2, and β3 are all at least transiently down-regulated (Ellerkmann *et al.,* 2003; Gastaldi *et al.,* 1998; Gorter *et al.,* 2006). This down regulation implies that patient seizure history may affect their β subunit expression and in turn alter mutant channel behaviour. Nonetheless, single channel recordings by the same group revealed that R1648H increased the probability of channel openings after inactivation over a voltage range. Additionally, a smaller percentage of channels exhibited prolonged opening times (Vanoye *et al.,* 2006). Ensemble-average currents showed that both factors contributed to persistent currents (Vanoye *et al.,* 2006).

In the same year, the group published a computational analysis of $Na_V1.1$-R1648H based on a modified Markov model for $Na_V1.1$. They proposed that fast inactivation involves an intermediate inactivated, non-conducting, phase where the channel is inactivated but the IFM gate is not 'locked' (Kahlig *et al.,* 2006). The authors surmised that the mutation destabilizes the locked state and shifts the equilibrium to the intermediate 'unlocked' phase, increasing the likelihood of channels briefly returning to the open-state (Kahlig *et al.,* 2006). In comparable experiments involving the skeletal VGSC, $Na_V1.4$, a change in an analogous arginine, to a histidine, did not produce persistent currents (Alekov *et al.,* 2000) but a equivalent change in rat $Na_V1.2$ expressed in oocytes significantly slowed the rate of current decay, stabilizing the open state of the channel (Kühn & Greeff, 1999) implying that the position of the arginine mutation can influence different VGSCs in different ways.

If $Na_V1.1$-R1648H does de-stabilize inactivation, at a single-cell level it is likely it causes neuronal hyperexcitability. For example, a mutant $Na_V1.2$ channel shown to increase persistent currents in heterologous systems was used to generate a transgenic mouse model of epilepsy (Kearny *et al.,* 2001). These mice exhibited spontaneous seizures which were partly attributed to increased persistent currents in the CA1 region of the hippocampus. Kearny and colleagues hypothesized that the 2% augmentation in current increased the resting membrane potential, and could lead to pathological excitability. However, because $Na_V1.1$ is relevant in interneurons an increase in INa$_P$ at a system level might lead to net loss of activity through enhanced inhibition.

Indeed, an opposing observation from macroscopic currents of human $Na_V1.1$-R1648H expressed in tsa201 cells indicated they had a significant reduction in channel recovery from inactivation, which would lead to neuronal hypoexcitabilty, not hyperexcitablity (Lossin *et al.,* 2002). These experiments were the first indication that changes in the voltage sensor may introduce a loss of channel function. Two recent R1648H rodent models support this hypothesis, and suggest that activity of inhibitory neurons is particularly impaired. This impairment is consistent with the loss of *SCN1A* function, and reduced inhibitory interneuron excitability, that is associated with the more severe manifestation of SMEI/Dravet.

1.2.18 The transgenic mouse carrying R1648H

The first mouse model of GEFS+ generated used a bacterial artificial chromosome (BAC) to make transgenic mice (Tang *et al.,* 2009). The *SCN1A*-R1648H sequence was introduced into the pronucleus of a fertilized mouse egg with an additional mutation: E945Q, which conferred TTX and STX resistance. Addition of these toxins to extracellular recording solutions allowed the authors to isolate $Na_V1.1$-R1648H from endogenous sodium currents in neuronal cultures. The neuronal-type influenced channel behaviour. For instance, there was a significant reduction in inhibitory bipolar neuronal current density compared to excitatory pyramidal neurons. In the former, gating was unaffected, but the voltage dependence of inactivation was shifted to more negative potentials in excitatory cells. In contrast to the electrophysiological studies in tsa201 cells, in both types of neuron, there were no observed increases in persistent current (Lossin *et al.,* 2002). Moreover, $Na_V1.1$-R1648H slowed the recovery from inactivation and increased use-dependence inactivation.

86

This was more pronounced in GABAergic inhibitory cells and again differed from previous findings in heterologous systems (Spampanato *et al.,* 2001). The transgenic mice were not epileptic but were more susceptible to kainic acid induced seizures compared to transgenic wild-type animals (Tang *et al.,* 2009). Overall this study of transgenic mice supports the hypothesis that GEFS+ causes a loss in neuronal inhibition. However, the phenotype of the mice did not completely replicate GEFS+ and precipitation of seizures by 'fever' temperatures was not addressed. Recordings were carried out at room temperature and the expression of the transgenic gene was low, leading to low amplitude currents and poor quality recordings. Disruption of gene product expression and the broader mouse genome is a possibility with pronuclear injection of foreign DNA (Hickman-Davis & Davis, 2006). However, a more exact, knock-in mouse model demonstrated several parallels to the BAC transgenic model (Martin *et al.,* 2010).

1.2.19 The R1648H knockin mouse

In another study the R1648H mutation was introduced into the endogenous *SCN1A* mouse gene, allowing analysis of mice with one or two copies of the mutation. Results from heterozygous mice may better reflect the consequence of R1648H on neuronal behavioural as patients are also heterozygous for the mutation (Escagy *et al.,* 2000). Again, mutant sodium currents recorded from GABAergic inhibitory cells derived from homozygote and heterozygote animals had decreased current densities, delayed recovery from inactivation and elevated use-dependence inactivation compared to wild-type neurons (Martin *et al.,* 2010). These effects were not observed in excitatory neurons. In fact, channels expressed from glutamatergic cells from two-week $SCN1A^{RH/RH}$ mice recovered faster from

inactivation than wild-type channels: an unaccounted gain of function that did not affect use-dependence inactivation. Persistent currents originating from mutant channels were not detected from whole-cell voltage clamp recordings in either cell background (Martin *et al.,* 2010). Current clamp recordings suggested that R1648H caused a reduction in inhibition synaptic input in both cell types.

In Na$_V$1.1-R1648H homozygous mice the number of action potentials elicited by depolarizing injections over a current range were significantly decreased in both bipolar and pyramidal cells. A reduction in neuronal excitability was more evident at higher magnitudes of current for inhibitory cells but at lower levels for glutamatergic cells. The physiological relevance of this remains unclear. All *SCN1A$^{RH/+}$* neurons demonstrated similar neuronal excitabilities compared to wild-type cells. A reduction in GABAergic inhibition and failure to propagate action potentials in these cells resulted in an epileptic phenotype for *SCN1A^{R1648H}* mice. Homozygotes, for instance, exhibited spontaneous generalized often severe seizures and died, on average, within three weeks after birth. Heterozygotes had a comparable survival rate to wild-type littermates and demonstrated a milder phenotype. For example, only a small percentage of rodents exhibited infrequent spontaneous seizures and showed a decreased threshold to fluorthyl- but not kainic acid-induced seizures. For the kainic acid model, opposite observations made for the BAC transgenic model, perhaps reflecting possible differences in spatial and temporal expression of mutant sodium channel subunits between the two strains of mice. The knock-in study highlighted that both heterozygous and homozygous mutants showed a reduced threshold and latency to seizure onset in response to hyperthermia, implying the higher body

88

temperatures can undermine the function of these mutant channels. The relatively mild phenotype of the heterozygous mice is consistent with the incomplete penetrance and variable severity observed with this mutation in humans (see Figure 1.7).

Although the results from the two mouse models are not identical, they do suggest that Na$_V$1.1-R1648H channels compromise neuronal inhibition, which is likely to impair the control of postsynaptic glutamatergic neurons and in turn increase the probability of pathological network firing. Electrophysiological studies into other *SCN1A* GEFS+ and SMEI causing mutations expressed in HEK cells both corroborate and contradict this hypothesis suggesting the full mechanism of the disease may be more complex. A recently reported rat strain with a targeted mutation in *SCN1A* reinforces the suggestion that disruption of inhibition plays an important role in the mechanism of GEFS+ (Mashimo *et al.,* 2010).

1.2.20 Merging conflicting data on functional effects of GEFS+ mutations with a mechanism of seizures

As with the *in vivo* data, electrophysiological studies into heterologously expressed GEFS+ causing mutant Na$_V$1.1 channels also exhibit mixed biophysical properties, a few of which are summarized in Table 1.5. There are, however, large variations in the methodologies used to investigate these mutants. Earlier studies used Na$_V$1.2, Na$_V$1.4 or rat orthologs of Na$_V$1.1 because human Na$_V$1.1 is difficult to clone and manipulate. There are disparities in cell models, intracellular recording solutions, and the identity of splice variants are either

unrecorded, or different in themselves. β subunit co-expression is also inconsistent, and β3, β4 modulation has not been examined.

These inconsistencies in functional data raise the following questions:

1. What is the true pathological mechanism of SMEI and GEFS+ mutations?

2. Why do mutations that similarly alter channel function present in patients with dramatically different phenotypes?

3. How do AEDs that target sodium channel inactivation prevent seizures?

The answers in the field are ardently debated. A gain of function (for instance, an increase in persistent current) would elevate intrinsic neuronal excitability. This conforms to the hypothesis that seizures result from brain hyperexcitability, and AEDs act to block this activity by reducing sodium channel function.

Table 1.5 Functional effects of *SCN1A* mutations that cause GEFS+

Mutation	Channel	Region in Na$_V$1.1	Cell type	β subunit co-expression	Splice variant?	Functional effect	Gain or loss of function	Intracellular solution	
D188V	rNa$_V$1.2	D1/S2-S3 intracellular loop	HEK	β1	Adult	Decrease use-dependence; faster recovery from inactivation	Gain of function	Cesium-Aspartate	Cossette *et al.* (2003)
R859C	rNa$_V$1.1	D2/S4	*Xenopus* oocytes	β1	Adult	Positive shift of activation; slowed recovery from slowed inactivation; reduced current	Loss of function	-	Barela *et al.* (2006)
T875M	rNa$_V$1.1	D2/S4	*Xenopus* oocytes	β1	Adult	Enhanced slow inactivation	Loss of function	-	Spamanato *et al.*(2001)
	hNa$_V$1.4		tsa201	none	Adult	Increased fast and slow inactivation	Loss of function	Cesium Fluoride	Alekov *et al.* (2001)
	hNa$_V$1.1		tsa201	β1, β2	Adult	Increased persistent current	Gain of function	Cesium Fluoride	Lossin *et al.* (2002)
W1204R	hNa$_V$1.1	L2	tsa201	β1, β2	Adult	Increased persistent current	Gain of function	Cesium Fluoride	Lossin *et al.* (2002)
	rNa$_V$1.1		*Xenopus* oocytes	β1	Adult	Negative shift of activation and inactivation; negative shift of window current		-	Spamanato *et al.* (2001)
V1353L	hNa$_V$1.1	D3/S5	tsa201	β1, β2	Adult, Full-length	No sodium current	Loss of function	Cesium Fluoride	Lossin *et al.* (2003)
I1656M	hNa$_V$1.1	D4/S4	tsa201	β1, β2	Adult, Full-length	Positive shift of activation	Loss of function	Cesium Fluoride	Lossin *et al.* (2003)
R1657C	hNa$_V$1.1	D4/S4	tsa201	β1, β2	Adult, Full-length	Positive shift of activation; reduced expression	Loss of function	Cesium Fluoride	Lossin *et al.* (2003)
A1685V	hNa$_V$1.1	D4/S5	tsa201	β1, β2	Adult, Full-length	No sodium current	Loss of function	Cesium Fluoride	Lossin *et al.* (2003)
M1841T	hNa$_V$1.1	C-terminus	tsa201	β1, β2	Adult, Na$_V$1.1[-33]	Folding/trafficking defect	Loss of function	*N*-methyl-D-glucamine	Rusconi *et al.*(2007)
D1866Y	rNa$_V$1.1	C-terminus	*Xenopus* oocytes		?	Increased persistent current	Gain of function		Spampanato *et al.*(2004)
R1916G	hNa$_V$1.1	C-terminus	tsa201	β1, β2	Adult, Na$_V$1.1[-33]	Folding/trafficking defect	Loss of function	*N*-methyl-D-glucamine	Rusconi *et al.* (2009)

However, both SMEI genetics and data from GEFS+ rodent models suggest that it is more likely that neuronal inhibition is impaired in both of these diseases; this is the favoured hypothesis in the current literature (Ragsdale 2008; Catterall *et al.,* 2010) In support of this idea, GEFS+ or SMEI causing sequence aberrations in several GABA$_A$ subunit genes have been shown to reduce neuronal inhibition through defects in receptor trafficking, subunit oligomerization and folding (Kang & MacDonald, 2009). This implies that disruption in the control of network excitability through loss of inhibition is a common pathological cause for childhood epilepsies.

From clues given in disease models concerning different VGSCs, some argue that even an *increase in* persistent current would lead to a *loss* of inhibition. For example, specific mutations in the skeletal VGSC cause an increase in INa$_P$ but a paradoxical decrease in cellular excitability that leads to muscle inexcitability and episodes of paralysis. Cannon (2006) surmises that the increased INa$_P$ would depolarize the resting membrane potential and inactivate transient sodium currents responsible for the upstroke of the muscle action potential.

1.2.21 Interactions with other channels

As previously discussed, the genetic background significantly altered the severity of epileptic phenotype observed in *SCN1A$^{+/-}$* mice indicating that genetic modifiers may provide some explanation of patient phenotypic heterogeneities. For example, *SCN8A^{med-jo}* 'motor endplate disease' mice have a point mutation within the Na$_V$1.6 D3:S4-S5 intracellular linker and display an ataxic, 'jolting' phenotype (Kohrman *et al.,* 1996).

92

Compared to wild-type animals heterozygous $SCN8A^{med-jo}$ mice were more resistant to pharmacologically induced seizures (Martin *et al.,* 2007). Current clamp recordings demonstrated that spontaneous bursting activity in dissociated $SCN8A^{med-jo}$ cerebellar purkinje cells was significantly attenuated and $Na_V1.6$ was essential for the correct functioning of excitatory neurons (Raman *et al.,* 1997). Therefore, impairment in $Na_V1.6$ function (Smith & Goldin, 1999) may reduce neuronal excitability and elevate seizure resistance in mutant *SCN8A* mice. Martin and colleagues (2007) crossed $SCN8A^{med-jo/+}$ and $SCN1A^{+/-}$ animals to produce heterozygous $SCN8A^{med-jo/+}$/$SCN1A^{+/-}$ mice. After exposure to flurothyl, double heterozygote mice demonstrated comparable seizures thresholds to wild-type animals. Moreover, the $SCN8A^{med-jo}$allele prevented the premature deaths of $SCN1A^{+/-}$ mice and prolonged the survival of $SCN1A^{-/-}$ mice. The authors surmised that the reduction in excitability of pyramidal neurons opposed the attenuation of sodium current in inhibitory interneurons, rescuing the *SCN1A* knock-out phenotype. This implies that interactions between populations of VGSCs expressed in different cell types alter seizure severity and may partly explain the heterogeneity of SMEI and GEFS+ phenotypes.

May this kind of interaction be occurring in humans with SMEI/GEFS+? It is possible that some patients suffer harbour mutations in more than one ion channel gene, which may have an additive effect on their phenotype. For example, Ohmori *et al.* (2008) sequenced the coding regions of *SCN1B*, *GABRG2* and *CACNB4* genes in 38 SMEI patients. Abnormalities in both *GABRG2* (gamma-aminobutyric acid receptor gene) and *CACNB4* (voltage dependent calcium β4 subunit gene) cause a broad spectrum of childhood epilepsies (Wallace *et al.,* 2001; Herrmann *et al.,* 2005). One AED-resistant SMEI patient

inherited a point mutation in the c-terminus of calcium channel β4 subunit from his father. The c-terminal of the β subunit is involved in trafficking the α channel-forming subunit to the plasma membrane. Electrophysiological analysis in Baby Hamster Kidney fibroblast (BHK) cells demonstrated that an alteration in the β-α interaction introduced by β4-R468Q significantly increased the current density of P/Q type calcium channels. Unfortunately this patient suffered with severe generalized convulsions and died at a young age. His father, however, only suffered with a febrile seizure in his childhood. Further screening of this patient identified a *de novo* premature stop codon, R568X, within the region coding for the first intracellular loop of $Na_V1.1$. Therefore, the haploinsufficiency of *SCN1A*, specifically a loss of neuronal inhibition, in combination with increased levels of presynaptic calcium and therefore excitatory neurotransmitter release, appears to have dramatically exaggerated the milder epileptic *CACNB4* mutation phenotype (Ohmori *et al.,* 2008).

Other genetic modifiers are emerging in similar models of childhood epilepsies. Mice carrying a three point mutation in $Na_V1.2$ D3:S4-S5 intracellular linker, denoted $SCN2A^{Q54}$, demonstrated an increase in persistent current in their CA1 hippocampal neurons (Kearney, 2001); but the epileptic phenotype of these mice is strongly influenced by genetic background. For instance, the frequency of spontaneous seizures and animal lifespan were dramatically altered in two mouse strains carrying $SCN2A^{Q54}$ (Bergren *et al.,* 2005). The specific genes responsible for the severer phenotype were mapped to chromosomes 11 and 19 (Bergren *et al.,* 2005). A later study, however, showed that mutations in the voltage-gated potassium channel *KCNQ2* exacerbated the milder $SCN2A^{Q54}$ phenotype observed for one particular mouse strain (Kearney 2006). *KCNQ2* codes for a subunit that forms a

94

potassium channel that conducts the M-type current, this activates and inactivates slowly limiting neuronal excitability (Selyanko *et al.,* 2001). Two mutant *KCNQ2* mouse lines were crossed with *SCN2A$^{Q54/+}$* mice. The *Szt1* line has a 300 bp deletion in chromosome 3 that results in the deletion of the *KCNQ2* c-terminus and nicotinic acetylcholine receptor (CHRNA4) haploinsufficiency. Heterozygous *Szt1* mice have a lower resistance to proconvulsant drugs compared to wild-type mice (Otto *et al.,* 2004). Another *KCNQ2* mice line, *KCNQ2^{V182M},* was generated so that there was a point mutation in the third segment of the *KCNQ2* subunit; these mice did not exhibit spontaneous seizures. However, double heterozygotes, namely, *SCN2A$^{Q54/+}$/KCNQ2$^{szt1/+}$* and *SCN2A$^{Q54/+}$/KCNQ2$^{V182M/+}$* mice, demonstrated spontaneous generalized tonic–clonic seizures after P12 and on average died within a week of onset (Kerney *et al.,* 2006). The authors hypothesized that an increase in persistent sodium current on depolarization and the loss of M-current during repolarisation would spread hyperexcitability and lead to severe spontaneous seizures. No SMEI patients with inherited or *de novo* mutations of *SCN1A* carried mutant *KCNQ2* alleles (Kerney *et al.,* 2006); however, the sample size was too small to disregard *KCNQ2* as a gene modifier in these patients.

Previous functional characterization of GEFS+ causing mutations failed to determine why patients exhibit age-dependent changes in seizure frequency and severity. Changes in inhibition due to a developmental switch in GABA function may be one possible explanation (Ben-Ari 2002). In the developing nervous system the intracellular concentration of chloride is high because of the relative expression of two co-transporters with opposing functions: KCC2 causes chloride efflux and NKCC1 chloride influx (Ben-

Ari 2002). The latter is predominant in immature neurons. Outward GABA$_A$ chloride currents depolarize the membrane and in the developing brain may encourage seizure generation (Ben-Ari 2006). However, during development the expression levels of KCC2 and NKCC1 switch and in mature neurons GABAergic transmission becomes inhibitory as GABA$_A$ receptors pass an inward chloride current (Ben-Ari 2002).

Another possible explanation is that the immature nervous system comprises a different milieu of ion channels compared to the fully developed nervous system. During this gestation period the kinetics of ion channels expressed by immature neurons are different to those expressed by fully formed cells, and this establishes specific firing patterns essential for proper development (Moody & Bosma, 2005). Differences may be due to dissimilar channel expression (*SCN3A* dominates early on), or may result from alternative splicing (see below). Indeed, *SCN1A* is alternatively spliced producing developmentally regulated splice variant channels (Copley 2004).

1.3.1 Overview of alternative splicing

Alternative splicing is the mechanism by which a single transcript from a gene is processed into several possible mature mRNAs. In splicing introns (non-coding DNA regions, ranging between 200 to several 1000 nucleotides) are removed, and exons (coding DNA regions, ranging between 50–300 nucleotides) are connected together (Figure 1.8). Mature spliced mRNA is exported from the nucleus to the cytoplasm where it is translated by ribosomes, producing polypeptide chains that ultimately fold into functional proteins. It is estimated that 40-60 % of human genes are alternatively spliced, finely tuning physiological function

(Modrek & Lee, 2002). In a genome-wide analysis study of human tissue, the greatest numbers of tissue-specific splice variants were found in the brain (Xu *et al.,* 2002). Unsurprisingly the first example of tissue specific alternative splicing was identified in the brain, whereby a specific variant of the calcitonin gene related peptide gene was only upregulated in the hippocampus (Amara *et al.,* 1982).

Reports within the last 30 years suggest that alternative splicing in the nervous system has three primary functions (Blencowe & Graveley, 2007). Firstly, alternative splicing expands whole-brain neuronal structure. For example, splice variants of pre-synaptic receptors called neurexins only bind to particular isoforms of post-synaptic ligands called neuroligins, establishing and regulating specific synapses within the brain (Chih *et al.,* 2006). Secondly the diversity that arises from splicing can widen neuronal responses to network activity. Genes encoding ion channels, including VGSCs, undergo extensive alternative splicing (Blencowe 2006), and in some cases this links network activity to channel behaviour. For instance, neuronal activity dictates the ER export of splice isoforms of the NMDA receptor. Increased activity favours the inclusion of one exon and activity blockade biases the expression of another. This splicing mechanism helps regulate NMDA receptor cell-surface expression (Mu *et al.,* 2003). Lastly, alternative splicing is thought to diversify protein function within neuronal subtypes. For example, two isoforms of the voltage gated calcium channel $Ca_V2.2$, which differ in their c-terminal domains are differentiately expressed in particular cell types. One variant is specifically expressed in nociceptive sensory neurons and demonstrates altered biophysical properties compared to the other variant that is upregulated in most neuronal tissues (Bell *et al.,* 2005).

Short consensus sequences along the length of introns are essential for alternative splicing. The 5' and 3' end of most mammalian introns contain the specific sequences GU and AG respectively, and preceding AG is an intronic polypyrimidine tract. In vertebrates, approximately 10-40 nucleotides upstream of the polypyrimidine rich-region is the branchpoint sequence: 5'-CURAY-3' (Figure 1.8 B; Turner *et al.,* 2001). In simplified terms splicing occurs in two-steps (Figure 1.8 A). The bond after the 5'-end G residue, that is the 5'-splice-site, is attacked by a 2'-hydroxyl group of the A nucleotide within the branchpoint sequence (Turner *et al.,* 2001). This creates a loop of mRNA called the lariat and liberates the first exon (Figure 1.8). During the second stage, pre-mRNA is cleaved at the 3'splice-site, that is, after the G at the 3' end of the intron. The two exons ligate and the lariat is released and rapidly degraded (Turner *et al.,* 2001).

Five small nuclear ribonucleoproteins (snRNPs) U1, U2, U4, U5, U6, working with a collection of regulatory proteins and ATP, catalyze alternative splicing (Turner *et al.,* 2001). The 5' end of U1 base-pairs with the 5' splice site. A sequence within U2 base-pairs with the branchpoint sequence (Lodish *et al.,* 2000). U4 and U6 base-pair to form a molecule that binds to U5. The U4/U5/U6 complex binds to the pre-mRNA and undergoes a series of re-arrangements, so that the pre-mRNA is held in the correct orientation for splicing (Lodish *et al.,* 2000). This complex of snRNPs and pre-mRNA is called the spliceosome (Figure 1.8 B) and catalyzes two transesterification reactions that free the lariat (Lodish *et al.,* 2000; Turner *et al.,* 2001). Splicing can occur in either a constitutive fashion whereby exons are combined or excluded in series (Figure 1.8 C) or are mutually exclusive in which one exon is included, and another excluded, in the final mRNA

98

transcript (Figure 1.8 C). Other methods of alternative splicing are also extensively used;

for example, intron retention and usage of alternative 5' donor and/or 3' acceptor splice

sites (Lee & Irizarry, 2003).
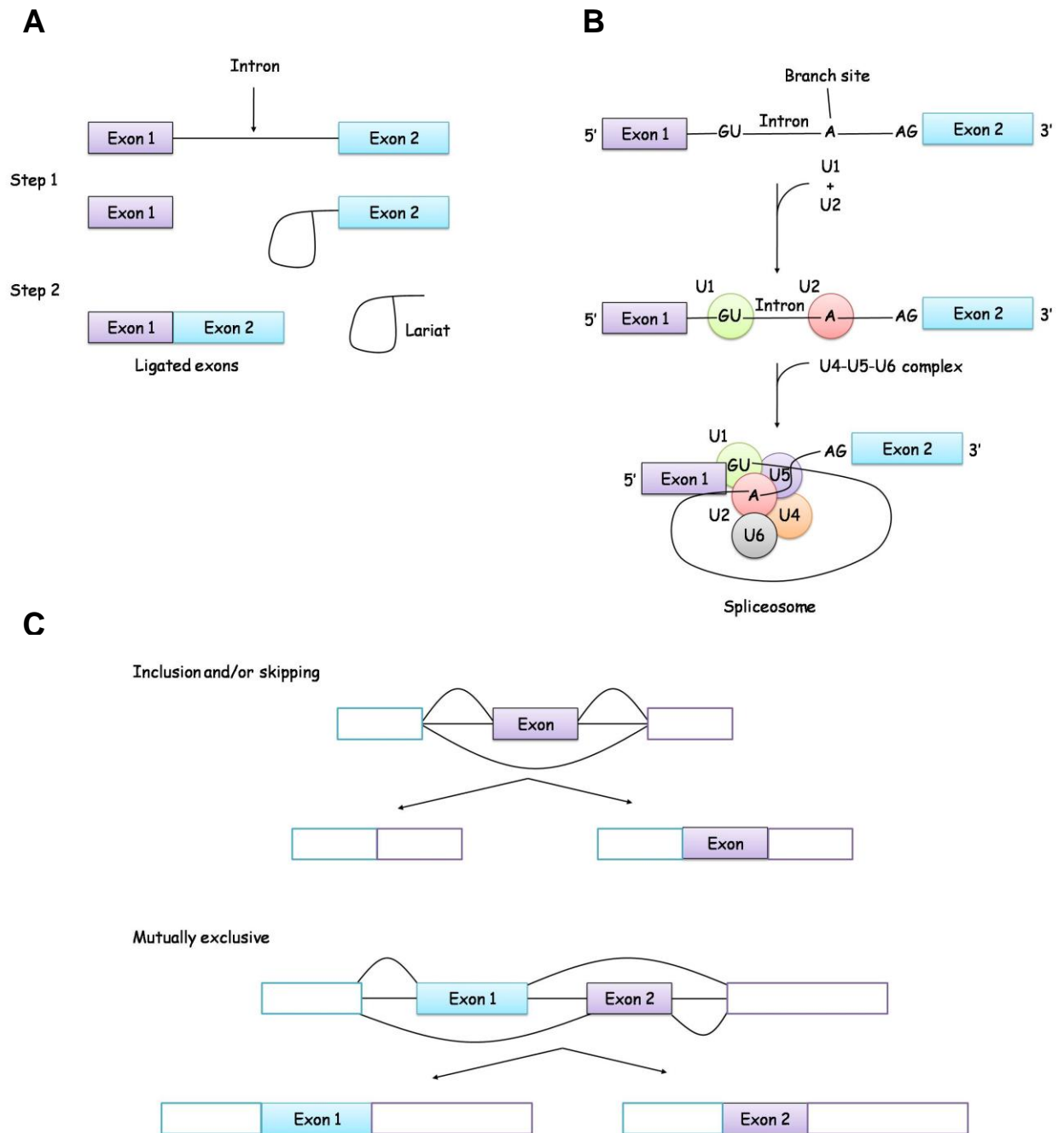
Figure 1.8 Splicing of eukaryotic pre-mRNA *A.* The two-step reaction. *B.* Involvement of snRNPs in spliceosome formation. *C.* Two forms of regulated alternative splicing: consecutive exon inclusion or skipping splicing (top) or mutually exclusive splicing (bottom). Abbreviations as in text. Redrawn from Turner *et al.* 2001 and Lipscombe 2005.

1.3.2 Alternative splicing in SCN genes

SCN1A is alternatively spliced at exon 5. *SCN1A* contains two copies of exon 5. These isoforms are denoted 5N and 5A or *N*eonatal and *A*dult according to their relative expression during development but both are expressed in the human adult brain (Tate *et al.,* 2005). Both copies of exon 5 encode nearly identical sequences in domain I. However, three amino acid changes in the extracellular loop between S3 and S4 differ between the two exons (adult to neonatal): Y203F, D207N, and V211F (Copley 2004; Figure 1.9). Alternative splicing of exon 5 *SCN1A* is partly modulated by the splice-modifier protein Nova2. Increased expression of Nova2 biases splicing towards the neonatal exon (Heinzen *et al.,* 2007). Microarray studies on brain tissues from *Nova2* null mice revealed that this protein coordinated exons in genes expressed mainly in inhibitory neuronal synapses, supporting the role of $Na_V1.1$ in inhibition (Ule *et al.,* 2005). Exon 5N and 5A encode channels that differ in a domain of the ion channel thought to be important for voltage-sensing. Consequently, even subtle effects of alternative splicing might have important consequences for neuronal behaviour. An additional five VGSCs undergo similar alternative splicing, including *SCN2A*, *SCN3A* (Sarao *et al.,* 1991; Gustafson *et al.,* 1993; Lu & Brown 1998), *SCN8A* (Plummer *et al.,* 1997) and *SCN9A* (Belcher *et al.,* 1995), replacing a neutral residue, typically asparagine, with a negatively charged aspartate when switching from exon N to A in this region. Within *SCN5A*, analogous alternate splicing replaces a positively charged lysine with aspartate (Schaller *et al.,* 1992; reviewed in Copley 2004; see Figure 1.9).

A

Exon 4   5N   5A   Exon 6

B
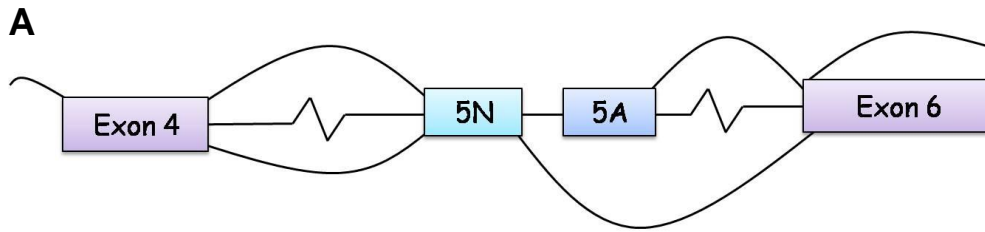
SCN1A Nav1.1	ITFAFVTEFVNLGNFSALRTFRVLRALKTISVIPGLKTI
	ITFAYVTEFVDLGNVSALRTFRVLRALKTISVIPGLKTI
	•••• ••••• ••• ••••••••••••••••••••••

SCN2A Nav1.2	ITFAYVTEFVNLGNVSALRTFRVLRALKTISVIPGLKTI
	ITFAYVTEFVDLGNVSALRTFRVLRALKTISVIPGLKTI
	•••••••• •••••••••••••••••••••••••••

SCN3A Nav1.3	IVMAYVTEFVSLGNVSALRTFRVLRALKTISVIPGLKTI
	IVMAYVTEFVDLGNVSALRTFRVLRALKTISVIPGLKTI
	•••••••••• ••••••••••••••••••••••••••

| SCN4A Nav1.4 | IMMAYLTEFVDLGNISALRTFRVLRALKTITVIPGLKTI |
| | (no evidence for alternative exon 5) |

SCN5A Nav1.5	IIMAYVSENIKLGNLSALRTFRVLRALKTISVIPGLKTI
	IIMAYTTEFVDLGNVSALRTFRVLRALKTISVISGLKTI
	••••• • ••• •••••••••••••••• •••••

SCN8A Nav1.6 PN4	IMMAYITEFVNLGNVSALRTFRVLRALKTISVIPGLKTI
	IMMAYVTEFVDLGNVSALRTFRVLRALKTISVIPGLKTI
	••••• •••• ••••••••••••••••••••••••••

SCN9A Nav1.7 PN1	IVFAYLTEFVNLGNVSALRTFRVLRALKTISVIPGLKTI
	IVFAYVTEFVDLGNVSALRTFRVLRALKTISVIPGLKTI
	••••• •••• ••••••••••••••••••••••••••

| SCN10A Nav1.8 PN3 | ITLAYVGTAIDLRGISGLRTFRVLRALKTVSVIPGLKVI |
| | (no evidence for alternative exon 5) |

| SCN11A Nav1.9 PN5 | IGIAIVSYIPGITIKLLPLRTFRVFRALKAISVVSRLKVI |
| | (no evidence for alternative exon 5) |

C
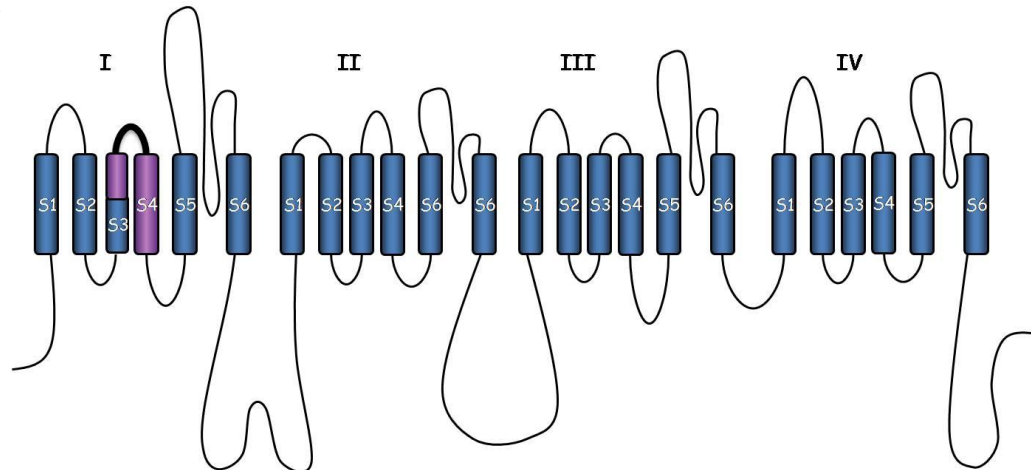
Figure 1.9 (previous page) Molecular differences between 'neonatal' and 'adult' VGSC splice variants *A*. The genomic structure of human VGSC genes surrounding neonatal (N, green) and adult exons (A, blue) Exon 5N encodes the neonatal isoforms of human *SCN1A* (Na$_V$1.1), *SCN8A* (Na$_V$1.6) and *SCN9A* (Na$_V$1.7) and Exon 6N the neonatal isoforms of human *SCN2A* (Na$_V$1.2), *SCN3A* (Na$_V$1.3) and *SCN5A* (Na$_V$1.5). *B.* The peptide sequences of VGSCs genes encoded by the alternative 'neonatal' exon are shown on the *top line* and the sequences encoded by the 'adult' exon are shown on the *bottom line*. Table taken from Raymond *et al.,*2004. *C.* Schematic indicating the region of VGSCs encoded by exon 5N/6N or 5A/6A in the first domain of the channel. This region, corresponding to the end of the third transmembrane segment (S3), a short extracellular linker (thick black line) and the entire voltage-sensing fourth transmembrane segment (S4; indicated in purple).

Within the analogous rodent intronic region to human *SCN1A* exon 5N (Gazina *et al.,* 2010) there is a premature stop-codon; therefore, only the adult isoform is expressed in rats and mice. Consequently, determining the relative expression of Na$_V$1.1-5N and Na$_V$1.1-5A *in vivo* is problematic, and expression of exon 5N may not be physiologically relevant in *SCN1A* in rodents. However, northern blot and quantitative PCR studies performed in rodents suggest that *SCN1A* is strongly upregulated during the first week of birth, being detectable at E10 but escalating to peak at P15 (Beckh *et al.,*1989; Gazina *et al.,* 2010). *SCN1A* is most abundant in midbrain areas, thalamus and cerebellum, and displays a weaker mRNA signal in the cortex and hippocampus (Beckh *et al.,* 1989; Gazina *et al.,* 2010). The remaining VGSC genes shown in Figure 1.9 B are alternatively spliced in rats and mice, as well as in all other mammalian sequences known. Although denoted 'neonatal' and 'adult', studies in rodents suggest that this nomenclature may be misleading. For example, there are conflicting reports of the relative expression levels of Na$_V$1.3-6N and Na$_V$1.3-6A during development. Gustafson *et al.* (1993) showed that rat Na$_V$1.3-6N was predominant isoform at E18, by P4 levels of Na$_V$1.3-6N and Na$_V$1.3-6A were equal

and by P10 the adult isoform replaced $Na_V1.3\text{-}6N$ expression. However, a more recent quantitative PCR report performed in mice implied that $Na_V1.3\text{-}6A$ was predominant between P0 and P15 (Gazina *et al.,* 2010). Similarly, in three reports the adult isoform of *SCN8A* was the primary channel in newborn and two-week old rodent brains (Raymond *et al.,* 2004; Mechaly *et al.,* 2005; Gazina *et al.,* 2010). However, a recent quantitative PCR study suggest that *SCN2A* expression follows the 'neonatal' and adult' paradigm. In the newborn mouse cortex and hippocampus, $Na_V1.2\text{-}6N$ expression levels were at least 1.5 times that of $Na_V1.2\text{-}6A$ (Gazina *et al.,* 2010); this supported earlier data described by Gustafson *et al.* (1993). A previous investigation using the same technique showed that $Na_V1.7\text{-}5N$ was the main channel expressed not only in fetal but also the adult brain (Raymond *et al.,* 2004). The same study demonstrated that $Na_V1.7$ is dramatically upregulated in fetal compared to adult brain; data corroborated by a later PCR study where overall $Na_V1.7$ expression was detected in rat cortex at stage P1 but not P13 (Mechaly *et al.,* 2005). $Na_V1.5\text{-}6N$ was observed in the neonatal (P1) mouse brain (Chioni *et al.,* 2005), but the relative expression levels between $Na_V1.5\text{-}6N$ and $Na_V1.5\text{-}6A$ was undetermined.

1.3.3 Alternative splicing in VGSC genes during epilepsy

Interestingly, in experimental epilepsy and/or following seizures, the neonatal channel isoform is upregulated in multiple sodium channels, including *SCN1A*. In one study, $Na_V1.1\text{-}5N$ was upregulated in resected temporal lobe tissue from patients (Tate *et al.,* 2005), but this finding was not replicated in a follow-up study (Heinzen *et al.,* 2007), whereby neonatal transcripts had a trend towards downregulation in comparable tissues. Unlike *SCN1A*, other channel mRNAs can be investigated in rodent models of epilepsy

where the N>A splicing is conserved. $Na_V1.3$-6N and $Na_V1.2$-6N were both transiently upregulated for approximately 12 hours in the rat hippocampus, following kainate-induced seizures (Gastaldi *et al.,* 1997). After electrically-induced status epilepticus (SE), another epilepsy rodent model, the neonatal transcripts of $Na_V1.2$ and $Na_V1.3$ were persistently upregulated in the hippocampus for 3 months, while the adult isoforms were transiently upregulated for only 4 hours (Aronica *et al.,* 2001). In both studies the dentate gyrus was particularly affected compared to other regions of the hippocampus. In similar epilepsy models, three other GEFS+ genes were persistently up- (*GABRA2*) and down-regulated (*GABRD* and *HCN2*) in the dentate gyrus (Sperk *et al.,* 1998; Nishimura *et al.,* 2005; Powell *et al.,* 2008). This implies that gene transcription in this area is more susceptible to long-term changes in response to neuronal hyperexcitability, but the implications for GEFS+ epileptogenesis are unknown.

1.3.4 Functional studies of SCNnA splice variants

Although the N>A alternative splicing changes the linker adjacent to the voltage sensor its functional impact remains controversial. Functional effects have been shown for splicing in several related sodium channels, including $Na_V1.2$, $Na_V1.7$ and $Na_V1.5$ and these are summarized in Table 1.6 (references therein). However, these heterologous expression studies are compromised by limitations similar to those described for $Na_V1.1$-R1648H channels. Extrapolation to $Na_V1.1$ is also limited because there are several amino acid substitutions between $Na_V1.1$ and other VGSCs splice variants. In addition, in spite of the role of VGSCs in the pharmacology of AEDs (discussed below) no report addresses the pharmacological consequences of alternative splicing in a VGSC. Nonetheless from these

studies, inactivation, particularly the rate of current decay and recovery from inactivation are two properties affected by alternatively splicing in these genes (Table 1.6). Interestingly, these parameters of CNS VGSCs are also modulated by AEDs. Moreover, no mutations have been found to affect $Na_V1.1$-5A and $Na_V1.1$-5N splicing *per se* but a cluster of missense and frameshift mutations at amino acids 211-213, around the third amino acid switch (residue 211) are found in GEFS+ patients, suggesting that D1:S3-S4 loop is functionally important in GEFS+.

Table 1.6 Functional differences between 'neonatal' and 'adult' VGSC channel isoforms

Channel	Cell type	β subunit expression?	Functional differences between variants	Intracellular solution	
$rNa_V1.2$	*Xenopus* oocytes	none	No differences	-	Auld *et al.,*1990
$hNa_V1.2$	HEK 293	none	**Neonatal variant:** ↓ rate of current decay, **Adult variant:** depolarizing shift inactivation, ↑ recovery from inactivation	Cesium Fluoride	Xu *et al.,*2007
$hNa_V1.2$	tsa201	β2,β2	No differences	Cesium Fluoride	Liao *et al.,*2010
$hNa_V1.5$	EBNA-293	All isoforms endogenously expressed	**Adult variant:** depolarizing shift activation; ↑ rate current decay; ↓ recovery from inactivation	Cesium Chloride	Onkal *et al.,*2008
$hNa_V1.7$	tsa201	β1	**Adult variant:** slower development of inactivation	Cesium Fluoride	Chatelier *et al.,*2008
$hNa_V1.7$	HEK 293	β1,β2	**Adult variant:** ↑ ramp current	Cesium Chloride	Jarecki *et al.,*2009

1.3.5 Biophysical consequences of disease causing mutations in SCNnA splice variants

Different mutations in both $Na_V1.7$ and $Na_V1.2$ are differentially affected by changes in the D1:S3-S4 linker (Xu *et al.,* 2007; Liao *et al.,* 2010; Jarecki *et al.,* 2009; Choi *et al.,* 2010). Studies into the effects of heterologously expressed $Na_V1.2$-6N and $Na_V1.2$-6A containing

BFIC mutations demonstrated subtle biophysical differences (Xu *et al.,* 2007; Liao *et al.,* 2010). For example, a mutation in D4:S4 accelerated the rate of channel inactivation but only in the neonatal background (Xu *et al.,* 2007). A later study showed that a mutation in the pore region of D1 did not change its gating in either splice variant background. In contrast, a mutation in the same region demonstrated an increase in persistent current in $Na_V1.2$-6N channels (Liao *et al.,* 2010). Similarly, a mutation in $Na_V1.7$ D1:S1 did not have an effect on either channel isoform (Jarecki *et al.,* 2009) but a mutation in the inactivation gate, slowed channel current decay and increased ramp currents in the adult but not neonatal background. Results from these studies imply that changes in neuronal excitability can be altered by alternative splicing but are a dominant effect of individual mutations.

1.3.6 Alternative splicing in other VGSC regions

First intracellular loop

VGSCs are extensively alternatively spliced to produce a myriad of channel isoforms but little is known about their biophysical properties (Diss *et al.,* 2004). For clarity select variants, particularly $Na_V1.1$ isoforms, found in mammalian neuronal tissues will be discussed. *SCN1A* is alternatively spliced in exon 11, which codes for a region within the first intracellular loop. Two additional shortened isoforms are generated: $Na_V1.1$[-33] and $Na_V1.1$[-88]which lack 11 and 28 amino acids respectively, compared to the full length protein (Lossin *et al.,* 2002). The clone used in this study was $Na_V1.1$[-33] and is the

predominant isoform in rat brain (Schaller *et al.,*1992). The functional consequence of exon 11 splicing in $Na_V1.1$ is unknown (Lossin *et al.,* 2008).

$Na_V1.3$, $Na_V1.6$ and $Na_V1.7$ channels are spliced in the same region producing at least two more isoforms for each channel (Schaller *et al.,* 1992; Klugbauer *et al.,* 1995; Dietrich *et al.,* 1998; Plummer *et al.,* 1998). $Na_V1.3$ and $Na_V1.6$ splice variants are found in the rodent brain (Schaller *et al.,* 1992; Plummer *et al.,* 1998; Diss *et al.,* 2004). One $Na_V1.3$ isoform is truncated within the loop producing a channel with one domain but its biophysical properties are yet to be elucidated (Diss *et al.,* 2004). $Na_V1.7$ isoforms play a role in the PNS and non-neuronal tissues (Klugbauer *et al.,* 1995; Sangameswaran *et al.,* 1997; Toledo-Aral *et al.,* 1997). Splicing in this region is hypothesized to regulate channel phosphorylation because within the first intracellular loops of VGSCs there is a high concentration of serine residues; however, longer $Na_V1.1$ isoforms do not contain putative phosphorylation sites (Berendt *et al.,* 2010).

Second intracellular loop

In rat brain alternative splicing of exon 16 within *SCN2A* and *SCN3A* and exon 17 within *SCN9A* introduces a premature stop codon within the second intracellular loop producing two domain channels (Kerr *et al.,* 2008). Human analogues of these channels have not been identified but the authors argue the alternative splicing sequences for these channels are highly conserved in humans (Kerr *at al.,* 2008). Similarly, isoforms of $Na_V1.5$ produced by alternative splicing have second intracellular loops with variable lengths and are found in rodent brain (Korsgaard *et al.,* 2004). Shortening of this region by 53 amino acids altered

108

the gating and TTX sensitivity of Na$_V$1.5 in an embryonic precursor cell line (Korsgaard *et al.,* 2004). This effect maybe dependant on cell background as no changes in Na$_V$1.5 properties were observed from this isoform expressed in HEK 293 cells (Zimmer *et al.,* 2002c). *SCN5A* and *SCNA10* are also alternatively spliced in this region to produce an isoform with a deletion of a glutamine. However, the electrophysiological properties of these Na$_V$1.5 and Na$_V$1.8 isoforms are indistinguishable from their full-length counterparts (Schoeter *et al.,* 2010; Schirmeyer *et al.,* 2010).

Third domain

Exon 20 of Na$_V$1.1 is alternatively spliced producing one isoform truncated in the third domain and another with a structurally distinct pore loop in the same region (Oh & Waxman, 1998). These isoforms were detected in rat spinal cord astrocytes and were inducible upon cAMP administration. It is undetermined how these variants change the functional properties of Na$_V$1.1 channels (Oh & Waxman, 1998). Exon 18 of human *SCN8A*, Na$_V$1.6, is also alternatively spliced in the same domain, generating two developmentally regulated splice variants 18A and 18N. Na$_V$1.6-18N is truncated at D3:S3 and upregulated in the fetal brain (Plummer *et al.,* 1997). Na$_V$1.6-18A is a full length isoform that is expressed only in adult brain (Plummer *et al.,* 1997). There are no reports on the functional significance of these isoforms but Na$_V$1.6-18N is predicted to form non-functional channels (Diss *et al.,* 2004). The voltage sensor of the third domain, in one Na$_V$1.9 variant weakly expressed in the brain, is truncated by splicing (Jeong *et al.,* 2000).

1.3.7 Functional significance of VGSC splice variants

The few functional reports on VGSC splice variants suggest that channel isoforms possess subtly different biophysical properties. No studies have investigated how the VGSC splice variant profile of individual neurons affects their cell-specific output. However, a recent SC-RT-PCR study into the crab VGSC: *CbNaV*, which undergoes alternative splicing to produce nine splice variants showed that 10 different cell types from the Stomatogastric Ganglion had specific *CbNaV* splice variant profiles (Dai *et al.,* 2010). Splice variant expression was heterogeneous not only between cholinergic and glutamatergic cells but also within the same cell type (Dai *et al.,* 2010). This suggests that sodium channels within each neuron, particularly within this small circuitry neuronal system, play a very specific role. Moreover, Mechaly and colleagues (2005) combined SC-RT-PCR and electrophysiology techniques to characterize the gating properties of VGSCs expressed in rat hippocampal pyramidal and utricular hair cells. Individual cells expressed up to three combinations of VGSCs but splice variants were unspecified. Single hippocampal and utricular cells with the same VGSC expression profile showed different action potential profiles and *I*Na gating. Although the authors speculated that this likely to result from alternative splicing of VGSC genes (Mechaly *et al.,* 2005) they did not fully investigate this possibility.

1.3.8 Alternative splicing GEFS+ syndromes

Aberrant splicing in *SCN1A* causes severe epilepsy phenotypes; 65 mutations in splice acceptor or donor sites within the majority of *SCN1A* introns cause SMEI but only one

mutation in a donor site causes GEFS+ (Table 1.4). In the report discussed previously, which provides evidence that mutations in *SCN9A* may act as a genetic modifier in SMEI harbouring *SCN1A* mutations, several splice site mutations in *SCN1A* were investigated (Singh *et al.,*2009). In a cohort of 109 patients with SMEI, 7 individuals had mutations in both genes, of which 3 had changes that affected splice donor and acceptor sites in *SCN1A*. Aberrant splicing also occurs in other GEFS+ genes. For example, a patient with febrile seizures who later developed childhood absence epilepsy harboured a splice-donor mutation rendering the γ2 subunit non-functional (Kananura *et al.,* 2002).

1.3.9 AEDs and splicing

Many AEDs inhibit VGSC including established drugs like phenytoin and carbamazepine and newer anticonvulsants, for example, lamotrigine. Phenytoin, like many neuromodulatory drugs (Keiser *et al.,* 2009) has off-target effects and has been reported to bind to calcium and potassium channels (Remy & Beck, 2006). Although structurally distinct (Figure 1.10 A) VGSC blockers have two common features: a positively charged nitrogen group and an aromatic group at opposite ends (Mantegazza *et al.,* 2010). AEDs bind to an inner vestibule of the pore formed by S6 residues within all domains but D2 (Mantegazza *et al.,* 2010; see Figure 1.10 B for details). Other AEDs, for example, specifically block calcium channels and facilitate potassium channels and other agents enhance GABAergic neurotransmission (Rogawski & Löscher, 2004).
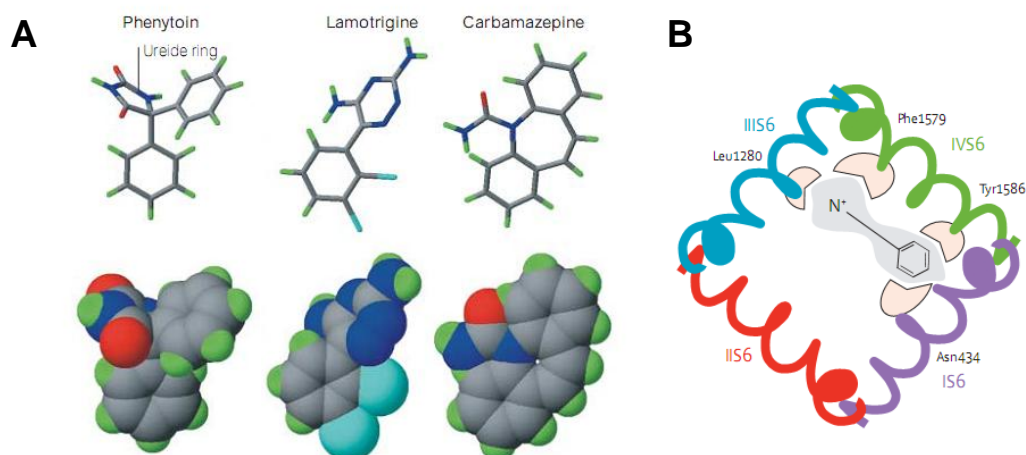
Figure 1.10 The structure and binding sites of AEDs *A*. "Stick and space-filling views showing the ureide ring $(CO(NH_2)_2)$ common to the sodium-channel-blocking antiepileptic drugs phenytoin, lamotrigine and carbamazepine". Explanation and figure taken from Rogawski & Löscher 2004. *B.* "**Molecular modelling of the drug binding site suggests that the positively charged amine interacts strongly with a phenylalanine in domain IV and, to a lesser extent, with a leucine in domain III, whereas the aromatic group interacts with a tyrosine in domain IV and an asparagine in domain I". Explanation and figure taken from Mantegazza *et al.* 2010.

1.3.10 Can alternative splicing affect AED efficacy?

At present, AED treatment of epilepsy is unpredictable; approximately 30% of patients are resistant to the first two to three drugs they are administered (Remy & Beck, 2006). The cause of pharmacoresistence is obscure. SMEI patients have been reported to be not only resistant to particular AEDs but their seizures can be aggravated by the VGSC blockers carbamazepine and lamotrigine (Wakai *et al.,* 1996; Guerrini *et al.,* 1998; Abe *et al.,* 2008), although phenytoin is less aggravating (Genton 2000). Drug sensitivity may alter due to subtle differences in multi-drug transporters, voltage-gated channels, neurotransmitter systems and genetics between individuals (Remy & Beck, 2006; Schaub *et al.,* 2007). Indeed in a rat experimental epilepsy model, one strain was subdivided into two groups that

either responded or did not respond to phenytoin (Löscher & Rundfeldt, 1993), a difference not found in another phenytoin-responsive breed (Löscher et al., 1998).

A seminal study exploring whether a European heterogeneous population of 425 epilepsy patients were genetically predisposed to respond to specific anti-epileptics, demonstrated that a SNP, rs3812718, in *SCN1A* was associated with a significant shift in the maximal dosage of two AEDS: phenytoin and carbamazepine (Tate et al., 2005; Figure 1.11). The polymorphism rs3812718 is located in the consensus sequence of the 5' splice donor site downstream of the neonatal exon 5N (exon 5N+5G>A). The alleles of the SNP, the 'ancestral' allele G and the 'mutant' allele A, are approximately equally prevalent in humans chromosomes (Heterozygous = 0.50 ± 0.05 (average $\pm$SEM); NCBI refSNP Cluster Report; Weale et al., 2003). The G allele is conserved across vertebrates (Zhang 1998) and is present in homologous CNS VGSC genes that are alternatively spliced within D1:S3-S4. Since the +5G site is located within the spliceosome recognition sequence, it is possible that a switch to the A allele at this site interrupts recognition of the neonatal exon by the U1 snRNA (Zhang & Weiner, 1986). Indeed, in temporal lobe neocortex taken during autopsy of healthy individuals, the exon 5N+5G$\rightarrow$A variant (AA) was associated with a significantly lower proportion of neonatal transcripts. The ratio of exon 5N transcripts increased sequentially in brain tissue taken from people with AG and GG genotypes (Heinzen et al., 2007). The disruption of the splice recognition site by the A allele was confirmed by a minigene assay in HEK cells (Heinzen et al., 2007). Tissue from epilepsy patients demonstrate comparable genotype-phenotype correlations (Heinzen et al., 2007), but as discussed, it is ambiguous whether seizures cause an up or down-regulation of the

113

neonatal variant in *SCN1A* (Tate *et al.,* 2005; Heinzen *et al.,* 2007). Mammals have

divergent mechanisms of splice site recognition and alternate exons are known to use

multiple mechanisms to regulate their inclusion, so an absolute effect of splicing *in vivo* is

not predictable from the nucleotide sequence alone. For instance, increased levels of

NOVA2 mRNA expression correlated with an upregulation of exon 5N transcripts in

homozygous AA healthy and epileptic individuals (Heinzen *et al.,* 2007).
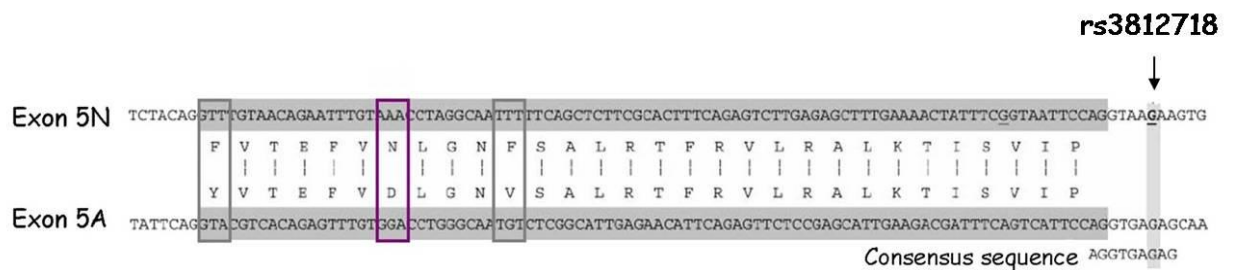
Figure 1.11 The complete sequence of *SCN1A* exon 5 aligned with exon 5A. The codons
encoding the three amino acid changes between exon 5N and 5A are boxed. The conserved
amino acid switch is boxed in purple. The location of rs3812718 is indicated by the arrow.
Redrawn from Tate *et al.* (2005)

Tate *et al.* (2005) demonstrated that maximum AED dosage consecutively decreased in

epilepsy patients with AA, AG and GG genotypes. As maximum dosage is not an accurate

determinant of drug efficacy the original study was repeated on a Chinese cohort of 71

patients, and Tate *et al.* (2006) confirmed that rs3812718 was associated with phenytoin

serum concentration at maintenance dose (Tate *et al.,* 2006). Because this significance was

marginal, the authors tentatively postulated that individuals that express a greater

percentage of 5N, that is carry the G allele of the SNP on one or both their alleles, may

require a lower drug maximum dosage. One aim of this study is to link the effect of the

114

rs3812718 on splicing of exon 5N, together with a demonstration that splicing has a biophysical and pharmacological consequence for $Na_V1.1$. This could provide a mechanistic explanation for the association between this polymorphism and AED dosage. Since the polymorphism is extremely common, a mechanism connecting it to the treatment of epilepsy would imply that genetic variability of *SCN1A* has a far broader impact for epilepsy in the population than currently appreciated from rare, individual mutations. In fact, the AA genotype conferred a three-fold increased risk of developing childhood febrile seizures in an Austrian cohort (Schlachter *et al.,* 2009). However, the same group did not find an association in a cohort of 558 Australian epilepsy patients (Petrovski *et al.,* 2009).

A similar association between rs3812718 and lamotrigine serum levels in 50 Russian patients has been recently reported (Krikova *et al.,* 2009), providing evidence that this SNP affects the dosage of a range of AEDs. Moreover, another study of 222 Japanese epilepsy patients demonstrated that individuals with the AA genotype were on average, nearly three times more resistant to carbamazepine (Abe *et al.,* 2008). However, the effects of rs3812718 should be treated with some scepticism. Two studies have failed to replicate the Tate *et al.* findings (2005, 2006). The maintenance dosage of carbamazepine in 369 Austrian patients did not correlate with genotype (Zimprich *et al.,* 2008) and no relationship was found in 377 Chinese patients between sodium channel blocking AEDs and rs3812718 (Kwan *et al.,* 2008). One may argue, therefore, that this association is unproven but the positive findings may still provide a plausible hypothesis connecting patient genotype with drug response. Since discrepancies between these studies may result from varying cohort size, heterogeneity of epilepsy syndromes in population samples and

differences in ethnic backgrounds. These studies focus on sodium channel blocking drugs and within the cohorts the cause of epilepsy is unknown. Different cohorts may have different ratios of genetically-related and non-genetically related epilepsy syndromes, which may or may not involve *SCN1A* or other VGSCs genes. Therefore, the effect of rs3812718 on AED dosage may be obscured or overridden in some populations. As previously discussed studies involving experimental epilepsy models imply that there is a significant change in neuronal phenotype in response to seizures, which may change responses to AEDs (Gastaldi *et al.,* 1997; Aronica *et al.,* 2001). Indeed, SC-RT-PCR and electrophysiological analysis of dentate granule cells from a rat pilocarpine model of epilepsy demonstrated that the subunit composition of $GABA_A$ receptors was altered which in turn reduced zolpidem (an anticonvulsant) sensitivity (Brooks-Kayal *et al.,* 1998). One aim of this study is to determine whether phenytoin differentially affects the biophysical properties of $Na_V1.1$-5N and $Na_V1.1$-5A channels, to provide a potential mechanistic explanation for AED discrimination.

1.3.11 Mechanism of AED block on VGSCs

Phenytoin is effective at protecting against GTCS and partial epilepsy. Its mechanism is typical of sodium channel blockers and dependent on channel conformation (Figure 1.12). AEDs like phenytoin selectively block high-frequency repetitive firing and only weakly suppress normal nerve activity (Rogawski & Löscher, 2004; Mantegazza *et al.,* 2010). The modulated receptor hypothesis assumes that phenytoin-like drugs strongly bind to inactivated or open VGSCs channels, at more depolarized potentials, and have weaker affinity for resting channels at more negative potentials (McLean & MacDonald, 1983;

116

Ragsdale *et al.,* 1991). AED action is 'use-dependent', that is, inhibition is significantly increased during rapid trains of depolarizing pulses, similar to sustained firing during ictal episodes (Matsuki *et al.,* 1983; Kuo & Bean, 1994). During each pulse a greater proportion of channels open and inactivate: conformations that enhance drug binding. Both phenytoin and lamotrigine bind to and dissociate from VGSCs slowly (Rogawski & Löscher, 2004). Therefore firstly, the normal time-course of VGSC gating is unaltered and 'normal' firing is mostly unaffected. Secondly drug dissociation is slower than VGSC recovery from inactivation enabling block to accumulate during rapid, prolonged firing (Ragsdale & Avoli 1998). Moreover, VGSC blockers stabilize the inactivated state, decreasing channel availability, shifting the voltage dependence of VGSC inactivation in a hyperpolarized direction (Ragsdale *et al.,* 1991). In a heterologous system persistent sodium currents were more sensitive to several AEDs, including phenytoin, and were blocked at lower dosages compared to transient currents (Kohling 2002). *In vivo* neuronal INa$_P$ have also been reported to be inhibited by phenytoin and lamotrigine (Chao & Alzheimer 1995; Gebhardt *et al.,* 2001).

A Recovery from inactivation

B Closed   Inactivated
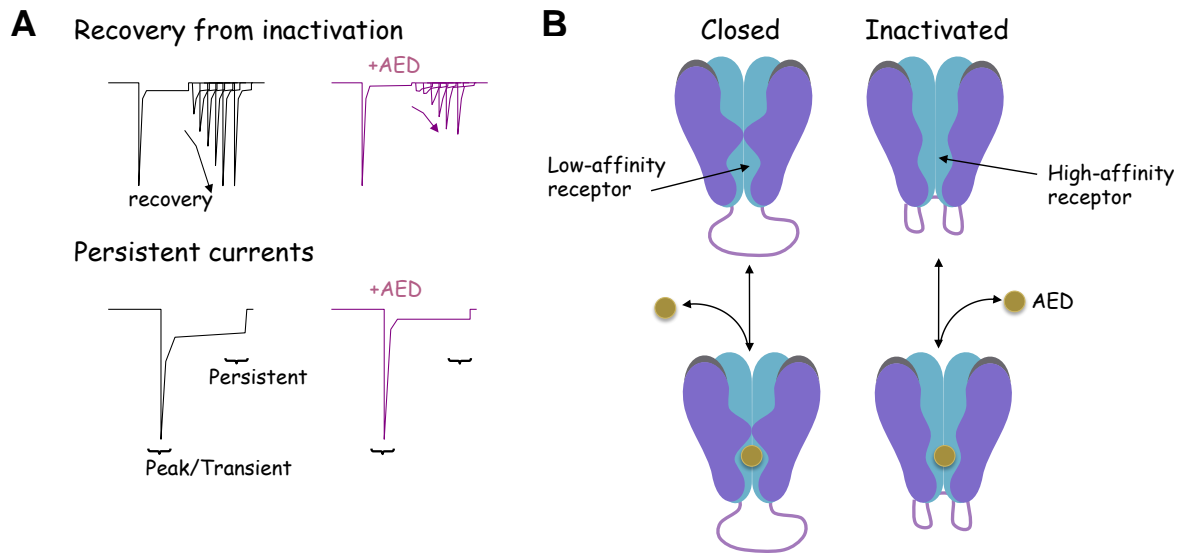
Figure 1.12 Effects of AEDs on VGSCs *A*. (Top panel) the first pulse is unaffected by AED administration. However, recovery from inactivation is inhibited and this is the mechanism underling 'use-dependent' inhibition. (Bottom panel) when peak sodium currents are <10% blocked persistent sodium currents are ~60% inhibited. This has only recently been recognized as an important feature of AED inhibition. The net effect is a reduction of sodium currents by the drugs, particularly during strong activation of neurons**. *B*.** The modulated receptor model. "In this model, the drug binds with higher affinity to inactivated channel states than to resting channel states". Explanation taken and figure redrawn from Mantegazza *et al.* 2010.

It is unknown what the impact of $Na_V1.1$-R1648H and other mutations is on channels in a neonatal 'background', or if rs3812718 contributes to the variability of GEFS+ Type 2 phenotypes. Mutant VGSCs like $Na_V1.1$-R1648H may increase persistent currents (Lossin *et al.,* 2002). Because AEDs disproportionably inhibit INa$_P$ another aim of this study is to determine if phenytoin differentially affects $Na_V1.1$-R1648H in exon 5N and 5A backgrounds. This may provide another possible mechanism for the association of genetics with drug dosage. Further, if $Na_V1.1$-5N is upregulated early in development, this may partly explain why the syndromes associated with *SCN1A* mainly manifest during

childhood. However, as suggested by the variable results of biophysical investigations into the consequences of the $Na_V1.1$-R1648H mutation, it is likely that any assessment of the functional impact of inclusion of exon 5N or 5A will be highly sensitive to recording conditions. Given the temperature sensitivity of the seizure disorders associated with *SCN1A* and elevated temperatures are known to reduce VGSC blocker affinity (Strichartz & Zimmermann 1983), temperature may also play an important role in modulating channel and variant function in the presence or absence of AEDs.
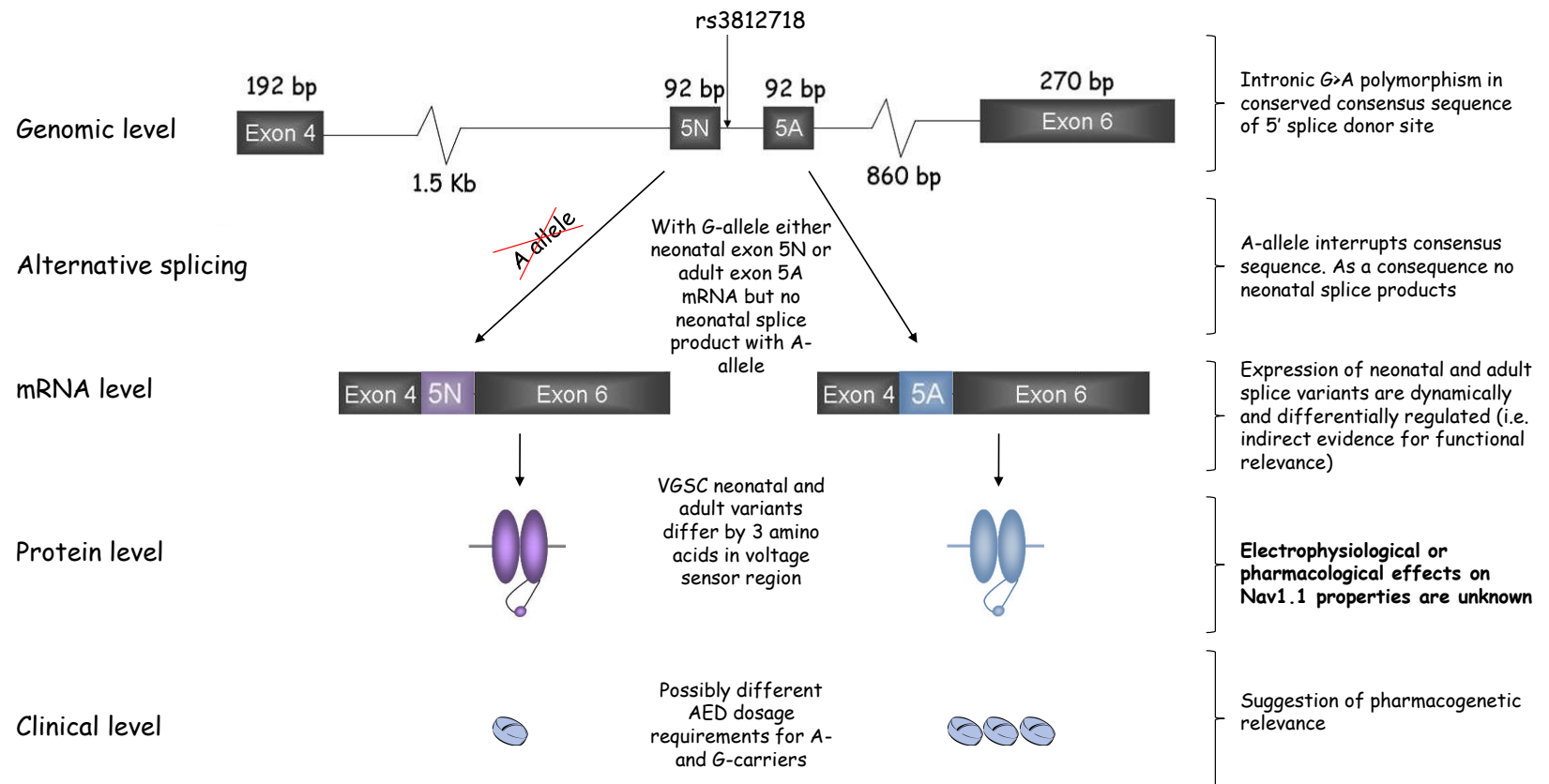
Figure 1.13 The rs3812718 SNP in the SCN1A gene can affect the alternative splicing of exon 5. $Na_V1.1$-5N and $Na_V1.1$-5A are likely to have different biophysical properties. This may explain why patients have altered AED requirements depending on their genotype. (Redrawn from Loscher *et al.*, 2009).

1.4.1 Overview of modulation of Na$_V$1.1

A large part of this work was focused on determining the conditions where the different splice variants of *SCN1A* could be studied in isolation. A major hurdle to this sort of comparison is that even in heterologous cells that express few other channels, many endogenous and exogenous factors modify sodium channel behaviour. For the purposes of this project, to attempt to clamp the channels in comparable states three broad sources of variability were controlled and one pharmacological test was used: firstly, G-proteins, which are known to modulate these channels, and which are present and can be constitutively active in all cells. Secondly, temperature is, as described previously, an important precipitant of seizures in patients with mutations in *SCN1A*. However many recordings of these channels are carried out at room temperature, therefore the effects of temperature were investigated. Finally, for convenience and stability many heterologous recordings use fluoride based intracellular solutions. This work early on identified fluoride as an unpredictable modifier of sodium channel gating, and therefore recordings were carried out to compare the effects of this anion on channel behaviour. Pharmacologically, sodium channels are sensitive to many AEDs, and the genotype of the SNP in *SCN1A* associated with splicing changes AED dosage. For these reasons, the impact of a representative AED was tested against splice variants of *SCN1A*.

1.4.2 G-protein regulation of Na$_V$1.1 derived INa$_P$

One aim of this project is centred on untangling the interactions between Na$_V$1.1 splice variants and Gβγ subunits. Many ion channels are regulated by neurotransmitters and

121

hormones via G-protein coupled receptors (GPCRs). Upon ligand binding, GPCRs undergo a conformational change and activate heteromeric G-proteins. These are composed of three subunits: α, β and γ. This structural change promotes the exchange of GDP for GTP at the Gα subunit, followed by the disassociation of Gα-GTP and G$\beta\gamma$ (Figure 1.14). The functions of G-proteins are principally dictated by their α subunits (Figure 1.14). These are encoded by 16 genes and are split into four groups Gαs, Gαi/o, Gαq/11 and Gα12 (Gomperts *et al.,* 2002). Stimulated Gαs and Gαi subunits activate and inhibit respectively, adenylate cyclase. Gαq/11 stimulates Phospholipase C-beta (PLCβ) another enzyme involved in cellular signalling pathways, and Gα12 regulates the activity of tyrosine kinases and GTPases. Activated Gα subunits can modulate ion channels via direct physical interactions or indirectly through protein kinases and second messengers (Dascal 2001).

Alternatively, the liberated G$\beta\gamma$ subunits can directly modulate target proteins. Indeed, G$\beta\gamma$ subunits modulate Na$_V$1.1-derived persistent currents (Ma *et al.,* 1997; Mantegazza *et al.,* 2005). G$\beta\gamma$ modulation has been widely investigated for two ion channel families: G-protein activated inwardly rectifying K+ channels (GIRKs) that are activated by G$\beta\gamma$, and voltage-dependent Ca^{2+} channels, which are inhibited by G$\beta\gamma$ (Dascal 2001). There are 5 subtypes of Gβ subunits and at least 12 subtypes of Gγ proteins, which are tethered to the membrane by post-translational fatty acid modification of Gγ. The number of potential G$\beta\gamma$ complexes is potentially vast. However, some combinations do not occur, for instance, Gβ2γ1, and some are tissue specific like Gβ1γ1, which is only found in the retina (Gomperts *et al.,* 2002). Nonetheless, six different combinations of G$\beta\gamma$ subunits have been shown to differentiately regulate the open probability of a heart potassium channel

122

(Wickman *et al.,* 1994). It is possible that particular Gβγ subunits may distinguish between different VGSCs and even their splice variants.
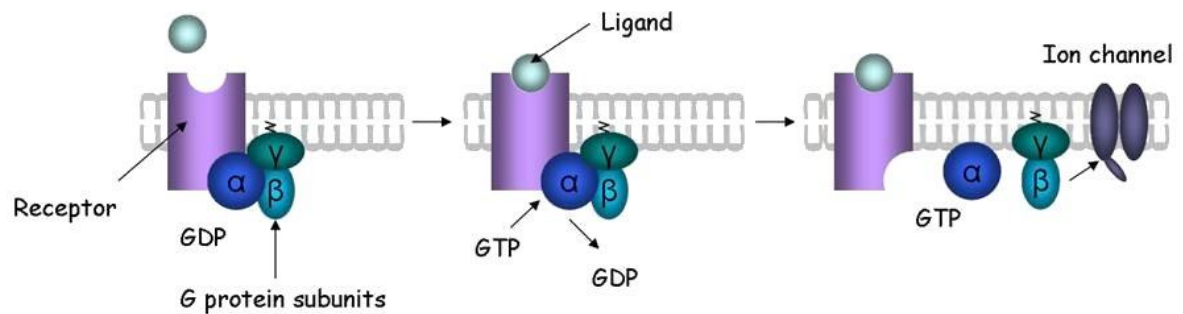
Figure 1.14: The disassembly of an activated G-protein into signalling components. (left) In the unstimulated state, the receptor and the G protein are both inactive. In some cases they are associated in a preformed complex. (middle) Binding of an extracellular ligand to the receptor changes the conformation of the receptor, which in turn alters the conformation of the G-protein that is bound to the receptor. The alteration of the α subunit of the G-protein allows it to exchange its GDP for GTP. (right)This causes the G-protein to break up into two active components - an α subunit and a βγ complex, the latter regulates the activity of voltage-gated ion channels. Redrawn and explanation from Alberts *et al.* (2002).

Few studies have investigated the regulation by Gβγ of VGSC α subunits. Ma *et al.* (1997) were the first to show that in tsa201 cells overexpression of several combinations of Gβγ including Gβ2γ3, with rNa$_V$1.2-6A, produced INa$_P$ that was not attenuated by the presence of β1. This increase in persistent current was not mediated by Gα subunits because co-expression of rNa$_V$1.2-6A with pertussis toxin sensitive Gα subunits, known to modulate rNa$_V$1.2-6A transient currents (Ma *et al.,* 1994) did not up-regulate INa$_P$. GTPγS is a non-hydrolysable analogue of GTP that binds to all G-protein α subunits, locks them in the 'active' form and in turn releases βγ subunits (Figure 1.14). In control recordings, up-

123

regulation of rNa$_V$1.2-6A derived INa$_P$ was not observed from tsa201 cells dialyzed with GTPγS (Ma *et al.,* 1997). *In vivo* kinases, namely PKC and PKA, inhibit Na$^+$ persistent currents (Cantrell & Catterall, 2001) but in the Ma *et al.* study intracellular dialysis of a PKC inhibitor had no effect on rNa$_V$1.2-6A derived INa$_P$ (Ma *et al.,* 1997).

The authors demonstrated that in the presence of Gβ2γ3 the voltage dependence of activation for both rNa$_V$1.2-6A persistent and transient currents were comparable. However, the voltage dependence of inactivation of the slow/incomplete current was shifted positively compared to transient current inactivation. Interestingly, only an excess of Gβγ subunits up-regulated persistent currents since co-expression of Gα$_i$ with Gβ2γ3 in the presence or absence of GTPγS masked the effect of the Gβγ proteins (Ma *et al.,* 1997). The sequence motif, QxxER is found within many proteins that interact with Gβγ subunits, including G protein-dependant receptor kinases (GRKs). This consensus sequence is also found within the c-terminal tail of rNa$_V$1.2-6A. Ma and colleagues designed a Gβγ binding 25 amino acid peptide based on this region within rNa$_V$1.2-6A that incorporated QxxER. Micromolar concentrations of the peptide introduced via the recording pipette solution significantly decreased rNa$_V$1.2-6A Gβ2γ3 modulated persistent currents and the authors hypothesized that it was through interactions with c-terminal tail binding motif. Marin *et al.* (2001) showed that Gβ co-immunoprecipitates with VGSC α subunits expressed by mice cortical neurons providing evidence that there is a direct interaction between VGSC α subunits and G-proteins.

A major advantage of the Ma *et al.* study was that the main intracellular anion was aspartate, not fluoride which disrupts the function of G-proteins (see discussion of anions below). A more thorough investigation, that also used an aspartate-based intracellular, was carried out by Mantegazza and colleagues (2005). In their experiments overexpression of Gβ2γ3 in the tsa201 cells substantially increased both rNa$_V$1.2-6A and hNa$_V$1.1-5A derived persistent currents. This indicates that Gβγ modulation is not species specific or unique to Na$_V$1.2 channels. Additionally Gβ2 alone was sufficient to increase rNa$_V$1.2-6A persistent currents (Mantegazza *et al.,* 2005). In the absence of exogenous Gβγ subunits, two clonal cell lines stably expressing hNa$_V$1.1-5A demonstrated varying levels of persistent current, suggesting that even subtle changes in cellular background can dramatically alter INa$_P$. Mutagenesis and channel chimera studies illustrated that the QxxER sequence alone was insufficient to regulate persistent currents, in contrast to the earlier report. However, more distal residues within the last 28 amino acids of the rNa$_V$1.2 c-terminal tail were essential for Gβγ modulation of persistent currents. Sequence alignments show that Na$_V$1.1, Na$_V$1.3 and Na$_V$1.7 share a high sequence identity with the last 28 amino acids of rat and human Na$_V$1.2 (Figure 1.15). Unlike other PNS, cardiac and skeletal sodium channels (Figure 1.15). Indeed, the c-terminal of Na$_V$1.3 has been shown to interact with Gβ1γ2 subunits (Lenkowski *et al.,* 2004). Therefore it is possible that Na$_V$1.1 channels are modulated in a similar manner. Moreover, Mantegazza and colleagues (2005) surmised that the QxxER motif could tether Gβγ to the pore region, thereby concentrating subunits in the correct channel region and increasing the likelihood of channel regulation in low Gβγ conditions.

```
                         ↓
rNav1.2  PPSYDSVTKPEKEK---FEKDKSEKEDKGKD---IRESKK-------
hNav1.2  PPSYDSVTKPEKEK---FEKDKSEKEDKGKD---IRESKK------- 100
hNav1.3  PPSYDSVTKPDKEK---FEKDKPEKESKGKE---VRENQK------- 79
hNav1.7  PPSYDSVTKPDKEK---YEQDRTEKEDKGKD---SKESKK------- 79
hNav1.1  PPSYDRVTKPIVEK---HEQEGKDEKAKGK--------------- 55
hNav1.6  LPSYDSVTKPEKEKQQRAEEGRRERAKRQKE---VRESKC------- 44
hNav1.5  PPSYDSVTRATSDNLQVRGSDYSHSEDLAD----FPPSPDRDRESIV 26
hNav1.8  PPSYESVTRGLSDRVNMRTSSSIQNEDEATSMELIAPGP-------- 23
hNav1.4  GPTMGLMPISPSDT--AWPPAPPPGQTVRPG---VKESLV------- 14
hNav1.9  -P-LQTLCNGDLSS---FGVAKGKVHCD------------------ 8
             *     :       .
```

Figure 1.15 The c-terminal tails of human VGSCs aligned to the last 28 amino acids of rNa$_V$1.2 (indicated by arrow). These residues were essential for Gβγ modulation of persistent currents in the Mantagazza *et al.* 2005 study. Human brain VGSCs show a higher sequence identity than cardiac, skeletal and PNS VGSCs. Figures indicate the percentage amino acid similarity compared to rNa$_V$1.2. All sequences are derived from the full transcripts published by the Ensembl database

Experimental standards used to determine whether an ion channel is modulated by G-protein subunits have been established from studies involving potassium and calcium channels. These criteria are taken from Dascal 2001:

1. **"Co-expression or direct application of the G-protein subunit mimics the effect of the transmitter; sequestration or knockdown of the G-protein subunit removes the effect of the transmitter".**

2. "The protein mimics the effect of the neurotransmitter in a membrane delimited fashion".

3. "The G-protein subunit physically interacts with the channel".

4. "Prevention of G-protein binding to its established binding site (by competition and/or by mutation of the binding site) abolishes the regulation".

In determining whether $Na_V1.1$ is modulated by $G\beta\gamma$ part of the first and third criteria had been fulfilled by studies previously mentioned. In this study a second approach was employed to complete the first category, whereby scavenger proteins were used to selectively reduce endogenous $G\beta\gamma$ subunits. The c-terminal tails of GRKs have been extensively used as $G\beta\gamma$ sequesterants (Faivre *et al.,*2000; Lei *et al.,*2000; Lohberger *et al.,*2000; Kammermeier *et al.,*2000; Fernández-Fernández *et al.,*2001; Melliti *et al.,*2001; Guo & Schofield 2002; Meza *et al.,*2007; Thapliyal *et al.,*2008; Figure 1.16 B). GRKs are involved in GPCR endocytosis by β-arrestins and GRK translocation to the membrane during this process is aided by $G\beta\gamma$ subunits. There are seven members of the GRK family, GRK 1-7, of which GRK2-3 and GRK5-6 are widely expressed including the brain (Penela *et al.,* 2003). However, only GRK2 and GRK3 have $G\beta\gamma$ binding domains at their c-terminal ends that are 39% identical (Pitcher 1998). This sequence variability results in the two proteins binding to specific and overlapping Gβ subunits. For example, only GRK3ct binds to $G\beta_3$, but both GRK3ct and GRK2ct were co-purified with $G\beta_1$ and $G\beta_2$ (Daaka *et al.,* 1997). It is thought that the Gγ subunits confer different Gβ-GRK binding affinities (Pitcher 1998).

In this report GRK2ct and GRK3ct were co-expressed with $Na_V1.1$ splice variants to selectively sequester $G\beta\gamma$ subunits and GRK5ct was used as a control peptide. A fatty acid signal (myristic acid) was attached to the peptides to promote membrane delimited protein interactions (Toby *et al.,* 1997). Administration of a neurotransmitter to initiate dissociation of Gαβγ is not essential because GPCRs are constitutively active in continuous cell lines (see Figure 1.16 A, Hart *et al.,* 1998; Gomperts *et al.,* 2002) including HEK 293 cells used

127

in this study (data not shown). In response to a hyperpolarizing ramp protocol, for example, endogenous HEK 293 cell Gβγ subunits amplified GIRK currents that were attenuated by GRK2ct (Lei *et al.,* 2001).   Since the specific GPCR(s) that Gβ2γ3, and $Na_V1.1$, directly/indirectly interact with are speculative no ligand was applied to the cells.

Another Gβγ sequesterant tool is Gα transducin (Gαt; Figure 1.16 B). This Gα subunit transduces light signals via the GPCR rhodopsin exclusively in retinal cells (OMIM 139330). Gαt non-selectively sequesters Gβγ subunits because it possesses a high affinity for rhodopsin; therefore, if Gαt is exogenously over-expressed in HEK cells it is likely that Gαtβγ is formed. This 'mops up' endogenous Gβγ as the Gαtβγ complex would only disassociate on rhodopsin stimulation (Federman *et al.,* 1992; Barren *et al.,* 2006). Similar to GRKct peptides Gαt has been used extensively in potassium and calcium channel research (Let *et al.,*2001; Cantí & Dolphin 2003; Filippov *et al.,*2004; Meza *et al.,*2007; Rangel *et al.,*2010). In a recent study, GTPγS up-regulated $Na_V1.9$ derived persistent currents in small diameter sensory neurons (Ostman *et al.,* 2008). Although in the Ma *et al.* (1997) study no increase of $rNa_V1.2$ currents were observed by GTPγS stimulation and the Mantegazza *et al.* (2005) paper demonstrates that this maybe due to cell background. Therefore, this analogue of GTP was also used to assess G-protein subunit regulation of $Na_V1.1$ splice variant persistent and transient currents.
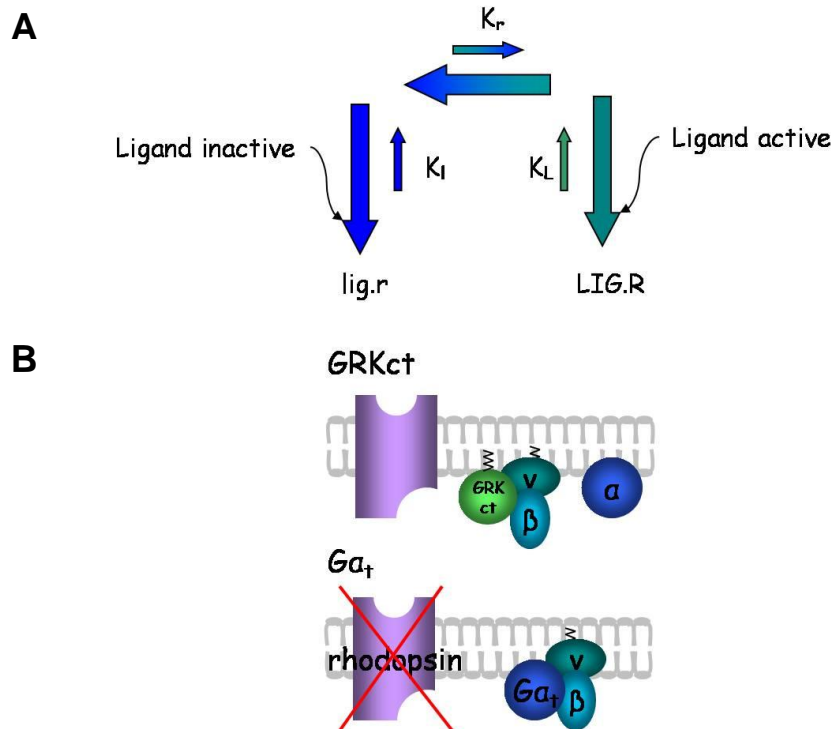
Figure 1.16 Gβγ sequesterant peptides. *A.* Endogenous GPCR receptors can exist in two conformation states inactive (left large arrow, r) and active (right large arrow, R). In an active conformation GPCRs can initiate downstream events. The equilibrium between these two states exists regardless of the presence or absence of a ligand. Therefore, Gβγ sequesterant peptides are still effective in the absence of an agonist. However, for completeness, agonists bind to the active conformation (LIG.R) and will increase the rate constant (K.L) so that the percentage of active receptors is greater. Inverse agonists bind to the inactive receptor conformation (lig.r) shifting the equilibrium, rendering a greater number of receptors inactive (Redrawn from Gomperts *et al.,*2002). *B.* The c-terminal tails of GRK2 and GRK3 act as selective sequesterants (top) and Gαt as a non-selective sequesterant of Gβγ subunits (bottom).

1.4.3 The effect of temperature

It is likely that the influence of both genetic and environmental factors generates FS in the developing brain of infants. FS can be triggered by fevers in response to infection, inflammation or stress (Vezzani & Granata 2005). Indeed, an inflammatory response, involving the secretion of cytokines is triggered in the brain area of seizure onset and

129

propagation in FS rodent models (Vezzani & Granata 2005). One inflammatory mediator is Interleukin-1β (IL-1β), a pyrogenic cytokine that may directly evoke FS in the developing rodent brain (Dube *et al.,* 2005; Vezzani & Granata 2005). IL-1β receptor null mice demonstrated significantly increased hyperthermic promoted seizure thresholds. Large doses of IL-1β elicited seizures without additional stimuli in healthy young mice but not their mutant IL-1β receptor counterparts (Dube *et al.,* 2005). Moreover, increased levels of IL-1β have been found within CSF samples taken from children suffering with FS (Tütüncüoğlu *et al.,* 2001; Haspolat *et al.,* 2003). The pathological mechanism of IL-1β is undetermined but may deleteriously affect NMDA receptor function (Dube *et al.,* 2005; Dube *et al.,* 2009). In animal models hyperthermia induced hyperventilation and alkalosis induced FS (Schuchmann *et al.,* 2006; Dube *et al.,* 2007). An elevation in rat brain pH can be epileptogenic (Aram & Lodge 1987) but the role of alkalosis in human FS is controversial and its etiological contribution unknown (Dube *et al.,* 2009). TRP (transient receptor potential) channels are non-selective cation pores that open in response to various stimuli. TRPV1 and TRPV4 are heat activated and may be involved in the epileptogenesis of FS. TRPV4 channels have been shown to regulate the resting membrane potential in the hippocampus (Shibasaki *et al.,* 2007). However, at fever temperatures these channels are up-regulated and may disrupt neuronal homeostasis. Furthermore, TRPV1 knockout mice were less susceptible to hyperthermic induced seizure thresholds compared to wild-type littermates (Kim *et al.,* 2008). These studies imply that increased brain temperature may be sufficient to provoke FS.

A rare syndrome, hot-water epilepsy, has been documented in individuals who suffer either complex partial seizures or GTCS on exposure to hot water between $40 - 50^{\circ}$C but underlying genetic causality is undetermined (Satishchandra 2003). Similar findings have been observed in SMEI patients (Fukada *et al.,* 2009). Seizures are also induced in healthy rodent pups exposed to hyperthermic stimuli (Holtzman *et al.,*1981; Morimoto *et al.,*1991; Toth *et al.,*1998; Dube *et al.,*2000) but in one report different mouse strains demonstrated distinctive temperature induced seizure thresholds (Dube *et al.,*2005). This suggests that genetic factors are not necessary to cause FS but can greatly influence their severity. The Oakley *et al.* (2009) study discussed previously, which involved the SMEI mouse model showed that network vulnerabilities in the developing brain caused by reduced $Na_V1.1$ expression were only exposed at higher temperatures. At a molecular level, studies suggest that increased temperatures may perturb the trafficking of GEFS+ mutant channels. For example, immunofluorescence investigations showed that HEK cells transfected with $GABA_A$ receptors containing one of the three mutant γ2 subunits previously described, at 'fever' temperatures demonstrated γ2 and α subunit trafficking and membrane expression deficits. Under the same conditions patch-clamp recordings of mutant channels showed significantly attenuated chloride currents compared to wild-type channels (Kang *et al.,* 2006). However, trafficking defective GEFS+ $Na_V1.1$ mutant channels are rescued when incubated at cooler temperatures (27°C; Rusconi *et al.,* 2007; Rusconi *et al.,* 2009).

The biophysical properties of wild-type and mutant $Na_V1.1$ channels are likely to be affected by temperature. In the advent of voltage clamp experiments clamping sodium currents was problematic because VGSCs would open before the charging of the membrane

131

capacitance was complete (Murray *et al.,* 1990 and references therein). This has circumvented by technical advances in equipment but maintaining a stable seal at higher temperatures is still challenging, especially in heterologous systems. This study does not directly address the effects of 'fever' temperatures on $Na_V1.1$ splice variants but the experiments were performed at physiological temperatures. This was essential because recordings at low temperatures may give inaccurate data or mask subtle variations in VGSC behaviour (Andersen & Moser 2005).

1.4.4 Intracellular anions

Most work on heterologously expressed $Na_V1.1$ employs intracellular solutions based on CsF to improve cell stability. Early experiments involving the squid giant axon, preparations perfused with fluoride ions demonstrated more stable resting membrane potentials, minimal action potential run-down, reduced leakage conductance and survived hours longer compared to axons perfused with chloride ions (Tasaki *et al.,* 1965; Adelman *et al.,* 1966; Chandler & Meves, 1970). The reason for this phenomenon is still eludes electrophysiologists (Lenz *et al.,* 1997; Coste *et al.,* 2004) but suggests that fluoride and chloride differentially affect the biophysical properties of sodium (and potassium) channels. Indeed, the gating and kinetics of $Na_V1.9$ in several studies was dependent on the intracellular halide ion (Rugiero *et al.,* 2003; Coste *et al.,* 2004; Maingret *et al.,* 2008).

Despite its advantages fluoride exerts deleterious affects on the function of intracellular proteins. For instance, if fluoride is combined with aluminium leached from borosilicate electrode glass, it can disrupt G-proteins, which as previously discussed, are central to the

regulating $Na_V1.1$ derived INa$_P$. Aluminium fluoride ions (fluoroaluminate, AlF^-_4) associate with GDP forming a complex similar to GTP in its transition state during the GTPase reaction (Bigay *et al.,* 1987). At lower, unspecified concentrations this activates G-proteins and in turn, affects the biophysical properties of G-protein modulated ion channels (Adams & Oxford, 1983; McCloskey & Cahalan, 1990; Ito *et al.,* 1994; Terzic *et al.,* 1994; Inoue & Imanaga 1995; Walsh *et al.,* 1996; Kamouchi *et al.,* 1997; Denson *et al.,* 2005). However, at higher concentrations of AlF^-_4 the affects of G-protein activity are suppressed (Harwood *et al.,* 1973a; Harwood *et al.,* 1973b). During experiments using CsF an unknown quantity of fluoroaluminate is formed and its consequences therefore are unpredictable, and may introduce variability between recordings.

Fluoride ions also inhibit phosphatases (Pinske *et al.,* 1999). These are enzymes that regulate protein activity by removing phosphate groups from serine, threonine, or tyrosine residues (Lodish *et al.,* 2000). Phosphatases modulate the activity of many voltage and ligand gated ion channels expressed in various cell types (Herzig & Neumann 2000). These include L-type calcium channels, GIRKs, NMDA receptors, $GABA_A$ receptors and other chloride channels to name a few (Herzig & Neumann 2000). Specific subtypes of phosphatases were shown to dephosphorylate rat neuronal VGSCs serine residues targeted by PKA (Chen *et al.,* 1995). It is likely, therefore, that high concentrations of fluoride ions introduce further inconsistencies by interfering with VGSCs kinase modulation. Because INa$_P$ is potentially contributing to drug effects, the properties of $Na_V1.1$ splice variants using CsF and CsCl-based intracellular solutions were compared to determine whether the identity of the anion altered the kinetics of macroscopic currents from these channels.

133

1.4.5 Cell models for characterization of VGSCs

It is clear from *in vitro* experiments that cellular background plays a vital role in α subunit regulation. It is possible that different splice variants are expressed in different types of neurons or astrocytes (Bordey & Spencer, 2004), or in the same neuron but in specific microdomains and could cause opposing effects. Non-neuronal cells do not replicate neuronal diversity, genetic background or subcellular specialization (Avanzini *et al.,* 2007). Studies, using primary cell cultures allow these properties to be retained. There are different disadvantages to neuronal cultures, for instance, neurons express a plethora of other channels and the channel of interest cannot always be pharmacologically isolated (Avanzini *et al.,*2007). Moreover, neuronal input and outputs are lost on cell dissociation; this process may change neuronal phenotype. Another aim of this study is to determine the phenotype of cultured cells using the SC-RT-PCR method. This enables the examination of gene expression from a single cell. This paper describes preliminary SC-RT-PCR investigations that determine the phenotype of two-week cultured rat hippocampal cells. Although $Na_V1.1$-5N is not produced in rodents, rat neurons were used to optimize this technically challenging method for use in other cell models.

1.4.6 Human neuronal cell models

Because of this loss of exon 5N in rodents, an additional aim is to find and optimize neurons or neuronal cells that do have alternative splicing at this site. This is difficult because primary cultures of human neurons cannot be used. A human cell line, 197VM, was investigated. These neural stem cells derived from the 10 week mesencephalon have

134

been engineered into a multipotent stable line that can be differentiated into neuronal-like cells within three weeks (Donato *et al.,* 2007). Using SC RT-PCR and the whole-cell patch technique, their gene expression and 'neuronal' functions were characterized to determine whether these cells were appropriate model candidates for use in $Na_V1.1$ splice variant physiology.

1.4.7 Animal neuronal cell models

A non-rodent mammal would have to be easily obtainable, economical and with a short life span. Both *Cavia porcellus* (guinea pig) and *Gallus gallus* (chicken), two potential animal neuronal models investigated, fulfill these criteria. Between the 1970-80s the Fayoumi epileptic strain (F.Epi) of chickens, a commonly used model for photosensitivity epilepsy, were extensively analyzed (Johnson & Tuchek 1987). The disease causing gene is still unknown but is inherited in an autosomal dominant manner (Sarkisian 2001). Although not a GEFS+ model *per se* both 2-5 day old F.Epi homozygous and heterozygous chicks displayed febrile GTCS induced by hyperthermia (Johnson *et al.,* 1983). This effect was not observed in adult mutant fowl (Johnson *et al.,* 1983). Additionally, their febrile seizures were resistant to particular AEDs including phenytoin but responded to phenobarbital (Johnson *et al.,* 1983). Therefore, if exon 5 splicing is retained in this animal it would prove to be neuronal model for studies into *SCN1A* mutations.

1.5 Experimental aims

- To determine whether exon 5 *SCN1A* alternative splicing changes the behaviour of $Na_V1.1$ channels.

135

- To evaluate the effect of intracellular anions and temperature on $Na_V1.1$ channel behaviour.

- To examine the effect of alternative splicing on the behaviour of $Na_V1.1$ channels containing the GEFS+ causing mutation R1648H.

- To assess the reponse of $Na_V1.1$ wild-type and mutant channel isoforms to phenytoin. In an attempt to reveal a mechanistic mechanism for the association of rs3812718 polymorphism and AED dosage in patients with or without a GEFS+ mutation.

- To characterize neuronal cell models to assess their suitability for investigating the behaviour of $Na_V1.1$ channels in a neuronal background.

- To examine the effect of G-protein regulation, in particular $G\beta\gamma$ modulation, of $Na_V1.1$ splice variants.

- To test whether distinct β subunit pairs differentially regulate the gating of $Na_V1.1$ isoforms.

Chapter 2: General materials and methods

2.1 Molecular biology methods

2.1.1   Bacterial media and reagents

2.1.1a LB Broth

20g LB Broth (Luria Bertani medium, Sigma) was dissolved in 1 litre of ddH_2O. Autoclaved and stored at RT.

2.1.1b LB agar

17.5g LB agar (Sigma) was dissolved in 500 ml of ddH_2O. Autoclaved and stored at RT.

2.1.1c Antibiotics, LB plates and broth

Antibiotic stocks were stored at -20^oC in 1 ml aliquots. Stock preparations and concentrations are shown in table 2.1. To prepare LB plates, agar was melted and cooled before the correct concentration of antibiotic(s) was added (table 2.1). Agar was poured into 10 cm plates (VWR international), allowed to set and stored at 4^oC. For culture of transformed *E.coli*, concentrations of antibiotics added to LB broth are also shown in table 2.1.

Table 2.1 Antibiotic stock concentrations and dilutions for preparation of selective agar plates and bacterial culture media

Antibiotic	Stock concentration	LB agar selection plate concentration	LB broth culture concentration
Ampicillin (Sigma)	100 mg/ml (ddH$_2$O)	100 μg/ml	100 μg/ml
Chloramphenicol (Sigma)	30 mg/ml (ddH$_2$O)	30 μg/ml	30 μg/ml
Kanamycin (Gibco)	50 mg/ml (ddH$_2$O)	50 μg/ml	50 μg/ml
Tetracycline (Sigma)	25mg/ml (100% ethanol)	5 μg/ml	5 μg/ml
Ampicillin & Tetracycline	(as above)	100 μg/ml & 5 μg/ml	100 μg/ml & 5 μg/ml

2.1.2 Bacterial culture

2.1.2a Preparation of competent bacteria

To prevent contamination equipment and surfaces were cleaned with 70% ethanol; glass- and plasticware were autoclaved and work was carried out in a fume cupboard (Fumair, Hertford, UK). 7 μl of either TOP10[®] or TOP10/P3[®] (Invitrogen) *E.coli* stock was grown overnight at 37°C on an agar plate. 2 ml of LB was inoculated with a single colony and incubated overnight with shaking at 37°C. The overnight culture was added to 500 ml of LB and incubated with shaking until OD$_{596nm}$ was $0.25 - 0.7$. Cells were placed on ice for 10 mins, centrifuged at 6000 rpm at 4°C for 10 mins (J2-21 High-Capacity Centrifuge, Beckman). Sterile filtered TB buffer prepared in 1 litre of ddH$_2$O (10 mM PIPES, 55 mM MnCl$_2$, 15 mM CaCl$_2$, 250 mM KCl, pH 6.7) was pre-chilled to 0°C. The pellet was resuspended in 160 ml in TB and incubated on ice for 10 mins. *E.coli* were harvested as

138

previously, and resuspended in 40 ml of TB. The suspension was gently swirled as 2.8 ml

DMSO was added dropwise to the bacteria. Cells were kept on ice for 10 mins, then

aliquoted into 1.5 ml tubes (Eppendorf). Aliquots were snap-frozen in liquid nitrogen and

stored at -80°C.

2.1.2b Transformation of *E.coli* by heat shock

50 µl of TOP10$^{®}$ *E.coli* was thawed on ice. 2 µl of 50 ng of supercoiled DNA or 5 µl

ligation reaction was added to the cells and incubated on ice for 30 mins. Bacteria were

heat shocked for 30 seconds at 42°C and returned to ice for 3 mins. Cells were diluted in

150 µl of S.O.C medium (20g/l (2% w/v) bacto-tryptone, 5g/l (0.5% w/v) bacto-yeast

extract, 5g/l NaCl, 10 mM MgCl$_2$, 10 mM MgSO$_4$, 2 mM glucose; Sigma), at 24°C before

being shaken (225 rpm, IKA Incubating Shaker) for an hour at 37°C. The transformation

volume was spread on an agar plate containing the appropriate antibiotic selection and

incubated at 37°C overnight.

2.1.2c Transformation of *E.coli* with Na$_V$1.1 constructs

2 µl *SCN1A* constructs and its variants were transformed into TOP10/P3$^{®}$ *E.coli* by heat-

shock as previously described. These bacteria contain a low copy-number plasmid, P3,

which includes tetracycline- and ampicillin-resistant genes. These are inactive during

normal *E.coli* life-cycle, since they carry amber mutations rendering them inactive. pcDM8

encodes the suppressorF gene that nullify these mutations, inducing bacterial resistance

(Invitrogen 2008; Figure 2.1).
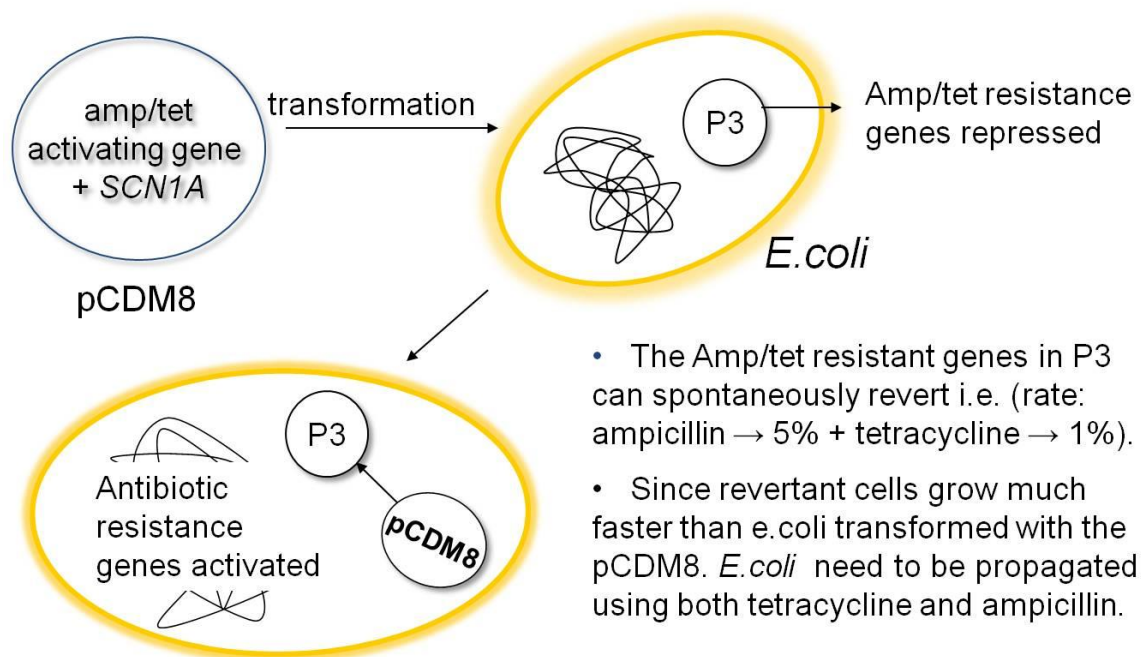
Figure 2.1 TOP10/P3 *E.coli* **transformations with** *SCN1A***-pcDM8** The antibiotic resistant genes in the P3 plasmid, within the *E.coli*, have an amber mutation (stop codon). *SCN1A*-pcDM8 contains repressor genes for the amber mutation. Therefore after transformation of this plasmid the resistant genes are switched on (i.e. the amber mutation is repressed). However, the amber mutation can revert i.e. mutate and the repressor genes can become in ineffective. This leads to excessive growth of non-transformed *E.coli* and poor DNA yields. This is prevented by growing bacteria in both antibiotics.

SCN1A has a high spontaneous mutation rate when propagated in bacteria (Mantegazza *et al.,* 2005). To minimise this phenomenon, during incubation cells were heated to 28$^{\text{o}}$C. In conjunction with using a low-copy plasmid, this reduced propagation and therefore, metabolic burden on the *E.coli*. To reduce reversion rates cell were grown on plates containing both ampicillin and tetracycline (Table 2.1; Figure 2.1).

2.1.2d Overnight cultures

To prepare cultures to purify approximately 100 ng/µl DNA or >500 ng DNA, 5 ml and 200 ml respectively, of LB broth containing the appropriate antibiotic(s) (Table 2.1) was inoculated with a single colony of transformed bacteria. Cultures were incubated with shaking until OD_{600nm} of 0.35 at 37^oC (TOP10$^®$ *E.coli*) or 28^oC (TOP10/P3$^®$ *E.coli*). Obtaining an OD_{600nm} of 0.35 was vital when culturing TOP10/P3$^®$ *E.coli* transformed with $Na_V1.1$ clones. Close monitoring of cell growth prevented bacteriophage infections, reduced mutation rates and DNA nicking.

2.1.2e Glycerol stocks

80% (v/v) glycerol was prepared and autoclaved. Equal volumes of the desired culture and glycerol were vortexed and aliquoted. Stocks were snap-freezed in liquid nitrogen and stored at -80^oC.

2.1.2f QIAfilter Maxi Plasmid Purification Kit

200 ml overnight bacterial cultures were centrifuged at 6 000 rpm, for 15 mins at 4^oC. Supernatants were removed and cell pellets resuspended in 10 ml of chilled P1 buffer (50 mM Tris/HCl pH 8.0, 10 mM EDTA, 100 µg/ml RNase A). Samples were vortexed for 30 secs to disperse bacterial clumps that can prevent effective lysis. Cells were lysed in 10 ml P2 buffer (200 mM NaOH, 1 % (w/v) SDS), inverted 10 times and incubated at RT for 5 mins. During incubation Qiagen tips were equilibrated with 10 mls of equilibration buffer (750 mM NaCl, 50 mM MOPS, pH7.0, 15% (v/v) ethanol 0.15% (w/v) Triton-X). These contain a membrane covered in resin that binds to plasmid DNA. Samples were treated

with 10 mls of chilled neutralization P3 buffer (3.0 potassium acetate pH 5.0) before being poured into the barrel of a Qiagen cartridge. These cartridges contain a filter membrane that separates plasmid DNA from bacterial proteins and DNA. Samples were incubated at RT for 10 mins before their lysates were filtered through into a Qiagen tip and allowed to flow through the resin by gravity. Tips were washed with 60 ml of QC wash buffer (1.0M NaCl, 50mM MOPS pH 7.0, 15% (v/v) ethanol) to remove smaller proteins and bacterial RNA. DNA was eluted in 15 ml of QF buffer (1.25 mM NaCl, 50 mM Tris/HCl pH8.5, 15% (v/v) ethanol) and desalted by the addition of 10.5 ml isopropanol. Samples were centrifuged at 2 500 rpm (Falcon 6/300R) for 90 mins at 4$^\text{o}$C. Pellets were washed with 5 ml 70% ethanol and centrifuged at 2 500 rpm for 30 mins at 4$^\text{o}$C. Finally, supernatants were removed and pellets air dried for 10 mins to allow for complete ethanol evaporation. DNA samples were resuspended in 150 µl ddH$_2$O, and stored at -20$^\text{o}$C.

2.1.2g GenElute™ Plasmid Miniprep Kit for purification of 100 ng/µl DNA

Although from a different company, this kit works on the same principles as the Qiagen purification maxiprep kit. 5 ml overnight bacterial cultures were pelleted at 4 000 rpm, for 10 mins at RT (MSE Micro Centaur Plus). The supernatant was removed before the pellet was processed as described above. 50 µl eluted DNA in ddH$_2$O was stored at -20$^\text{o}$C.

2.1.3 DNA manipulation

2.1.3a DNA quantification

The concentration of DNA samples were calculated using a spectrophotometer (Nanodrop ND-1000, Thermoscientific). Although a ratio of absorbance at 260 nm and 280 nm 1.8 indicates pure DNA this can alter depending on pH and the DNA nucleic acid content; therefore, samples <1.6 were discarded.

2.1.3b Digestion of plasmid DNA with restriction endonucleases

Restriction endonucleases stored in glycerol were obtained from New England Biosciences (NEB). Digests were based on the manufacturer's guideline: at least 10 U of enzyme was used to digest 1 µg DNA. A high concentration of glycerol increases the rate of enzyme star activity (Wei *et al*., 2008). Therefore, the final reaction was >10 times the volume of enzyme to reduce aberrant digestion. The reactions were supplemented with x1 enzyme buffer to stabilize the endonucleases, and 100 µg/ml BSA to prevent enzymes interacting with plastic and/or the air-liquid interface (Williams *et al.,* 1996). Typical digestion reactions are detailed in table 2.2 and were incubated for 1-12 hours at 37°C. Enzymes were subsequently inactivated by heating at 65°C for 20 mins. Digests were analyzed by agarose gel electrophoresis.

Table 2.2 Endonuclease enzyme recipes for digestion of DNA for various applications

Type of digest	Conc of DNA (ng)	Volume of enzyme (µl)	Units of enzyme (U)	Volume of enzyme buffer (µl)	Volume of x10 BSA (µl)	Final reaction volume in ddH₂O (µl)
Diagnostic digest	30	0.5	10	1.5	1.5	15
Large scale plasmid digest	150	5	100	20	20	200
PCR amplicon digest	50	5	100	20	20	200

2.1.3c Agarose gel electrophoresis

DNA samples were separated by gel electrophoresis using 1–3% (w/v) agarose gels. Smaller fragments (100-500 bp) were resolved in 3% gels and larger DNAs (<500bp) in 1.0% gels. Agarose (Sigma) was dissolved in x1 TBE (100 mM Tris, 83 mM Boric acid, 1mM EDTA) and boiled. 1 µg/ml of ethidium bromide (Molecular Probes, Invitrogen) was added and the mixture was poured into an electrophoresis tray and allowed to set. On exposure to UV light, ethidium bromide bound to DNA fluoresces more intensely and permits nucleic acids detection. Prior to loading, one fifth total volume of 6x Orange G dye (10 mM Tris-HCl (pH 7.6), 0.15% orange G, 0.03% xylene cyanol FF, 60% glycerol, 60 mM EDTA; Fermentas Life sciences) was added to each sample to monitor DNA migration. Reference molecular weight markers: 1kb and 100 bp DNA ladders (NEB) were run either side of the samples. Gels were electrophoresed at 100 V for an hour and

visualized using a UV-light transilluminator. Records were photographed digitally using the Gene Genius BioImaging System (Syngene).

2.1.3d DNA fragment purification from agarose gels

DNAs were run on TBE buffered agarose gels and viewed using a long wavelength (365) UV lamp to reduce mutations. Bands were cut from the gel using a sterile scalpel. DNA was extracted and purified using the QIAGEN DNA gel extraction kit following the manufacturer's instructions.

2.1.4 Cloning

2.1.4a Mutagenesis reactions

Mutations were introduced into plasmid DNA using the QuikChange™ mutagenesis (Stratagene, CA) protocol. Mutagenesis primers were designed using the Primer X (website: http://www.bioinformatics.org/primerx/). All enzymes were chosen for their high fidelity in the amplification of DNA fragments of up to 12 kb. All PCRs were performed using a 2720 thermal cycler (Applied Biosystems) and constructs were sequenced at the Wolfson Institute for Biomedical Research, Scientific Support Services, UCL, to confirm successful mutagenesis and sequence integrity.

The three amino acid changes encoded by exon 5N and D207N were introduced into the human *SCN1A* cDNA in the pcDM8 vector, using the following primers, reactions and cycling parameters:

5N primers from 5' to 3' sequence

Forward:

CATTACATTTGCGTTCGTCACAGAGTTTGTGAACCTGGGCAATTTCTCGGCATT
GAG

Reverse:

CGAGAAATTGCCCAGGTTCACAAACTCTGTGACGAACGCAAATGTAATGACAG
TG

D207N primers from 5' to 3' sequence

Forward: CAGAGTTTGTGAACCTGGGCAATGTCTC

Reverse: ACATTGCCCAGGTTCACAAACTCTGTGAC

- *Polymerase chain reaction*: 100 μl volume of 50 ng of DNA, 75 pmol each primer, 200 μM mixed dNTPs, 10μl native *Pfu* 10x buffer (Stratagene) and 2.5 U of native *Pfu* polymerase (Stratagene).

- *Thermal cycling method:* 95°C for 45 s, followed by 18 cycles of 95°C for 45 s, 55°C for 45 s, 72°C for 15 mins and 72°C for 30 mins.

The 5N primers and the above PCR conditions were also used to mutagenize *SCN1A*-R1648H-pcDM8 to *SCN1A*-R1648H-5N.

2.1.4b Mutagenesis of β subunits tricistronic construct

SCN1B - ECMV IRES - *SCN2B* - polio IRES – EGFP was a kind gift from Professor John Wood, UCL. Unfortunately, this construct had a premature start codon before the *SCN2B* sequence. Therefore to introduce a stop codon three nucleotides upstream of the *SCN2B* ATG codon the following mutagenesis reaction was performed:

Primers from 5' to 3' sequence

Forward: GAAAAACACGATGATAATTAGGCCACAACCATGCACAG

Reverse: CTGTGCATGGTTGTGGCCTAATTATCATCGTGTTTTTC

PCR conditions:

- *Polymerase chain reaction*: 100 µl volume of 50 ng of *SCN1B* - ECMV IRES - *SCN2B* - polio IRES – EGFP, 25 pmol each primer, 200 µM mixed deoxynucleotide triphosphatases (dNTPs), 10 µl native *Pfu* 10x buffer (Stratagene) and 2.5 U of native *Pfu* polymerase (Stratagene).

- *Thermal cycling method:* 95°C for 45 s, followed by 18 cycles of 95°C for 45 s, 60°C for 45 s, 68°C for 16 mins and 68°C for 20 mins

This plasmid was then used as a template for *SCNXB* - ECMV IRES - *SCN2B* - polio IRES – EGFP (Figure 2.2).
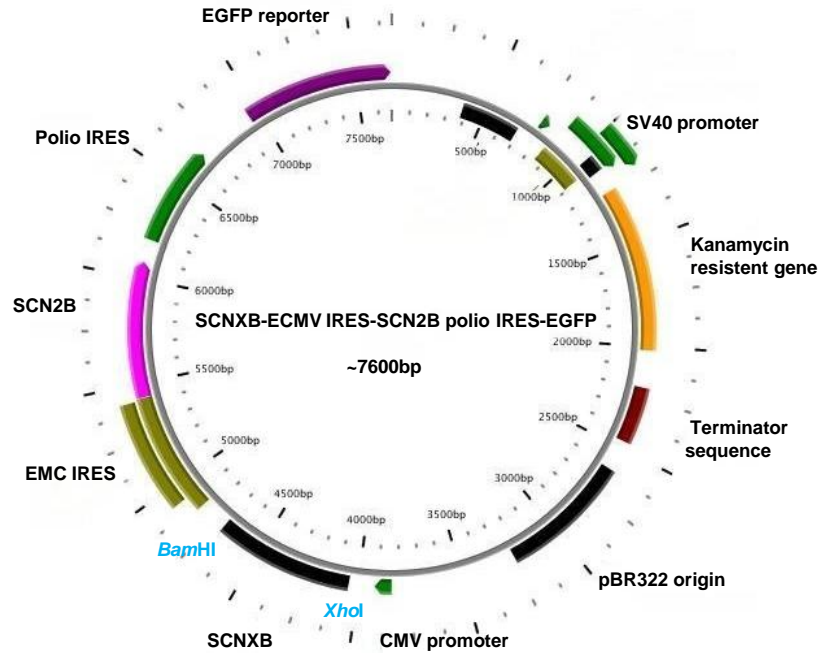
Figure 2.2 Schematic of the tricistronic vector *SCNXB* - ECMV IRES - *SCN2B* - polio IRES – EGFP Vector. *SCN1BB* and *SCN3B* were subcloned after the CMV promoter into the *Xho*I and *Bam*HI cloning site (blue letters). RNA polymerase binds to the CMV promoter to initiate transcription. EMV IRES is internal ribosome entry site originated from encephalomyocarditis virus and allows for translation initiation within the mRNA sequence. The EGFP reporter gene is under the control of a second, weaker IRES site derived from the polio virus. All three genes are therefore translated from a single strand of mRNA. The kanamycin resistant gene allows for selection and is under control of SV40 promotor, cloned from the Simian virus 40. Terminator denotes the polyadenylation signal site which allows the end of transcription. pBR322 origin of replication ensures the vector is replicated in HEK 293 cells. It is derived from the pBR322 vector designed by Bolivar & Rodriguez, 1977.

2.1.4c Amplification of β subunits

Non-mutagenic primers were designed using Primer3 available at http://workbench.sdsc.edu/. Annealing temperatures were $5^{o}C - 10^{o}C$ lower than the primer melting temperatures (T_m) calculated by the software. All primers were bought from Sigma-Aldrich. Extension times and temperatures were ascertained from the polymerase protocols provided by the manufacturer.

SCN3B was amplified from human whole brain obtained from the Human Developmental Biology Resource at the Institute of Child Health (ICH). Reverse transcription is described in section 2.4. The coding sequence of *SCN3B* was amplified using the following Primers (designed against sequence NM_018400+3) and PCR conditions:

Primers from 5' to 3' sequence

Forward: CACCATGCCTGCCTTCAATAGATTGTT

Reverse: TCACACTGCTCCTGTTCTATTCC

PCR conditions:

- *Polymerase chain reaction*: 100 µl volume of 50 ng of DNA, 25 pmol each primer, 200 µM mixed dNTPs, 10 µl native *Pfu* 10x buffer (Stratagene) and 2.5 U of native *Pfu* polymerase (Stratagene).

- *Thermal cycling method:* 95°C for 45 s, followed by 35 cycles of 95°C for 45 s, 55°C for 45 s, 72°C for 1 min and 72°C for 5 mins.

Following protocols the PCR fragment was cleaned using the QIAquick PCR Purification Kit and subcloned into pcDNA3.1/V5-His-TOPO using the pcDNA3.1 directional TOPO® Expression Kit (Invitrogen), following instructions. *SCN1B* splice variant B cloned into the pCMV6-XL5 mammalian expression vector was bought from Origene Technologies, USA. Both vectors were used as templates to amplify β subunit DNAs with 5' *Xho*I and 3' *Bam*HI restrictions sites ready to be subcloned into *SCNXB* - ECMV IRES - *SCN2B* - polio IRES – EGFP. The following primers and PCR condition were used (lower case letter indicate enzyme recognition sequences):

SCN3B Primers from 5' to 3' sequence

Forward: CCGctcgagCACCATGCCTGCCTTCAATAGATTGTT

Reverse: CGCggatccTCACACTGCTCCTGTTCTATTCC

SCN1BB Primers from 5' to 3' sequence

Forward: ACGctcgagCACCATGGGGAGGCTGCTGGCC

Reverse: CGCggatccTCAAACCACACCCCGAGA

PCR conditions:

- *Polymerase chain reaction*: 22.5 μl volume of Accuprime *pfx* supermix (Invitrogen) with 50 ng of DNA, 25 pmol each primer.
- *Thermal cycling method:* 95°C for 5 mins, followed by 30 cycles of 95°C for 15 s, 55°C for 30 s, 68°C for 1.5 min and 68°C for 10 mins.

SCN1B was excised from *SCNXB* - ECMV IRES - *SCN2B* - polio IRES – EGFP using appropriate restriction endonucleases (New England Biolabs, following the digestion protocol in Table 2.2). 100 μl linearized vector was ethanol precipitated in 900 μl 99% ethanol (VWR) and 40 μl 0.3M sodium acetate. The mixture was spun for 10 mins at 12 000 rpm and washed in 500 μl 70% ethanol. After aspiration of the wash, the vector was air-dried for 10 mins before resuspension in 25 μl ddH20. The vector and PCR fragments were gel and column purified respectively. *SCN3B* and *SCN1BB* were inserted into vector using a 10 μl ligation reaction containing 1 μl 50ng vector, 1 μl 50ng insert, 1 μl ligase x10 buffer (Promega) and 1U T4 ligase (Promega).

2.1.4d Attachment of myristic acid attachment signals to the family of GRKs c-terminals:

The c-terminal (amino acids 495-689) of human GRK2, was amplified from whole human brain acquired from Institute of Child Health, UCL using the following primers (designed against sequence NM_001619+3) and PCR procedure:

GRK2ct primers from 5' to 3' sequence

Forward: CACCATGGGAATCAAGTTACTGGACAGTGATCAGG

Reverse: CAGAGGCCGTTGGCACTG

PCR conditions:

- *Polymerase chain reaction*: 100 µl volume of 50 ng of DNA, 25 pmol each primer, 200 µM mixed dNTPs, 10 µl native *Pfu* 10x buffer (Stratagene) and 2.5 U of native *Pfu* polymerase (Stratagene), 8 µl dimethyl sulfoxide.

- *Thermal cycling method:* 95°C for 45 s, followed by 35 cycles of 95°C for 45 s, 57°C for 45 s, 72°C for 2 mins and 72°C for 5 mins.

The DNA fragment was cleaned and subcloned into pcDNA3.1/V5-His-TOPO. The latter was a template for a second PCR reaction, where the c-terminus was amplified using the conditions above, with sense and antisense oligonucleotides containing *Eco*RI and *Not*I restriction sites, respectively:

Forward: GTGgaattcGGAATCAAGTTACTGGACAGTGATCAGG

Reverse: GTGgcggccgcCAGAGGCCGTTGGCACTG

The mammalian expression vector pGTM (Toby *et al.,* 1998) and was linearized with the appropriate restriction endonucleases (New England Biolabs), ethanol precipitated and gel purified. The cleaned c-terminus of GRK2 was inserted in-frame with a myristic acid attachment signal (MAS) within pGTM using the ligation reaction just described.

GRK3 and GRK5 subcloned into bacterial expression vectors were acquired from Geneservice Ltd, Cambridge, UK. These constructs were used as templates to amplify the c-terminals of GRK3 and GRK5 (corresponding amino acids 495-687 and 464-638; Figure 2.3) using sense and antisense oligonucleotides containing *Eco*RI and *Not*I restriction sites respectively:

GRK3ct primers from 5' to 3' sequence

Forward: GTGgaattcGGGATTAAGCTACTTGATTGCGAC

Reverse: GTGgcggccgcCTAGAGGCCGTTGCTGTTTC

GRK5ct primers from 5' to 3' sequence

Forward: GTGgaattcGGGATTAAGCTACTTGATTGCGAC

Reverse: GTGgcggccgcCTAGAGGCCGTTGCTGTTTC

PCR conditions for amplification of both products:

- *Polymerase chain reaction*: 100 µl volume of 50 ng of DNA, 25 pmol each primer, 200 µM mixed dNTPs, 10 µl native *Pfu* 10x buffer (Stratagene) and 2.5 U of native *Pfu* polymerase (Stratagene)

- *Thermal cycling method:* 95°C for 45 s, followed by 25 cycles of 95°C for 45 s, 57°C for 45 s, 72°C for 4 mins and 72°C for 20 mins.

GRK3ct and GRK5ct were subcloned into pGTM as described for GRK2ct.

```
GRK3    VNAADAFDIGSFDEEDTK GIKLLDCDQELYKNFPL-VISERWQQEVTETVYEAVNADTDK

GRK2    VNAADAFDIGSFDEEDTK GIKLLDSDQELYRNFPL-TISERWQQEVAETVFDTINAETDR

GRK5    VYCKDVLDIEQFS--TVK GVNLDHTDDDFYSKFSTGSVSIPWQNEMIETECFKELNVFGP

        *  . *.:** .*.   .* *::* . *:::* :*.   :*  **:*: **          .



GRK3    IEARKRAKNKQLGHEEDYALGKDCIMHGYMLKLGNPFLTQWQRRYFYLFPNRLEWRGEGE

GRK2    LEARKKAKNKQLGHEEDYALGKDCIMHGYMSKMGNPFLTQWQRRYFYLFPNRLEWRGEGE

GRK5    NGTLPPDLNRNHPPEPP-------------------------------------------

         :        *::   *



GRK3    SRQNLLTMEQILSVEETQIKDKKCILFRIKGGKQFVLQCESDPEFVQWKKELNETFKEAQ

GRK2    APQSLLTMEEIQSVEETQIKERKCLLLKIRGGKQFILQCDSDPELVQWKKELRDAYREAQ

GRK5    --------------------KKGLLQRLFKRQHQNNSKSSPSSKTSFNHHINSNHVSSN

                            :* :* ::   ::   . .* .. ..:::.:.. . .::



GRK3    RLLRRAPKFLNKPRSGTVELPKPSLCHR-NSNGL

GRK2    QLVQRVPKMKNKPRSPVVELSKVPLVQRGSANGL

GRK5    STGSS-----------------------------
```

Figure 2.3 GRK3 and GRK5 were aligned with GRK2ct to determine their analogous c-terminal regions. Sequences were aligned using the multiple sequence alignment program, ClustalW (http://www.ebi.ac.uk/Tools/clustalw2/index.html)

2.1.4e Subcloning G-protein βγ subunit sequestering constructs into IRES-DsRed2

Gαt cDNA cloned into pcDNA3.1 was purchased from Missouri S&T. For identification of successful transfections all G-protein βγ subunit sequestering constructs were subcloned into the pIRES2-DsRed2 vector (Takara/Clontech, France, Figure 2.4). DNAs were amplified with forward primers containing a *Nhe*I site and reverse primers containing

*Bam*HI (GRKXct-MAS) and *Eco*RI (Gαt) restriction sites (Figure 2.4). The oligonucleotides and PCR procedures are as described:

GRKxct-MAS primers from 5' to 3' sequence

Forward: GTGgctagcCGACTCACTATAGGGAGACCC

Reverse: GTGggatccGCCTAGCATTTAGGTGAACTA

Gαt primers from 5' to 3' sequence

Forward: gctagcGTTTAAACTTAAGCTT

Reverse: GTGgaattcGTTTAAACGGGCCCTCTAGAT

PCR conditions

- *Polymerase chain reaction*: 22.5 μl volume of Accuprime *pfx* supermix (Invitrogen) with 50 ng of DNA, 25 pmol each primer.

- *Thermal cycling method:* 95°C for 5 mins, followed by 30 cycles of 95°C for 15 s, 52°C for 30 s, 68°C for 1.5 min and 68°C for 10 mins.

A

pBR322 origin

CMV promoter

*Nhe*I

MAS-GRK2ct

*Bam*HI

EMC IRES

DsRed2

SV40 promoter

Kanamycin

Terminator sequence

pIRES-DsRed2-MAS-GRK2ct
5902bp

500bp
1000bp
1500bp
2000bp
2500bp
3000bp
3500bp
4000bp
4500bp
5000bp
5500bp

B

pBR322 origin

CMV promoter

*Nhe*I

MAS-GRK2ct

*Bam*HI

IRES EMC

DsRed2

SV40 promoter

Kanamycin

Terminator sequence

pIRES-DsRed2-MAS-GRK5ct
5627bp

500bp
1000bp
1500bp
2000bp
2500bp
3000bp
3500bp
4000bp
4500bp
5000bp
5500bp

C

Plasmid map of pIRES-DsRed2-MAS-Gαt (6367bp), showing the following labelled regions: pBR322 origin, Terminator sequence, Kanamycin, SV40 promoter, DsRed2, IRES EMC, *Eco*RI, Gα Transducin, *Nhe*I, CMV promoter. Scale markers: 500bp, 1000bp, 1500bp, 2000bp, 2500bp, 3000bp, 3500bp, 4000bp, 4500bp, 5000bp, 5500bp.

Figure 2.4 Schematics of the bicistronic vectors pIRES-DsRed2-MAS-GRK2ct (A), pIRES-DsRed2-MAS-GRK5ct (*B*) and pIRES-DsRed2-MAS-Gα*t* (*C*). Regions are described in Figure 2.2. DNAs were subcloned into sites denoted in blue letters. DsRed2 is the reporter gene.

Ligations were carried out as described previously. GRK3ct-MAS-pIRES2-DsRed2 was made by Klaus Wanisch within Dr Schorge's lab. Sources of all other plasmids used in this study are detailed overpage.

Table 2.3 Sources of plasmids used in this study

Protein	Vector	Source
$Na_V1.1$-5A	pcDM8	Prof. Massimo Mantegazza, Milan University, Milan
$Na_V1.2$-6N	pcDNA3	Prof. Holger Lerche, Ulm University, Germany
$Na_V1.2$-6A	pcDNA3	Prof. Holger Lerche
$Na_V1.1$-5A R1648H	pcDM8	Prof. Holger Lerche
GIRK 1,4	GIRK1-IRES-GIRK4/pcDNA3	Prof. Andrew Tinker, UCL, London
Voltage-gated sodium channel subunits β1, β2	SCNxB - ECMV IRES - SCNxB - polio IRES - EGFP	Prof. John Wood, UCL, London
Voltage-gated sodium channel subunit β1 splice variant 1B	pCMV6-XL5	Origene Technologies, USA
DsRed2	pIRES2	ClonTech, France
GRK3	pCMV-sport6	Geneservice Ltd, Cambridge, UK
GRK5	pOTB7	Geneservice Ltd, Cambridge, UK
Gαt	pcDNA3.1	Missouri S&T, USA

2.2 Cell culture

2.2.1   HEK 293 cell culture and transfection

HEK 293 cells were maintained in Dulbecco's Modified Eagles medium (D-MEM Sigma), supplemented with 10% (v/v) foetal calf serum (Gibco), 1 % glutamine (2 mmol/l, Invitrogen) and 1 % penicillin–streptomycin solution (Pen/Strep 10 000 IU/ml to 10 000 IG/ml, Gibco) at 37^oC in a humidified atmosphere of air: CO_2 (95:5%).   Cultures were passaged twice weekly by trypsination (Gibco ∕ Invitrogen). 24 hours prior to transfection,

cells were grown to 20 - 30% confluency in 35 mm dishes (Nunc, Denmark) that contained sterilized 13 mm poly-D-lysine-coated coverslips (Menzel-Glaser). Transfections were performed using Lipofectamine 2000 (Invitrogen) according the manufacturer's recommendations. 3 ug of total plasmid DNA was used. GFP was used as an indicator of successful transfectants.

2.2.2a 197VM culture

Non-differentiated 197VM cells were maintained in B27 growth medium supplemented with B27 neural cell supplement mix (Gibco), L-Glutamine (2 mM, Gibco), heparin (10 Units/ml, Sigma), Gentamicin (50 μg/ml, Gibco), bFGF (10 ng/ml, Invitrogen) and EGF (20 ng/ml, Sigma). Cells were grown on laminin (Invitrogen) coated T25 cm^2 flasks (Nunc Easyflask) in a humidified atmosphere of air: CO_2 (95:5%). If cells became over 80% confluent cell viability and differentiation potential was dramatically reduced (Donato *et al.,* 2007). Therefore, cells were strictly passaged every three days. Two hours prior to passaging, uncoated flasks were incubated with 20 μg/μl laminin diluted in 2.5 ml ice cold DMEM:F12 (Invitrogen), at 37°C. Monolayers were washed with 10 ml HBSS minus Ca^{2+}/Mg^{2+} (Invitrogen) and treated with 2.5 ml x10 trypsin (Sigma) until cell detachment. 5 ml of soyabean-trypsin inhibitor (Sigma) was added and cells were centrifuged at 500 g × for 5 min. Coated flasks were washed with 5 ml warmed DMEM:F12 and cells were replated at 3.5 x10^3 cells/cm^2 in fresh growth medium.

2.2.2b 197VM differentiation

In growth medium, cells were seeded at 10,000 cells/well in an uncoated 96-well plate (Corning Incorporated) and left to form aggregates for 7 days. After gentle titration,

dissociated masses from each well were plated on a corresponding 13 mm laminin coated Thermanox (Nalge Nunc International) coverslip. These were contained in 4 well plates (Corning Incorporated) and maintained for 3 – 4 days. Differentiation was started by starving the cells of growth factors for a specific time: 10 days for SC-RT-PCR analysis and 4 – 6 weeks prior to patch clamping. Media was routinely changed weekly.

2.2.3   Rat hippocampal neurons

Primary hippocampal cultures from newborn Sprague-Dawley rats were cultured under standard conditions and obtained from Dr Kirill Volynski, UCL.

2.2.4   Chicken neuronal cultures

Fertilized chicken eggs were obtained from Winter Egg Farm, Hertfordshire, UK. A E14 White Leghorn chicken embryo was decapitated. Its telencephalon, identified as two prominent lobes behind the optic cups, was dissected. Immature cerebral tissue was immediately digested in 500 µl trypsin and triturated using a 1 ml sterile pasteur pipette for 2 mins. To aid dissociation cells were trypsinized for a further 14 mins. Cells were pelleted (300 rpm, 5 mins) and resuspended into DMEM supplemented with 10% FBS. Neurons were spun as before and washed in 2 mls ice-cold Hanks balanced salt solution (Gibco⁄Invitrogen). The suspension was centrifuged and resuspended in DMEM supplemented with 2% of the serum-free supplement B27 (Gibco⁄Invitrogen). 20 µl of the suspension was plated onto Poly-D-Lysine coated coverslips in 4-well plates and left at 37°C in a humidified atmosphere of air: CO_2 (95:5%) for 7 days. The culture medium was changed every 3 days.

2.3   *Electrophysiology*

2.3.1   Voltage clamp recordings in the whole-cell configuration

Voltage clamp recordings were made in the whole-cell configuration to functionally characterize macroscopic currents from transiently transfected $Na_V1.1$ and GIRK 1,4 channels. The same configuration was used to investigate whole-cell currents from 197VM differentiated neurons and chicken neurons.

Details of components within the electrophysiological rig used in this study are shown in Figures 2.5 & 2.6, some are briefly discussed here. The Axoclamp 700B is an operational amplifier that not only maintained the voltage clamp, but also measured the macroscopic current. It received two inputs: the recorded potential and the holding potential (voltage clamp). An electronic feedback system compensated for differences between these two signals by injecting a current that was representational but opposite in polarity of the membrane current. The latter was sent as an analogue signal to an analogue-digital converter (BNC-2090A, National Instruments), which relayed digitized signals to the computer to for manipulation/storage. Conversely, command digital signals from the computer, via the analogue-digital converter, were delivered to the amplifier to control the membrane potential clamp.

Within the micropipette was a reversible $Ag/AgCl_2$ electrode, which allowed electrons to flow from a copper wire connected to the Axoclamp 700B amplifier to the bath solution or vice versa. This reaction is finite and AgCl coating would wear off by either chemical or mechanical means. This occasionally would result in polarisation of the electrode and lead to drifting tip potentials in recordings. Therefore at the start of weekly experiments the

silver wire was chlorinated with household bleach overnight. Additionally, the chamber was regularly cleaned to prevent crystallized salt forming around the bath introducing ground loops. All perfusion tubing was regularly washed with 70% ethanol to avoid bacterial and fungal growth.

Typically 24-72 hours post-transfection, cell-attached coverslips were placed in a microscope-mounted recording chamber (Olympus; Figure 2.5) that was continually perfused (~1 ml/min, Figure 2.5) with extracellular solutions either at ~21°C or at 35 – 39°C using a heated perfusion tube (Figure 2.6). Cultured neurons were only perfused in room temperature solution. It was essential that perfusion was stable before recording started to reduce noise. Recordings were made using filamented borosilicate glass pipettes (GC120F-10, Harvard Appparatus) pulled to resistances of 1-3 MΩ (P-87 microelectrode puller; Sutter instrument company). Under coarse control the electrode was lowered into the bath. A 10 mV seal test was used to calculate the resistance of the pipette, by clicking the resistance checkbox on the Axoclamp 700B commander (this can also be calculated using Ohm's Law: by dividing the test potential amplitude by the current response amplitude). Positive pressure was then applied to prevent debris blocking the end of the micropipette.

Cells were chosen based on size, that is, cells with a capacitance more than 40 pF were discarded to avoid space-clamp errors and shape, preferentially convex. The micropipette was manoeuvred under fine control to hover over the cell before the positive pressure was released. To ensure the command and membrane potentials were equal, the pipette offset was immediately zeroed manually or using the amplifier commander. The pipette was

lowered so that it touched the membrane indicated by a slight reduction in the current response from the seal test. Gentle suction was then applied until a two gigaohm seal was formed between the micropipette and the cell lipid bilayer. The membrane was clamped to a holding potential of -80 mV to encourage seal formation. Once achieved, fast and slow capacitance transients were cancelled using the amplifier software. At higher temperatures it was essential that a good quality seal was formed, before a brief, forceful suck was applied rupturing the membrane, to form a whole cell configuration.

The seal test was removed and whole-cell toggle on the software was clicked. This allowed for large transients formed by cell capacitance in series with pipette and access resistance to be cancelled (Molleman 2007). The cell capacitance and series resistance were also calculated using the amplifier software. At higher temperatures the series compensation on the Axoclamp 700B was unreliable and through an unknown mechanism would often introduce large transients. Therefore, in the majority of recordings the series resistance was <2 MΩ and compensation was avoided. Voltage protocols were started immediately as cell viability significantly reduced after 10 mins at physiological temperatures. Current traces were Bessel filtered at 10 kHz and were acquired at a rate of 50 kHz.

Analogue - digital converter (BNC-2090A, National Instruments).

Operational amplifier (Multiclamp 700B, Molecular devices).

Oscilloscope This was used to monitor current responses during voltage-clamp experiments (Tektronic TDS 100 2B, National Instruments)

PC Allowed for data acquisition and analysis (Dell). The amplifier was controlled by Multiclamp 700B commander software (Molecular Devices). Voltage clamp protocols were performed using custom programs in Labview 8.0 (National Instruments).

Gravity perfusion system Extracellular solutions were poured into two 50 ml syringes and flow was controlled by multi-way taps. Superfusates streamed into the bath via plastic tubing under gravity. This allowed for phenytoin administration during experiments. Rate of flow was 1 ml/min.

Faraday cage Blocked environmental electrical noise (inherited from DMK).

Recording chamber

Inverted microscope (Olympus IX71) Cells were viewed under x10 and x40 magnifications. Fluorescence was excited by 120-watt lamp (X-cite series 120, Exfo) and wavelengths were filtered by low signal to noise ratio cubes. This allowed visualization of red (DsRed2) and green (GFP) fluorescence. Cubes were fitted into the filter turret. Cells could also be viewed in bright field.

Micromanipulator (arrow points to control cube) Two manipulators (Patchstar) both with coarse and fine controls were used to position the headstage and micropipette across the X,Y and Z axis.

Suction pipette

Perfusion waste was aspirated (by a Watson Marlow 5058 pump) and collected into a 5 litre round bottom flask.

Anti-vibration table Prevented the introduction of mechanical noise. It was cushioned by pressurized nitrogen gas (donated by DMK).
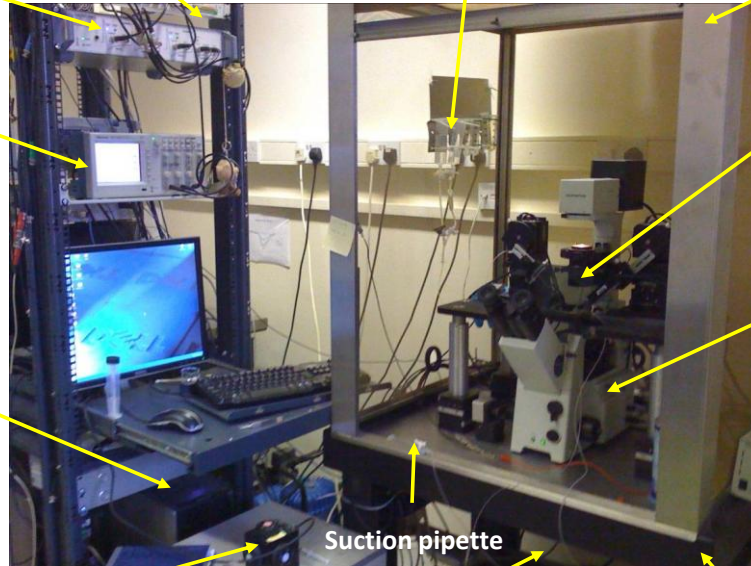
Figure 2.5 Components of the electrophysiological rig

164

Bath Chamber in which cells were perfused with extracellular solution

Temperature probe Measured the bath temperature and was monitored electronically by ALA Scientific Instruments software installed on the PC.

Micromanipulator

Silver / silver chloride ground pellet Grounded the bath solution to ensure low-noise during recordings (Warner Instruments).

Tube leading to suction pipette

Heated Perfusion Tube The perfusion tubing was inserted into a heated aluminum coil. To obtain temperatures of 37°C the coil was heated to 51°C and externally controlled by software installed on the PC (HPT-2a, ALA Scientific Instruments software).

Waste aspirator

Micropipette holder Secured the position of the microelectrode during experiments (G23 Instruments, UCL)

Figure 2.6 Components of the electrophysiological rig surrounding the bath

2.3.2 Electrophysiology solutions

- HEK 293 cells were perfused with (mM): NaCl 145, KCl 4, $CaCl_2$ 1.8, $MgCl_2$ 1, HEPES 10, (pH 7.35 with NaOH) and patch electrodes were filled with either (in mM): **CsCl** 150, EGTA 10, HEPES 10, (pH 7.35 with CsOH) or **CsF** 130, CsCl 10, EGTA 10, HEPES 10 (pH 7.35 with CsOH). For potassium channel recordings the following intracellular solution was used (in mM): KCl 150, EGTA 10, HEPES 10 (pH 7.35 with KOH).

- The extracellular solution used for 197VM and rat hippocampal neurons was (in mM): NaCl 125, KCl 2.5, $CaCl_2$ 2, $MgCl_2$ 2, Glucose 30, HEPES 25, NBQX 10 μM (pH 7.4 with NaOH), and intracellular solution (in mM) KMS 135, HEPES 10, Na-Phosphocreatine 10, $MgCl_2$ 4, Na-ATP 4, Na-GTP 0.4 (pH 7.2 with KOH).

- Chicken neurons were perfused with (mM): 140 NaCl, 1.5 KCl, 2.5 $CaCl_2$, 1 $MgCl_2$, 11 glucose, 10 HEPES (pH 7.4 with NaOH) and patch electrodes were filled with (in mM) 100K-gluconate, 40 KCl, 10 HEPES, 0.1 $CaCl_2$, 2 $MgCl_2$, 1.1 EGTA, 2 Na-ATP (pH 7.2 with KOH).

2.3.3 Voltage clamp analysis software

Labview 8.0 (National Instruments) was used to design and control voltage protocols and analyze recorded current traces. Raw data was exported to Microsoft Excel and subsequent curve fitting and statistical analysis was performed by GraphPad Prism 5 (GraphPad Software, Inc, USA). Membrane potentials were not corrected offline for the liquid junction potentials but were calculated as -4.4 mV in the Cesium chloride based intracellular solution, -9.3 mV in the Cesium fluoride based internal solution, -16.9 mV in

197VM stem cell recording solutions and -13.1 mV in chicken neuronal recording solutions using Clampex software (Molecular Devices).

2.3.4   Current-voltage protocols and analysis

From a holding potential of -80 mV, 100 ms voltage steps in 10 mV increments were administered every 10 seconds from -100 mV to +60 mV. From this protocol, normalized conductance curves, peak transient current densities, persistent current-voltage relationships, rate of current decay and $10 - 90$ % current rise times were calculated as described below.

2.3.4a Normalized conductance curves

For individual cells the peak current amplitude at voltages $10 - 30$ mV was plotted against the voltage step and fitted with a linear regression (y = mx + c). The reversal potential was x when y = 0. Conductance was calculated using the following equation: $G = I/(V-V_{rev})$, where G is conductance (Siemens), I is the peak current (pA), V is the membrane potential (mV) and V_{rev} is the calculated reversal potential (mV). Conductance was normalised so that values were a fraction of the maximum conductance. Normalized conductance against voltage potential (-60 mV to +20 mV) was fitted with a Boltzmann equation: $G/Gmax = (A+(B-A))/(1+\exp((V_{50}-V)/k))$, where G/Gmax is the normalised conductance value, A is bottom of the curve (lowest value), B is the or top of the curve (highest value), V_{50} is the potential for half maximum normalized conductance, V is the test potential and k is the slope factor. Boltzmann curves were fitted from average conductance values for each experiment. Mean V_{50} and slope factors were derived from Boltzmann fits of normalized

conductance-voltage data (-60 mV to -20 mV) from individual cells.

2.3.4b Peak current density

Currents from individual cells were normalized to their cell capacitance (pA/pF). The maximum current densities for each experiment were averaged.

2.3.4c Persistent current-voltage relationships

The mean current during the 20 – 30 ms after the initiation of the voltage step was normalized to cell capacitance. Mean current densities were plotted against the membrane potential (-100 mV - +60 mV).

2.3.4d 10 – 90 % current rise times

10 – 90 % rise-time to peak was calculated from normalized current from individual cells after a step from -80 mV to test potentials ranging between -20 mV and +20 mV.

2.3.4e Rate of current decay (τ_h)

The normalized current from individual cells was fit to a one-phase exponential decay from a holding potential of -80 to steps between -20 mV and +20 mV from 90% of peak current amplitude. The following equation was used: Y=(Y0 - Plateau)*exp(-K*X) + Plateau. Where Y is the normalized current, Y0 is the normalized current value when X (time) is zero (pA), Plateau is the normalized current at infinite times (pA), K is the rate constant (1/ms; taken from GraphPad prism 5)

2.3.5 Voltage dependence of fast inactivation and percentage persistent current

The voltage dependence of fast inactivation and percentage persistent current were assessed

using the following protocol: from a holding potential of -80 mV, cell membranes were voltage clamped with a run of -100 mV-+60 mV 100 ms prepulses, in 10 mV increments followed by a 30 ms test pulse to −10mV every 10 seconds.

2.3.5a Fast inactivation

Peak currents elicited by the test pulse were normalised as before described for conductance. Boltzmann curves were fitted from average normalized current values against voltage (-100 mV − 10 mV) for each experiment using the following function: $I=(A+(B-A))/(1+\exp((V_{50}-V)/k))$ where I is the fraction of normalized current available, A is the bottom - , B top - of the curve, V_{50} is the voltage giving the half-maximal current, V is the test potential and k is the slope factor. Mean V_{50} and slope factors were derived from Boltzmann fits of normalized current-voltage data (-100 mV − 10 mV) from individual cells.

2.3.5b Percentage persistent current

%INa$_P$ was calculated as the mean current from the last 10 ms of the -10 mV test pulse from -80mV and expressed as a fraction of the maximum transient current. Due to the variability of this parameter the INa$_P$ from each voltage clamp protocol cycle, run during a single recording, was calculated from each cell and averaged. For each experiment mean values from single cells were used to calculate the total mean %INa$_P$.

2.3.6 *Recovery from fast inactivation*

Recovery from inactivation in the presence or absence of 50 μM Phenytoin (PHT) was assessed using two-pulse protocol consisting of initial step to -10 mV for 100 ms,

169

sequential recovery intervals of 2 ms, 10 ms and 20ms at -80mV, and a test step to -10 mV for 30 ms. The current amplitude of the test pulse was expressed as a fraction of the current from the initial step to give a measure of fractional recovery, expressed as a percentage.

2.3.7 Phenytoin preparation

Stock solutions of PHT 100 mM were prepared in DMSO was stored at $-20^{o}C$. Prior to electrophysiological recording, 50 µM PHT was prepared in extracellular solution and administered via the gravity perfusion system.

2.3.8 GIRK 1,4 voltage protocols and analysis

A 0.9 second ramp hyperpolarisation was applied from a holding potential of -50 mV down to -140 mV.   Mean values of the potassium conductance recorded from individual cells was calculated from a linear regression fit to the slope of the current-voltage data from -100 to -120mV.

2.3.9 Differentiated 197VMs voltage protocols and analysis

Cells were held at -80 mV and stepped 100 ms to voltages between -100 and +40 mV in 10 mV intervals every 10 seconds.   Individual currents recorded from the differentiated 197VMs cells were normalized to their cell capacitance. Average values were plotted against the membrane potential.

2.3.10 Chicken neuron voltage protocols

To assess macroscopic neuronal currents, cells were held at -80 mV and stepped to voltages between -100 and +30 mV in 10 mV intervals every 10 seconds. After attaining the whole-cell configuration the resting membrane potential (RMP) was measured in the current-

clamp I = 0 mode.

2.3.11 Leak subtraction

Leak current was subtracted online using a *-P*/4 protocol. This involved subtracting summated, passive current responses to small positive voltage steps, from macroscopic waveforms produced after each test pulse.

2.3.12 Statistics

Results are expressed as means (±SEM) and graphing of the data and statistical analyses were performed using GraphPad Prism 5. Individual statistical analyses are described in the text and a statistical significance was considered $P<0.05$.

2.4 SC-RT-PCR

The principle of nested SC-RT-PCR is shown overleaf in Figure 2.7.

Figure 2.7 Principle of nested SC-RT-PCR

Contents of a single cell

DNA digest

Reverse transcription using
gene specific primers

First-round PCR
with outer oligonucleotides

Second-round PCR
with nested oligonucleotides

Genes detected by ethidium bromide gel
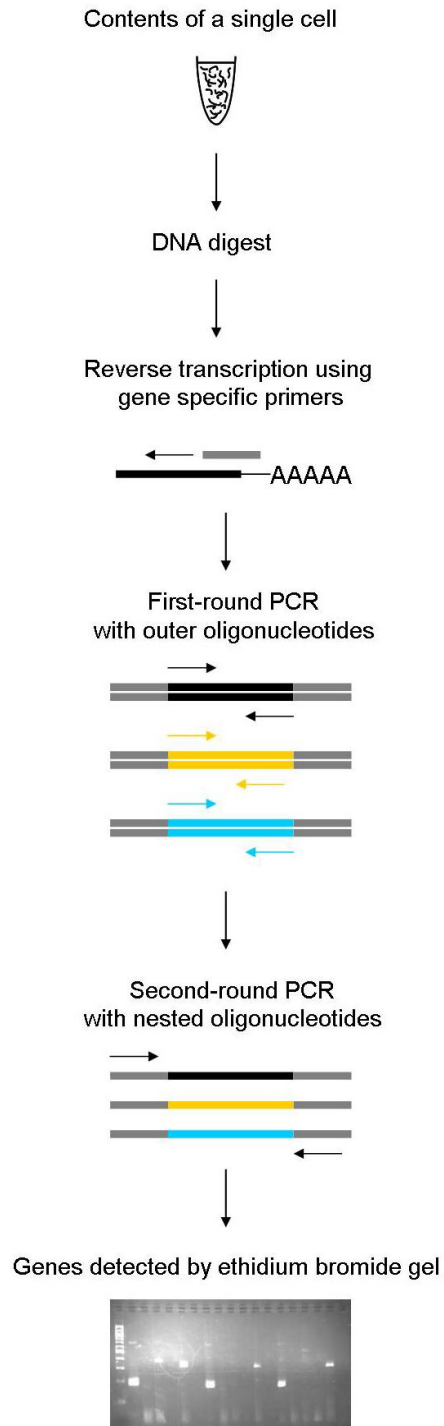
2.4.1 Prevention of RNase contamination

High levels of RNase's are found in bodily fluids therefore, equipment was handled with gloves. Working spaces and equipment were cleaned with 70% ethanol and Microsol™ (Anachem) to remove potential RNase sources. This was followed by treatment with an RNase decontamination solution RNAse-Zap (Ambion). Aerosol resistant tips (Axygen) were used to prevent RNase/DNA contamination via the pipettors. Tips, Ultrapure™ water (Invitrogen) and 0.2 ml thin walled tubes (Thermoscientific) were RNase-free. Glassware and plasticware used to prepare solutions were autoclaved. Where possible, equipment was stored in an air tight box to prevent environmental RNase contamination.

Electrophysiological solutions were not prepared under strict RNAase-free conditions. However, all chemicals were opened using RNase-Zap decontaminated gloves and handled with RNAse-free tools. Before each experiment, both intracellular and extracellular solutions were 0.2 µm syringed-filtered (Supelco). The electrode-wire was rechlorinated at the start of each session or when RNase contamination was suspected.

2.4.2 Cell harvesting & DNA decontamination

Under visual observation, cell content including the nucleus, was aspirated using gentle negative pressure, into a <2MΩ pipette containing 6 µl intracellular solution. Care was taken to avoid DNA/RNA contamination from the bath solution and neighbouring cells. Using an adapted 1ml syringe content was injected into a chilled 0.2 ml thin-walled tube (Thermoscientific) containing 40U RNasin, a ribonuclease inhibitor (Promega). The

solution was decontaminated from genomic and stray DNA using the TURBO DNA-*free*™ kit (Ambion) following the manufacturer's instructions

2.4.3 RNA reverse transcription

1.5mM of mixed deoxynucleotide triphosphatases (dNTPs, Invitrogen) and 50 pmol of each oligonucleotide (Sigma), to amplify selected RNAs (Tables 3-6), were added to the single-cell content. The mixture was incubated at 70°C for 7 mins before being cooled at RT for a further 7 mins. Contents were collected by a brief centrifugation before 4ul of Superscript™ 5x first-strand buffer (Invitrogen), 1μl of dithiothreitol (DTT, 0.1M, Invitrogen), 1μl of 200U Superscript™ III reverse transcriptase (Invitrogen) were added. To propagate cDNA synthesis samples were warmed to 55°C for an hour, followed by a 15 min 70°C incubation to inactivate the enzyme. Samples were stored at -20°C until further processing.

2.4.4 Amplification of cDNAs

Each gene was amplified in a single 0.2 ml tube containing 2 μl template cDNA, 200 pmol outer oligonucleotides (Table 3-6), 200 μM mixed dNTPs (Invitrogen), 1mM $MgCl_2$, 5μl 10x Thermo-start® buffer (Promega) and 3U Thermo-start® DNA polymerase (Promega) in a final volume of 25 μl. A first polymerase chain reaction (PCR) consisted of 15 min hot start at 95°C followed by 25 cycles: 95 ^{o}C for 45 secs, 57 ^{o}C for 45 secs and 72 ^{o}C for 60 secs; followed by a final elongation step at 72 ^{o}C for 10 mins. A second, comparable PCR reaction was conducted with 'nested' oligonucleotides using 2μl of the previous reaction as a template (Tables 2.4-2.7). The amplification protocol was repeated but reactions went

through 35 PCR cycles. The final products were visualized by ethidium bromide staining after electrophoresis in 3% agarose gels. Cells were considered positive for a given gene if the correct base-pair amplicon size was detected (Tables 2.4-2.7).

Successful cellular aspiration and reverse transcription were only considered in reactions where either glyceraldehyde-3-phosphate dehydrogenase (GAPDH) or βIII tubulin (TUBB3) mRNAs were detected. For each PCR amplification, controls for contaminating artifacts were performed by using sterile water, intracellular solution and extracellular solution removed from the bath instead of cDNA. Since the nucleus was harvested, the detection of genomic DNA was avoided by treating the aspirated contents with DNase and designing primers that targeted only exons.

Table 2.4: List of all nested oligonucleotides used in rat hippocampal SC-RT-PCR studies

mRNA	Seq reference number	Oligo	Primers from 5' to 3' seq	Amplicon size (bp)
GADPH	NM_017008	Sense	AGACAGCCGCATCTTCTTGT	142
		Antisense	TGATGGCAACAATGTCCACT	
SLC17A7	NM_053859	Sense	TGAGGATCCTTCAGGGATTG	169
		Antisense	TACTGTACCAGGACCCCAGC	
GAD67	M76177	Sense	GTTTGATCCGATCCAGGAGA	126
		Antisense	TCTATGCCGCTGAGTTTGTG	
TH	NM_012740	Sense	CAGGGCTGCTGTCTTCCTAC	247
		Antisense	GGGCTGTCCAGTACGTCAAT	
ChAT	XM_224626	Sense	TCATTAATTTCCGCCGTCTC	173
		Antisense	CCGGTTGGTGGAGTCTTTTA	

Table 2.5: List of all outer oligonucleotides used in rat hippocampal SC-RT-PCR studies

mRNA	Seq reference number	Oligo	Primers from 5' to 3' seq	Amplicon size (bp)
GADPH	NM_017008	Sense	TCTCTGCTCCTCCCTGTTCT	308
		Antisense	GATCTCGCTCCTGGAAGATG	
SLC17A7	NM_053859	Sense	GTCTTTGGCTTTGCCATTGT	315
		Antisense	CAGGTACCAAAAGATCCCGA	
GAD67	M76177	Sense	ACAAAAGGGATTTGTTCCCC	316
		Antisense	CTGGAAGAGGTAGCCTGCAC	
TH	NM_012740	Sense	CAGGGCTGCTGTCTTCCTAC	296
		Antisense	CTCCAAGGAGCGCTGGAT	
ChAT	XM_224626	Sense	TGGCCCAGAAGAGCAGTATC	275
		Antisense	CTCGATCATGTCCAGGGAG	

Table 2.6: List of all nested oligonucleotides used in 197VM SC-RT-PCR studies

mRNA	Seq reference number	Oligo	Primers from 5' to 3' seq	Amplicon size (bp)
GADPH	NM_002046	Sense	GAGTCAACGGATTTGGTCGT	185
		Antisense	GACAAGCTTCCCGTTCTCAG	
SLC17A7	NC_000019.8	Sense	CCATGGTCAATAACAGCACG	225
		Antisense	CTGAGGGGATCAGCATGTTT	
GAD67	NM_000817	Sense	CCAACAGCCTGGAAGAGAAG	324
		Antisense	GGTGGTCAGAGAGCTCCAAG	
TH	NC_000011.8	Sense	AGTGCACCCAGTATATCCGC	203
		Antisense	GAACTCCACCGTGAACCAGT	
ChAT	NC_000010.9	Sense	TTTTGTGAGAGCCGTGACTG	283
		Antisense	CACAGGACCATAGCAGCAGA	
TUBB3	NC_000016.8	Sense	CAGATGTTCGATGCCAAGAA	162
		Antisense	GGGATCCACTCCACGAAGTA	

Table 2.7: List of all outer oligonucleotides used in 197VM SC-RT-PCR studies

mRNA	Seq reference number	Oligo	Primers from 5' to 3' seq	Amplicon size (bp)
GADPH	NM_002046	Sense	ACAGTCAGCCGCATCTTCTT	312
		Antisense	TTGATTTTGGAGGGATCTCG	
SLC17A7	NC_000019.8	Sense	ATGAGTGGTCTGGGCTTCTG	324
		Antisense	CACGAAGATGACACAGCCAT	
GAD67	NM_000817	Sense	CAGAAAACTGGGGCTCAAGA	404
		Antisense	TGTCTCTGCAGTCAACCAGG	
TH	NC_000011.8	Sense	GGGAAGACAATATCCCCCAG	484
		Antisense	GTCTGGTCTTGGTAGGGCTG	
ChAT	NC_000010.9	Sense	ACAACATCAGATCGGCCACT	275
		Antisense	GTAGCAGGCACCATACCCAT	
TUBB3	NC_000016.8	Sense	GCGCCTGCACTTCTTCAT	250
		Antisense	GGCCACCTTCACGTTGTT	

2.4.5 G-protein α subunit expression profiles in HEK 293s

Confluent HEK 293 cells grown in T25 flasks from three different passages were harvested by scraping in 1 ml cold PBS (Gibco). Total RNA was extracted using Trizol agent (Invitrogen) following the manufacturer's instructions and stored at -80°C until further processing. Reverse transcription and a single round of cDNA amplification was carried out as described in section 2.4.3. Due to cDNA volume limitations, a maximum of seven oligonucleotides priming for specific genes, per reverse transcriptase reaction were used (Tables 2.8-2.10).

2.4.6 Sequencing of SCN1A R1648H patient DNA

Patient genomic DNA (150-650 ng/ul) was received from Dr Stephanie Baulac, Université Pierre et Marie Curie, France. Patient DNA was processed, sequenced and analyzed by Klaus Wanisch, a postdoc with Dr Stephanie Schorge's lab.

Table 2.8: List of all nested oligonucleotides used to amplify G-protein α subunits

mRNA	Expression[1]	Seq reference number	Oligo	Primers from 5' to 3' seq	Amplicon size (bp)
GNAS	Ubiquitous	NM_016592	Sense	GCCCAGTACTTCCTGGACAA	459
			Antisense	CTCGGGAGTAGCATCCTCAG	
GNAI1	Widely distributed	NM_002069	Sense	TTTTAGGGTGATGGCTTTGG	299
			Antisense	GTTGATCCAAAGGCAGGTGT	
GNAI2	Ubiquitous	NM_002070	Sense	CAGCCATCATCTTCTGCGTA	136
			Antisense	ATGGACGTGTCTGTGAACCA	
GNAI3	Widely distributed	NM_006496	Sense	ATCATAAGAGCCATGGGACG	174
			Antisense	GCTGAAGCAAGCTTGTACCC	
GNAO	Neuronal	BC030027	Sense	TTTCCTGAATACACAGGCCC	258
			Antisense	CAACAGCAAAGAGTCCGTGA	
GNAZ	Neuronal	NM_002073	Sense	ATGACTACGGCAAATCAGGC	357
			Antisense	GGGCTGCTTCTTTTTCCTCT	
GNAQ	Ubiquitous	NM_002072	Sense	GGATCAACGACGAGATCGAG	242
			Antisense	TGGGATCTTGAGTGTGTCCA	
GNA11	Ubiquitous	NM_002067	Sense	GTCAGTGCCATCAAGACCCT	286
			Antisense	TCACGTTCTCAAAGCAGTGG	

[1] Wettschureck & Offermanns, 2005

Table 2.9: List of all nested oligonucleotides used to amplify G-protein β subunits

mRNA	Expression[1]	Seq reference number	Oligo	Primers from 5' to 3' seq	Amplicon size (bp)
GNB1	Widely distributed	NM_002074	Sense	CTTGTGATGCTTCAGCCAAA	166
			Antisense	TCAGCACGAAGGTCAAACAG	
GNB2	Widely distributed	NM_005273	Sense	CTGGGTAATGACCTGTGCCT	193
			Antisense	CCCAGAGCTGGTGATGATTT	
GNB3	Widely distributed	NM_013530	Sense	ACAACCTCAAATCCCGTGAG	236
			Antisense	CCCCGAAATGAAGAGATTGA	
GNB4	Widely distributed	NM_021629	Sense	GCCAGGTCACACAGGGTACT	129
			Antisense	CCAGTGAATGTGGTGGTCTG	
GNB5	Neuronal	NM_016194.3	Sense	GGGAACAAAGTCCTGTGCAT	193
			Antisense	TATCCAAACCACCACAAGCA	

[1] Wettschureck & Offermanns, 2005

Table 2.10: List of all nested oligonucleotides used to amplify G-protein γ subunits

mRNA	Expression[1]	Seq reference number	Oligo	Primers from 5' to 3' seq	Amplicon size (bp)
GNG3	Brain, blood	NM_012202	Sense	CACTTCGGAGAACCCCTTC	267
			Antisense	CATATCTCTGGGGTGCTTGG	
GNG4	Brain	NM_004485	Sense	AGCCTGTATGGACAGGGTCA	248
			Antisense	ATGCATGGTCTCTACAGGGG	
GNG5	Widely distributed	NM_024377	Sense	ACCATGTCTGGCTCCTCCAG	297
			Antisense	GCTTTTGTACAGGCTTCAAATGT	
GNG7	Widely distributed	NM_024138	Sense	CATCTCAAGTCCCCAAAACC	489
			Antisense	GGGTTCAACCATCACAATCC	
GNG8	Olfactory epithelium	NM_010320	Sense	AGACGGTGGAACAGCTGAAG	172
			Antisense	AGCAGAACACAAAAGAGGCG	
GNG10	Widely distributed	NM_001017998	Sense	CAGCTGCAGAGCTTCAACAGT	300
			Antisense	TTCACCCAGTTTTCTCACTCAA	
GNG11	Widely distributed	NM_004126	Sense	TAACCCTCATCTAGCACCCG	363
			Antisense	TGCAACTTCACTTCTTTGCG	
GNG12	Widely distributed	NM_018841	Sense	CTCTCCTTGTCCCAGCTTTG	358
			Antisense	TGTGAGGGCTATATTTGGGC	
GNG13	Brain, taste buds	NM_016541	Sense	CCCGACCTGATGAAGAACAA	224
			Antisense	TCACAGGATGGAGTGAATGG	

[1] Wettschureck & Offermanns, 2005

183

2.4.7   *Microarray analysis of HEK 293 cells*

Messenger RNAs from three passages of HEK 293 cells, one passage harvested in 2007 and another two in 2009 were extracted as above. Samples were decontaminated from genomic and environmental DNA using the TURBO DNA-*free™* kit (Ambion) following the manufacturer's instructions. The quality of mRNA was verified by spectrophotometry and samples with a 260/280 ratio below 1.8 were rejected. 50 μg mRNA was processed and hybridized to Affymetrix Human Gene 1.0 ST Arrays. All microarray and computational analysis using Affymetrix Expression Console™ was performed by Dr Simone Sharma and Mrs Priya Banerjee, at the Wolfson Institute for Biomedical Research, Scientific Support Services, UCL.

2.4.8   *Analysis of SCN1A splicing in Guinea Pig*

Cavia porcellus leg muscle was obtained from Pnemolabs (UK). DNA from 100 mg tissue was extracted using the Wizard genomic purification kit® (Promega) according to the manufacturer's recommendations. The published guinea pig *SCN1A* sequence (Ensemble transcript ID ENSCPOT00000002700) is incomplete and therefore, it was impossible to determine whether the region that codes for DI:S3 was alternatively spliced. The neonatal human *SCN1A* sequence lies within introns 4-5 (Vega transcript ID OTTHUMT00000102661). Nucleotides 570-578 within human exon 4 align to nucleotides 186-194 within guinea pig exon 2. It was reasoned that the unpublished guinea pig exon 3 aligned to human exon 5 sequence. The following primers were used to amplify guinea pig exon's   2   to   5:   sense   TTACTTTCCTTCGAGATCCAT,   antisense:

TGACTTCCAGTCAAACTCGTACA. In a final volume of 100 µl the 3kb DNA fragment was amplified with 50 ng of DNA, 25 pmol each primer, 200 µM mixed dNTPs, 10µl native *Pfu* 10x buffer (Stratagene) and 2.5 U of native *Pfu* polymerase (Stratagene). The PCR reaction was performed as follows: 95°C for 45 s, followed by 35 cycles of 95°C for 45 s, 50°C for 45 s, 72°C for 4 min with a final extension of 72°C for 10 mins. Intron 2 was then sequenced using the following forward primer: TGTTTATCA TTTAAAATCACCAGGAA.

2.4.9   Analysis of VGSC expression the chicken embryo

The immature cerebral lobes from two E14 chicken embryos were dissected as previously described in section 2.2.5. Tissue was grounded with a chilled dounce homogenizer. Total mRNA was extracted immediately using Trizol agent (Invitrogen) following the manufacturer's protocol. Primers were designed using predicted and verified sequences from the Ensembl database and are shown in table 2.11. Extreme care was taken in ensuring primers did not anneal to overlapping regions due to VGSCs sharing a high sequence similarity. Reverse transcription reactions and nested PCR protocols were performed as described in sections 2.4.3 and 2.4.4 (primers are listed in Table 2.11).

Table 2.11: List of all oligonucleotides used to amplify chicken VGSC genes

mRNA	Ensembl Seq reference number	Oligo	Outer primers from 5' to 3' seq	Inner primers from 5' to 3' seq	Inner amplicon size (bp)
SCN1A	XM_422021.2	Sense	TGTACCACCAGGACCAGACA	TGTACCACCAGGACCAGACA	227
		Antisense	TGACAGTGAAATCGAGCCAG	CCATATCTTCCAAGGGCTCA	
SCN2A	O42420_CHICK	Sense	ATTTCGCAAATCCGAATCAG	TTCTCTTCCCCACACCAGTC	107
		Antisense	GGCAGAAGCTGTCCAGTAGG	ACATCCTTTGCACGACCTCT	
SCN3A	scn3a_predicted_ when_aligned_with_human	Sense	GATTGCTGGAGTCCATGGTT	TGGAGTCCATGGTTAAAAGTAAAA	113
		Antisense	GGTTTCCCACAGAAAGGACA	TCCATGGCCATAAACAAGGT	
SCN4A	IPI00820559.1	Sense	CCATATTCGGGATGTCCAAC	ATCCTAAACAGTGGTCCCCC	141
		Antisense	GTCCAGGCAGTGGATTTTGT	ATTGACCACGATGAGGAAGG	
SCN5A	O42418_CHICK	Sense	TTGTCTATGGAGTCGAGGGG	ACTGCAGCAGAGCTCACAAA	141
		Antisense	GCAAACTCAGGGATCTGCTC	CACTGTGCTGCCTTCAGAAA	
SCN8A	IPI00602451.2	Sense	CTACGTTGGAGGAGGCAGAG	ACGGTCTCTGAGGATGCTGT	138
		Antisense	CCTTCCGACAGCTCTTTGTC	CGACAGCTCTTTGTCCTTCC	
SCN9A	O42419_CHICK	Sense	GGGTGGTTGTGAATGCTCTT	CTTGGGAACACTGCATCAGA	141
		Antisense	TACATGGGCTGCTTCCCTAC	CCTAGAGTCAACGGCAGCAT	
SCN10A	scn10a_predicted_ when_aligned_with_human	Sense	CCTTCAGACTGCTGAGGGTC	GTCCTGGCAATCATCGTTTT	109
		Antisense	CCCTTATGAATCCGAGCAAA	GCCAGCGTATTTCACCATTT	
SCN11A	scn11a_predicted_ when_aligned_with_human	Sense	GCGCAGAAAGTTGTGTCAAA	AAGTTTCCAGGCAGCACTTG	223
		Antisense	CTGAGAGACTTCAGGGCACC	CCCATTTCAGAAGCATCTCC	
TUBB3	TBB3_CHICK	Sense	GCTGAACGTGCAGAACAAAA	TCTGCCACGTTCATTGGTAA	134
		Antisense	GAACAAAGGAGACGAGCCTG	TGTGAATTCCATCTCGTCCA	

186

2.5   Immunofluorescnce

2.5.1   Preparation of 4% Paraformaldehyde

20g paraformaldehyde (PFA, Sigma-Aldrich) was dissolved in 500 ml of 1x PBS (Sigma-Aldrich), pH 7.4. The solution was heated to 55ºC for two hours to encourage the PFA to dissolve. Using 1M NaOH the pH was adjusted to 7.4. The solution was 0.2 μm syringed-filtered and stored at -20ºC in 40 ml aliquots.

2.5.2   Preparation of Immunocytochemistry buffers

250 mg of Albumine Bovine (Sigma-Aldrich) was dissolved 5 ml of 1x PBS to make 5% BSA. This was further diluted in 50 ml PBS to make the block buffer: 0.5% BSA. 1 ml of 0.1% Triton (Sigma-Aldrich) was dissolved in 10 ml of block buffer to prepare the permeabilization buffer. All solutions were stored at 4^oC for up to a week.

2.5.2   Immunocytochemistry

Prior to transfection HEK 293 cells were grown on sterilized 13 mm Poly-D-lysine coated glass coverslips. Cells were (co-) transfected for 12hrs with the appropriate DNA using Lipofectamine 2000. Cells were fixed directly in DMEM using 4% PFA for 3 mins and washed in 1x PBS three times. Cells were permeabilized for 5 mins using the 0.1% Triton in block buffer and were washed in 1x PBS three times and blocked in 0.5 % BSA for 1 hour. All antibodies were diluted in block buffer. To detect $Na_V1.1$, cells were incubated with diluted 1:200 rabbit anti-$Na_V1.1$ (Millipore) for 24 hours at 4^oC. Cells were washed three times in 1x PBS for 10 minutes. Coverslips were then incubated with fluorophore conjugated secondary antibodies: donkey anti-rabbit Alexa Fluor® 568 (Invitrogen),

diluted 1:1000, for 1 hour at RT. Cells were washed in distilled water and paper-blotted to prevent salt crystallization. Coverslips were mounted using Moviol (Calbiochem) containing 25mg/ml DABCO anti-fade reagent. Cells were viewed using a Zeiss AxioImager A1 fluorescent microscope. The microscope and immunofluorescence images were manipulated by Mr George Chennell at the Wolfson Institute for Biomedical Research, Scientific Support Services, UCL. The same protocol was repeated by Elin Reeves in immunocytochemistry experiments using CHO cells. Specific antibodies are noted in the text.

Chapter 3: The functional characterization of Na$_V$1.1 splice variants

3.1 Hypothesis and aims

Hypothesis: Since splicing changes part of the ion channel thought to be important for sensing changes in membrane voltage, it was surmised that Na$_V$1.1-5A and Na$_V$1.1-5N would possess different biophysical properties. It was predicted that these would be altered by different intracellular anions, known to distinctively act on downstream signalling pathways and by temperature. The AA genotype of the rs3812718 polymorphism is associated with higher phenytoin dosage suggesting that its efficacy is decreased when acting on a higher proportion of the 5A variant. It was therefore hypothesized that phenytoin would demonstrate an enhanced effect when acting on Na$_V$1.1-5N compared to Na$_V$1.1-5A channels.

Many of the α subunits of sodium channels are alternatively spliced in their first domain and one amino acid in the extracellular linker is consistently different between the two exons. Whereby neonatal exon encodes a neutral amino acid, asparagine, the adult exon encodes a negatively-charged amino acid, aspartate. It was hypothesized that any channel behavioural differences between the two isoforms would be due to this conserved amino acid change.

Experimental aims: There were several aims to this chapter. The main aim was to investigate the impact of exon 5N on the Na$_V$1.1 channels and secondary to this, to assess the impact on channel gating by the conserved amino acid change. Therefore, in transfected

HEK cells, using whole-cell patch clamp, the macroscopic properties of $I\text{Na}_\text{T}$ and $I\text{Na}_\text{P}$ of the two splice variants and $\text{Na}_\text{V}1.1$-D207N were assessed. Another aim was to establish optimal physiological recording conditions; therefore the impact of internal solutions, cell background and temperature on $\text{Na}_\text{V}1.1$ behaviour were examined. The last aim was to reveal a mechanistic mechanism for the association of rs3812718 polymorphism and AED dosage; consequently, $\text{Na}_\text{V}1.1$ splice variant sensitivity to phenytoin was investigated.

The results are divided into the following sections:

1. Genetic and electrophysiological evaluation of HEK 293 cells.

2. Comparison of $\text{Na}_\text{V}1.1$ splice variant channel behaviour at RT using CsCl and CsF-based internal solutions.

3. Assessment of $\text{Na}_\text{V}1.1$ splice variant and $\text{Na}_\text{V}1.1$-D207N gating at 37$^\text{o}$C using CsCl-based intracellular solutions.

4. Comparison of RT and 37$^\text{o}$C $\text{Na}_\text{V}1.1$ macroscopic recordings using CsCl-based intracellular solutions.

5. Assessment of the recovery from inactivation of $\text{Na}_\text{V}1.1$ isoforms and $\text{Na}_\text{V}1.1$-D207N in the presence and absence of phenytoin.

3.1.1: Controls: Untransfected HEK 293 cells do not express voltage-activated currents

Endogenous channels would potentially distort data from the expressed channels. The clone of HEK 293 cells used in these experiments (derived from ATCC) was assessed for currents during protocols used for comparing sodium channels. The HEK 293 cell line is an

established expression system used for electrophysiological studies into voltage-gated ion channels. Immunocytochemistry and microarray analysis suggest that these cells belong to a neuronal (Shaw *et al.,* 1992) rather than a metanephric lineage (Graham & Smiley, 1977). Indeed, endogenous voltage-activated currents are present in particular HEK 293 cell lines, including currents from voltage-gated sodium, calcium, chloride and potassium channels (Ukomadu *et al.,* 1992; Cummins *et al.,* 1993; Berjukow *et al.,* 1996; Zhu *et al.,* 1998; Avila *et al.,* 2004). Although in the Zhu *et al.* 1998 study the potassium currents were blocked by cesium within the internal solutions.

To detect possible intrinsic voltage-activated currents recordings were performed at room temperature from untransfected HEK 293 cells using the whole-cell configuration. Both 150 mM CsCl and 130mM CsF based internal solutions were used. Cells were held at -80 mV and stepped to voltages between -100 mV and +60 mV in 10 mV steps. The current density for each cell was calculated by normalizing the current amplitude in the last millisecond of the 100 ms voltage step to cell capacitance. Small inward and outward currents peaking at +60 mV were observed using CsCl (mean ±SEM = -17.1 ± 3.5 pA/pF; *n*=5), and CsF (mean ±SEM = 23.3 ± 14.2 pA/pF; *n*=7; Figure 3.1 A) solutions respectively. At -10 mV - an experimentally relevant voltage with regards to calculating percentage persistent current (see chapter 6) - negligible peak current densities were observed: using CsCl, mean (±SEM) non-specific currents were -5.2 ± 2.1 pA/pF (*n* = 5, Figure 3.1) and using CsF 4.9 ± 4.3 pA/pF (*n*=7; Figure 3.1 A).
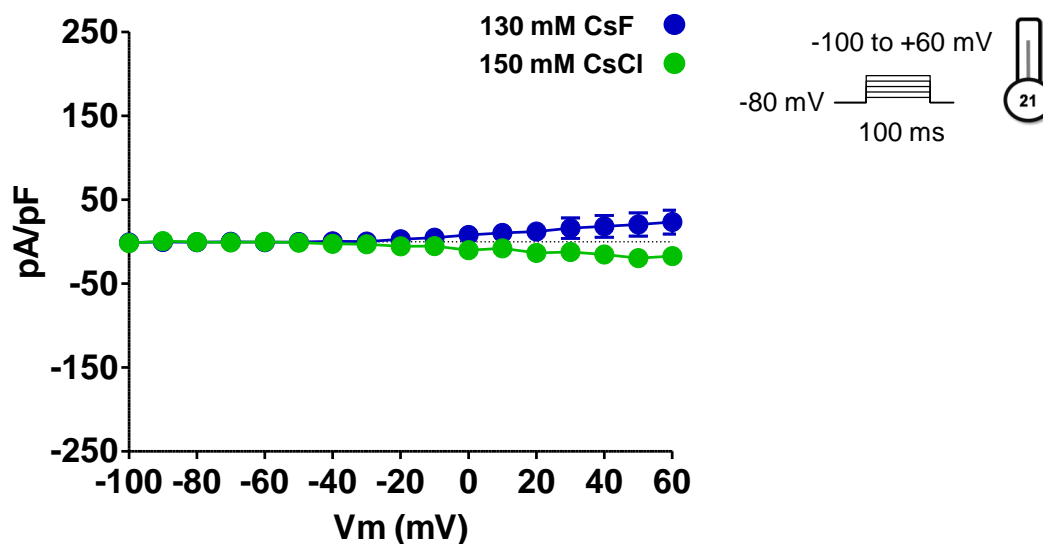
Figure 3.1 Electrophysiological properties of untransfected HEK 293 cells used in this study. At room temperature negligible currents were observed from whole-cell patch clamp recordings of untransfected HEK 293 cells using either a 150 mM CsCl (*n*=5) or 130mM CsF (*n*=7) based intracellular solutions. Cells were held at -80 mV and stepped to voltages between -100mV and 60 mV in 10 mV intervals (inset). Currents were normalized to cell capacitance.

3.1.2: Controls: The gene expression profile of three HEK 293 passages used in this study were comparable

Several groups have noted the properties of cell lines can change over time (reviewed in Hughes *et al.,* 2007), and these changes can introduce non-intrinsic changes to heterologously expressed ion channels (for example by altering kinase/phosphatase activity). The experiments described here were carried out over many months and to assure the cells used were comparable, gene expression was examined in three different batches of HEK cells from timepoints spanning more than one year.

It is unsurprising that the behaviour of $Na_V1.1$ channels, which are heavily modulated by intracellular signalling pathways are dramatically altered by cellular background (Avanzini

et al., 2007). This is particularly significant when considering INa$_P$ current. A previous study demonstrated that levels of Na$_V$1.1-5A derived INa$_P$ was considerably altered within two clonal lines originating from the same HEK 293 cell line (Mantagazza *et al.,* 2005). Therefore to accurately characterize and compare both splice variants it was essential to establish that cell background conditions were stable.

The mRNA harvested from three batches of HEK 293 cells was subjected to microarray analysis as described in the methods (Chapter 2). Briefly, one batch of mRNA originated from a passage of cells from in 2007 and two batches were from different passages in 2009 (the majority of electrophysiological recordings were carried out in 2009). A Pearson's ranked correlation determines the extent of fluorescent signal linearity between mRNA samples: a rank of '1' indicates a perfect correlation, while '0' indicates no correlation between groups. There was a strong correlation between the normalized fluorescence between the three passages (Figure 3.2). The two RNA batches from cells harvested in 2009 demonstrated a higher linearity at ~0.99,   compared to the passage from 2007 at ~0.95 (Figure 3.2).   Unfortunately there were too few samples to provide an accurate indication of the relative abundance of VGSC transcripts. Nevertheless electrophysiology and microarray data confirmed that this HEK 293 cell line was a suitable cell model for electrophysiological investigations, and that gene expression in these cells was relatively stable over different batches.
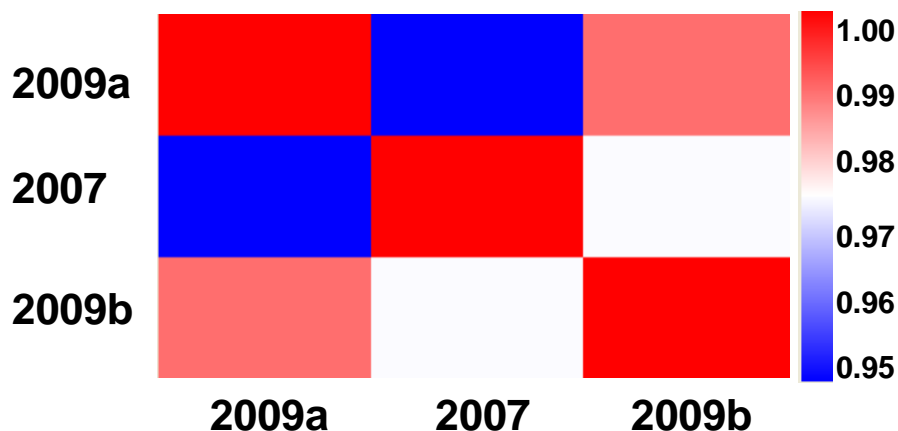
Figure 3.2 Gene expression profiles of three HEK 293 passages used in this study were indistinguishable. Messenger RNA was harvested the same HEK 293 cell line but from three different passages in years 2007 and 2009. Each passage was analyzed by microarrays. The above Pearson's correlation plot, where 1 indicates a perfect correlation and 0 no correlation, shows that the normalized fluorescence between the three passages was highly linear. Note the scale begins at a very high correlation of 0.95 (blue).

3.1.3: Controls: Endogenous currents and filtering at physiological temperatures

Because voltage-gated ion channels can be activated at higher temperatures (Dhaka *et al.,* 2006), control recordings were repeated on untransfected HEK 293 cells, in bath solutions at $34 \pm 3^{o}C$ using CsCl-based intracellular solutions. In addition, because sodium channels activate and inactivate significantly faster at physiological temperatures, the distortion introduced by filtering that is acceptable in RT recordings, may distort currents at higher temperatures. Thus the peak currents were compared for currents filtered at decreasing bandwidths to determine what cut-off provided the best compromise between noise and peak dampening. As at room temperature, minimal currents were recorded, with a mean (±SEM) peak inward current of -4.0 ± 1.6 pA/pF (*n*=26) at 50 mV. At -10 mV the mean (±SEM) current was −1.8 ± 0.5 pA/pF (*n*=26, Figure 3.3 A).
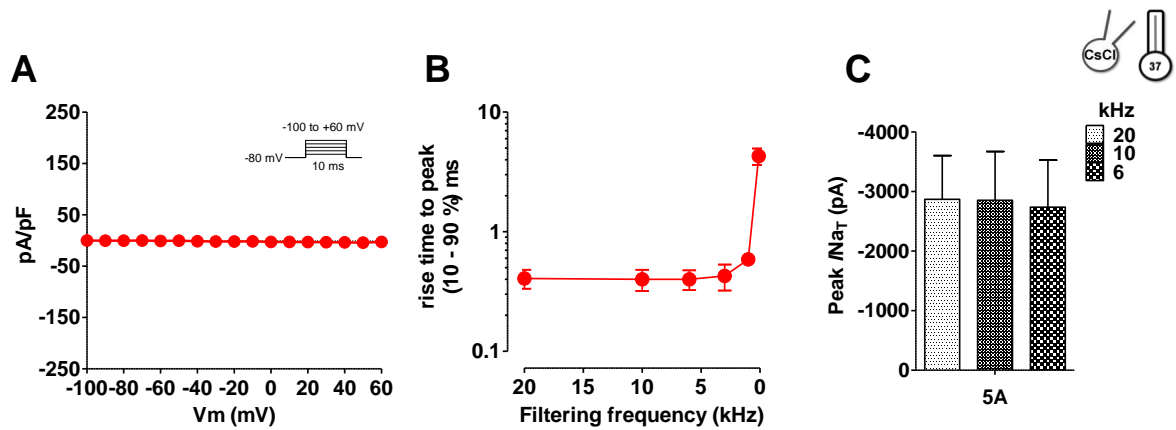
Figure 3.3 10 kHz filter is optimal for recording Na$_V$1.1 currents at biological temperatures. *A.* At temperatures averaging 34°C negligible currents were observed from whole-cell patch clamp recordings of untransfected HEK 293 cells using CsCl (*n*=26) based intracellular solutions. Cells were held at -80 mV and stepped to voltages between -100mV and 60 mV in 10 mV intervals (inset). Currents were normalized to cell capacitance. *B.* Mean (±) 10-90% rise times to peak were calculated from Na$_V$1.1-5A currents (*n*=3) elicited by a test pulse to -10 mV from -80 mV. Currents were filtered at frequencies ranging from 20-0.1 kHz. Little variation in rise times weas observed between 6 and 20 kHz (P=0.9; one-way ANOVA). Since the peak current *(C)* decreased at 6 kHz, and 20 kHz may have introduced too much noise, 10 kHz was selected.

The MultiClamp 700B possesses a 4-pole Bessel filter and at room temperature whole-cell currents were filtered at 10 kHz and sampled at 50 kHz. However, at increased temperatures a 10 kHz cut-off frequency may have not been adequate. To prevent the distortion of data currents need to be filtered approximately ten times faster than the expected 10-90% rise time of a step input. "The filtered 10-90% risetime (Tr, in ms) of a step input depends on fc (in kHz) approximately as: Tr ≈ 0.35/fc" (Axoclamp 700B manual). To determine which fc was optimal at physiological temperatures cells transfected with Na$_V$1.1-5A were held at -80 mV and stepped to a -10 mV – a potential estimated to elicited ~90 % peak sodium current - for 100 ms for six cycles. Each cycle was filtered at a different frequency ranging from 0.1 to 20 kHz (Figure 3.3 B). Experiments were performed at 37 ± 4 °C. The mean 10-90% rise time to peak at 20 kHz, 10 kHz and 6

kHz was 0.4 ms (*n*=3; Figure 3.3 B). According to the above equation 10 kHz was optimal, as 20 kHz may have introduced too much noise and at 6 kHz the peak current was clipped (Figure 3.3 C).

3.2 Comparing Na$_V$1.1 splice variants in conditions typical in literature and those more relevant to physiology

It was important to establish recording conditions that would allow accurate measurement of the effects of AEDs, namely phenytoin, on the biophysical properties of the two splice variants. This is because altered phenytoin dosage is associated with rs3812718 and this drug is thought to work via two mechanisms: either delaying recovery from inactivation and /or blocking persistent sodium current (Matsuki *et al.,* 1984; Kuo & Bean 1994; Chao & Alzheimer, 1995; Gebhardt *et al.,* 2001). Both of these processes are likely to be sensitive to different recording conditions.

In the literature investigations into heterologously expressed Na$_V$1.1 predominantly use CsF-based intracellular solutions (Lossin *et al.,* 2002; Spamanato *et al.,* 2001) as the electrophysiologist can achieve rapid gigaohm seals and whole-cell recordings are more stable. Aluminium fluoride ions, however, are known to disrupt the functions of G-proteins and phosphatases, both of which are known to regulate VGSC derived *I*Na$_P$ (Cantrell & Catterall, 2001; Mantegazza *et al.,* 2005). Since persistent current is a potential target of phenytoin, and an important modulator of neuronal excitability, the presence of fluoride could potentially obscure the physiological impact of this drug. The first portion of this section (Fluoride/chloride: 3.2.1) compares the transient and persistent currents of Na$_V$1.1 splice variants using CsF- and CsCl-based intracellular solutions. The results presented

here demonstrate that a change in internal anion significantly affects $Na_V1.1$ splice variant behaviour for several biophysical parameters. The purpose of these experiments was to establish whether CsF, a less physiological solution, did significantly alter channel gating not to reveal a physiological mechanism for these changes.

A second potential difference between the work reported here and most published data on cloned sodium channels is the temperature of recordings. Most reports on heterologously expressed sodium channels use RT recordings; however sodium channels may behave differently at RT and 37^oC. Additionally, the epilepsies associated with sodium channels, are profoundly sensitive to changes in temperature. In fact, fever-induced seizures are a hallmark of genetic epilepsy caused by mutations in *SCN1A*. The second part of this section (Temperature: 3.2.2) systematically compares the effects of increasing temperatures on $Na_V1.1$ splice variants.

3.2.1 Fluoride/Chloride 1: $Na_V1.1$ transient current density is unaffected by intracellular anion

HEK 293 cells were transiently transfected with either $Na_V1.1$-5N or $Na_V1.1$-5A. Macroscopic currents were recorded in the whole-cell configuration. Example traces of sodium currents from $Na_V1.1$-5A and $Na_V1.1$-5N, evoked from voltage steps shown in the inset, recorded using CsF- (top panel) and CsCl- (bottom panel) based intracellular solutions are shown in Figure 3.4 A. To obtain the current-voltage relationships for each $Na_V1.1$ splice variant, cells were held at -80 mV and stepped to voltages between -100 and +60 mV in 10 mV intervals for 100ms.The *transient* current density, at each test potential, for each cell, was calculated by normalizing current amplitude to cell capacitance (pA/pF).

A two-way ANOVA reveals that the mean (±SEM) peak current density for $Na_V1.1$ was unaffected by splicing or intracellular anion (P=0.2; Figure 3.4 B).
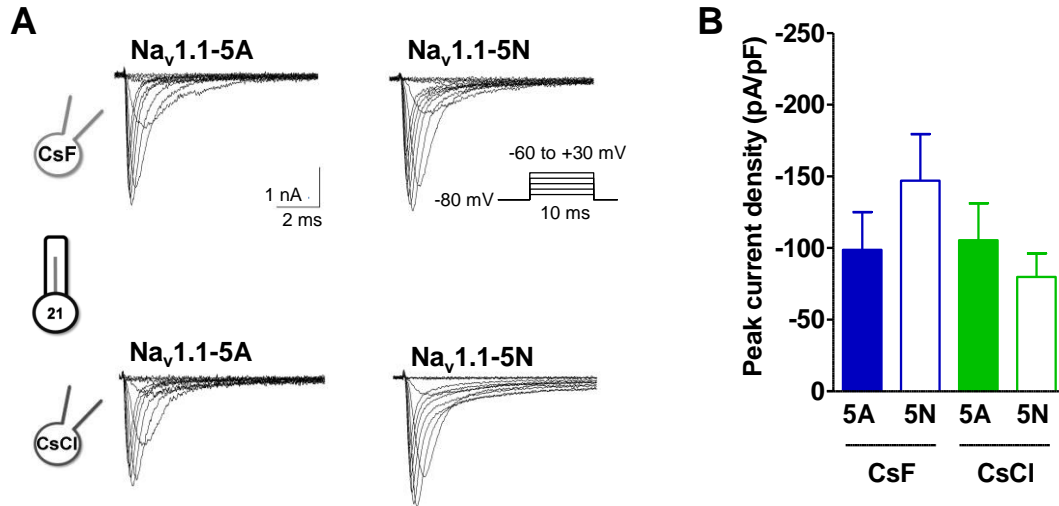
Figure 3.4 Peak current densities of $Na_V1.1$ splice variants were not affected by intracellular anions *A.* Raw traces of $Na_V1.1$-5A (left) and 5N (right) sodium currents using CsF (top) and CsCl (bottom) intracellular solutions. Sweeps were recorded from the current protocol depicted in the inset. *B.* Mean (±SEM) peak current densities were calculated from I-V relationships of individual cells normalized to cell capacitance. A two-way ANOVA did not reveal any differences between the splice variants.

3.2.1 Fluoride/Chloride 2: $Na_V1.1$ derived persistent current is more stable using CsCl based solutions

The current density of the persistent, or non-inactivating, current was calculated from the activation current protocol. The mean current during the 20-30 ms after the initiation of the voltage step was normalized to cell capacitance (Figure 3.5 A). As shown in Figure 3.5 B the $Na_V1.1$ persistent current was voltage dependent, peaking at -10 mV using CsF-based solutions and 0 mV using CsCl-based solutions (mean ± SEM peak current density: CsF 5A: -9.4 ± 3.0 pA/pF, *n*=9; 5N: -3.5 ± 1.3 pA/pF, *n*=14; CsCl 5A: -15.2 ± 6.5 pA/pF, *n*=14; 5N: -13.6 ± 2.3 pA/pF, *n*=11). At no voltage step was the persistent current density

198

significantly different between the two splice variants using CsCl-based solutions (P=0.2, two-way ANOVA). Using CsF internal solutions, however, the average current density between the two isoforms was significantly different (P=0.005, two-way ANOVA). At -10 mV and 0mV with Na_V1.1-5A demonstrated a greater ~ 5pA/pF current density compared to Na_V1.1-5N (P<0.05, Bonferroni's post test).
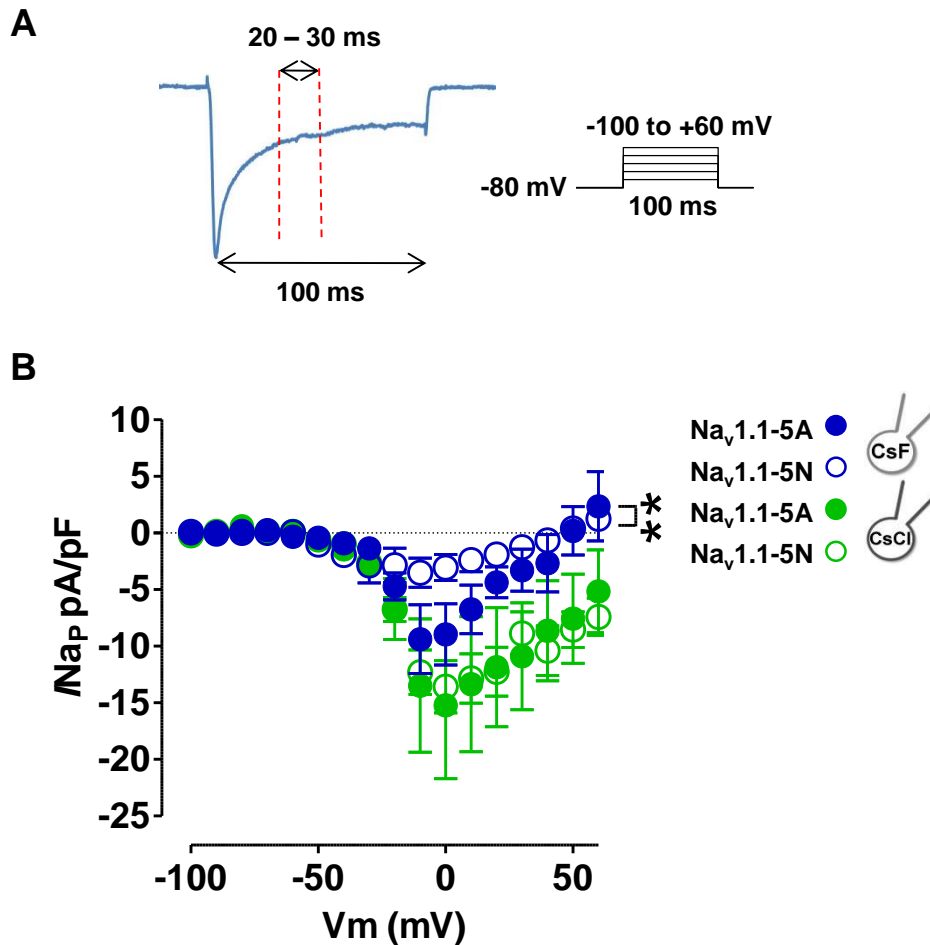
Figure 3.5 At RT Na_V1.1 persistent current is voltage dependent and was greater using CsCl-based solutions *A.* The current density of the persistent current was calculated from the activation current protocol (right). The mean current during the 20-30 ms after the initiation of the voltage step was normalized to cell capacitance. Times shown in the figure are estimates. *B.* I-V relationship of persistent currents derived from Na_V1.1 splice variants all conditions. Using CsF- and CsCl-based solutions the persistent current was voltage dependant and in latter more stable. Na_V1.1-5N persistent current was significantly reduced in fluoride compared to Na_V1.1-5A channels (two-way ANOVA, **P=0.005).

It was assumed that persistent current was a proportion of heterologous expressed $Na_V1.1$ that remained active. $\%INa_P$ was calculated from the inactivation protocol, as the mean current from the last 10 ms of the -10 mV test pulse from -80mV and expressed as a fraction of the maximum transient current (Figure 3.6 A). In agreement with the current density data there were no differences in the $\%INa_P$ between the splice variants using CsCl (5A versus 5N, P=0.9, 2-tailed t-test) but there was a significant increase in persistent current derived from $Na_V1.1$-5A (7.8 ± 1.7%, n=12) compared to $Na_V1.1$-5N channels (3.6 ± 1.1%, n=13) using CsF (P=0.04, two-tailed t-test; Figure 3.6 B).
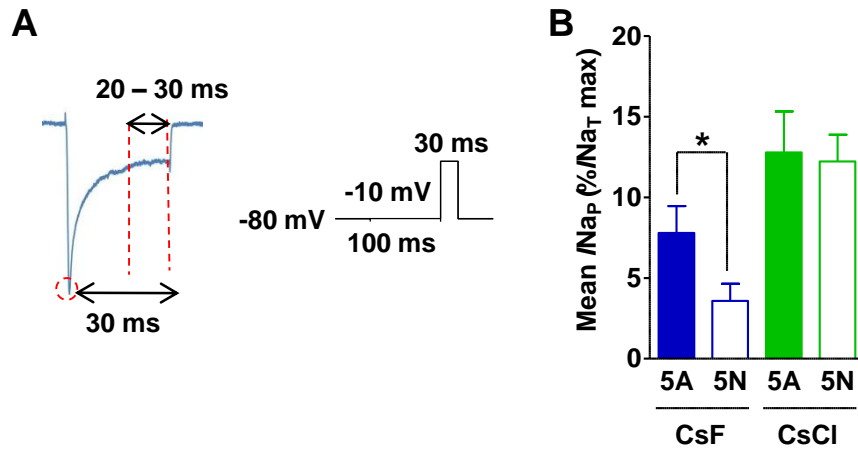
Figure 3.6 The $Na_V1.1$-5A persistent currents were significantly increased using CsF solutions only *A.* $\%INa_P$ was calculated from the inactivation protocol (right), as the mean current from the last 10 ms of the -10 mV test pulse from -80mV (indicated by arrow) and expressed as a fraction of the maximum transient current (red circle). The mean $\%INa_P$ was then calculated for individual cells representing the average INa_P over the complete timecourse of recordings. *B.* Mean (±SEM) $Na_V1.1$-5A derived $\%INa_P$ was significantly increased using CsF but nor CsCl internal solutions compared to $Na_V1.1$-5N channels. *P=0.04, two-tailed t-test.

In presence of chloride the persistent component of the current was more stable and this effect was more pronounced for $Na_V1.1$-5N channels. A change in anion did significantly

alter $Na_V1.1$-5A persistent current density overall (CsF versus CsCl P=0.003, two-way ANOVA) but not at a specific voltage (Bonferroni's post-test). However, $Na_V1.1$-5N was more sensitive to the change in intracellular anion. A significantly greater persistent current at voltages between -10 mV and + 60 mV was observed using CsCl compared to CsF based intracellular solutions (P<0.001, for each noted test potential, two-way ANOVA, Bonferroni's post test).

The persistent current was extremely variable both between cells and over time within the same recording. The scatter plot in Figure 3.7 shows that %INa$_P$ at -10 mV at 4, 8 and 12 minutes after whole-cell configuration, for both splice variants in the two internal solutions. Times are approximate because experiments were stopped for brief intervals to correct for small changes in capacitance and series resistance. This plot presents an example of the temporal aspect of $Na_V1.1$ persistent current (although for clarity, in the remainder of the study the average persistent currents accounting for all time intervals will be used). In support of the current density data presented in Figures 3.5 and 3.6, the persistent current was more prominent in the presence of chloride, with $Na_V1.1$-5N having a significantly greater average %INa$_P$ compared to CsF recordings (Mean ± SEM %INa$_P$ CsF 3.6 ± 1.1%, n=13; CsCl 12.2 ± 1.7, n=8; P<0.01, two-way ANOVA, Bonferroni's post-tests). There was also a similar but non-significant trend for $Na_V1.1$-5A (Mean ± SEM %INa$_P$ CsF 7.6 ± 1.7%, n=12; CsCl 12.8 ± 2.5, n=10, Figure 3.6). As demonstrated by Figure 3.7 it is only after 8 minutes into whole-cell the $Na_V1.1$-5N persistent current significantly reduces using CsF internal solutions (at 8 and 12 minutes, CsF, 0.5 ± 1.5 %, n=10; 0.9 ± 0.8, n=10 versus CsCl, 15.0 ± 2.3%, n=6; 10.9 ± 2.2 %, n=4; P<0.001; two-tailed t-test; Figure 3.7).

This effect was less marked for 5A-containing channels (Figure 3.7).
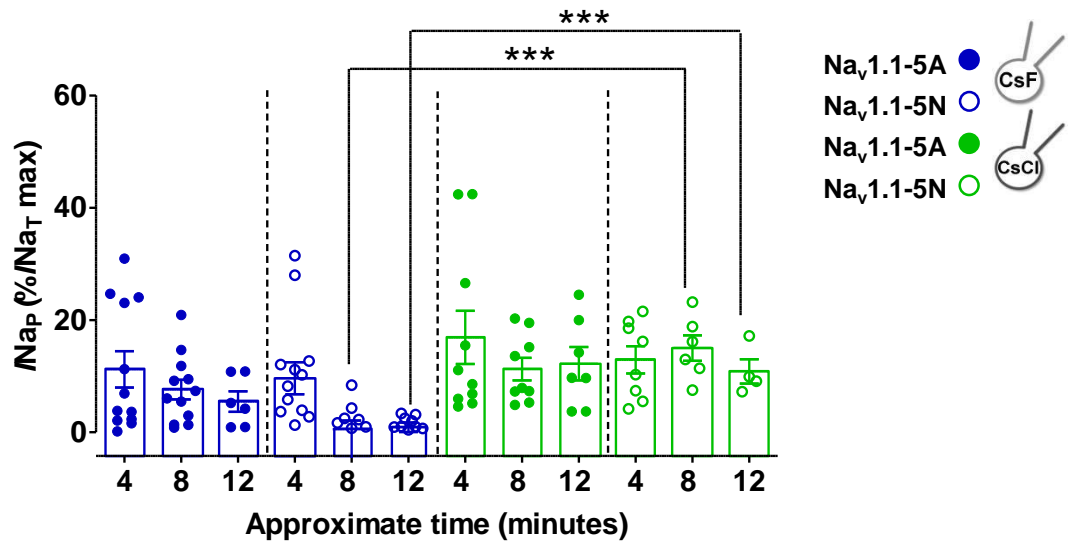
Figure 3.7 Persistent currents from the two splice variants are variable in HEK cells but remain stable during the timecourses of recordings using CsCl but not CsF. %INa$_P$ was calculated as shown in Figure 3.6 A. The graph shows the persistent current from individual cells at 3 times points during a single recording. Unlike 5A-containing channels, using CsF after 8 minutes after obtaining whole cell configuration, the amount of Na$_V$1.1-5N persistent current significantly decreases (***P<0.0001, two-tailed t-test). Additionally, post 8 minutes both splice variants consistently produce larger persistent currents in the absence of fluoride.

3.2.1 Fluoride/Chloride 3: Na$_V$1.1 splice variant rate of current decay is slowed in the presence of chloride

The normalized current from individual cells was fit to a mono-exponential decay after a step from -80 mV to test potentials ranging between -20 mV and +20 mV from 90% of peak current amplitude. The mean (±SEM) rate of decay (τ_h) was calculated from individual fits at each test voltage. This increased stability of non-inactivating current in chloride is consistent with the slower rate of inactivation for both variants in this intracellular solution. In fluoride the Na$_V$1.1-5N currents decayed significantly faster

between -10 mV and 20 mV compared to in chloride, (P<0.001, at each potential, two-way ANOVA, Bonferroni's post-tests). Although the $Na_V1.1-5A$ rate of inactivation overall was faster in fluoride (P=0.002, two-way ANOVA), there was no significant change in rate at any individual voltage (Bonferroni's post-test; Figure 3.8).

In the same intracellular anion, the rate of inactivation between splice variants was different. For example, using CsCl solutions the overall rate of inactivation for $Na_V1.1-5N$ was significantly slower than $Na_V1.1-5A$ (P=0.003, two-way ANOVA). Using CsF solutions, however, the opposite was the case: $Na_V1.1-5A$ rate of current decay was significantly slower (P=0.01, two-way ANOVA). As seen in Figure 3.8 this reversal in the relative rate of inactivation was due to the much larger shift experienced by $Na_V1.1-5N$ channels when the anion was changed (open symbols). Compared to channels with the 'adult' exon, channels with exon 5N, appeared much more sensitive to intracellular fluoride, slowing ~4 fold at several potentials, while $Na_V1.1-5A$ channels only slowed ~2-fold at similar potentials (e.g. 0 to 20 mV). These data are consistent with data in Figure 3.8 showing only $Na_V1.1-5N$ channels had increased persistent currents using CsCl. Current decay for these channels appears to be both slower and less complete in chloride than in fluoride, while decay of currents from $Na_V1.1-5A$ was less sensitive to changes in anion.
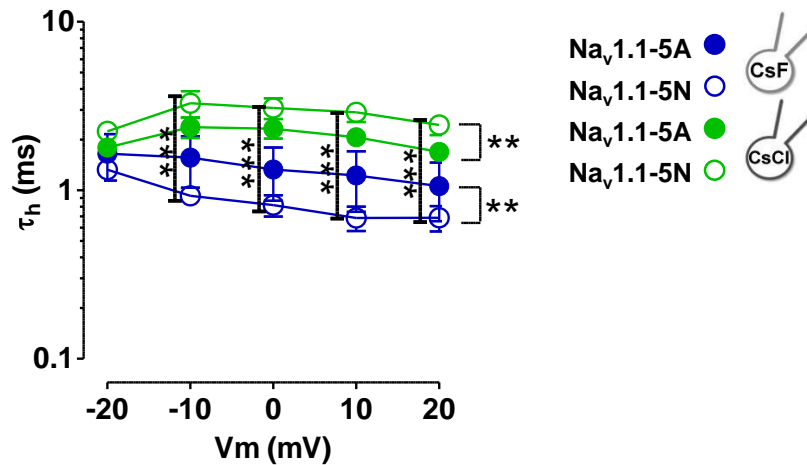
Figure 3.8 Semilogarithmic plot of the fast time constants derived from mono-exponential fits to the decay of the current over a range of test potentials. The rate of current decay was significantly slowed in the presence of CsCl compared to CsF for $Na_V1.1$-5N only (***$P<0.0001$, two-way ANOVA, Bonferroni's post test). Moreover, the $Na_V1.1$ do show a differential rate of current decay in both solutions (**$P<0.01$; two-way ANOVA, Bonferroni's post test) but using CsCl $Na_V1.1$-5A currents decay faster and conversely using CsF more slowly, compared to $Na_V1.1$-5N channels.

3.2.1 Fluoride/Chloride 4: Both $Na_V1.1$ splice variants have more hyperpolarized voltage dependence of activation in fluoride

Not only did the change in anion alter the rate of inactivation and stability of persistent currents as might be predicted from disruption of G-proteins (Figure 3.9 B), but the presence of fluoride also changed the voltage-dependence of activation (Figure 3.9 A). However, unlike inactivation the effect of fluoride on activation was similar for both splice variants. The V_{50} activation for both splice variants was significantly shifted by ~ 6 mV in depolarizing direction in the presence of chloride (mean ±SEM V_{50act} CsF: 5A -21.2 ± 1.7 mV, n=9 versus CsCl 5A -15.4 ± 1.3 mV, n=18, $P<0.01$; CsF: 5N -22.8 ± 1.2 mV, n=14 versus CsCl 5N -17.8 ± 1.3 mV, n=13, $P<0.01$, two-way ANOVA, Bonferroni's post-test). The voltage sensitivity of activation was unaffected by intracellular anion (mean ±SEM k:

204

CsF versus CsCl: P=0.7, two-way ANOVA; Figure 3.9 B). Additionally the time course of activation was significantly accelerated for both splice variants in presence of fluoride (mean ±SEM ms: 5A CsF versus CsCl: P=0.02; 5N CsF versus CsCl: P<0.0001, two-way ANOVA; Figure 3.9 B).

These results also indicate that within the same internal solution the activation midpoints of $Na_V1.1$ splice variants were comparable (mean ±SEM V_{50act}: CsF 5A versus 5N: P=0.4; CsCl 5A versus 5N: P=0.3, two-tailed t-test). However, using CsCl-based solutions $Na_V1.1$-5N time-course of activation was significantly slowed compared to $Na_V1.1$-5A, which was not the case in fluoride (between -20 mV and + 20 mV mean ±SEM ms: CsF 5A versus 5N P=0.7; CsCl 5A versus 5N P=0.03, two-way ANOVA: Figure 3.9, C), suggesting fluoride conceals possible differences in the activation kinetics between the two splice variants. The 10 – 90 % rise-time to peak was calculated from normalized current from individual cells after a step from -80 mV to test potentials ranging between -20 mV and +20 mV.

A

B

C
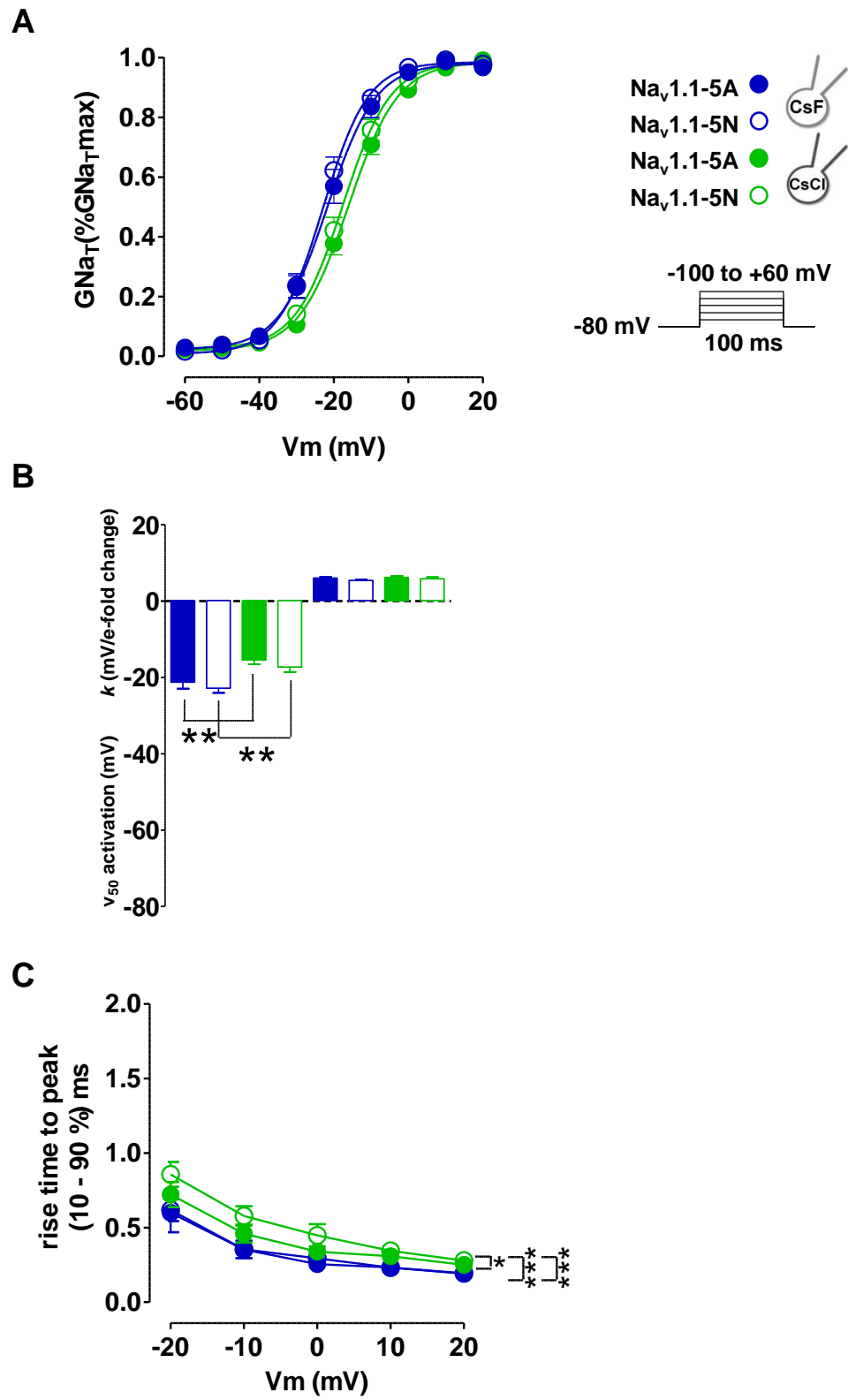
Figure 3.9 (previous page) A change in the intracellular anion changes the gating and kinetics of Na$_V$1.1 splice variant activation Normalized conductance of Na$_V$1.1 splice variants using CsCl and CsF based solutions (***A***) and mean ($\pm$SEM) $_{V50}$ of activation derived from Boltzmann fits of individual cells (***B***) show that the voltage dependence of Na$_V$1.1 splice variant activation is shifted in a more depolarized direction in the presence of chloride (**P=0.01, two-way ANOVA, Bonferroni's post-tests. Voltage protocol as in inset. Mean ($\pm$ SEM) steepness of curves (k) were unaffected. ***C.*** In the presence of fluoride, the kinetics of Na$_V$1.1 splice variant activation were accelerated (***P<0.001; two-way ANOVA) and concealed a slowing of Na$_V$1.1-5N channels exposed using CsCl intracellular solutions (*P<0.05; two-way ANOVA). Conductance was calculated from the current-voltage curve as described in the methods. The mean ($\pm$SEM) V$_{50}$ values and slopes factors (k) were calculated from Boltzmann fits of individual cells. The V$_{50}$ for activation is the voltage at which 50% channels are activated. The slope of describes the steepness of the curve and is an indicator of the voltage dependency of activation.

3.2.1 Chloride/Fluoride 5: Voltage dependence of inactivation is less sensitive to changes in intracellular solutions

Figure 3.10 A shows the relationship between prepulse potential and current available at -10 mV for both splice variants using CsCl- and CsF-based internal solutions. The mean ($\pm$SEM) V$_{50}$ values and slope factors (k) of inactivation were calculated from Boltzmann fits of individual cells (Figure 3.10 B). V$_{50}$ of inactivation represents the voltage that produces half maximal channel inactivation. Only fast inactivation was assessed using a protocol that looked at the current available at -10 mV, 30 ms test pulse following a range of voltage prepulses lasting 100 ms.

The V$_{50}$ of inactivation for both splice variants was unaffected by a change in intracellular anion (two-way ANOVA, Bonferroni's post-test). However at individual points there were some small but significant differences in channel availability. At more hyperpolarized potentials (-60 mV and -50 mV) fewer Na$_V$1.1-5A channels were available using fluoride (CsCl versus CsF: P<0.01 for noted potentials, Bonferroni's post test). Additionally in the presence of this anion Na$_V$1.1-5A the mean ($\pm$SEM) slope factor was increased by 1.9 $\pm$ 1.0

mV/e-fold change suggesting decrease in voltage sensitivity (mean ±SEM k 5A: CsF 8.1 ± 0.9 ms, CsCl 6.2 ± 0.5 ms; CsCl versus CsF: P<0.05; Bonferroni's post test). The presence of fluoride altered voltage dependence of $Na_V1.1$-5N inactivation at more depolarized potentials, between -50 mV and -30 mV; again significantly fewer channels were available (CsCl versus CsF: P<0.05 for noted voltages, Bonferroni's post-test). Importantly, when compared using the same intracellular anion, the voltage dependence of inactivation between the splice variants was not significantly altered at any voltage (CsF: 5A versus 5N: P=0.13; CsCl: 5A versus 5N: P=0.4; two-way ANOVA).
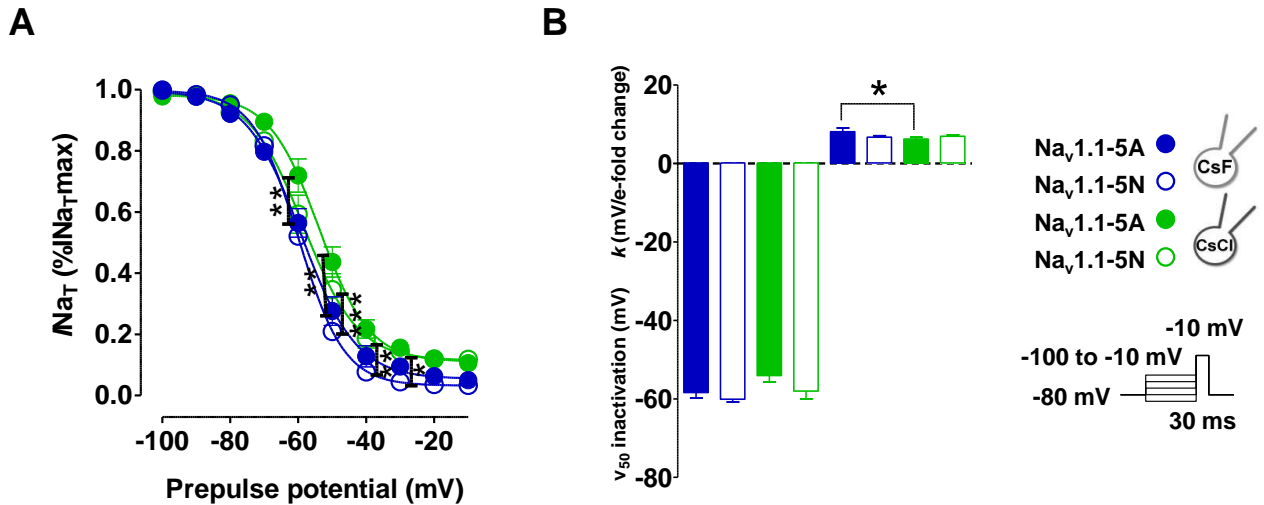
Figure 3.10 The voltage dependence of $Na_V1.1$ splice variant inactivation shifts to more depolarized potentials at specific voltages using CsCl intracellular anions. *A.* The voltage dependence of inactivation of maximal peak transient currents shows that at more hyperpolarized potentials significantly fewer $Na_V1.1$-5A channels were available in fluoride compared to chloride. **P<0.01; two-way ANOVA Bonferroni's post test. This was similar for $Na_V1.1$-5N but at more depolarized potentials. ***P<0.0001, *P<0.05, two-way ANOVA Bonferroni's post test. voltage protocol as in inset. *B.* In all conditions the mean (±SEM) $Na_V1.1$ midpoints of inactivation were comparable. The mean (±SEM) slope factor for $Na_V1.1$-5A was significantly increased using CsF but not CsCl based intracellular solutions; indicative of a decrease in voltage sensitivity of inactivation. *P<0.05, two-way ANOVA, Bonferroni's post-test.

3.2.1 Chloride/Fluoride 6: Summary

Not only did the change in anion alter the stability of persistent currents and rate of inactivation but the presence of fluoride also changed the voltage-dependence of activation, and to a lesser extent voltage-dependence of inactivation. Voltage dependence of activation is not thought to be a key target of AEDs; however, the rate of inactivation and stability of INa$_P$ are both likely to contribute to the two mechanisms of AED block. Consequently, changes introduced by the presence of fluoride, including those which are more pronounced in Na$_V$1.1-5N, could obscure the impact of AEDs on the splice variants. The remainder of this study was completed using CsCl-based solutions.

3.2.2 Temperature 1: The effects of elevated temperatures on the biophysical properties of Na$_V$1.1 splice variants

Mutations in *SCN1A* are associated with temperature dependence of epilepsy symptoms and the polymorphism rs3812718 may be associated with vulnerability to febrile seizures. Therefore it was investigated whether the Na$_V$1.1 splice variants were also different when currents were recorded at physiological temperatures.

A

Na$_v$1.1-5N   ITFA**F**VTEFV**N**LGN**F**SALRTFR
Na$_v$1.1-5A   ITFA**Y**VTEFV**D**LGN**V**SALRTFR
Na$_v$1.1-D207N ITFA**Y**VTEFV**N**LGN**V**SALRTFR

B

Na$_v$1.1-5A ■   Na$_v$1.1-5N □

1 nA
2 ms

Na$_v$1.1-D207N ▲

-60 to +30 mV
-80 mV
10 ms

CsCl   37

C

INa$_P$ (%INa$_T$ max)

5A   5N   D207N

D

τ_h (ms)

Vm (mV)

E

Peak current density (pA/pF)

5A   5N   D207N

F

GNa$_T$(%GNa$_T$-max)

Vm (mV)

G

rise time to peak (10 - 90 %) ms

Vm (mV)

H

INa$_T$ (%INa$_T$max)

Prepulse potential (mV)

210
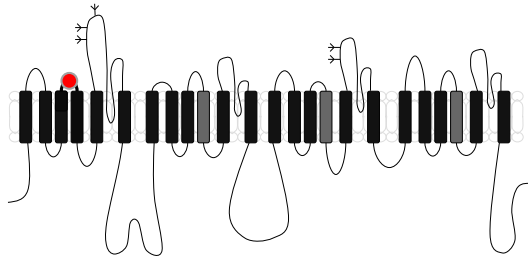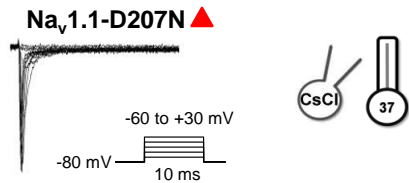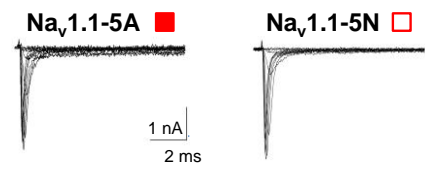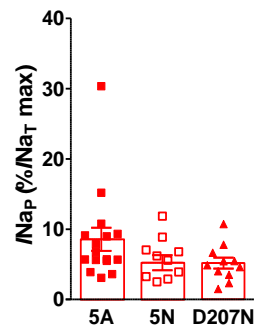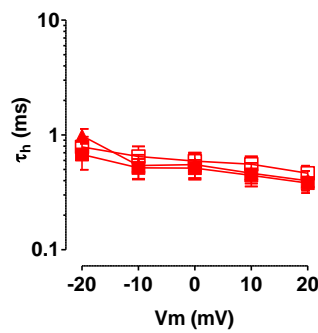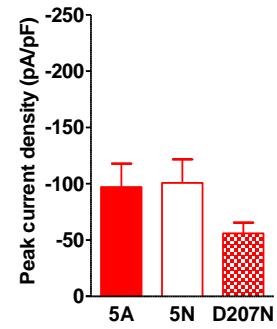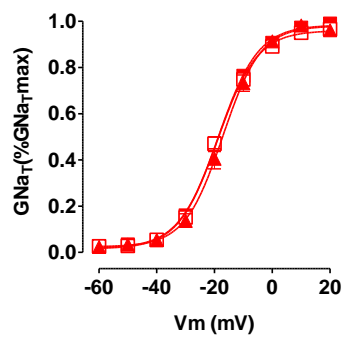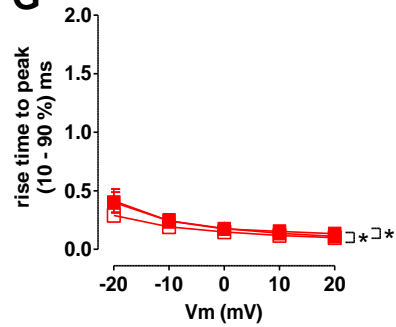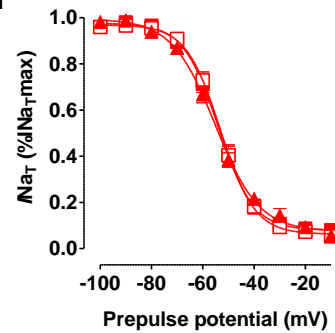
Figure 3.11 (previous page) at physiological temperatures both variants and the D207N mutant generate comparable macroscopic currents *A.* The sequence of the DI:S3-S4 linker encoded by exon 5N, 5A and by the D207N mutant that differs from exon 5A only by the single conserved amino acid, D207N. Topology of Na$_V$1.1 showing the location of D-N substitution (bottom panel). *B.* Representative traces from a cell expressing Na$_V$1.1-5A, Na$_V$1.1-5N and Na$_V$1.1-D207N. *C.* At physiological temperatures all three variants have small but stable persistent currents (P=0.1, one-way ANOVA) *D.* Changes in the D1 S3:S4 linker do not alter the rate of inactivation (decay) over a range of test potentials (5A vs 5N, P=0.2; 5A vs D207N, P=0.3; 5N vs D207N, P=0.8; two-way ANOVA) *E.* Current densities for all three channels are similar (P=0.3; one-way ANOVA). *F.* There are no differences in voltage dependence of activation (5A vs 5N, P=0.2; 5A vs D207N, P=0.1; 5N vs D207N, P=0.6). *G.* Na$_V$1.1-5N kinetics of activation were significantly faster than Na$_V$1.1-5A, and Na$_V$1.1-D207N channels over the voltage range, 5A vs 5N, *P=0.02, 5N vs D207N, *P=0.04 two-way ANOVA. This parameter was indistinguishable between Na$_V$1.1-5A and Na$_V$1.1-D207N channels (P=0.9, two-way ANOVA). *H.* Steady state inactivation between the three channels was similar (5A vs 5N, P=0.6; 5A vs D207N, P=0.8; 5N vs D207N, P=0.9).

3.2.2 Temperature 2: At physiological temperatures splicing has little effect on macroscopic currents from Na$_V$1.1 channels

The raw traces of Na$_V$1.1 splice variant sodium currents are shown in Figure 3.11 A and were evoked from current protocol shown in the inset. At physiological temperatures, averaging 37 ± 2 ^{o}C, Na$_V$1.1-5A and Na$_V$1.1-5N had comparable mean (±SEM) percentage persistent currents (5A: 8.5 ± 1.6%, *n*=16; 5N: 5.2 ±1.0 %, *n*=11; P=0.2, Mann-Whitney; Figure 3.11 B); although, %*I*Na$_P$ was variable among individual cells transfected with either variant. The values calculated for Na$_V$1.1-5A derived mean %*I*Na$_P$ displayed a larger 27% range (*n*=15) compared to 13% calculated for Na$_V$1.1-5N mean %*I*Na$_P$ (*n*=11; Figure 3.11 A). Consistent with %*I*Na$_P$ results, the overall rate of inactivation was comparable between the two isoforms over a range of test potentials (P=0.2, two-way ANOVA; Figure 3.11 C). Moreover, the two channel isoforms had similar mean (±SEM) peak current densities (5A -97.1 ± 20.1 pA/pF; 5N : -100.9 ± 20.8 pA/pF; P=0.9; Mann-Whitney);

midpoints and slope factors of activation (V_{50act} (5A versus 5N P=0.8) 5A: -18.5 ± 0.9 mV, n=15; 5N: -18.8 ± 0.8 mV, n=18; k (5A versus 5N P=0.7); 5A: 6.7± 0.4 mV/e-fold change; 5N: 6.5 ±0.3 mV/e-fold change; Mann-Whitney) and V_{50} and slope factors of inactivation ($V_{50inact}$(5A versus 5N P=0.8) 5A: -54.2 ± 1.2 mV, n=14; 5N: -53.1 ± 1.3 mV, n=11; k (5A versus 5N P=0.9); 5A: 6.4 ± 0.3 mV/e-fold change; 5N: 5.9 ± 0.7 mV/e-fold change; Mann-Whitney; Figures 3.11 E-H). However, although the change was small, Na_V1.1-5N channels did activate significantly faster than Na_V1.1-5A channels (P=0.02; two-way ANOVA; Figure 3.11 G).

3.2.2 Temperature 3: Which amino acid?

Na_V1.1-5A and Na_V1.1-5N differ at three amino acids (Figure 3.11 A). As a further control, Na_V1.1-5A channels were engineered to contain only the D>N switch that is conserved in several channels belonging to the VGSC family (Figure 3.11 A, position shown in red in the channel topology diagram). Two phenylalanines are introduced at positions 203 and 211 in human Na_V1.1-5N in addition to the D>N substitution. (Figure 3.11 A). Further experiments asked whether these supplementary amino acid changes obscured possible differences created by the D>N change (Figure 3.11 A). However, apart from the kinetics of activation the biophysical properties of Na_V1.1-D207N were indistinguishable from either Na_V1.1-5A or Na_V1.1-5N (Figure 3.11, red triangles). Na_V1.1-5N did enter activation significantly faster than Na_V1.1-D207N channels, over the voltage range (5N, n=16; =11; P=0.04, two-way ANOVA).

3.2.2 Temperature$^+$ 4: Experiments conducted at 'fever' temperatures were too unstable to produce sufficient data

It is possible that an increase of temperature by a few degrees from 37°C to 40°C to replicate 'fever' conditions associated with seizures in GEFS+ and SMEI, could introduce new differences between the macroscopic properties of both splice variants. Unfortunately recordings at +40°C for Na$_V$1.1-5A were not stable enough to produce data sufficient to make statistical comparisons. However, the data collected between 38-39^{o}C for Na$_V$1.1-5A and between 38-41^{o}C for Na$_V$1.1-5N did not suggest there was a robust difference between the voltage dependence of activation (5A versus 5N: P=1.0, two-way ANOVA; 5A n=6; 5N n=8; Figure 3.12 A), or inactivation (5A versus 5N: P=0.7, two-way ANOVA; 5A n=4; 5N n=5; Figure 3.12 B). Therefore any differences between the variants, at slightly higher temperatures, were likely to be very subtle.
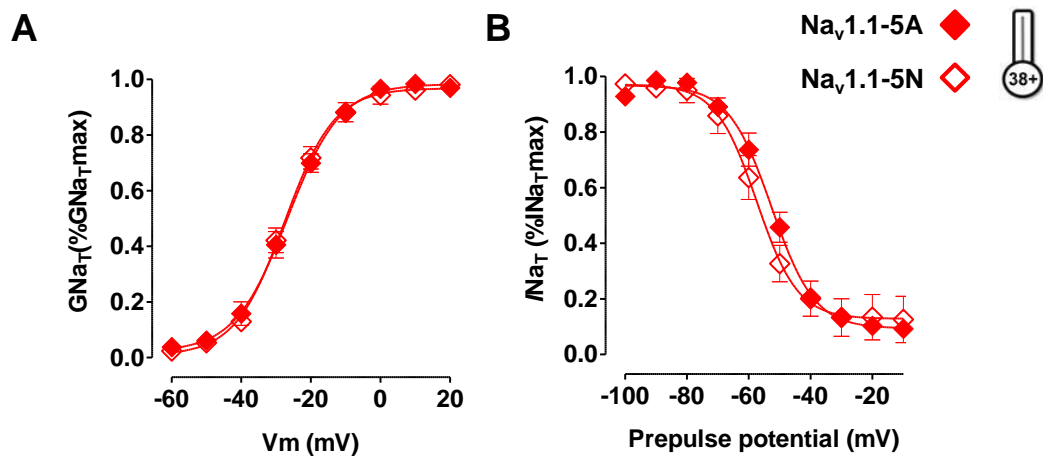
Figure 3.12 Preliminary experiments showed at 'fever' temperatures only subtle differences between Na$_V$1.1 splice variants gating were introduced. The voltage dependence of activation of peak conductance (*A*) and voltage dependence of inactivation maximal currents (*B*) for both splice variants calculated from recordings performed at

(previous page) temperatures above 38°C. No significant differences Na$_V$1.1 splice variants were revealed for these gating parameters (Activation: 5A vs 5N, P=0.7; Inactivation: 5A vs 5N, P=0.3, two-way ANOVA).

3.2.2 Temperature 5: On comparison of room and physiological temperature recordings the rate of current decay was most affected by changes in temperature

Several parameters altered by fluoride, particularly those associated with fast inactivation, were also altered by temperature in similar ways, and as with fluoride, Na$_V$1.1-5N channels appeared more sensitive to changing temperature than Na$_V$1.1-5A channels. Elevation to 37^{o}C reduced the %INa$_P$ for both splice variants compared to RT recordings. The mean (±SEM) %INa$_P$ derived from Na$_V$1.1-5N at 37^{o}C was significantly decreased from 12.8 ± 2.5% (*n*=10) at RT to 5.2 ± 1.1% (*n*=11) at 37^{o}C (P<0.05; two-way ANOVA, Bonferrroni's post-test, Figure 3.13 A). Na$_V$1.1-5A followed a similar, although statistically non-significant trend, demonstrating a reduction of mean (±SEM) %INa$_P$ from 12.2 ± 1.7 % (*n*=8) at RT to 8.6 ± 1.6 % (*n*=16) at 37°C. As expected the overall rate of inactivation was significantly accelerated overall by a minimum of 1.5 ms for both channel isoforms (5A 21°C versus 5A 36 ± 1°C: P<0.001; 5N 21°C versus 5N 36 ± 1°C: P<0.001; two-way ANOVA, Figure 3.13 B) suggesting that at higher temperatures the fast inactivation is enhanced and long or late openings are suppressed.
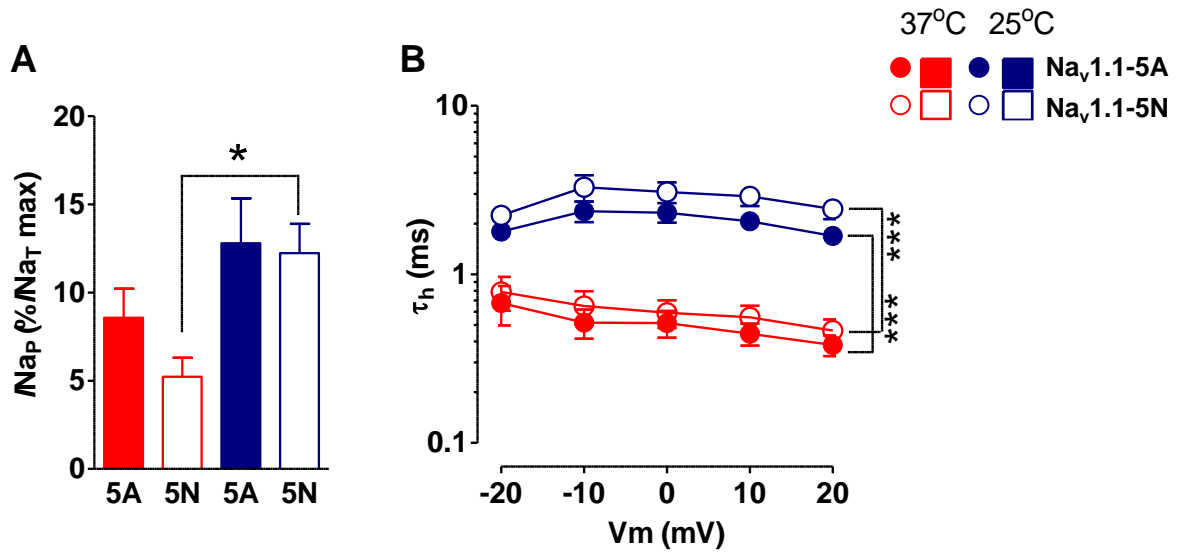
Figure 3.13 (previous page) Slow inactivation is more stable at lower temperatures. $Na_V1.1$-5N persistent current was particular vulnerable to change in temperature *P<0.05, two-way ANOVA, Bonferroni's post test (**A**) although the rate of current decay significantly accelerated at higher temperatures for both splice variants (**B**). ***P<0.0001, two-way ANOVA.

In contrast to the rate and stability of inactivation, the voltage-dependence of activation and inactivation were largely unaffected by an increase in temperature (Boltzmann fits activation 5A 21°C versus 5A 37±2 ^{o}C P=0.1; 5N 21°C versus 5N 37±1°C, P=0.6; two-way ANOVA, Bonferrroni post-tests; Figures 3.14 A & B) Although at -60 mV, at 37°C upon inactivation significantly more $Na_V1.1$-5N channels were available compared to those at 21°C (P<0.01; two-way ANOVA, Bonferrroni post-tests; Figures 3.14 C & D). This subtle change was not seen for 5A-containing channels (P=0.08; two-way ANOVA, Figures 3.14 C&D).
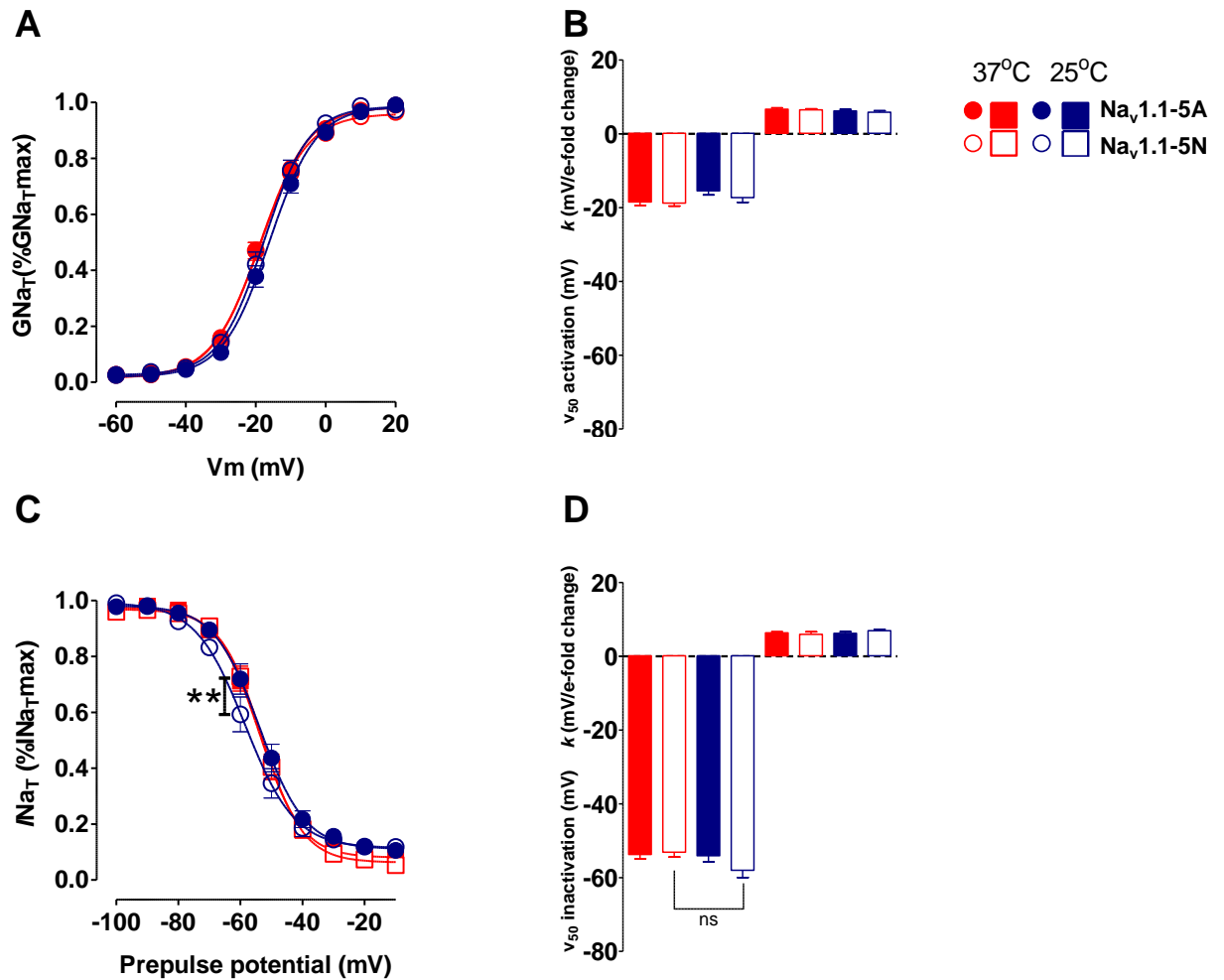
Figure 3.14 An increase in temperature has subtle effects on the gating of $Na_V1.1$ splice variants. The maximum conductance at several voltages, midpoints of activation and slope factors for both $Na_V1.1$ splice variants was unchanged by ~16°C increase in temperature (***A &B***) This was similar for the voltage dependence of inactivation although at -60 mV a greater proportion of $Na_V1.1$-5N channels had inactivated at RT. **P=0.01, two-way ANOVA, Bonferroni's post-test (***C &D***).

Although the voltage dependence of activation was unaffected at biological temperatures,

the time-course of activation was significantly accelerated for both $Na_V1.1$-5A and $Na_V1.1$-

5N (P<0.001; 37°C versus 21°C for both splice variants, two-way ANOVA; Figure 3.15).

This implies that overall temperature affects the kinetics of gating rather than its voltage

dependency. This is in contrast to the effects of fluoride, which although showing a similar

trend for effects on rate of inactivation were different on activation: Fluoride altered the voltage-dependence of activation for both splice variants, but temperature had no effect on voltage-dependence.
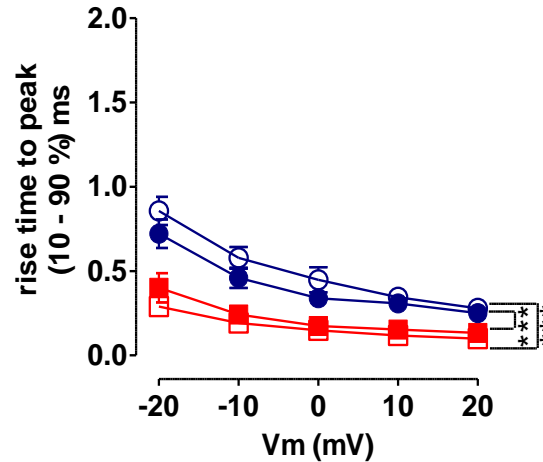
Figure 3.15 The timecourse of activation is significantly slowed at RT for both channel isoforms. ***$P<0.0001$, two-way ANOVA. A slowing in of $Na_V1.1$-5N rise to peak at RT compared to $Na_V1.$-5A channels is suppressed at higher temperatures. ***$P<0.0001$, two-way ANOVA.

3.2.2 Temperature 6a: $Na_V1.1$-5N recovers more rapidly from inactivation compared to $Na_V1.1$-5A at biological temperatures

Recovery from inactivation is thought to underlie the use-dependence of anti-epileptic drugs, including phenytoin. Splice variants were investigated for whether they differed in this parameter at physiological temperatures. Recovery from inactivation was assessed using a two-pulse protocol consisting of an initial step to -10 mV for 100 ms, a recovery interval of 2 ms, 10 ms and 20 ms at -80mV, and a test step to -10 mV for 30 ms. The current amplitude evoked by the test pulse was expressed as a fraction of the current from the prepulse to give a measure of fractional recovery. The raw trace in Figure 3.16 A show

217

the individual sweeps elicited from the recovery protocol from a cell transfected with $Na_V1.1$-5N. Unfortunately, at physiological temperatures, cells were too unstable to complete a detailed time course of recovery from inactivation.

The $Na_V1.1$-5N channels were significantly faster than $Na_V1.1$-5A over the time range tested (5A $n=8$, 5N $n=10$; P<0.0001; two-way ANOVA; Figure 3.16 A) and particularly at longer time intervals. At 10 ms and 20 ms proportionally more $Na_V1.1$-5N channels had recovered compared to 5A-containing channels (5A versus 5N at 10 ms, P<0.01; 5A versus 5N at 20 ms, P<0.05; Bonferroni's post test). Additionally, this difference appears to depend entirely on the D>N substitution, as $Na_V1.1$-D207N channels were indistinguishable from $Na_V1.1$-5N channels (D207N $n=13$; P=0.06, two-way ANOVA; Figure 3.16 C). In contrast over the complete time course $Na_V1.1$-D207N channels were significantly faster than $Na_V1.1$-5A channels (P=0.0018, two-way ANOVA; Figure 3.16 C).
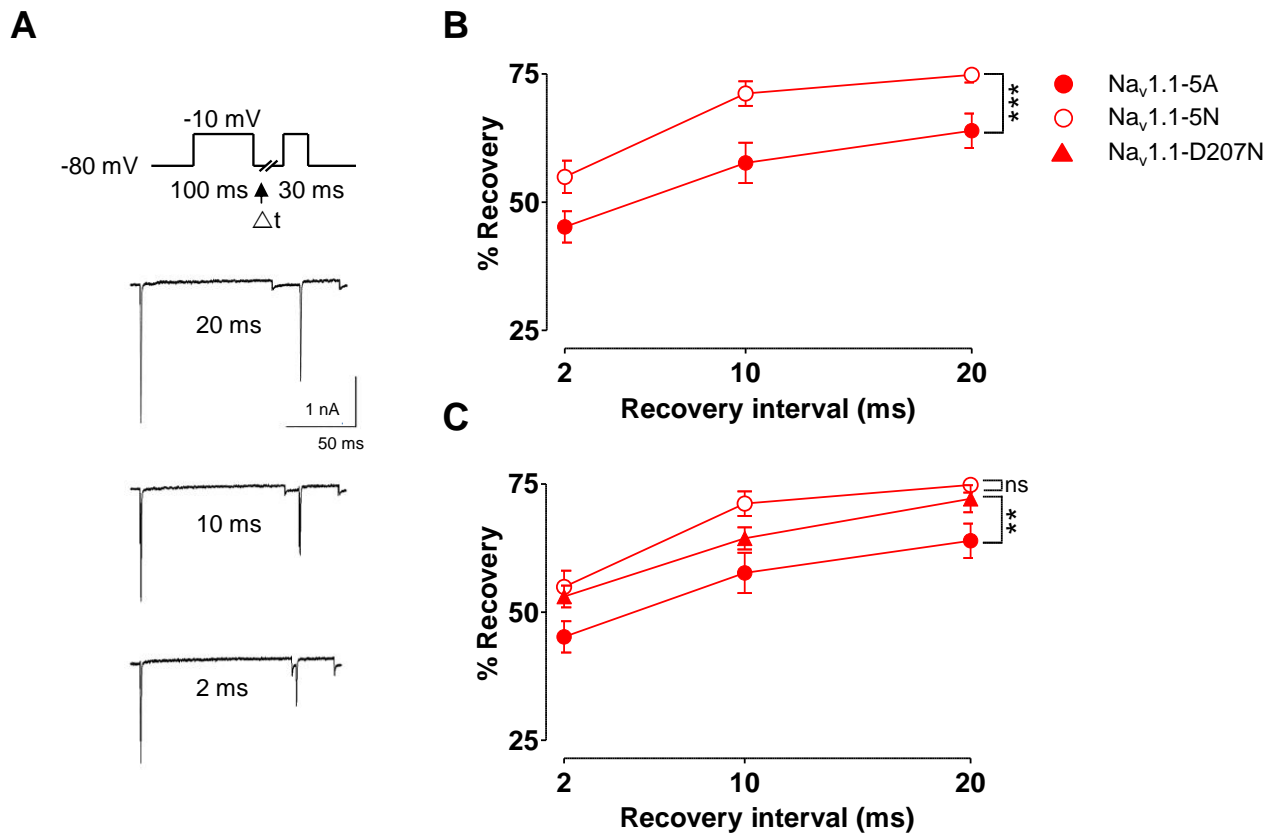
Figure 3.16 Channels containing exon 5N recover more rapidly from inactivation and the conserved amino acid change D207N is sufficient to account for the change. *A.* Raw traces from cells transfected with $Na_V1.1$-5N. Currents were evoked using the protocol at top. *B.* $Na_V1.1$-5N channels are more available for activation than $Na_V1.1$-5A channels for time points between 2 and 20 ms after prolonged depolarisations. ***P<0.0001 *C.* $Na_V1.1$-D207N is not different from $Na_V1.1$-5N. P=0.06, two-way ANOVA. But this mutant does recover faster from inactivation than $Na_V1.1$-5A channels **P=0.002, two-way ANOVA.

3.2.2 Temperature 6b: Phenytoin masks differences in recovery from inactivation between $Na_V1.1$ splice variants

Figures 3.17 A & B show preliminary $Na_V1.1$-5A phenytoin dose-response curves at 11 ms and 19 ms recovery intervals, performed by Stephanie Schorge. These experiments were lengthy and were recorded at RT to improve stability and allow multiple drug doses to be tested on individual cells. The calculated IC_{50} at 11 ms and 19 ms were 53 μM and 64 μM

(*n*=3-6) respectively. In the following experiments, therefore, 50 μM phenytoin was used, as this concentration is similar to clinically relevant serum levels (Scheyer *et al.*, 1994).

A

B
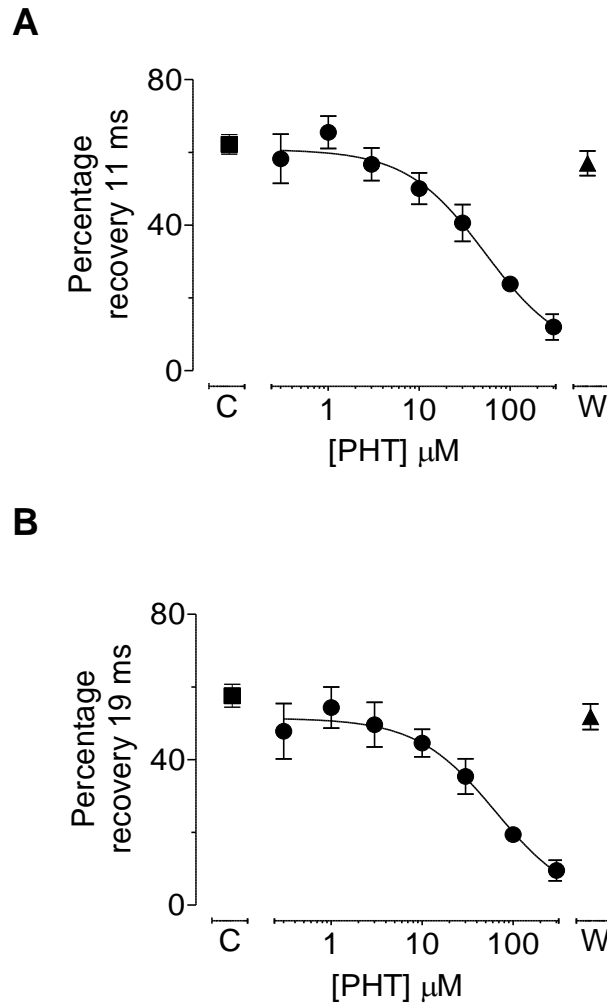
Figure 3.17 Concentration response curve for Na$_V$1.1-5A at RT. Recovery from inactivation for Na$_V$1.1-5A channels after 11 ms (**A**) or 19 ms (**B**) in control (C, squares), phenytoin (circles), and wash (W, triangles). n=3-6 for all points. IC$_{50}$ at 11 ms was 53 μM. IC$_{50}$ at 19 ms was 64 μM.

A two-way ANOVA revealed in the presence of phenytoin the difference in the rate of recovery from inactivation over the time-interval range between the splice variants was concealed (5A *n*=8, 5N *n*=6; P=0.3; Figure 3.18 A). This suggests that individuals with a

higher percentage of the neonatal variant may have proportionately larger effects on the recovery from inactivation in the presence of clinically relevant doses of phenytoin. Moreover, because over the experimental time range $Na_V1.1$-5N and $Na_V1.1$-D207N were comparable in their response to this drug (D207N n=6; P=0.6; two-way ANOVA; Figure 3.18 B), and in control conditions, the change in drug efficacy may also be relevant to other VGSCs containing the conserved D>N substitution.

A

B

Legend:
- ● $Na_V1.1$-5A
- ○ $Na_V1.1$-5N
- ▲ $Na_V1.1$-D207N
- ----- 50 μM PHT
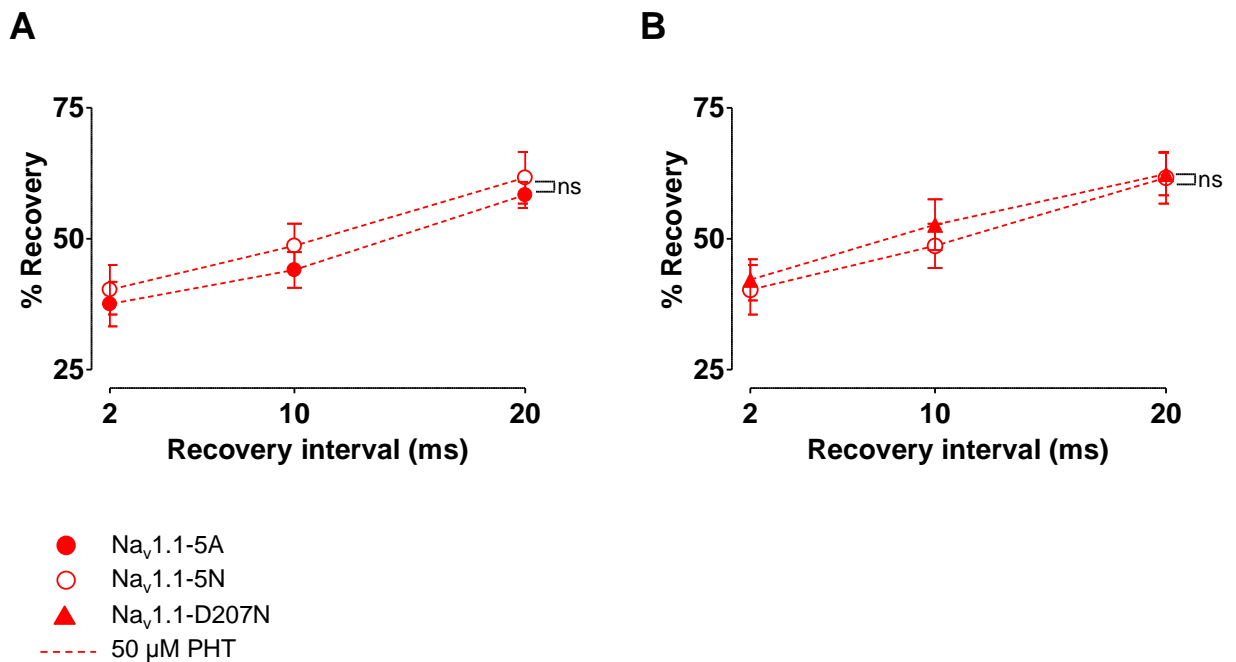
Figure 3.18 Addition of phenytoin (PHT) obscures the difference in recovery from inactivation. *A.* There is was no difference in the recovery from inactivation between the splice variant channels in the presence of 50 μM PHT. P=0.3, two-way ANOVA. *B.* $Na_V1.1$-D207N is reduced to a similar rate of recovery of $Na_V1.1$-5N channels. P=0.6, two-way ANOVA.

221

3.3 Discussion

The main aim of this chapter was to determine whether biophysical differences between $Na_V1.1$-5A and $Na_V1.1$-5N could explain the link between the rs3812718 polymorphism in *SCN1A* and altered drug responsiveness in patients. $Na_V1.1$ splice variants differ in a region close in proximity to the voltage sensor in the first domain, providing a molecular rationale behind this hypothesis. Several reports indicate that patients homozygous for the mutant A allele are expected to have a greater proportion of $Na_V1.1$-5A (Tate *et al.,* 2005; Heizen *et al.,* 2007) require higher phenytoin and lamotrigine dosages at maintenance and serum levels respectively (Tate *et al.,* 2006; Krikova *et al.,* 2009). In another study involving a large Japanese cohort, homozygous AA patients were more likely to be resistant to carbamazepine (Abe *et al.,* 2008). However not all studies have shown a relationship between the SNP and AED therapy (Kwan *et al.,* 2008; Zimprich *et al.,* 2008). To determine the possible functional impact these two splice variants in the presence or absence of phenytoin, macroscopic currents from whole-cell voltage clamp of HEK 293 cells transfected with $Na_V1.1$ splice variants were analyzed.

Ideally these experiments would have been performed in neurons. Neuronal models were investigated and are detailed in Chapter 6; but because of the technical difficulties with cloning unstable *SCN1A* cDNAs into mammalian expression vectors, this experimental avenue could not be pursued. Because the cell background was non-neuronal several measures were taken to make other recording conditions as comparable to the environment $Na_V1.1$ channels experience *in vivo* as possible. These focused on altering intracellular solutions to remove fluoride and, because GEFS+ causing mutations in *SCN1A* are

222

associated with fever, temperature. The latter was particularly important as the rs3812718 AA genotype has also shown to contribute to the development of childhood febrile seizures (Schlachter *et al.,* 2009).

The main findings of this chapter will be discussed in order of importance:

1. $Na_V1.1$-5N channels recover faster from inactivation compared to $Na_V1.1$-5A channels, which is dependant on a conserved amino acid change.

2. Phenytoin disproportionally inhibits $Na_V1.1$-5N channel recovery from inactivation.

3. Internal anions and temperature have significant effects on $Na_V1.1$ channel behaviour and therefore establishing accurate physiological recording conditions is essential.

4. Differences between $Na_V1.1$ splice variant behaviour were not due to changes in HEK 293 cell background or endogenous currents.

3.3.1 Recovery from inactivation

$Na_V1.1$-5N channels recovered significantly faster than $Na_V1.1$-5A over the time range tested and relied on the D207N change, as $Na_V1.1$-D207N channels were indistinguishable from $Na_V1.1$-5N channels. This suggests that the changes seen in recovery from inactivation of $Na_V1.1$-5N at physiological temperatures may also be present in other sodium channels with the D>N substitution at this site. Summarized in Table 1.6 (page 106) are the effects VGSCs exon 5 (or 6) splice variants at RT, heterologously expressed in various cell backgrounds, in the presence or absence of different combinations of β subunits and internal solutions. In support of this report this table demonstrates that in a

variety of conditions kinetics of inactivation, stability of slow inactivation and recovery from fast inactivation are primarily affected by splicing. Unfortunately, only Xu *et al.* 2007 (Na$_V$1.2) and Onkal *et al.* 2008 (Na$_V$1.5) used comparable intracellular solutions to this study. Unlike Na$_V$1.1 channels, the recovery of Na$_V$1.2-6A was significantly faster compared to Na$_V$1.2-6N channels; a smaller difference was shown for Na$_V$1.5 splice variants. It is difficult to determine whether the variation in recovery from channel inactivation is VGSC sub-type specific or simply that channels behave differently at lower temperatures, because Na$_V$1.1 splice variants share a high sequence identity to Na$_V$1.2 isoform. There is only the conserved asparagine to aspartate switch between Na$_V$1.2 isoforms but a (positive) lysine to aspartate between Na$_V$1.5 splice variants, plus an additional six amino acid changes (Figure 1.9). Onkal *et al.* 2008 mutangenized the Na$_V$1.5-6N lysine to aspartate and showed that the mutant channel recovered from inactivation faster than both Na$_V$1.5 channel isoforms. Together with the results in this study, this shows that a change in the amino acid in a position analogous to Na$_V$1.1-D207 has significant consequences for recovery from inactivation for another sodium channels. Onkal *et al.* 2008 surmised that this residue changes the local electric field detected by D1:S4 changing its outward movement depending on the charge of the critical residue. However Na$_V$1.1 and Na$_V$1.2 neonatal channels have a neutral charge at 207 but opposing inactivation recovery times compared to adult exon containing channels. Na$_V$1.1-5N contains additional changes in the S3-S4 linker, two large non-polar phenylalanines, which are less hydrophobic, compared to Na$_V$1.2-6N valines in comparable positions (Engelmen *et al.,* 1986), which may change the channel conformation in the lipid bilayer. Additionally differences in Na$_V$1.1 and Na$_V$1.2 may result from changes in experimental temperatures or

cell background.

The cellular localization of $Na_V1.1$ suggests that these channels contribute to action potential generation and propagation in GABAergic interneurons. From these data it is possible that patients homozygous for the mutant A allele experience a disproportionately slower recovery from $Na_V1.1$ inactivation which may disproportionately alter inhibition. In the immature nervous system, decreased inhibitory firing rates may be pro-excitatory at elevated body temperatures. Interestingly, different neuronal types show varying responses to changes in temperature (Guatteo *et al.,* 2005). In rat dopaminergic neurons elevated temperatures caused cellular depolarization and increased firing rates (Guatteo *et al.,* 2005) but in rat cortical visual cells under similar conditions contrasting effects were observed (Volgushev *et al.,* 2000). Therefore, it is possible that, in humans, inhibitory interneurons are particularly vulnerable to fever temperatures and the onset of febrile seizures may be coupled with the switch in *SCN1A* splicing in addition to other neuronal sodium channels. If the change in recovery from inactivation is only influenced by splicing in *SCN1A*, then inhibitory interneurons would be more sensitive to temperature-dependent changes in recovery from inactivation. However, it is possible that cells relying on *SCN2A/SCN8A* also have altered recovery from inactivation which is toggled as splicing shifts during development. In rodents, because *SCN1A* is not alternatively spliced, the comparison to humans is complicated, and only cells relying on *SCN2A/SCN8A* are likely to be affected by changes in splicing, including any changes in recovery from inactivation. It should be noted that although in rodents $Na_V1.1$ is upregulated in inhibitory interneurons it is not known whether this is mirrored in humans (Kalme *et al.,* 2007).

Briefly, what is the physiological role of Na$_V$1.1-5N during development? The immature nervous system comprises a different milieu of ion channels compared to the fully developed nervous system. Neurons within the immature nervous system are spontaneously active. This activity initiates an increase in intracellular calcium transients, which in turn switches on gene expression, leading to the transcription of growth factors, ion channels and other cellular machinery that eventually forms the mature nervous system (Moody & Bosma, 2005). During this gestation period the kinetics of ion channels expressed by immature neurons are different to those expressed by fully formed cells. This establishes specific firing patterns essential for proper development (Moody & Bosma, 2005) and may partly result from alternative splicing. It is difficult to select example studies of spontaneous immature neuronal activity that may be informed by splicing in *SCN1A* because many investigations use rodents models (Nam & Hockberger, 1997). However, clues to the role of Na$_V$1.1-5N may be given by Na$_V$1.3 channels, which are predominantly expressed in neonatal tissues (Felts *et al.,* 1997, but it should be noted that the function of *SCN3A* exon 6 splice variants is undetermined). Nonetheless, within rat DRG, like Na$_V$1.1-5N channels, Na$_V$1.3 channels were found to recover from inactivation rapidly (Cummins *et al.,* 2001) and their transient up-regulation corresponds to a period of spontaneous activity in immature rat DRGs, which may play a role in their normal development (Felts *et al.,* 1997; Cummins *et al.,* 2001; Moody & Brosma, 2005). Moreover, Na$_V$1.3 is expressed in Cajal-Retzius cells of the mouse preplate which are precursors of cortical neurons (Albrieux *et al.,* 2004). After birth Na$_V$1.3 expressing cells are capable of fast firing rates (Radnikow *et al.,* 2002). Controversially, this neuronal activity may contribute to their excitotoxic cell death, thought to be an important end process in corticogenesis (Radnikow

et al., 2002; Albrieux *et al.,* 2004). Interestingly, in both hippocampal cells from *SCN1A* knock-out mice (Yu *et al.,* 2006) and axotomized rat DRG cells (Cummins *et al.,* 2001) $Na_V1.3$ is upregulated. Perhaps this is either a neuronal compensatory mechanism or a marker of a pathological state?

3.3.2 The effects of Phenytoin

The main aim of this chapter was to determine why patients homozygous for the G allele of rs3812718, with an increased expression of exon 5N in $Na_V1.1$ respond better to AEDs and in particular phenytoin (Tate *et al.,* 2005; Tate *et al.,* 2006). From these results phenytoin obscured the difference in recovery from inactivation between the $Na_V1.1$ splice variants. Therefore patients homozygous for the wild-type allele of rs3812718, that is, with a greater proportion of $Na_V1.1$-5N channels, would undergo a more pronounced inhibition of $Na_V1.1$ activity compared to their AA homozygous counterparts (Figure 3.18 A). This demonstrates that alternative splicing of exon 5 in *SCN1A* alters recovery from inactivation: a biophysical parameter specifically targeted by AEDs. In terms of $Na_V1.1$ localization and *SCN1A* pathology these data are paradoxical because a complete loss of $Na_V1.1$ function leads to SMEI. Secondly, $Na_V1.1$ predominates in GABAergic interneurons and increased $Na_V1.1$ inhibition would lead to instability in the control of network excitability as GABAergic activity was surpressed, encouraging ictal activity. Possibly, the altered response is modified by other changes in $Na_V1.1$. *SCN1A* is not only alternatively spliced in exon 5 and incorporation/exclusion of other *SCN1A* regions may change the behaviour and drug response of $Na_V1.1$-5A or $Na_V1.1$-5N; although further work is needed determine their precise effects.

However, another perspective is that a reduction in inhibition of $Na_V1.1$ via the predominant expression of $Na_V1.1$-5A may be therapeutically beneficial. It is highly likely that *in vivo* phenytoin does not act solely on $Na_V1.1$ channels as it does not discriminate between VGSCs and can also bind to voltage-gated calcium and potassium channels. Therefore, patients with the AA genotype, which promotes the skipping of exon 5N, may tolerate increased levels of phenytoin because they have *less* inhibition of $Na_V1.1$ channels in GABAergic neurons, relative to inhibition in other cell types. This may result in less off-target AED reduction of inhibition, or shift the balance of AED block towards excitatory neurons.

The heterogeneity in GEFS+ patient AEDs drug response who harbour the same *SCN1A* mutation and the discrepancies in studies associating rs3812718 with drug dosage suggest that the molecular mechanisms of AEDs are not straightforward. Similar splicing occurs in other VGSCs, expressed in different neuronal types and could result in comparable interactions with phenytoin. For example, $Na_V1.2$ and $Na_V1.6$ are up-regulated in excitatory neurons (Chen *et al.,* 2002) and conserve the D>N switch; therefore, a change in splicing could alter drug efficacy in these neurons. Moreover in experimental epilepsy neonatal VGSCs are upregulated including $Na_V1.2$-6N (Aronica *et al.,* 2001). $Na_V1.2$-6A channels recover from inactivation faster than $Na_V1.2$-6N channels (Xu *et al.* 2007) but as discussed above their behaviour at elevated temperatures and interactions with AEDs is unknown. Further experiments assessing whether $Na_V1.1$-5N channels recover faster from inactivation and have a greater AED inhibition compared to $Na_V1.2$ and $Na_V1.6$ splice variants may help to explain why people with the AA genotype might tolerate higher dosages, that is, have proportionately less inhibition of interneurons for the same dose of

228

AED.

The association between rs3812718 and AED dosage is inconsistent (Zimprich *et al.,* 2008; Kwan *et al.,* 2008). Therefore, AED maintenance dosages in patients are likely to result from cumulative differences in genetic background or the association is spurious. Other SNPs within intronic and exonic regions of *SCN1A* and *SCN2A,* and another GEFS+ gene *GABRA2* also conferred multidrug resistance in ethnically diverse epilepsy patients (Chou *et al.,* 2003; Wang *et al.,* 2008; Kwan *et al.,* 2008; Lakhan *et al.,* 2009). There are also genetic variations in the genes encode proteins that absorb, distribute, metabolize and eliminate AEDs, which contribute to the maintained dose of GEFS+ patients (Loscher *et al.,* 2009). For example, several SNPs within the drug-transport pump gene *ABCB1*, which is expressed in the BBB and large intestine, significantly altered patient phenytoin plasma levels and efficiency of drug transport into the brain (Kerb *et al.,* 2001; Simon *et al.,* 2007). Additionally, in epilepsy models, post SE three GEFS+ genes coding for GABA$_A$ receptor subunits and the *HCN2* channel are dynamically regulated. This may affect in parallel neuronal, particularly GABAergic, phenotypes (Sperk *et al.,* 1998; Nishimura *et al.,* 2005; Powell *et al.,* 2008). The large problem with drug association studies is that there is limited information on the specific cause of epilepsy. If genetic, and a patient has severe mutation in *GABRA2* for example, the relative expression of Na$_V$1.1-5N or Na$_V$1.1-5A may be inconsequential. Moreover, phenotypic variation maybe further introduced by mutations in genetic modifier genes like *SCN9A*. Interestingly, Na$_V$1.7-5N is the main isoform expressed within the brain, which may also contribute to the sensitivity to phenytoin. Therefore, AED is likely to be a compromise between effectiveness and tolerability.

Although these results do not explain why in one report individuals with the AA genotype were significantly more resistant to carbamazepine (Abe *et al.,* 2008), observations do imply that the conserved D>N amino acid was a target of phenytoin, and perhaps therefore other AEDs. As shown in Figure 1.10 A, the structures of phenytoin and carbamazepine are dissimilar and it is possible that the configuration of $Na_V1.1$-5N is more effectively blocked by the carbamazepine. AEDs could be designed to specifically to block $Na_V1.1$ splice variants or, more likely, other VGSCs splice variants expressed in varying neuronal types. This may be feasible because both $Na_V1.1$ and $Na_V1.5$ for instance, have several amino acid differences in the D1:S3-S4 linker. Similar future experiments could determine the effects of sodium channel blockers like carbamazepine on VGSC splice variants. Splice variants of a cockroach VGSC that undergoes analogous splicing are pharmacologically distinct, with significantly different responses to the insecticide deltamethrin (Tan *et al.,* 2002), and demonstrates the possibility of distinguishing between closely related sodium channel variants.

3.3.3 $Na_V1.1$ macroscopic gating properties are changed by intracellular ions

One aim was to establish intracellular solution recording conditions that would allow reproducible measurements of the intrinsic macroscopic gating properties $Na_V1.1$ splice variants; particularly concerning the effects of phenytoin. At RT, the presence of fluoride changed the gating of both $Na_V1.1$ isoforms, shifting the voltage-dependence of activation (and to a lesser extent inactivation) in a leftward direction. Hyperpolarizing shifts in gating voltage dependency has also been observed in cell types in which $Na_V1.9$ channels are thought to predominate (Coste *et al.,* 2004): guinea pig (V_{50} activation only) and rat

myenteric sensory neurons (SNaC currents) and rat small DRG neurons (NaN currents; Rugiero *et al.,* 2003; Coste *et al.,* 2004). This change in gating was not observed in medium sized rat DRG neurons that express SNS/Na_V1.8 currents, suggesting that the effects of fluoride maybe dependant on cell background/VGSC sub-type. Indeed, the presence of fluoride also rendered Na_V1.1-5A channels to be less sensitive to voltage changes, suggesting that different internal ions can change distinctive channel properties.

The Costa *et al.* (2004) study is the most comprehensive report that has compared the properties of macroscopic sodium currents using either CsF or CsCl-based intracellular solutions. In the literature it is advised that cells expressing VGSCs should be dialyzed with CsF for at least 30 mins before voltage-clamp protocols are begun. In the whole-cell configuration, after 30 minutes of intracellular CsF equilibration Vanoye *et al.* (2006) demonstrated that the voltage dependence of activation was shifted in a ~7 mV hyperpolarizing direction from heterologously expressed Na_V1.1-5A channels. In this study currents were analyzed from recordings taken between 5 – 10 mins, not 30 mins, after breakthrough. Firstly, because fluoride shifted the voltage dependence in a hyperpolarizing direction compared to chloride, a longer dialysis time may have exacerbated this affect and not provided greater information about Na_V1.1 gating. Shorter experiment times prevented washout of intracellular regulatory proteins. Fluoroaluminate disrupts downstream signalling pathways and therefore persistent fluoride dialyzation may have increased the likelihood of uncontrolled variability in ion channel modulation by disrupted G-protein signalling. Lastly, preparations at elevated temperatures were stable for ~15 mins; therefore, longer experiment times would have made comparisons between recordings performed at RT and 37°C unreliable. It should be noted that Coste and colleagues (2004)

also allowed a shorter 5 – 8 mins intracellular solution equilibration time after breakthrough.

In the presence of chloride, the non-inactivating component of $Na_V1.1$ splice variant currents was more stable. Control recordings from untransfected HEK cells suggested that the persistent current component was derived from $Na_V1.1$, not endogenous channels. This was supported by $Na_V1.1$ channel overexpression in HEK cells and the voltage dependency of the persistent currents (Figure 3.5). The length of the voltage clamp protocol was not sufficient to determine whether there was a shift in the V_{50} of activation or inactivation for $I\text{Na}_P$. To assess $Na_V1.1$ slow inactivation/persistent currents the prepulse to -10 mV in the availability protocol would be extended from 100 ms to 1 sec, to allow for complete channel recovery from fast-inactivated states.

The kinetics of $Na_V1.1$ splice variant gating and in particular $Na_V1.1$-5N were significantly slower in the presence of chloride. This suggests that the three amino acid switch, in particular changing the surface-charge of the protein by the neutralization the extracellular D1:S3-S4 aspartate, may have affected the speed of $Na_V1.1$ activation and current decay (Hille 2001). Negatively charged sialic acids are attached to the Ig domain of β1 subunits and when associated with α-subunits contribute to a negative surface potential (Johnson *et al.,* 2004). CHO cells co-transfected with either $Na_V1.7$ or $Na_V1.2$ and un-sialylated β1 subunits demonstrated slower current decays compared to those transfected with wild-type β1 subunits (Johnson *et al.,* 2004), implying that a loss in surface-charge may slow channel gating. However, this hypothesis is highly speculative as between $Na_V1.1$-5A and $Na_V1.1$-5N there is only one charge change, and the solutions used in the latter study contained

CsF. However, from studies involving heterologously expressed channel chimeras of skeletal and cardiac VGSCs, D1 does appears to play a predominant role in the in the development of slow inactivation (Chahine *et al.,* 1996; O'Reilly *et al.,* 1999). Again, in these papers preparations were at RT, chimera channels were of mixed rat and human origin and the authors used CsF-based intracellulars. As discussed in the introduction it is extremely difficult to make strict comparisons with data in the literature because there are too many variables between papers and because slow inactivation/persistent currents are poorly understood and defined.

It is not clear why a change in current decay of $Na_V1.1$-5N was only revealed in chloride. Several intracellularly applied chemical agents and enzymes including tannic acid, formaldehyde, glyoxal, trypsin, slow VGSC inactivation (Hille 2001); but their chemical groups and actions are varied and provide little explanation into the selective mechanism of internal ions. It may not be the intracellular anion *per se* but G-protein regulation. Intracellular solutions used in by Coste *et al.* were supplemented with 0.4 mM GTP and slow inactivation and persistent currents derived from NaN and SNaC currents, both sensitive to changes in intracellular solution in this study, were similar in the presence of both halides. However when the CsCl and CsF intracellular solutions were not supplemented by GTP, the V_{50} of $Na_V1.8$, that is, sodium currents shown by Coste *et al.* not to be affected by intracellular ions, inactivation was shifted to the *right* (Saab *et al.,* 2003). This implies that G protein activity may cancel the affects of metal ions acting on 'less sensitive' channels and differentially modulate VGSC voltage dependency and the kinetics of inactivation.

During the first 12 mins after going whole-cell (Figure 3.7) $Na_V1.1$-5A derived $\%INa_P$ was stable in both intracellular solutions. However, only in chloride was the proportion of $Na_V1.1$-5N derived persistent currents stable during the whole recording. During the first few minutes after breakthrough, in fluoride, neonatal channel derived $\%INa_P$ was a similar proportion of peak INa_T compared to $Na_V1.1$-5N $\%INa_P$ recorded in chloride. Yet after 4 mins $Na_V1.1$-5N slow inactivation stabilized to a smaller $\%INa_P$ state. Again, this highlights the temporal aspect of fluoride in changing VGSC properties (Vanoye *et al.,* 2005; Coste *et al.,* 2004). From these results $Na_V1.1$-5N $\%INa_P$ maybe particularly sensitive to changes in modulatory proteins activated by AlF_4^- over time and/or are more sensitive to accumulating concentrations of fluoroaluminate.

To avoid changes due to the presence of fluoride, experiments were completed in 'more physiological' chloride. This was especially important because the rate of inactivation and stability of INa_P were both likely to be sensitive to AED block as well as because $Na_V1.1$-5N channels were more sensitive to fluoride than $Na_V1.1$-5A. Moreover, through single-channel analysis of SNaC currents, Coste *et al.* demonstrated that the properties of Ensemble currents best resembled macroscopic currents recorded using CsCl and not CsF. However, physiologically only 8 mM of Cl^- is found within cells (McCormick 1990), which is nearly 19-fold less than the contents of the intracellular pipette used in this study. It is possible, therefore that abnormal concentrations of Cl^- ions may also have had adverse affects on channel gating. High concentrations of intracellular chloride significantly attenuated G-protein regulated currents recorded from rat hippocampal neurons, compared to currents recorded in higher concentrations of methane-sulfonate (Lenz *et al.,* 1997). The authors surmised that chloride ions may also disrupt G-protein function or the directly

membrane channels expressed by CA1 neurons (Lenz *et al.,* 1997).

Coste and colleagues (2004) tried to address why fluoride affected the gating of specific VGSC currents by measuring the effects different internal solutions on NaN and SNS gating currents. From their results the authors surmised that through an unknown dynamic mechanism fluoride traps the voltage sensor in a pre-open closed state, preventing it returning to deeper closed states that perhaps can occur in chloride. Consequently a smaller change in the voltage across the membrane is required to open the channel. The authors hypothesized that fluoride could exert this effect via three mechanisms:

1. Fluoride may screen the surface-charges more effectively compared to chloride, changing voltage sensor properties. Although they argued this theory was improbable because no effects were observed for SNS currents and both halide ions have the same valency number.

2. Fluoride ions may bind to positive surface charges on the channel decreasing surface charge concentrations and potentials. Again Coste *et al.* 2004 dismissed this hypothesis as fluoride ions have a very low affinity to positively-charged groups.

3. Lastly, fluoride may exert its effects indirectly through downstream signalling pathways. The authors favoured this explanation as this may also account for why distinct VGSC currents were differentially affected.

The third hypothesis could be tested by supplementing the intracellular solutions with deferoxamine, an aluminium chelator; this would prevent the formation of AlF_4^- ions. This is not common practice and in this study deferoxamine was not used as experiments

involving $Na_V1.1$-R1648H could not have been compared to those in the literature. Moreover, the effects of protein kinases could also could be assessed by supplementing different internal solutions with agents that manipulate their function; for instance, the non-selective Isoquinoline sulfonamide protein kinase inhibitor, H7 (Saab *et al.,* 2003).

3.3.4 The effects of temperature on $Na_V1.1$ behaviour

In the presence of chloride, at elevated temperatures both the voltage dependency and kinetics of gating of $Na_V1.1$ splice variant and $Na_V1.1$-D207N channels were indistinguishable. This implies that *in vivo* there are no differences in these parameters for $Na_V1.1$ splice variant channels. Experiments conducted above $38^{o}C$ suggested that at fever temperatures the voltage dependency of activation and inactivation of $Na_V1.1$ isoforms are also similar. However, because too little data was collected for extensive biophysical analysis, differences in other parameters cannot be excluded. A few cells did survive high temperatures, but were often larger than normal HEK cells (~60 pF) and derived from a 'healthier' low passage number. Although these studies would be feasible in future experiments the integrity of the cell membrane was probably better preserved in larger cells and this would pose problems for clamping the membrane. Therefore, it is unlikely that these studies could be routine and would have to be performed in a low passage 'window'.

Elevating the temperature of recordings to $37^{o}C$ significantly reduced %INa$_P$ from $Na_V1.1$-5N. Additionally, the rate of current decay and entry into activation was significantly accelerated for both $Na_V1.1$ splice variants at biological temperatures. This implies that higher temperatures increased the kinetic rates of gating and therefore slower states of inactivation observed at RT are more likely to reflect a reduction in kinetic energy rather

than a true physiological property. The voltage dependency of activation and inactivation were largely unaffected by a change in temperature. However, at lower temperatures significantly fewer $Na_V1.1$-5N channels were available at -60 mV. Perhaps at this voltage neonatal channels are closer to an inactivated state compared to adult channels, a difference which is concealed at higher temperatures.

This is the first study to examine the effects of temperature on VGSC splice variant channels. A similar study was performed using $Na_V1.2$-5A channels expressed in HEK 293 cells (Thomas *et al.,* 2009). The voltage dependency of activation and inactivation was sequentially shifted to more depolarized potentials with increasing temperatures: $22^oC \rightarrow 37^oC \rightarrow 41^oC$. However, a CsF-based intracellular was used and only an *n* of 4 was obtained for 41^oC recordings, therefore the results may be unreliable. Similar to the results in this study the speed of sodium current inactivation was accelerated at higher temperatures (Thomas *et al.,* 2009). Similarly, the kinetics of fast inactivation for $Na_V1.4$ channels were significantly slower at RT compared to recording performed at 30-32^oC (Sugiura *et al.,* 2003; Carle *et al.,* 2009). The voltage dependence of $Na_V1.4$ gating at different temperatures differed between the two studies but experiments were performed in varying internal solutions.

The biophysical effects of elevated temperatures on the VGSCs *in vivo* have been investigated intermittently over the past 30 years. However, recordings originate from different preparations and species and contain mixed populations of channels. At one extreme, VGSC gating at room and physiological temperatures is indistinguishable in human myoballs, rat peripheral myelinated nerve balls and skeletal muscle (Schwarz 1986;

Pröbstle *et al.,* 1988; Ruff 1999). In guinea pig cardiac myocytes, however, the voltage dependence of activation and inactivation was shifted depolarized potentials (Murray *et al.,* 1990). Other effects observed included increased sodium current density and channel Na+ conductance at higher temperatures (Murray *et al.,* 1990). Lastly, similar to reports involving heterologously expressed VGSCs the rate of current decay sodium currents *in vivo* are significantly faster at biological temperatures, suggesting that the kinetics of inactivation are particularly affected by temperature (Schwarz 1986; Pröbstle *et al.,*1988; Murray *et al.,*1990; Ruff 1999).

Changes in gating parameters are not readily separable using macroscopic data. Therefore from this study it cannot be determined absolutely whether changes in temperature and intracellular solutions resulted from alterations in activation or inactivation. From a biophysical perspective it would be interesting to gain a better understanding of $Na_V1.1$ splice variants function under different conditions. The ideal strategy would be to record from the splice variants in single-channel out excised patch configuration. At a single channel level it is possible to accurately determine whether more rapid current decays are coupled with faster inactivation and slow activation or slow inactivation and fast inactivation combined with a lowered probability of activation (Hille 2001 – p590). In addition, these recordings could determine if changes in persistent currents were due to late re-openings or to longer individual or bursting open states.

3.3.5 HEK 293 cell line is suitable cell model for investigating the biophysical properties of $Na_V1.1$ splice variants

Further controls demonstrated that untransfected HEK 293 cells at RT in the presence of

both fluoride and chloride and at $37^{\circ}C$ in chloride did not express contaminating currents. Microarray analysis demonstrated that the cellular background only slightly altered year to year. This may be due to changes in cell-culturing conditions, for example, serum changes within growth media. Although the samples were quality checked before hybridization the older mRNA sample was frozen at $80^{\circ}C$ and prolonged storage may have degraded the mRNA with periodic drops in temperature increasing the possibility of RNase activity. Nonetheless, from these results it is likely that the biophysical differences observed between $Na_V1.1$ splice variants in this study were physiological and not artefacts resulting from endogenous currents or cell background. Although the latter cannot be completely excluded and the numbers of HEK 293 microarray mRNA samples were too small to determine the expression levels of individual genes. This would have been helpful in determining the relative expressions of modulatory proteins including protein kinases. Despite this disadvantage the overall genetic background was consistent. This was particularly important with regards to $Na_V1.1$ persistent currents and β subunit regulation as both factors have been reported to be dramatically altered either by differential gene expression or cell type (Mantegazza *et al.,* 2005; reviewed in Avanzini *et al.,* 2007).

The experimental design of the microarray analysis could have been improved. The samples were not taken at consistent time-points throughout the three years of the study and the passage numbers were random. As mentioned previously the properties of cell lines can change with passage number (Hughes *et al.,* 2007). Using a one-way ANOVA algorithm, the microarray analysis software, Affymetrix Expression Console™ requires at least six samples to identify differentially expressed genes (UCL Scientific Support Services). The fluorescent value for each gene was normalized to a median value of all the 1000s of

239

probes on the array to ensure that individual signals were above the background levels of fluorescence. A change in fluorescent intensity was a deviation from the overall signal of the array. Another way to assess the change in abundance of a gene would be to compare relative signal between the gene of interest and a reference (housekeeping) gene. Housekeeping genes are thought to be highly expressed in all somatic cells, under all conditions but cell confluency can affect their gene transcription levels (Greer *et al.,* 2010). In numerous cell lines, however, β-actin is stably expressed at varying cell confluences (Greer *et al.,* 2010). Therefore, to achieve more reliable results the cells would be harvested at 50% confluency in 35 mm dishes, similar to transfected HEK cells plating conditions. The relative intensities would be compared to β-actin signal to try to eliminate inconsistencies in gene expression caused by passage number and cell density.

The control recordings demonstrated that the sampling rate and filtering conditions used in this study were adequate for recording sodium currents at physiological temperatures. In the past, electrophysiologists have been reluctant to record INa at 37°C. The kinetics of sodium channels are too fast for older amplifiers to achieve successful voltage clamp. VGSC would open during the charging of membrane capacitance, before the membrane had been properly voltage clamped (Murray *et al.,* 1990). Improvements in the speed of modern amplifier circuits, ensuring that the series resistance was maintained below 2 MΩ and the small capacitance of HEK cells (average around 15 pF with a range up to 30 pF, personal estimation) circumvented this problem. Indeed, labs now routinely record sodium currents expressed in smaller cells at physiological temperatures (Cooper *et al.,* 2005). In this report series resistance compensation was very carefully used. Using a CsCl-based intracellular solution can be technically demanding as it often introduced a drop in holding

current of up to 200 pA, but only after going whole-cell. This is partly why many experimenters prefer to use CsF-based intracellulars. In these 'leaky' CsCl conditions, if the recording was stable series resistance compensation or supercharging was not used because the increased holding current would introduce fluctuating capacitance transients. However, compensation was often unnecessary if low series resistance was maintained by patching with wide-tipped, 1-2 MΩ, pipettes. According to the Axoclamp 700B manual, if the series resistance was 1 MΩ and cell capacitance 20 pF, in response to a voltage command the amplifier would clamp the membrane potential with a time constant of 20 µS, which is much faster than the opening of sodium channels even at physiological temperatures (10-90% rise time >100 µS). Moreover, the low series resistance combined with relatively small currents (typically less than 2 nA) ensured that even during peak inward currents the error introduced was less than 4mV during a voltage step. In addition, the voltage clamp was assessed off-line to permit confirmation of the raw-data that the voltage clamp was accurate.

3.3.6 Summary

In summary, recovery from inactivation, the parameter that robustly differs between $Na_V1.1$ channel isoforms is significantly attenuated by phenytoin, with $Na_V1.1$-5N channels demonstrating a greater sensitivity compared 5A-containing channels. These data provide two possible explanations for the association of the mutant allele with higher phenytoin dosage levels (Tate *et al.,* 2005; Tate *et al.,* 2006). The same concentration of the drug would demonstrate a smaller affect on channel availability in AA homozygous individuals, perhaps leading to a dose increase. However, *in vivo* the loss of $Na_V1.1$ results in severe

epilepsy, and changes that reduce inhibition of $Na_V1.1$ that is, splicing of *SCN1A* could be protective. Therefore, patients with a decreased transcription of exon 5N may tolerate higher doses of phenytoin because they experience less inhibition of $Na_V1.1$ channels. Future studies are necessary to determine whether conserved splicing in additional VGSCs also change drug efficacy. This may be relevant to drug actions throughout the central and peripheral nervous systems and in the heart and may impact future treatment for VGSC related pathologies.

In addition the biophysical properties of $Na_V1.1$ channels containing the neonatal exon are particularly affected by internal anions and temperature changes. These variables would be important to control in future work.

Chapter 4: The functional effect of splicing on the GEFS+-associated *SCN1A* mutation R1648H

4.*1 Hypothesis and aims*

Hypothesis: Since Na$_V$1.1-5N is upregulated in early development and patients with GEFS+ frequently exhibit age-dependent changes in seizure frequency and severity; it was hypothesized that the GEFS+-associated *SCN1A* mutation R1648H would differentially affect Na$_V$1.1-5N and Na$_V$1.1-5A. Because many individuals with mutations in *SCN1A* manifest seizures with only an increase in body temperature, it was surmised that recordings at higher temperatures would deleteriously alter the biophysical properties of both mutant channels.

Members of the family harbouring Na$_V$1.1-R1648H demonstrate a wide-ranging response to AEDs. Another proposal for this work was that R1648H patients with comparable rs3812718 genotypes - and therefore a similar ratio of Na$_V$1.1 splice variant channels - would have similar drug histories. Because it was hypothesized that Na$_V$1.1-R1648H channels in alternative splice variant backgrounds would respond differently to AEDs, particularly phenytoin.

Background and experimental aims: Missense mutations in *SCN1A* are associated with several monogenetic epilepsy syndromes, which often manifest during early childhood that may continue into adulthood with variable phenotypes. The aim of this section was to determine whether changes in alternative splicing could play a role in modifying disease severity, by altering the functional impact of mutations in *SCN1A* that cause epilepsy. *In*

vitro electrophysiological experiments using $Na_V1.1$-5A indicate that these mutations cause relatively subtle effects on channel behaviour, particularly on persistent currents. One mutation, R1648H, is associated with GEFS+ and in heterologous systems has been shown to produce an increased persistent current. This mutation affects a conserved positively charged arginine in the voltage sensor of the fourth domain. As previously discussed the GG genotype of rs3812718in *SCN1A* is associated with lower phenytoin dosage. This may result from this drug delaying proportionally more $Na_V1.1$-5N channel recovery from inactivation. The widely reported increase in $Na_V1.1$-R1648H derived persistent current may be an additional target for phenytoin, and it may be modulated by the altered inactivation of channels containing exon 5N.

4.2 Genetic background: R1648H is likely to co-exist with exon 5N in $Na_V1.1$

The original multigenerational family in which R1648H was identified provides an opportunity for determining whether the mutation in *SCN1A* segregates with the SNP rs3812718 which alters splicing in this gene. Although the mutation is too far from the SNP to determine directly whether the polymorphism and the mutation are allelic, segregation analysis can be used to show co-inheritance. The identity of the second allele of the SNP should be correlated with a varying amount of $Na_V1.1$-5N during development. If the presence of $Na_V1.1$-5N alters severity of epilepsy or seizures, then individuals with different alleles of the SNP may display different manifestations. While the distance between the SNP and the mutation are too far for direct sequencing, they are too closely linked for recombination to be likely even in a relatively large family. Therefore, only the allele of the SNP on the chromosome without the mutation is likely to vary. As detailed

phenotypic data for this family is available (Baulac *et al.,* 1999; Escagy *et al.,* 2000), it should be possible to determine whether clinical manifestation is correlated with the genotype of the SNP.

Analysis performed by Klaus Wanisch (a postdoc in the lab) showed that of the original $Na_V1.1$-R1648H pedigree (Escayg *et al.,* 2000; Figure 4.1) all 12 affected individuals for whom DNA was available, carried at least one G allele of the SNP rs3812718. Of these, over 50% were homozygous for the SNP (the genotype of one patient was unidentified). There was no obvious difference in phenotypes when comparing between GG and GA individuals, although the sample size was small. Two healthy individuals were AA; which would provide them with a bias towards the adult exon. Because the G allele is present in all affected individuals, patients carrying the R1648H mutation are likely to have a larger proportion of $Na_V1.1$-5N channels, and it is probable that the mutation is carried with the G allele, although this would need to be confirmed. Investigating the properties of $Na_V1.1$-R1648H in exon 5N background is therefore important because previous reports have used only investigated the behaviour of adult mutant isoform.
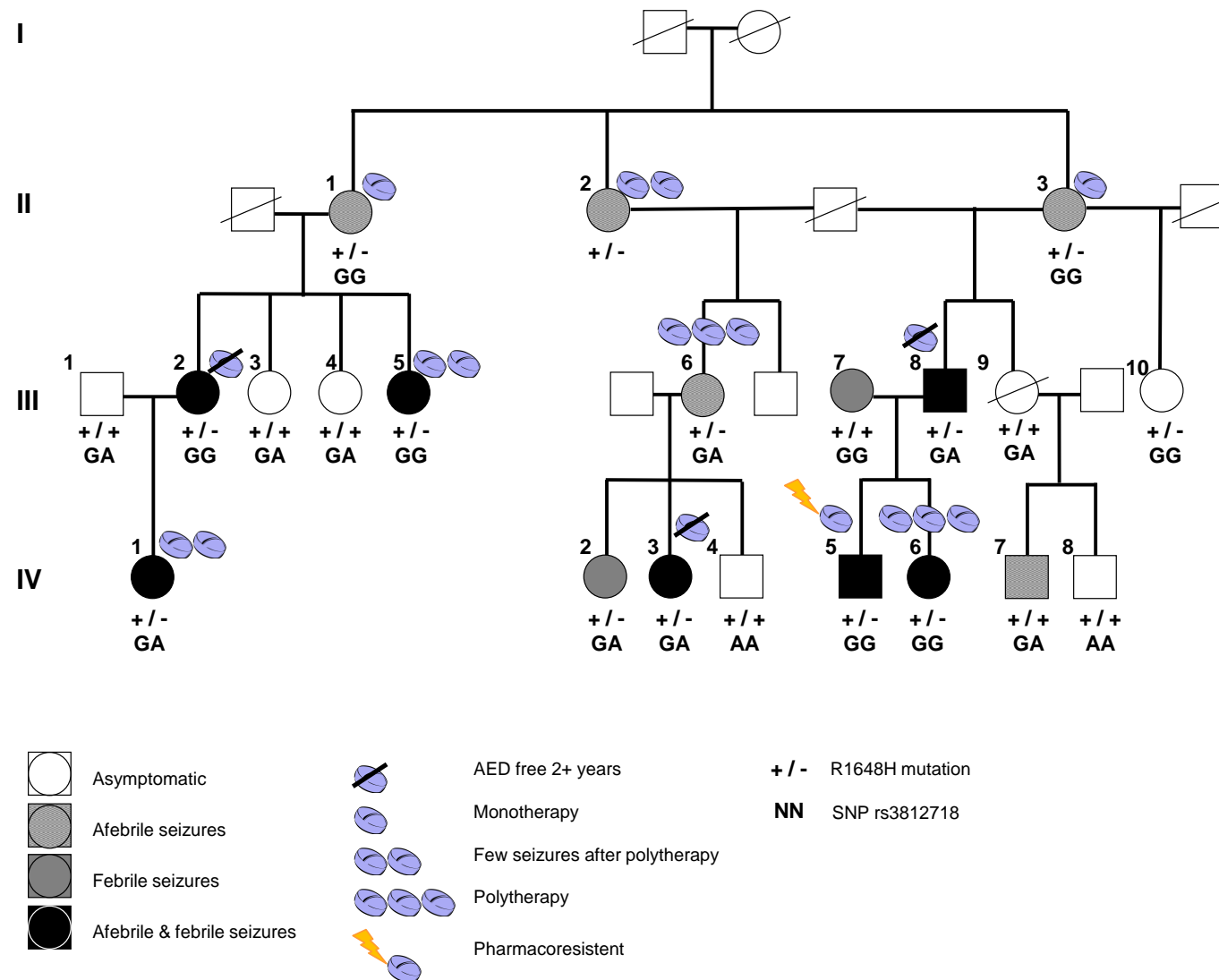
Figure 4.1 R1648H pedigree detailing patient rs3812718 genotype. The original pedigree is based on information from Baulac *et al.* 1999 and Escagy *et al.* 2000.

4.3 Effects using CsF-based intracellular solutions 1: $Na_V1.1$-5A derived persistent currents were unaffected by R1648H using CsF-based solutions

To establish a comparison with the data describing functional effects of $Na_V1.1$-R1648H-5A heterologously expressed in HEK cells, the two splice variants were initially compared using CsF-based intracellular solutions at RT. $Na_V1.1$-5N channels were engineered to carry the R1648H mutation (Figure 4.2 A, top panel). Raw traces are shown in Figure 4.2 A (bottom panel, current protocol shown in the inset). Peak transient current density of $Na_V1.1$ was not significantly affected by splicing or the R1648H mutation (P=0.7, two-way ANOVA). Unlike previous reports, using the CsF-based internal solution used in this study, $Na_V1.1$-R1648H-5A demonstrated indistinguishable mean (±SEM) %INa$_P$ to wild-type channels (5A: 7.8 ± 1.6 %, n=12 versus R1648H-5A: 7.4 ±1.3 %, n=13; P>0.05, two-way ANOVA, Bonferroni's post-test; Figure 4.2 B). This was not the case for $Na_V1.1$-5N, as mutant channels displayed a greater mean (±SEM) %INa$_P$ (8.1 ±1.6 %, n=9) compared to wild-type channels (3.6 ± 1.0 %, n=13). However, this was not significant when accounting for the combined influences of splicing and the mutation using a two-way ANOVA with Bonferroni's post-tests (P>0.05, Figure 4.2 B). Nonetheless, $Na_V1.1$-R1648H-5N channels demonstrated a significantly slowed rate of inactivation between -20 mV and + 20 mV, compared to wild-type $Na_V1.1$-5N channels (P<0.0001, two-way ANOVA; Figure 4.2 C).
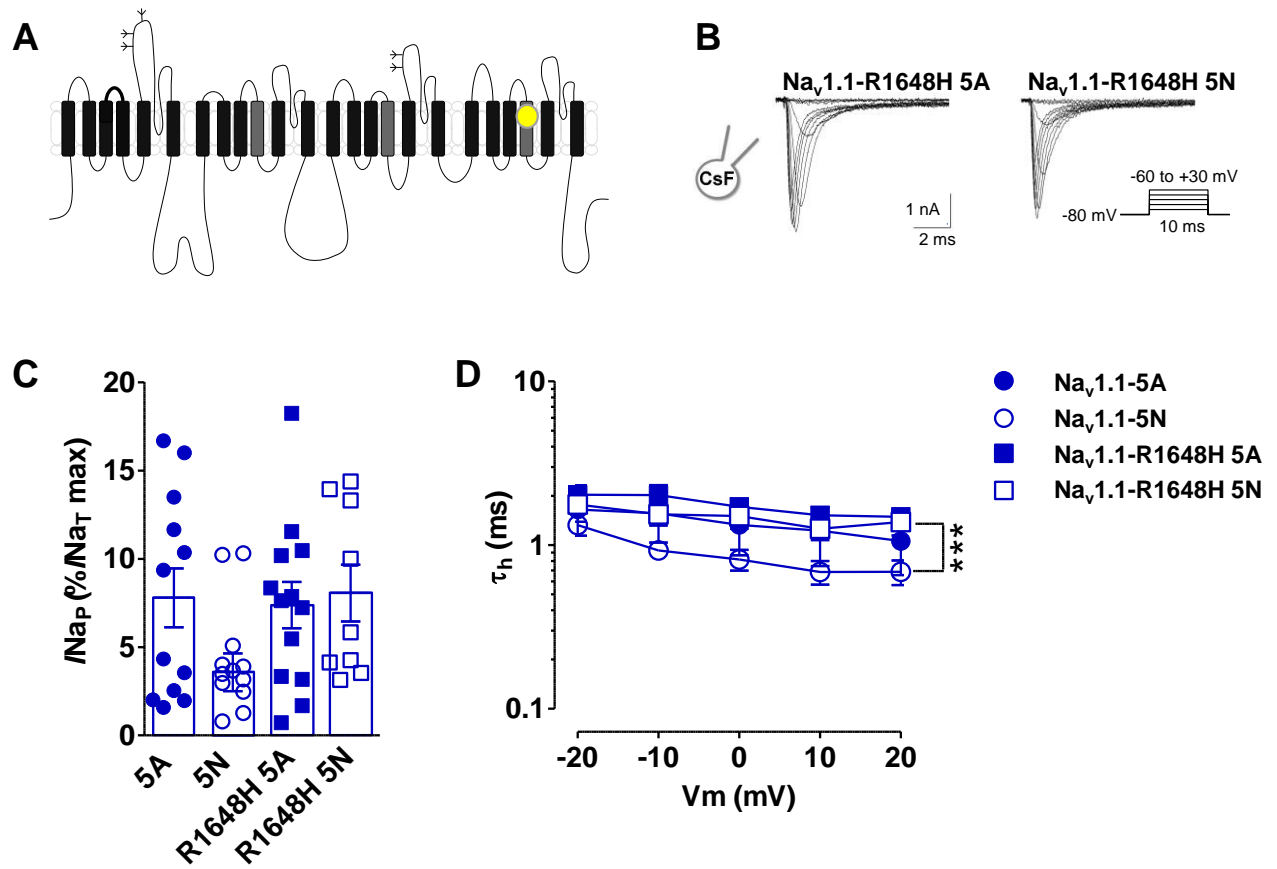
Figure 4.2 The non-inactivating component of Na$_V$1.1-R1648H 5N transient currents is more stable compared to wild-type channels *A.* Location of the R1648H mutation in the voltage sensor in the fourth domain is shown by the yellow circle. The region changed by alternative splicing of *SCN1A* exon 5, is shaded a darker grey. ***B.*** Representative traces from cells transfected with Na$_V$1.1-R1648H-5A or 5N. Currents elicited by protocol as in inset *C.* Na$_V$1.1-R1648H-5A does not increase mean ±SEM %*I*Na$_P$, although this may have been a qualitative effect for 5N containing channels; reflected in the slowing of Na$_V$1.1-R1648H 5N mean ±SEM current decay, over a range of voltages compared to wild-type channels (*D*). ***P<0.0001, two-way ANOVA.

4.3 Effects using CsF-based intracellular solutions 2: R1648H does not alter splice variant voltage dependence of activation or inactivation

Other reports did not detect changes in voltage dependence of activation or inactivation of Na$_V$1.1-R1648H-5A channels expressed in HEK 293 cells (Lossin *et al.,* 2002; Kahlig *et al.,* 2006; Vanoye *et al.,* 2006). In these conditions the voltage dependence of

inactivation was also unaffected for both splice variants carrying the mutation (5A versus R1648H-5A, P=0.9; 5N versus R1648H-5N, P=0.9, two-way ANOVA; Figure 4.3 C&D).

There was a trend for $Na_V1.1$-R1648H voltage dependence of activation to be shifted ~ 3 mV to more depolarized potentials in both splice variant backgrounds (clearly depicted in Figure 4.3 A), but a two-way ANOVA with post hoc tests revealed no significant differences in the mean (±SEM) midpoints (V_{50act} 5A versus R1648H-5A, P>0.05; 5N versus R1648H-5N, P>0.05; Figure 4.3 B). In contrast, the same statistical tests indicated that the voltage dependency of the mutation in the neonatal splice variant background was significantly reduced with an increase of 1.1± 0.1 mV/e-fold change (mean ±SEM *k*: 5N, *n*=14, versus R1648H 5N, *n*=8, P<0.05). Lastly, the time-course of activation was unchanged in mutant channels compared to wild-type channels (data not shown, 5A versus R1648H 5A, P=0.06; 5N versus R1648H 5N, P=0.1; two-way ANOVA).
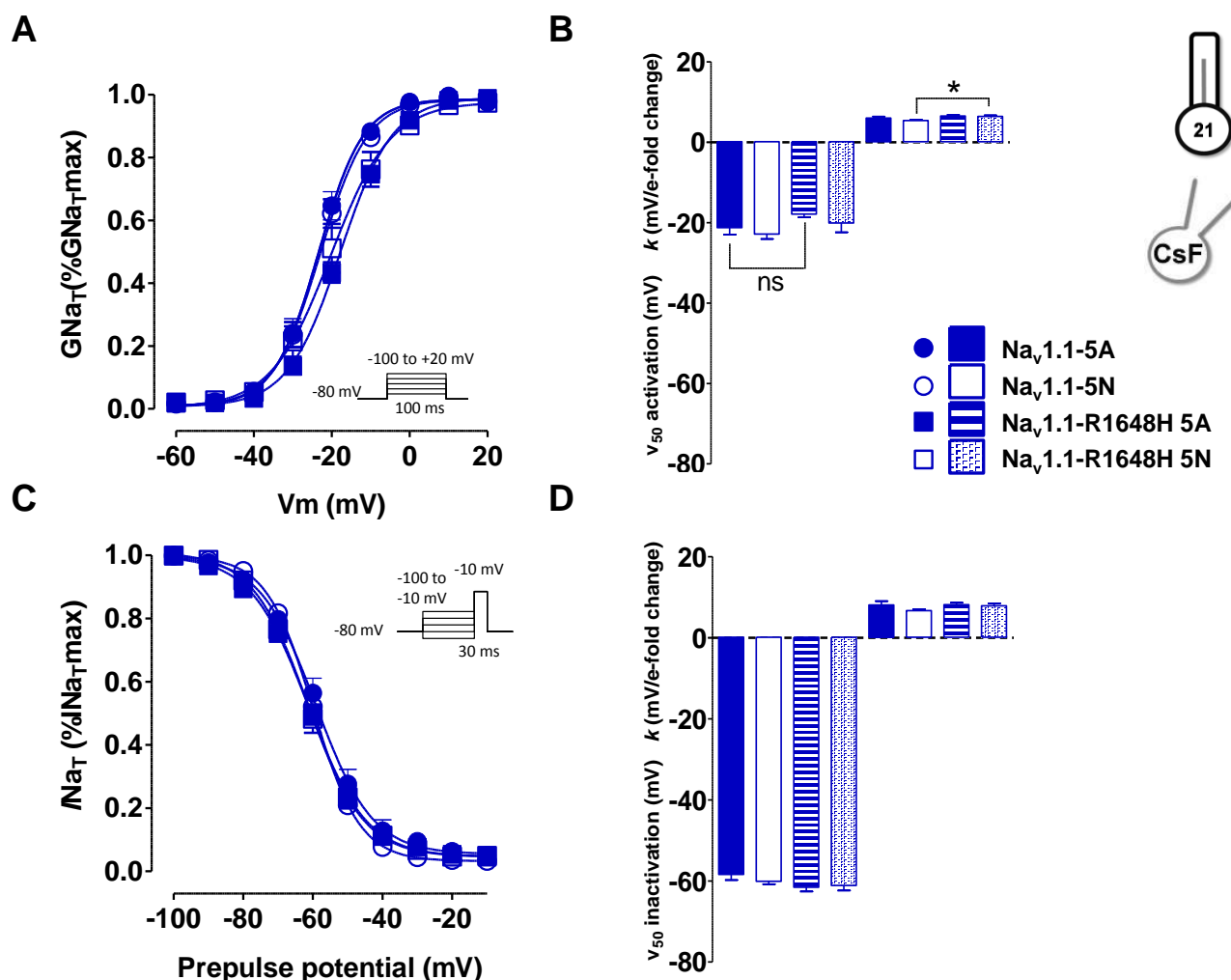
Figure 4.3 Na_V1.1 splice variants voltage dependence activation and inactivation is largely unaffected by R1648H A greater percentage of $Na_V1.1$-R1648H mutant isoforms activated at more depolarized potentials (*A*), but the mean±SEM midpoints were not significantly changed (*B*) but the voltage sensitivity of $Na_V1.1$-R1648H-5N activation was significantly decreased (*B*). *$P<0.05$, two-way ANOVA, Bonferroni post test. *C, D.* In all conditions, the voltage dependence of inactivation was unaffected over the voltage range and no change was observed in the mean±SEM V_{50} inactivation or slope factors of Boltzmann fits. Currents elicited by protocol as in insets.

At RT in the presence of fluoride, the inclusion of exon 5 altered the stability of $Na_V1.1$-R1648H persistent currents. In contrast to the literature, the non-inactivating component of $Na_V1.1$-5A was unaffected by R1648H (Lossin *et al.,* 2002; Vanoye *et al.,* 2006).

Because patients with GEFS+ frequently exhibit fever associated seizures, it was asked next whether the R1648H mutation was differentially affected by splicing at physiological temperatures using fluoride free solutions. Experiments were attempted at $40^{o}C$ in the presence of CsCl to replicate pathological conditions but cells transfected with the mutated channels were too fragile for recordings (data not shown).

4.4 Physiological conditions 1: The R1468H mutation significantly increases persistent currents in both splice variant backgrounds

In Chapter 3 it was shown that the gating of $Na_V1.1$ channels is altered in several ways. In particular, increasing the temperature of recordings suppressed persistent currents by increasing fast inactivation, and equalized the voltage-dependence of macroscopic gating between the two splice variants. The goal of this section was to determine how the mutation interacted with the different splice variants in more physiological conditions.

As clearly depicted in the raw traces shown in Figure 4.4 A, at elevated temperatures and using CsCl-based solutions the $Na_V1.1$-R1648H persistent currents in both splice variant backgrounds were pronounced. The current-voltage relationship in Figure 4.4 A shows that persistent currents from $Na_V1.1$-R1648H-5N were significantly larger compared to wild-type 5N channels (5N, $n=18$ versus R1648H-5N, $n=13$ P=0.02; two-way ANOVA). A significant increase of persistent current between $Na_V1.1$-R1648H-5A and wild-type 5A channels was also observed over the voltage range (5A, $n=10$ versus R1648H-5A, $n=8$ P=0.008; two-way ANOVA). Persistent currents derived from mutant channels were also voltage dependant, peaking at -10 mV and 0mV respectively.

$Na_V1.1$-5N mean (±SEM) peak current density was -11.1 ± 3.4 pA/pF (n=8), ~ 7 pA/pF greater than $Na_V1.1$-5A at -3.9 ± 1.3 pA/pF (n=12; difference in pA/pF was not significant, P=0.3; two-tailed t-test). However over the voltage range $Na_V1.1$-R1648H-5N persistent currents were significantly increased compared to 5A-containing mutant channels (P=0.0006, two way ANOVA).

There are two possible ways of comparing INa$_P$ measured from mutant and normal channels. Differences may be measured as changes in the percent of current that is persistent as a proportion of the total 'peak' transient current, or changes may be more directly measured as simple amplitude of INa$_P$ density. In previous reports, single-channel analysis has shown that persistent currents derived from heterologously expressed $Na_V1.1$-R1648H channels resulted from the late re-openings of the pore. These data suggest that the same channels underlie both the early fast transient openings, and the late 'persistent' openings. Therefore, %INa$_P$ may be a more direct representation of this channel property than total amount of INa$_P$, because %INa$_P$ reflects the proportion of channels that re-open as a part of the total channels available. In contrast, a direct comparison of INa$_P$ current density from different channels would be confounded by any changes in channel expression levels, as well as changes in likelihood of channels re-opening later in voltage-steps.

$Na_V1.1$-R1648H-5N mean (±SEM) %INa$_P$ was dramatically increased compared to wild-type channels (5N R1648H 15.2 ± 3.2%, n=13 versus 5N 5.2 ± 1.1%, n=11; P<0.01, two-way ANOVA, Bonferroni's post-test; Figure 4.4 C). Comparable observations were made for $Na_V1.1$-5A mutant compared to wild-type channels

channels (R1648H-5A 17.6 ± 1.7%, n=17 versus 5A 8.5 ± 1.6%, n=16; P<0.01, two-way ANOVA, Bonferroni's post-test; Figure 4.4 C).

The proportion of persistent current for both channels was comparable (P=0.2, two-tailed t-test; Figure 4.4 C). Overall the transient current was unaffected by splicing and the R1648H mutation (P=0.6, two-way ANOVA; Figure 4.4 D), although there was a trend towards smaller peak transient currents from Na_V1.1-1648H-5A channels compared to Na_V1.1-1648H-5N channels (25.6 ± 18.3 pA/pF, P=0.2, two tailed t-test; clearly shown in Figure 4.4 D). The increase of INa$_P$ from the mutant channels is consistent with the significant deceleration of inactivation seem over a range of voltages (5A versus R1648H 5A, P=0.01, 5N versus R1648H 5N, P=0.02; two-way ANOVA; Figure 4.4 D). Splicing did not affect this parameter as both mutant channels had comparable rates of current decay (P=0.5, two-way ANOVA, Figure 4.4 E).
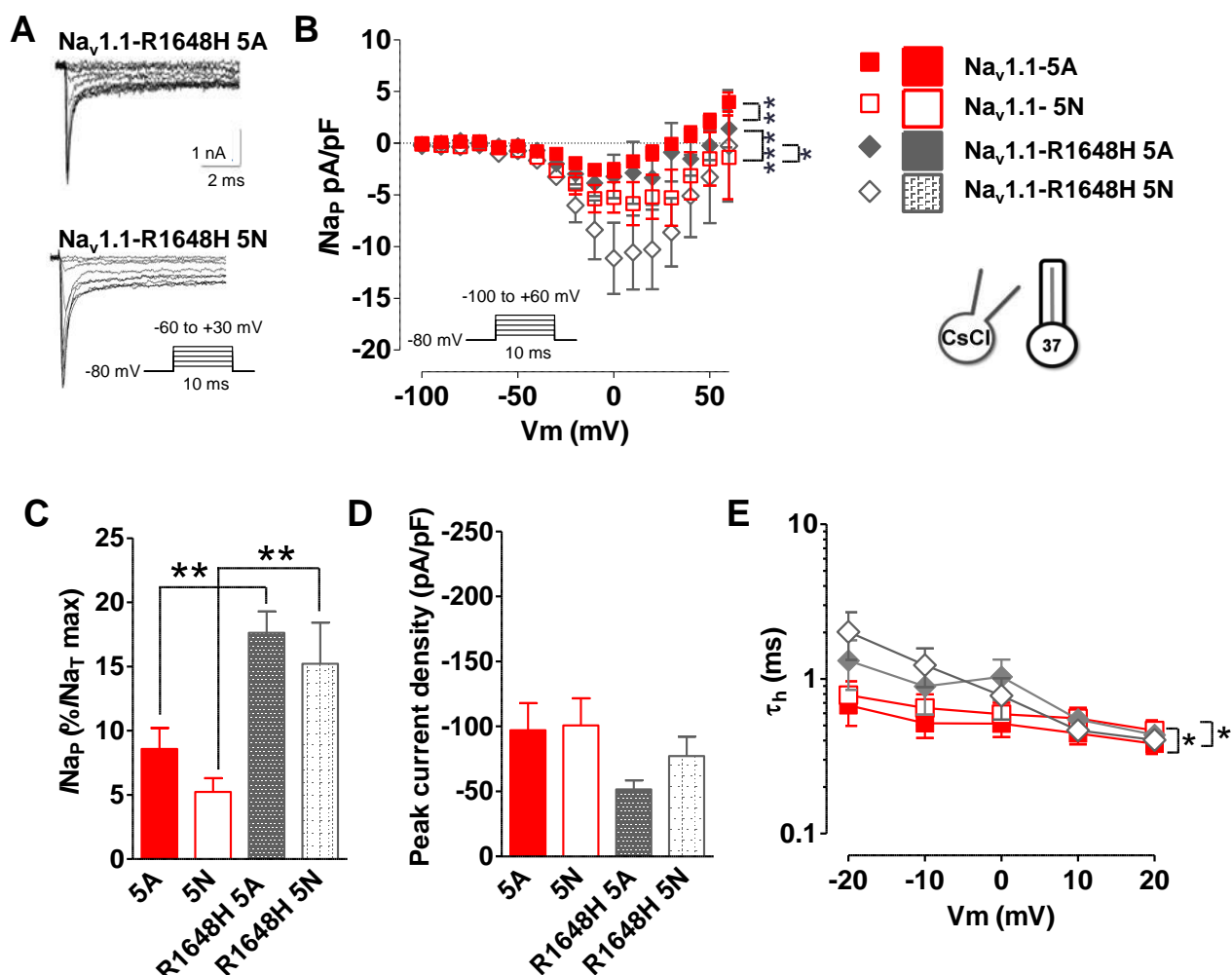
Figure 4.4 Na$_V$.1-R1648H increases persistent current in both splice variant backgrounds at biological temperatures *A.* Raw traces of Na$_V$1.1-R1648H 5A-containing channels (top) and 5N-containing channels (bottom). *B.* Mean (±SEM) persistent current density of wild-type and mutant channels. Persistent currents derived from Na$_V$1.1-R1648H were significantly increased compared to wild-type channels, and were voltage dependant. 5A vs R1648H-5A **P=0.008; 5N vs R1648H 5N *P=0.02, two-way ANOVA. *C.* Splicing did not affect the mean (±SEM) increase in %INa$_P$ for Na$_V$1.1-R1648H channels, but %INa$_P$ was significantly increased for both mutants compared to wild-type channels. **P<0.01, two-way ANOVA, Bonferroni's post-test *D.* The R1648H mutation and splicing did not significant change mean (±SEM) peak current density of Na$_V$1.1. Although there was a significant increase in the persistent current density for Na$_V$1.1-R1648H 5N channels (***P=0.0006, two-way ANOVA, *B*), the %INa$_P$ was similar for both mutant isoforms, because of a reduction in Na$_V$1.1-R1648H-5A transient peak current density. *E.* Consistent with a decreased stability of inactivation Na$_V$1.1-R1648H channels demonstrated a slower rate of current decay over a range of voltages compared to wild-type channels. 5A vs R1648H 5A, *P=0.01, 5N vs R1648H-5N, *P=0.02, two-way ANOVA.

4.4 Physiological conditions 2: The R1648H mutation causes a rightward shift in the

voltage dependence of activation of both splice variants

In both splice variant backgrounds, the midpoints of mutant channels were significantly

shifted by 6.5 ± 1.5 mV and 3.0 ± 1.3 mV in a rightward direction for 5A and 5N

containing channels respectively (5A -18.5 ± 0.9 mV, *n*=15 versus R1648H-5A -12.0 ±

1.2 mV, *n*=9; P<0.001; 5N -18.8 ± 0.8 mV, *n*=18 versus R1648H 5N -15.8 ± 1.0 mV,

n=13; P<0.05, two-way ANOVA, Bonferrroni's post tests; Figures 4.5 A&B). Moreover

Na_V1.1-R1648H-5A channels activated at significantly more depolarized potentials than

Na_V1.1-R1648H-5N channels (P=0.02, two-tailed *t*-test) suggesting that unlike Na_V1.1-

R1648H persistent currents, transient currents produced by this mutation were

differentially modulated by splicing. The kinetics of activation for both Na_V1.1-R1648H

splice variants were unchanged compared to wild-type channels over the voltage range

(5A versus R1648H 5A, P=0.7; 5N versus R1648H 5N, P=0.7; two-way ANOVA;

Figure 4.5 C).
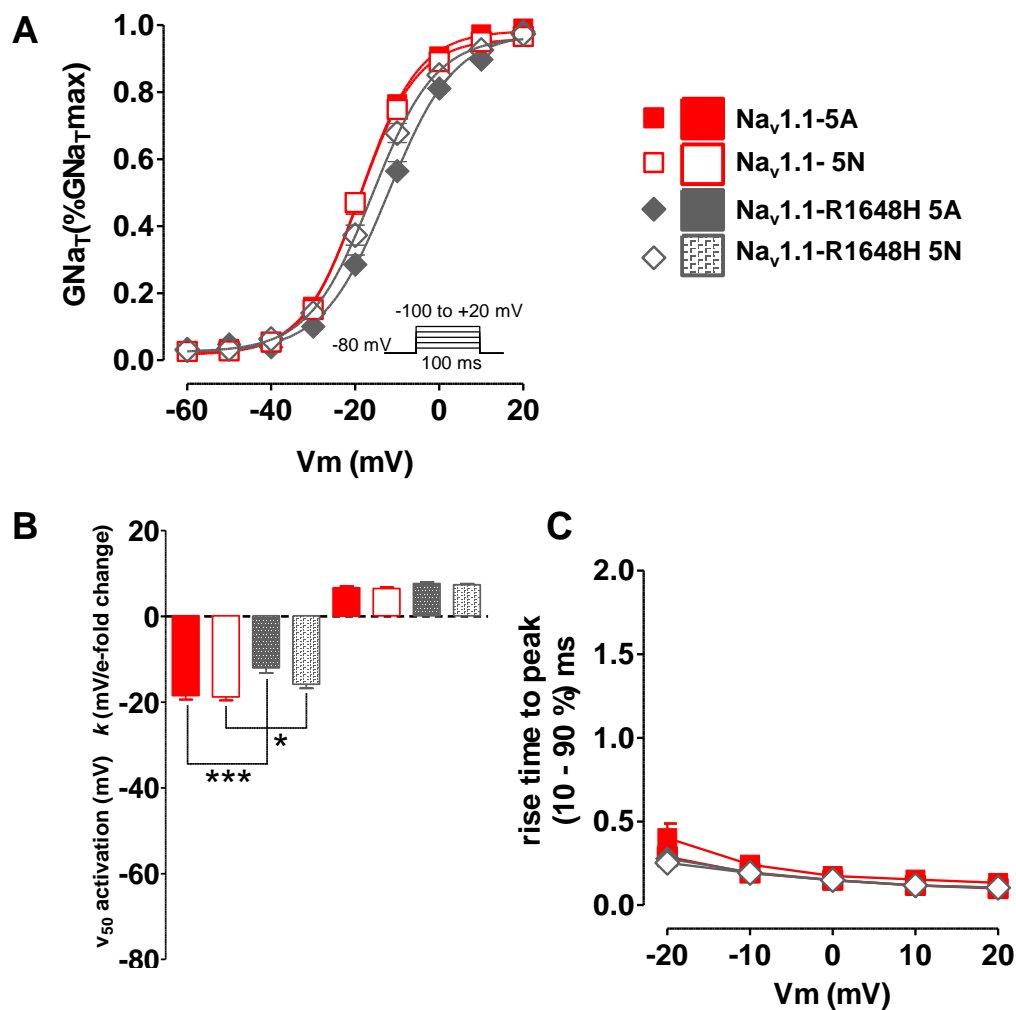
Figure 4.5 R1648H causes a loss of function in $Na_V1.1$ splice variant voltage dependence of activation *A.* The voltage dependence of activation for $Na_V1.1$-R1648H in both splice variant backgrounds was shifted in a rightward direction. Currents were elicited by protocol in inset *B.* 5A containing channels were more sensitive to a change in the voltage sensor and mean (±SEM) midpoints of activation were shifted to more depolarized potentials compared to wild-type channels and $Na_V1.1$-R1648H-5N. The average (±SEM) slope factors were comparable in all conditions. ***P<0.0001, *P<0.05, two-way ANOVA. Bonferroni's post-test. *C.* The mean (±SEM) 10-90 % rise time to peaks over a voltage range was similar for both $Na_V1.1$ splice variant wild-type and mutant channels.

4.4 Physiological conditions 3: The mutation R1648H decreased the voltage sensitivity of inactivation for both channel variants

The mean (±SEM) V_{50} of $Na_V1.1$ inactivation was unaffected by R1648H and splicing (P=0.5; two-way ANOVA; Figures 4.6 A&B). However the voltage dependency was reduced for both channels with an increase in the mean steepness of Boltzmann fits compared to wild-type channels (P=0.0005, two way ANOVA; Figure 4.6 A). More specifically, when considering individual channels increase of 1.7 ± 0.7 mV/e-fold change was observed in $Na_V1.1$-R1648H-5A channels compared to controls (P<0.05, two-tailed t-test; Figure 4.6 B). A similar decrease in the voltage dependency of inactivation was demonstrated by a -2.2 ± 0.8 mV/e-fold change increase slope factor $Na_V1.1$-R1648H-5N channels compared to $Na_V1.1$-5N channels (P<0.05, two-tailed t-test; Figure 4.6 B).
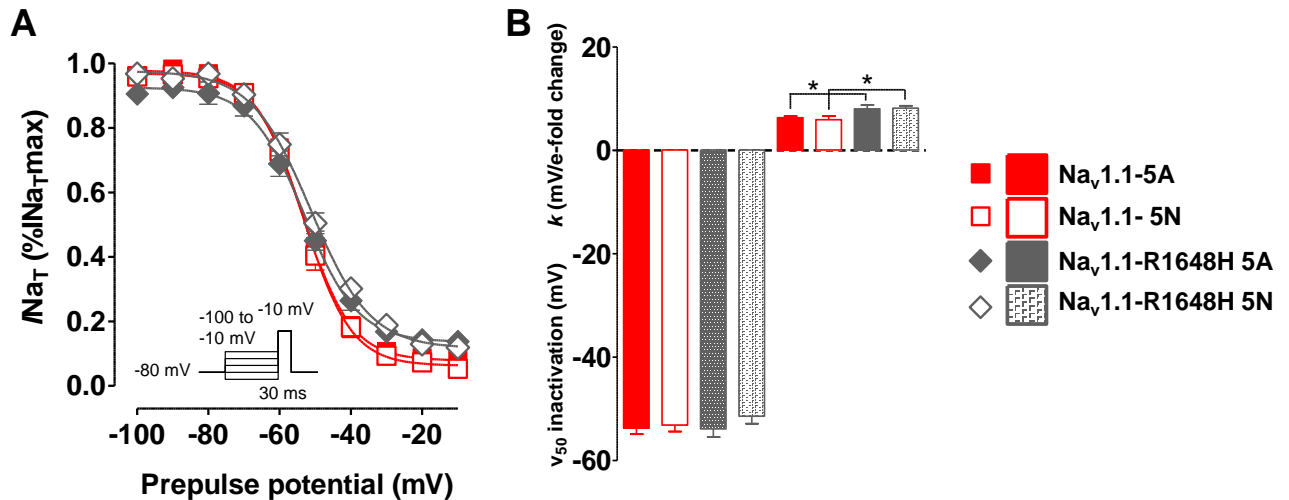
Figure 4.6 The voltage sensitivity of inactivation was decreased for $Na_V1.1$-R1648H splice variant channels. *A.* The voltage dependence of inactivation for $Na_V1.1$-R1648H channels was comparable to wild-type channels. ***B.*** The mean (±SEM) k values were significantly increased for both $Na_V1.1$-R1648H isoforms compared to wild-type channels. *P<0.05, two-way ANOVA, Bonferroni's post-test.

4.4 Physiological conditions 4: Phenytoin does not significantly reduce persistent currents derived from channels containing the R1468H mutation

In both splice variant backgrounds the mutation R1468H introduced a substantial increase in persistent current, which is a potential target for AED block. To assess the contribution of this parameter to phenytoin responsiveness the proportional difference in INa$_P$ between a 200ms -10 mV inactivating prepulse followed 18 ms recovery interval at -80 mV was followed by a -10 mV test potential. This protocol was preceded by a 20 ms interval sweep, to allow for the use-dependent block of AEDs. As expected phenytoin did reduce persistent currents for both wild-type and mutant channels (mean ±SEM % decrease INa$_P$: 5A 32.8 ± 8.2 %, n=8; 5N 21.0 ± 5.3%, n=6; R1648H-5A 35.9 ± 10.4%, n=7; R1648H 5N 44.7 ± 10.6%, n=7; Figure 4.7 B). However, a two-way ANOVA did not reveal a significant difference in the proportion of drug inhibition of Na$_V$1.1 compared to Na$_V$1.1-R1648H derived persistent currents (P=0.2), suggesting that phenytoin block INa$_P$ derived from mutant channels may not alter drug responsiveness in patients with this mutation.
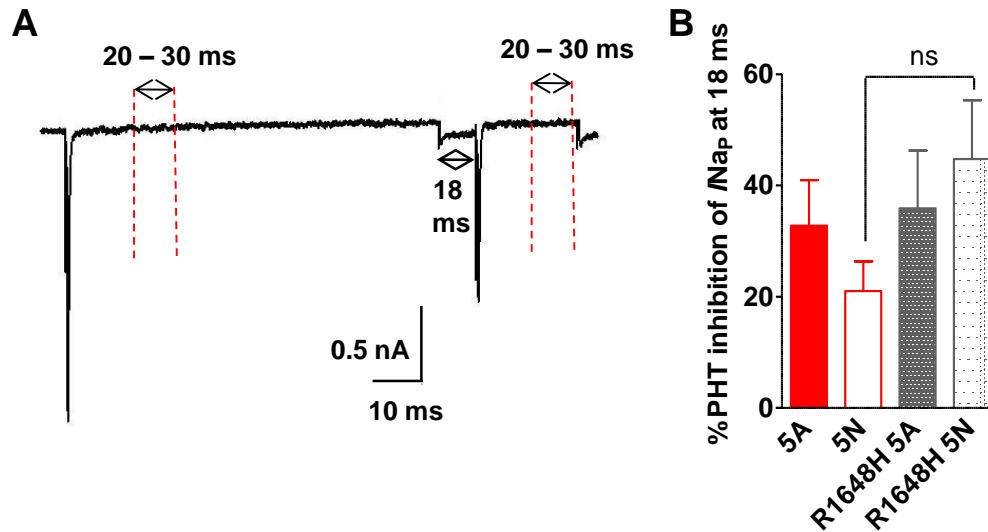
Figure 4.7 Phenytoin did not disproportionally inhibit Na$_V$1.1-R1648H persistent currents *A.* Schematic showing the parameters use to calculate proportional inhibition by phenytoin of persistent currents. Mean currents were taken from 20 ms – 30 ms after a -10 mV prepulse and 20 ms – 30 ms after a subsequent -10 mV test potential, following a 18 ms interval at -80 mV. The reduction in the persistent current from the second pulse for each cell was expressed as a percentage. *B.* In the presence of phenytoin persistent currents derived from all channels were proportionally reduced but no differences in percentage inhibition were observed between mutant and wild-type channels. NS: $P=0.2$, two-way ANOVA.

4.4 Physiological conditions 5: R1648H slows the recovery from inactivation for both splice variants

The remaining parameter targeted by both phenytoin and by alternative splicing is recovery from inactivation. The R1648H mutation is not located in the inactivation module, but as shown in previous studies R1648H slows the rate of recovery from inactivation (Martin *et al.,* 2010). Similarly, the changes in the voltage sensor caused by R1648H mutation in Na$_V$1.1-5N channels slowed recovery from inactivation (5N *n*=10, R1648H 5N *n*=8; P<0.0001; two-way ANOVA; Figure 4.8 A). This slowing was particularly pronounced at longer time intervals (10 ms and 20 ms, P<0.0001, Bonferroni's post-tests). R1648H had slightly smaller effects on recovery from

259

inactivation in Na$_V$1.1-5A compared to Na$_V$1.1-5N but these were not significantly different at any specific recovery time (5A *n*=8, R1648H-5A *n*=11; P=0.03; two-way ANOVA; Figure 4.8 B). However, the consequences of the larger inhibition of recovery in the Na$_V$1.1-5N background meant that the recovery from inactivation from both splice variants containing the mutation were comparable (P=0.7, two-way ANOVA; Figure 4.8 C).
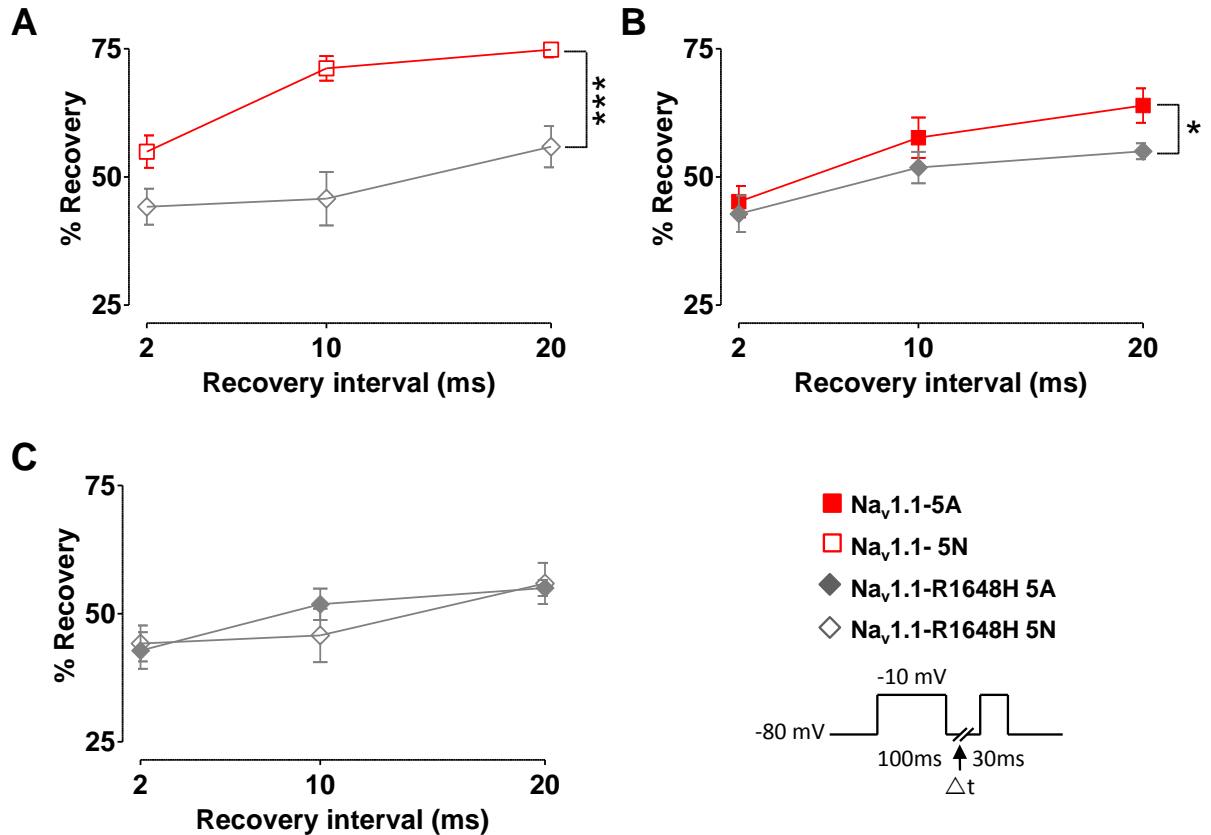
Figure 4.8 Channels containing R1648H recovered from inactivation more slowly compared to wild-type channels. The recovery from inactivation was significantly slowed at time points between 2 and 20 ms after prolonged depolarisations for 5N (*A*) and 5A (*B*) R1648H channels compared to wild-type channels ***P<0.0001, *P=0.03, two-way ANOVA. *C.* R1648H eradicated the difference between recovery from inactivation between wild-type channels. The recovery was reduced to similar percentages for Na$_V$1.1-R1648H channels in both splice variant backgrounds. P=0.7, two-way ANOVA. Currents were elicited as in inset.

4.4 Physiological conditions 6: Phenytoin demonstrates a proportionally greater inhibition when acting on R1648H channels in Na$_V$1.1-5N background

As expected, phenytoin significantly inhibited recovery from inactivation of both mutant channels in both splice variant backgrounds. This was true across the time-interval range (R1648H 5A, *n*=11, versus R1648H-5A + PHT, *n*=7; P=0.005; R1648H 5N, *n*=8, versus R1648H 5N + PHT, *n*=7; P<0.0001; two-way ANOVA; Figure 4.9 A&B). Interestingly, the AED had a significantly greater efficacy when acting on Na$_V$1.1-R1648H-5N channels compared to Na$_V$1.1-R1648H-5A (P=0.04; two-way ANOVA; Figure 4.9 C), indicating that splicing does alter the drug responsiveness of Na$_V$1.1-R1648H.
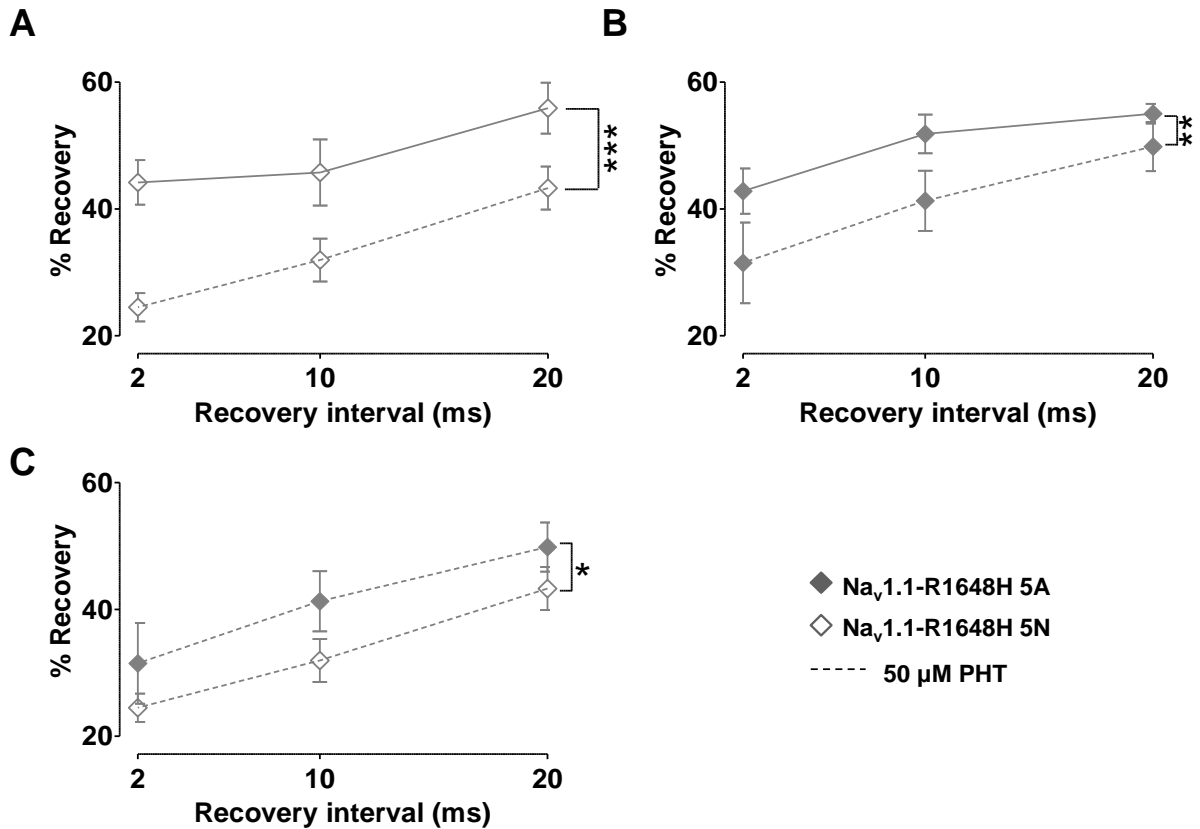
Figure 4.9. (previous page) Splicing significantly effects the drug responsiveness of R1648H channels *A, B*. 50 μM phenytoin significantly inhibited recovery from inactivation of both mutant channels at three times interval indicated. ***P<0.0001, **P=0.005, two-way ANOVA *C.* Recovery from inactivation of 5N-mutant channels was disproportionally decreased by phenytoin compared to $Na_V1.1$-R1648H-5A channels. *P=0.04, two-way ANOVA.

In the presence of phenytoin mutant $Na_V1.1$-5N channels were significantly delayed compared to wild-type channels (P<0.0001; two-way ANOVA; Figure 4.10 A). In contrast, under the same conditions 5A-containing channels were indistinguishable (P=0.1; two-way ANOVA; Figure 4.10 B). Implying that polymorphism rs3812718 and genetic heterozygosity, may have significant implications in drug treatment for inherited $Na_V1.1$ epilepsies.
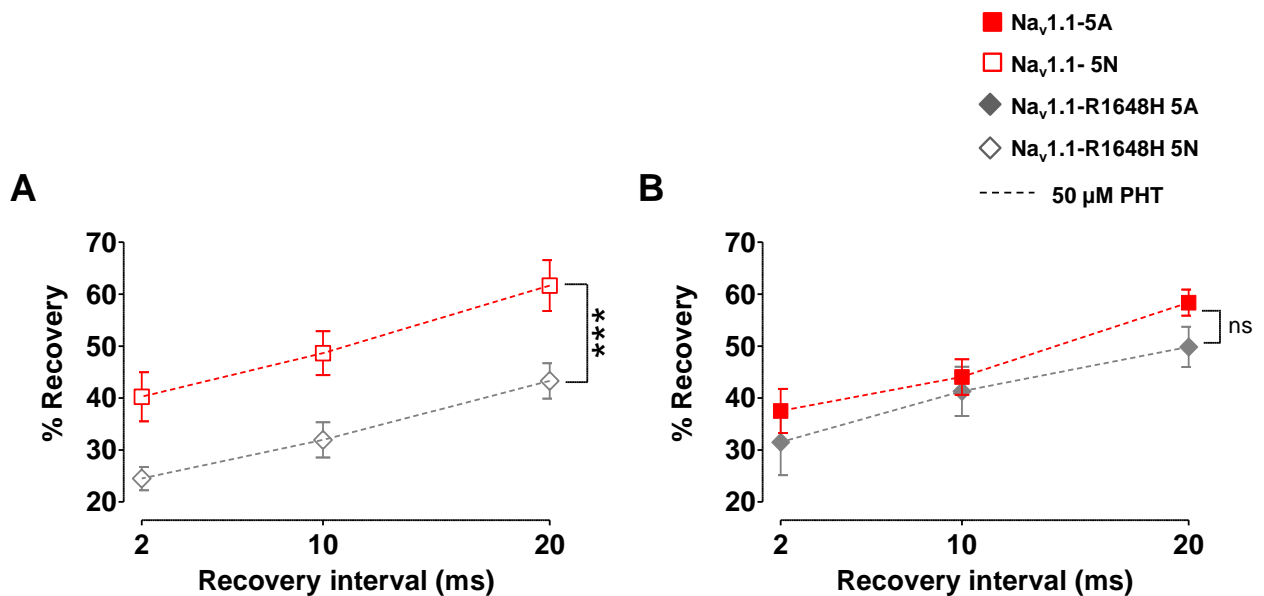
Figure 4.10 The effect of phenytoin on the recovery of inactivation for wild-type and mutant channels *A*. In the presence of phenytoin $Na_V1.1$-5N channels recovered more rapidly compared to $Na_V1.1$-R1648H 5N channels, over time intervals ranging from 2 -20 ms.***P<0.0001, two-way ANOVA. *B.* The drug responsiveness of mutant and wild-type 5A containing channels was comparable. P=0.1, two-way ANOVA.

262

4.5 Discussion

The main positive findings of this chapter were:

1. Patients harbouring the R1648H mutation had a least one copy of the G allele of rs3812718. This allele favours the inclusion of 5N. Therefore investigating the effects of this mutation in a neonatal 'background' was essential to understand its true biophysical consequences on $Na_V1.1$ behaviour.

2. The behaviour of $Na_V1.1$-R1648H channels presented in this work using CsF based internal solutions at RT did not compare with reports in the literature, highlighting the influence of cell background on channel properties.

3. At physiological temperatures R1648H causes both a loss and gain of $Na_V1.1$ function.

4. Alternatively splicing differentially affects $Na_V1.1$ mutant channel gating.

5. R1648H similarly slows channel recovery from inactivation of both $Na_V1.1$ isoforms and phenytoin disproportionally inhibits this parameter of $Na_V1.1$-R1648H-5N channels.

6. No direct link between patient AED phenotype/drug treatment, rs3812718 genotype and $Na_V1.1$-R1648H behaviour was revealed.

4.5.1 The G allele of rs3812718 is associated with R1648H

This chapter attempted to determine whether alternative splicing of $Na_V1.1$ would affect the behaviour and drug response of a GEFS+ mutation, R1648H. Genotyping the

members of this family that harbours R1684H showed that all affected individuals had at least one copy G allele of rs3812718. Therefore, as adults these individuals would express Na_V1.1-5N. However, because these patients are heterozygous for the mutation, further sequencing would ascertain whether the mutation and SNP are consistently located on the same chromosome. It is unlikely that in this pedigree, there is a direct association with drug dosage and rs3812718, because irrespective of their genotype each individual experienced varying responses to AEDs.

4.5.2 The behaviour of Na_V1.1-R1648H-5A channels in this report using CsF-based intracellular solutions at RT contrasted with earlier reports

Previous reports have investigated heterologously expressed Na_V1.1-R1648H-5A in HEK derivative cells, using CsF-based internal solutions. Results derived from this study in similar conditions, were different than those reported by other groups. One distinguishing feature of this mutation is that it increases the level of Na_V1.1-5A derived $\%I$Na$_P$ and does not alter the voltage dependence of Na_V1.1-5A gating (Lossin *et al.,* 2002; Kahlig *et al.,* 2006; Vanoye *et al.,* 2006). However, from these data no increase of $\%I$Na$_P$ was observed for Na_V1.1-R1648H-5A channels but a switch to exon 5N decreased the rate of current decay. Although not significant the mutation caused a mild loss of function in the voltage dependency of activation and the voltage sensitivity of Na_V1.1-5N channel activation was decreased. Together with the current decay observations these data imply that in fluoride, Na_V1.1-5N channel activation and inactivation are more sensitive to the loss of an arginine within the voltage sensor.

Discrepancies in Na_V1.1-R1648H-5A channel behaviour in this report and the literature

may result from several variables. For instance, the $Na_V1.1$ clone used in the Lossin *et al.* and Vanoye *et al.* investigations was the full length *SCN1A* gene, thus the shorter exon 11 $Na_V1.1[-33]$ variant used in this study may account for changes in $Na_V1.1$ activation. Indeed, DRG cells expressing a $Na_V1.7$ adult onset inherited erythermalgia mutation in an exon 5A with a longer exon 11 background had a reduced action generation threshold and firing compared to cells expressing shortened mutant channels containing 5N (Choi *et al.,* 2010). Alternatively β subunit modulation may have masked these subtle affects in previous reports or differences in cell background may have influenced channel gating. Because results from electrophysiology experiments using CsF are unlikely to represent the true physiology of these channels (Coste *et al.,* 2004), conclusions on the effect of R1648H on $Na_V1.1$ behaviour will be based on CsCl recordings at physiological temperatures.

4.5.3 $Na_V1.1$-R1648H increases %INa_P

Elevated temperatures revealed that R1648H causes an increase in %INa_P$ and a slowing of the rate of inactivation and this gain of function is unaffected by *SCN1A* alternative splicing. Therefore, a shift in the 5N/5A ratio would not change this parameter. Single channel analysis and computer modelling provided strong evidence that R1648H increases the probability late channel openings after inactivation, possibly by destabilizing the IFM inactivation gate (Kahlig *et al.,* 2006; Vanoye *et al.,* 2006). Mutations of $Na_V1.5$ inner D4:S4 arginines also increased persistent currents, suggesting that these residues play an important role in VGSC inactivation (Zimmer & Surber, 2005). Xu & Clancy (2008) demonstrated that $Na_V1.1$-R1648H derived persistent

currents encouraged neuronal bursting, in a single-compartment model of a CA3 hippocampal pyramidal neuron. However, If $Na_V1.1$ channels are upregulated in inhibitory interneurons in humans, how would a gain of channel function cause epileptogenesis? Some clues are given in disease models concerning different VGSCs. Specific mutations in the skeletal VGSC cause an increase in INa$_P$ but a paradoxical decrease in cellular excitability that led to muscle inexcitability and episodes of paralysis. Cannon (2006) surmises that the increased INa$_P$ would depolarize the resting membrane potential and inactivate transient sodium currents responsible for the upstroke of the muscle action potential. However, muscle and neuronal channels serve different physiological roles and it is likely that the Ensemble of channels plays a greater role. This is demonstrated by a loss of function mutation in $Na_V1.7$ that is associated with a pain disorder. The mutation, L858H results in hypo- and hyperexcitability of different PNS neurons which is explained by the presence of $Na_V1.8$ in one cell type but not the other. For example, in sympathetic neurons, cells that lack $Na_V1.8$, the mutation decreases cell excitability. In sensory neurons, however, $Na_V1.8$ is upregulated and in wild-type neurons $Na_V1.7$ is activated before $Na_V1.8$ which is resistant to inactivation at more positive potentials. The absence of this renders the sensory neurons hyperexcitable (Rush *et al.,* 2006). Because there was a pronounced increase in $Na_V1.1$-R1648H derived %INa$_P$ in this study, and in the previous reports (in the presence of β subunits), it is very surprising that persistent currents were not detected in neurons in both mouse models of this mutation (Tang *et al.,* 2009; Martin *et al.,* 2010).

4.5.4 Na$_V$1.1-R1648H also causes a loss of gating function

R1648H also introduced a loss of Na$_V$1.1 gating function, a rightward shift in the voltage dependence of activation and a decrease in the voltage sensitivity of inactivation. R1648H is a mutation in the fifth (out of six, closest to the extracellular side) arginine in Na$_V$1.1 fourth voltage sensor. Previous reports have neutralized or charge substituted the middle/outer arginines within D4:S4 of different VGSCs. Observations from whole-cell patch clamp experiments using heterologously expressed mutant channels are inconsistent. Some studies correlated with this study, that is, the voltage dependence of VGSC activation was shifted to more depolarized potentials, the voltage sensitivity of inactivation was decreased and/or that rate of current decay was slowed (Chen *et al.,* 1996; Wang *et al.,* 1996; Kuhn & Greeff, 1999; Frustaci *et al.,* 2005). Conversely other reports demonstrated that activation was unaffected and/or current decay was accelerated (Kontis *et al.,* 1997; Sheets *et al.,* 1999). Despite these discrepancies, the changes in Na$_V$1.1-R1648H gating shown in this study are consistent with a disruption of activation-inactivation coupling (Chen *et al.,* 1996) and a destabilization of fast inactivation (Kuhn & Greeff, 1999). Analogous residues within the D4:S4 of another to VGSC genes *SCN4A* and *SCN5A* are also mutation hotspots that cause hypokalemic periodic paralysis (Matthews *et al.,* 2009) and Brugada syndrome (Frustaci *et al.,* 2005) respectively.

The shift in the voltage dependency of Na$_V$1.1-R1648H activation is not observed in R1648H transgenic mice (Tang *et al.,* 2009; Martin *et al.,* 2010). The sodium current voltage dependency of activation and inactivation was unaffected in inhibitory

interneurons from both models (Tang *et al.,* 2009; Martin *et al.,* 2010). In excitatory neurons originating from the BAC transgenic model the midpoint of $Na_V1.1$-R1648H inactivation was shifted to the left and the voltage sensitivity was reduced; however, the latter was not highlighted by the authors (Tang *et al.,* 2009). Both mouse model studies demonstrated that peak sodium currents in GABAergic neurons were significantly reduced. This affect was not shown in these data from heterologous expression. This may result from a trafficking defect that could be masked by channel overexpression in non-neuronal cells, or interactions with specific neuronal proteins may hinder sodium permeation. Because there were differences in gating between excitatory and inhibitory neurons it is likely that the inconsistencies between these results and mouse models are due to cell background.

Based on the results *in vivo* how could a loss and gain of $Na_V1.1$ channel function cause GEFS+? Further insights may be given in a rat model of GEFS+ harbouring a mutation that caused opposing changes in $Na_V1.1$ channel function. Mashimo and colleagues (2010) introduced the missense mutation N1417H, into rat native *SCN1A* using a potent mutagen called *N*-ethyl-*N*-nitrosourea (EMU). Although not an epilepsy causing mutation *per se*, the pore of the third domain where this mutation occurrs is a mutation hotspot for SMEI and GEFS+ mutations in humans (Ohmori *et al.,* 2002; Sugawara *et al.,* 2002; Fujiwara *et al.,* 2003; Berkovic *et al.,* 2006; Mancardi *et al.,* 2006; Harkin *et al.,* 2007; Marini *et al.,* 2007; Zucca *et al.,* 2008). Similar to R1648H models the main deleterious effects of N1417H were observed in GABAergic hippocampal neurons from homozygous pups. Recordings from *SCN1A*[N1417H/N1417H] excitatory neurons showed no changes in the biophysical properties of mutant compared to wild-type channels.

Interestingly, $Na_V1.1$-N1417H channels in both HEK cells and hippocampal inhibitory interneurons showed a significant increase in persistent current and a shift to the left in voltage dependency of channel inactivation. This was a similar contrasting gain and loss of a function observed for $Na_V1.1$-R1648H in this study. It could be argued that functional discrepancies of $Na_V1.1$-R1648H in mouse neurons and HEK cells may not rely on cellular background but species. However, mouse full length *SCN1A* has 2% more sequence identity to human *SCN1A* than to the rat gene (unpublished alignment), so this seems an unlikely explanation. Alternatively, the variability of functional effects on interneurons, may partly contribute to variability of severity and manifestation of seizures. Indeed, homozygous $Na_V1.1$-N1417H rats did not exhibit spontaneous seizures, although they were extremely susceptible to hyperthermic stimuli compared to heterozygous and wild-type littermates. Approximately 20% *SCN1A*$^{\text{N1417H/+}}$ rats exhibited clonic seizures after submergence into a 45°C bath, an 80 % reduction compared to *SCN1A*$^{\text{N1417H/N1417H}}$ animals.

A later study by the Mashimo group (Ohno *et al.,* 2010) measured *in vivo* responses of *SCN1A*$^{\text{N1417H/N1417H}}$ CA1 hippocampal pyramidal cells to test or pair-pulse stimulation of the Schaffer collateral pathway. Implementing the latter, CA1 cells can receive $GABA_A$ receptor (inhibitory) and NMDA receptor (excitatory) mediated inputs (Ohno *et al.,* 2010). Single test pulses stimulating the stratum radiatum elicited normal CA1 responses in both wild-type and mutant rats. However, paired-pulsed stimulation of *SCN1A*$^{\text{N1417H/N1417H}}$ CA1 neurons showed a significantly greater number of spikes compared to healthy cells. This result could be reproduced in the wild-type rats in the presence of biciulline, a $GABA_A$ antagonist suggesting that abnormal $Na_V1.1$ function,

not necessarily a gain or loss of function *per se*, disrupts GABAergic synaptic transmission in the rat hippocampus.

It is possible that the increase in $Na_V1.1$-R1648H %INa$_P$ may negate the loss voltage dependency of $Na_V1.1$ activation. However, as described in the introduction elevated temperatures attenuates GABAergic transmission, possibly through aberrant trafficking of GABA receptor subunits (Kang *et al.,* 2006). *SCN1A*$^{N1417H/N1417H}$ rats have a lower hyperthermia induced seizure threshold. Perhaps subtle alterations in $Na_V1.1$ and GABA$_A$ mediated inhibition are only revealed at elevated temperatures, promoting epileptogenesis. Similar brain slice recordings from R1648H rodents could determine whether this mutation has comparable deleterious affects. Because the voltage dependence of activation of $Na_V1.1$-R1648H-5A was significantly more depolarized than $Na_V1.1$-R1648H neonatal channels, individuals with GA rs3812718 genotype may be more vulnerable to FS. However, the seizure history of this family challenges this hypothesis. From a biophysical perspective these data suggest that the changes in the extracellular linker of domain D1 may play a secondary role in activation-inactivation coupling to the D4 voltage sensor. In future studies it would be interesting to investigate other $Na_V1.1$ GEFS+ mutations that do not lie within the voltage sensor.

4.5.5 $Na_V1.1$-R1648H slows channel recovery from inactivation

One common effect of this mutation in different cell models, including the HEK cells in this study, is that R1648H slows the recovery of $Na_V1.1$ inactivation (Lossin *et al.,* 2002; Tang *et al.,* 2009; Martin *et al.,* 2010). This is the first report to show that both $Na_V1.1$-R1648H isoforms exhibited similar recovery from inactivation timecourses.

270

Consequently, irrespective of the rs3812718 allele, $Na_V1.1$-R1648H would hinder action potential propagation especially in parvalbumin-positive interneurons where $Na_V1.1$ is expressed at the AISs, axons and somata (Ogiwara *et al.,* 2007). It is expected that this loss of function would contribute to the impairment of GABAergic synaptic transmission similar to that observed for *SCN1A*[N1417H] rats (Ohno *et al.,* 2010). The family harbouring $Na_V1.1$-R1648H are heterozygous for the mutation and consequently their neurons would express both wild-type and $Na_V1.1$-5A mutation channels. Because wild-type $Na_V1.1$-5N channels recover faster from inactivation than $Na_V1.1$-5A channels, and mutant $Na_V1.1$-5N channel have a more hyperpolarized activation midpoint, homozygous GG individuals may be better protected from a loss of inhibition caused by R1648H compared to relatives with one copy each of the A. Again, the seizure history of the pedigree does not support this theory, suggesting that either these data do not represent the physiological affect of the mutation *in vivo*, or there are other modifying genetic or environmental factors that determine the phenotypic outcome of this missense mutation. Indeed two individuals: II-7 and IV-7 who do not harbour R1648H but exhibited febrile and afebrile seizures.

The therapeutic effectiveness of phenytoin treating seizures in this family is unknown. The $Na_V1.1$-R1648H persistent currents were not inhibited by phenytoin; thus, if *in vivo* R1648H does increase $\%I$Na$_P$ phenytoin is unlikely to reduce sodium currents by acting on this parameter. Ironically this may be therapeutically beneficial as increased persistent currents may maintain neuronal inhibition and phenytoin may disproportionally inhibit VGSCs expressed in pyramidal neurons reducing hyperexcitability. In fact, $Na_V1.1$-R1648H channels weakly expressed in glutamatergic

cells from two-week homozygous $SCN1A^{RH}$ mice recovered faster from inactivation than wild-type channels (Martin *et al.,* 2010). Phenytoin showed a proportionally greater inhibition of channel recovery from inactivation acting on $Na_V1.1$-R1648H-5N compared to both $Na_V1.1$-5N and mutant adult channels. Therefore, patients who are homozygous for the G allele experience greater inhibition. From these results it could be argued that heterozygous GA individuals may benefit better from AED treatment, but again the molecular, genetic and clinical data do not correlate (Baulac *et al.,* 1999; Escagy *et al.,* 2000; Tate *et al.,* 2006). Although the two GA patients may still have a large proportion of $Na_V1.1$-5N channels because this isoform is upregulated after ictal activity (Tate *et al.,* 2005). However, it does support the idea that the neonatal variant maybe a better substrate for phenytoin. In future, it would be useful to re-examine the clinical data and determine if a common AED is beneficial in treating this family. Its pharmacological affects could be assessed using electrophysiology.

These data also highlights the need for better detail in gene association studies. In future, to exploit the potential association between drug dosage and genetics fundamental questions need to be answered: What epilepsy syndrome does each patient suffer within the cohort? Do they harbour a genetic mutation; if so in which gene? The effects of SNPs for instance, can be assessed in three patient categories:

1. Individuals with structural/metabolic/unknown epilepsies.

2. Patients with mutations in the same SNP containing-gene.

3. Individuals harbouring mutations in the same gene.

Additionally, precise drug history is essential. Not all AEDs act on the same protein or have the same mechanism. As this study demonstrates it is unlikely that there is a single conserved pathological mechanism between patients, even within the same family. This is reflected in the variability of their phenotypes, even if their symptoms are classified as a part of the same syndrome. If the ideal is to be achieved, 'custom designed' AED treatment based on genotype, a greater scope of clinical data is needed. Basic science studies and in particular, electrophysiological investigations need to be consistent too. A large problem is that there are too many experimental inconsistencies between studies, and working in HEK cells can only provide information about the relative affects of alternative splicing or a mutation. The true physiological consequences of these mutations can only be determined *in vivo* where their consequences must be disentangled from closely-related, pharmacologically similar channels.

4.5.6 Can alternative splicing of exon 5 in SCN1A account for time dependent manifestation of GEFS+?

In the R1648H family three of 12 sufferers did not exhibit childhood FS (Baulac *et al.,* 1999); therefore, can alternative splicing fully account for the time-dependant manifestation of GEFS+? A similar question was asked by Liao and colleagues (2010) because alternative splicing did not dramatically alter the behaviour of $Na_V1.2$ BFIC mutations. They discovered in two regions of the rat hippocampus that a developmental switch caused $Na_V1.2$, which was dominant at P8, was largely replaced by P30 with $Na_V1.6$ which was significantly upregulated, while $Na_V1.2$ expression remained constant. The authors hypothesized that subtle changes in $Na_V1.2$ caused by mutations

may account for seizure generation at an early age, which remiss later because of increased $Na_V1.6$ expression. In future experiments it would be useful to determine if comparable developmental changes occur in GEFS+ mutant rodents in not only VGSCs but other GEFS+ genes, including $GABA_A$ subunits.

The study involving the *SCN1A*^{N1417H} rat compared the relative expression of *SCN1A* transcripts in wild-type and homozygous pups over 10 weeks. Susceptibility to hyperthermia induced seizures was correlated with lower levels of *SCN1A* for both wild-type and *SCN1A*$^{N1417H/N1417H}$ rodents. *SCN1A* expression peaked at 5 weeks for both genotypes, a time-point in which wild-type rats became resistant to hyperthermic stimuli. The mutant strain, however, continued to develop clonic seizures up to 10 weeks. This implies that the developing nervous system is vulnerable to hyperthermic stimuli, which may partly be caused by a reduction in $Na_V1.1$. However, because regulation of exon 5 *SCN1A* splicing in humans is not replicated in rodents it cannot be assumed that human $Na_V1.1$ channels are also developmentally downregulated.

For questions about the role of splicing the time-dependent manisfestation of GEFS+ symptoms, chicken neurons, discussed in Chapter 5, would be an ideal model to use because exon 5N is conserved. Electrophysiological experiments are described later the same chapter but the effect of knocking down each splice variant in a GEFS+ chicken model could be analyzed using siRNA delivered to the cell via genetically engineered viruses.

Chapter 5: The characterization of neuronal cell models

5.1 Background and aim: Why new neuronal models are needed

The Na$_V$1.1 channels encoded by *SCN1A* are almost exclusively restricted to excitable cells, particularly neurons. These channels are also known to be sensitive to intracellular signalling (Cantrell & Catterall 2001; Mantegazza *et al.,* 2005), and it is likely that pathways which target Na$_V$1.1 channels in neurons vary among different cell types. Since these channels seem to be specialised in interneurons (Yu *et al.,* 2006) they may have specific mechanisms in place to modulate them. In order to determine how or whether splicing alters the modulation of Na$_V$1.1 channels in neurons, it is necessary to express these channels in neuronal cells. The aim of this section was to explore different possible neuronal systems for characterising the modulation of Na$_V$1.1 channel splice variants.

5.2 Rodents: SC-RT-PCR analysis of rat hippocampal cells

One of the commonest neuronal models used in laboratory settings is the primary culture of neurons from neonatal rat pups. This model has the advantage that it is widely used and well studied, however, even when harvested from relatively homogenous hippocampal regions, the cultures contain a mixture of cell types. The first goal of this section was to establish, as much as possible, the identity and diversity of cellular phenotypes in primary neuronal cultures, and to develop SC-RT-PCR protocols that robustly identified different cell types when aspirated from individual cultures.

Methods that classify cellular phenotypes, for example, anatomy/morphology analysis, immunohistochemisty and *in-situ* hybridisation, are limited in determining molecular diversity of individual cells. For instance, adjacent cells with similar morphology may be functionally dissimilar. Imaging techniques typically allow only up to four markers to be analysed largely because of difficulties distinguishing between several coloured indicators. In this respect, SC-RT-PCR is a superior technique. It is possible to identify over 20 genes expressed in a single neuron (Richardson *et al.,* 2000). However, since only ~1pg of RNA can be harvested from a single cell the method is technically demanding. In preparation for future analyses this method was optimized using cultured P0 rat hippocampal cells (14 DIV). Cells analysed were taken from three separate cultures and broad neuronal phenotypes were classified using the following gene markers: cholinergic: choline acetyltransferase (ChAT); dopaminergic: tyrosine hydroxylase (TH); excitatory: sodium-dependent inorganic phosphate cotransporter, member 7 (SLC17A7); inhibitory: glutamate decarboxylase (GAD67) and control: Glyceraldehyde 3-phosphate dehydrogenase (GADPH).

Nearly 40% of neurons expressing the chosen markers were of a mixed inhibitory and excitatory phenotype. A quarter of the cells sampled were solely inhibitory and approximately 15% possessed an excitatory phenotype. One cell expressed both ChAT and GAD67. Approximately 20% cells could not be categorized into the chosen phenotypes (Figure 5.1). *In vivo*, it unlikely that the majority of hippocampal cells would possess a mixed phenotype. These data highlight the importance of neuronal inputs and outputs in maintaining phenotype, and suggest that neurons in culture may

fail to develop specialised phenotypes.
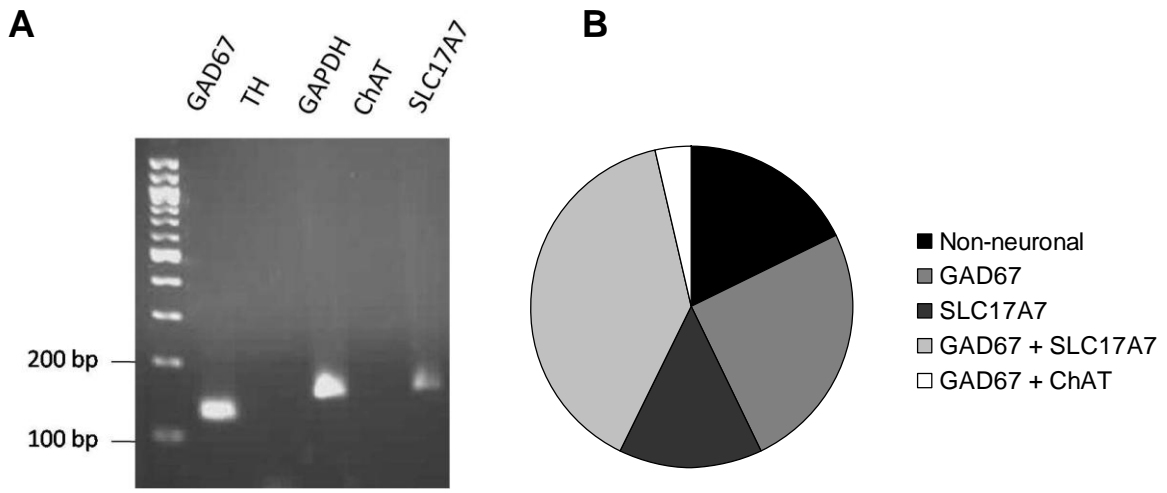
Figure 5.1: SC-RT-PCR was used to identify neuronal phenotype of two-week cultured rat hippocampal neurons. *A*. A typical photograph of the RT-PCR products from rat hippocampal cells showing GAD67 (inhibitory) and SLC17A7 (excitatory) mRNA expression. GAPDH is shown as a control marker. ***B*.** RNA was isolated and reverse transcription was performed with specific nested primers. Gene markers were amplified using the two-rounded nested primer method. Phenotypes (see legend) in order of lowest to highest percentage: GAD67 & ChAT, 4%; SLC17A7, 14%; GAD67, 25% and GAD67 & SLC17A7, 39%. 18% cells did not display a neuronal phenotype. (*n*=28).

5.3.1 Human neuronal cell lines: SC-RT-PCR analysis of 197VMs

Ideally, to fully understand the functional impact of $Na_V1.1$ splice variants recordings would be performed in human-derived neurons. This is of particular importance in studies concerning $Na_V1.1$ due to enormous variations in its regulation in different cell lines (Isom 2001) and its upregulation in inhibitory interneurons (Yu *et al.,* 2006). Primary cell cultures from rodents are simpler to obtain and more robustly (albeit not completely) neuronal in phenotype. However, exon 5 is not alternatively spliced in *SCN1A* in rodents (Tate *et al.,* 2005; Gazina *et al.,* 2010). A suitable alternative may be the 197VM cell line. This is an immortalized human fetal neural stem cell line derived

from the ventral mesencephalon that can potentially differentiate into cells with active sodium currents (Donato *et al.,* 2007). Briefly, the differentiation involved plating the multipotent cells onto uncoated plastic and allowing neurospheres to develop for a week. Cells were than transferred onto laminin and maintained for 4 days in the presence of growth factors. Finally, 197VMs were starved of growth factors for a following week, according to published reports (Donato *et al.,* 2007). To determine the success of the differentiation protocol, the phenotypes of undifferentiated cells were assessed using SC-RT-PCR. Two cells spontaneously differentiated into individual cholinergic and dopaminergic phenotypes. No cells expressed more than one marker and nearly 90% cells did not possess a categorized neuronal phenotype.

The Donato *et al.* study demonstrated that differentiated 197VMs stained positively for βIII tubulin, a neuronal microtubule protein, encoded by *TUBB3*. Therefore this gene was used a control marker to confirm successful cell aspiration in SC-RT-PCR experiments on differentiated cells. Additionally, immunohistochemisty staining suggested that when differentiated, 197VMs possessed a dopaminergic phenotype. This was confirmed in SC-PCR-RT experiments where 25% cells stained positively for TH (*n*=12; Figure 5.2 B). Some SC-PCR-RT rat hippocampal and 197VMs data had false GADPH positives, all these cells were discarded from further analysis.
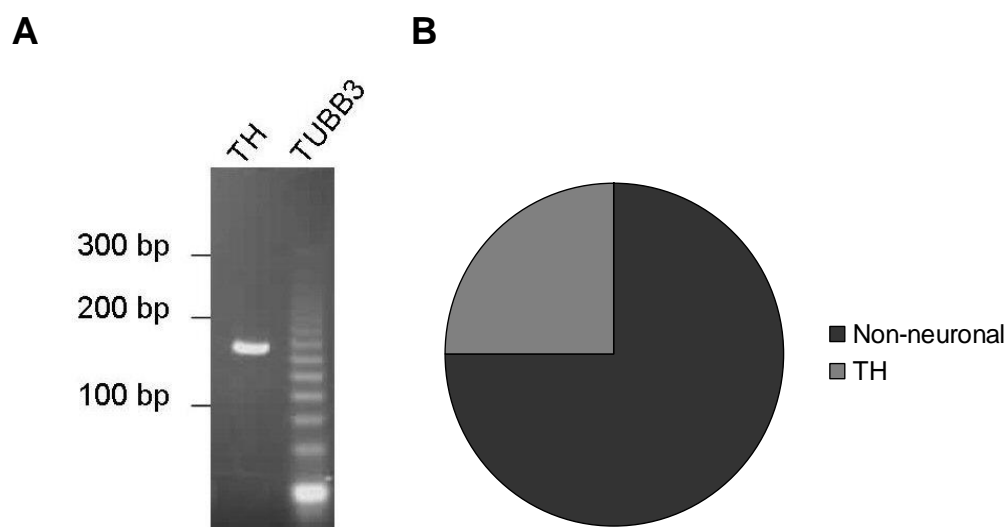
Figure 5.2: The percentage of differentiated 197VM cells that express TH mRNA
A. A typical photograph of the RT-PCR products from a differentiated 197VM showing TH and TUBB3 (control) mRNA expression. Ladder effect of TUBB3 amplicon indicated that this gene is abundantly transcribed. ***B.*** RNA was isolated and reverse transcription was performed with specific nested primers. Gene markers were amplified using the two-rounded nested primer method. 25% of cells possessed a dopaminergic phenotype (*n*=12).

5.3.2 Human neuronal cell lines: Electrophysiological characterization of differentiated 197VM cells

To investigate whether the SC-RT-PCR data was consistent with the electrophysiological behaviour of differentiated 197VM cells, their voltage-dependent currents were assessed. Donato *et al.* (2007) were able to elicit neuronal firing behaviour by stepping the current command from -60 to +20 mV in 20 mV steps from a resting potential of -75 mV using stem cells differentiated for two-weeks by starving them of growth factors. Additionally, recorded macroscopic TTX-sensitive sodium currents were recorded in Donato *et al.,* with an average amplitude of 200 pA. However, in the present

study, no sodium currents were recorded by initial whole-cell patch clamp on cells differentiated using the published protocol. Only an unspecified outward current was observed.

In the published report a small proportion of one-month differentiated 197VM cells still possessed firing properties. Consequently, electrophysiology investigations were extended to 197VMs differentiated for 4 – 6 weeks. Cells maintained in culture for longer than 4 weeks were held at -80 mV and stepped to voltages between -100 and +30 mV in 10 mV intervals. Again, an unclassified, although an outward current was recorded (Figure 5.3) with a maximal conductance of 537.3 ± 62.1 pS (n=8).
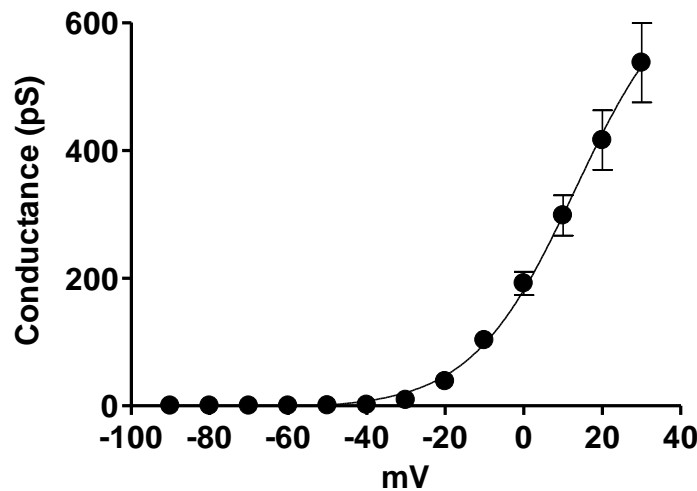
Figure 5.3: Average conductance-voltage relationship for 4 - 6 week differentiated 197VMs. A robust outward current was observed but no sodium currents (n=8)

5.4.1 Potential animal neuronal models: Online sequences of SCN1A exon 5N

The differentiation of human stem cell lines is unreliable, both in experiments tested here and within informal reports from other groups. RT-PCR data suggest these cells

produce ambiguous neuronal phenotypes. Electrophysiological data suggest they are not ideal for routine electrophysiology that requires close comparison of multiple recordings over long periods of time from different batches of cells.

The alternative approach to differentiating human stem cells into neurons is to use primary neuronal cultures from animal sources which do alternatively splice *SCN1A*. Consequently, alternative splicing in *SCN1A* throughout phyla was investigated using the sequences databases from NCBI and Ensembl. Unfortunately, of the laboratory animals approved for use in the UK, only *Monodelphis domestica* (Opossum) faithfully conserves splicing with human exon 5 in the published database (Figure 5.4).
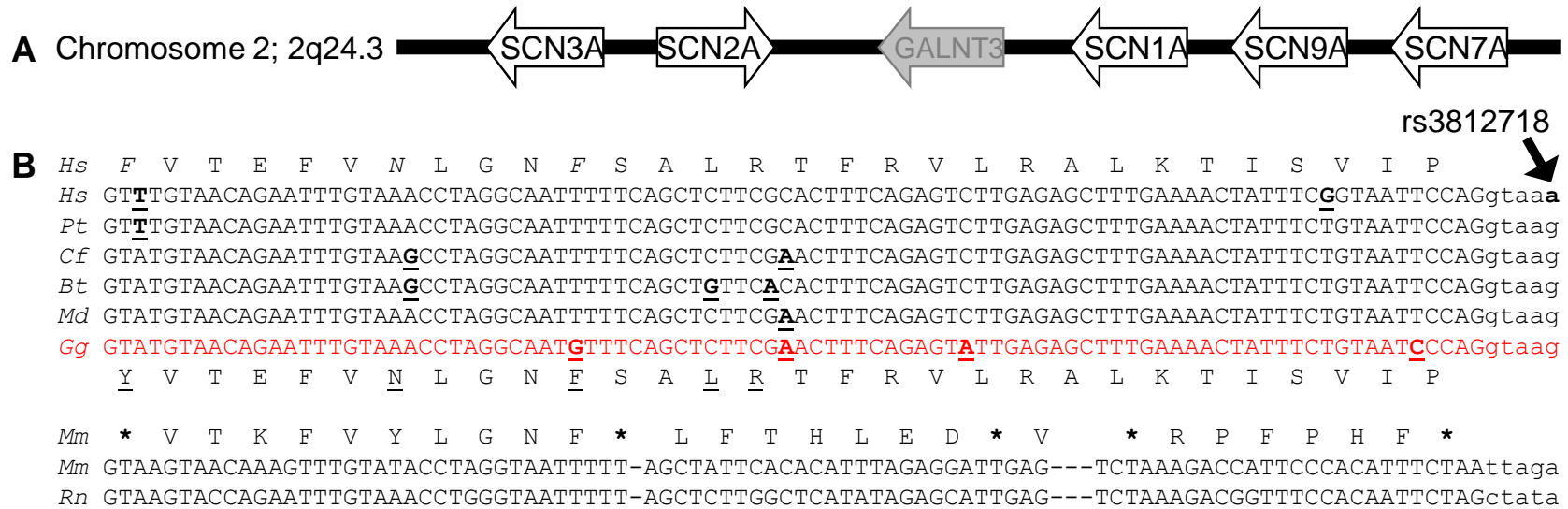
Figure 5.4 Exon 5N in *SCN1A* is widely conserved among amniota vertebrates, but is lost in rodents. *A.* Overview of sodium channel gene cluster on chromosome 2 in humans. The cluster is conserved among amniota vertebrates, and the position of surrounding sodium genes as well as GALNT3 was used to distinguish exon 5N in *SCN1A* from that of the nearby and closely-related sodium channel genes. *B.* Alignment of exon 5N and flanking 3'splice sequence from genomic sequences of a selection of amniota vertebrates. Individual nucleotides that vary are bold and underlined. The human translation is shown at top with residues that alter between exon 5N and 5A in humans italicised. The consensus translation of exon 5N in *SCN1A* is shown at the bottom of the alignment of conserved exons, with varying residues underlined (note that while the cow (Bt) has 3 varying residues, in all other cases 2 or fewer differ from the consensus translation). For comparison, the mouse (Mm) translation is shown above the rodent alignment. While the rat (Rn) and mouse nucleic sequences and translations differ substantially, as is usual for non-coding regions, the presence of 4 stop codons and the frameshift in exon 5N are conserved. For completeness, the position of rs3812718 is indicated as the A genotype in the human sequence to emphasize the conservation of this nucleotide among amniota vertebrates, excepting rodents. Hs = *Homo sapiens*, human NC_000002.10; Pt = *Pan troglodytes,* chimp NC_006470.2; Cf = *Canis familiaris,* dog NC_006618.2; Bt = *Bos taurus,* cow NW_980441; Md = *Monodelphis domestica,* opossum ENSMODG00000006537*;* Gg = *Gallus gallus, chicken* NC_006094*;* Mm = *Mus musculus*, mouse NC_000068.5; Rn = *Rattus norvegicus*, rat NC_005102.2. All sequences from NCBI genome data, except Md which is from Ensembl. Sequences were located using exon 5A, confirming the position of *SCN1A* in the gene cluster and searching the flanking intron for sequences homologous to exon 5N in humans.

282

5.4.2 Potential animal neuronal models: No exon 5 alternative splicing in Guinea Pig SCN1A

The *Cavia porcellus* (guinea pig) genome sequence was not published online in a complete form, however, guinea pigs are easy animals to acquire and handle. They are also approved for laboratory work in the UK. Exon 5 of human *SCN1A* is 92 nucleotides long. The guinea pig putative *SCN1A* sequence was available to mid intron 2. However, Ensembl predicted that exon 3 was 92 nucleotides long and consequently, could be the equivalent of human exon 5. Fortunately, the intron 4 sequence was available. Therefore, primers were designed to align to the end of intron 2 and the beginning of intron 4. A band approximately 4kb was amplified by PCR and sequenced. This sequence was aligned to human *SCN1A* in the region and it appears the guinea pig exon 3 corresponds to the human *SCN1A* exon 5A (Figure 5.5). The assumed guinea pig exon 5N sequence that lies with intron 2 has an in frame stop codon, indicating that guinea pig *SCN1A,* like rodent *SCN1A*, is not alternatively spliced in this region (Figure 5.5).

```
SCN1A 5N     GTTTGTAACAGAATTTGTAAACCTAGGCAATTTTTC
             .|...||||||||||.|||||. |||||||.|||||.
GP intron 2  ATACATAACAGAATGTGTAAG-CTAGGCACTTTTTAAGTTCTTTGCAATCTCATATTTTCCAG

             AATTTTGACAACTACTTACATAACCCAGAGTAAGAAGTAGTTAGTATAAAGCACAGATTCCTA

SCN1A 5A                                                             GTACGTCAC
                                                                     .|||||.||
GP exon 3?   CAACTCTTTCTTTGTGTCTTCTTGTTGTGTCTGTGTGTGAACTCCCTATTACAGATACGTGAC

             AGAGTTTGTGGACCTGGGCAATGTCTC
             |||||||||||||||||||||||||||
             AGAGTTTGTGGACCTGGGCAATGTCTCAGCGTTGAGAACATTCAGAGTTCTCCGAGCACTGAAA
```

Figure 5.5: Sequence alignments of the intron-exon border 2-3 of guinea pig *SCN1A* with human adult and neonatal *SCN1A* sequences. Nucleotide changes between the human splice variants are in bold. Sequence in blue is unpublished. The putative $Na_V1.1$-5N guinea pig sequence within intron 2 is interrupted by an in frame stop codon (red letters). The putative $Na_V1.1$-5A guinea pig in exon 3 is conserved with human $Na_V1.1$-5A.

5.4.3 Potential animal neuronal models: Chick embryonic neurons genotype and phenotype

Chicken *SCN1A* is alternatively spliced (Figure 5.4, in red), and conserves the D>N switch. Chick embryos are also used for primary cultures, albeit the anatomy is less well conserved, and cell types may be distinct from those found in humans and other mammals. Whole-cell patch clamp experiments were performed to establish if telencephalon neurons prepared at E14 and cultured for seven days exhibited neuronal sodium currents. After attaining the whole-cell configuration the resting membrane potential (RMP) was measured in the current-clamp I = 0 mode. Typical for immature neurons, the RMP of chick E14 neurons was depolarized (Belleau & Warren, 2000) at -8.4 ± 7.8 mV (*n*=3). To assess macroscopic neuronal currents, cells were held at -80 mV and stepped to voltages between -60 and +30 mV in 10 mV intervals. As demonstrated by the raw trace in Figure 5.6 these immature neurons expressed robust sodium and potassium currents. A number of cells were patched

but currents were too large to clamp efficiently (data not shown).

Figure 5.6 Immature chick cultured chick neurons are likely to express sodium and potassium currents. A 7-day cultured E14 chick neuron macroscopic current elicited at - 10 mV from a holding potential of – 80 mV,

A challenge to recording from heterologously expressed splice variants in neurons is isolating currents from the channels of interest in the presence of a complex background. One approach used by several groups is to isolate exogenous human $Na_V1.1$ currents in chick neurons by generating TTX-resistant mutant variants of the human channels. Through experimenting in the presence of TTX, the currents from each splice variant could be isolated from other TTX-sensitive channels in the chick cells. This depends on the currents in the chick neurons being sensitive to TTX. RT-PCR was used to determine which members of the VGSC were transcribed in the immature chick brain. At E14 only TTX-sensitive sodium channels were expressed (Figure 5.7) and confirmed that this neuronal model would be excellent for investigating in $Na_V1.1$ splice variants.
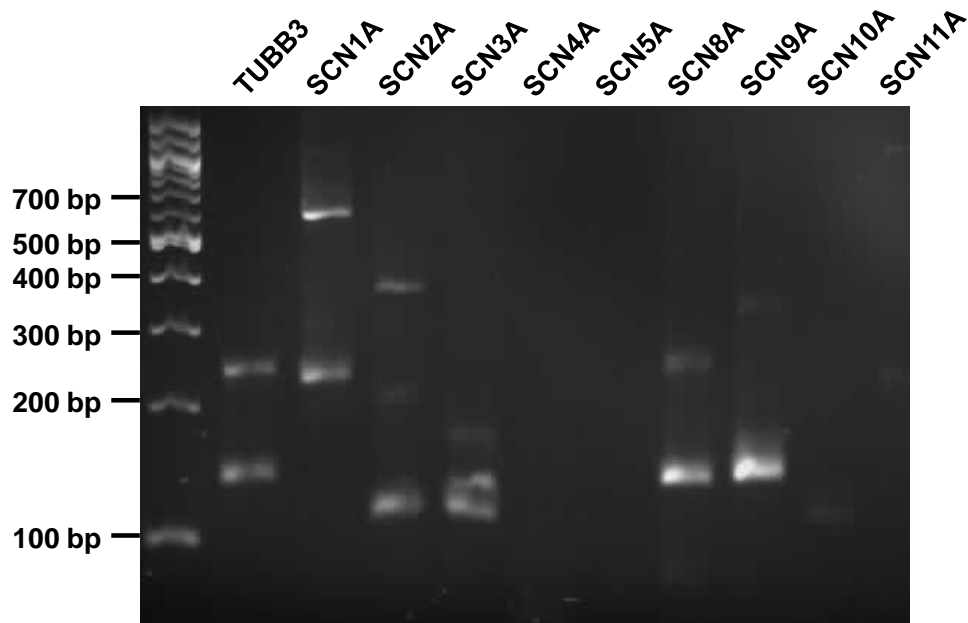
Figure 5.7: VGSC gene expression profile of the chick telencephalon at E14. RNA was isolated and reverse transcription was performed with specific primers designed using predicted chicken VGSC gene sequences published by Ensembl. PCR only detected the expression of TTX-sensitive sodium channels (from left to right) the control gene *TUBB3* (134 bp); *SCN1A* (227 bp); *SCN2A* (107 bp); *SCN3A* (113 bp); *SCN8A* (138 bp) and *SCN9A* (141 bp).

To avoid the toxicity of transfection reagents $Na_V1.1$ splice variants can be transduced into chicken neurons using lentiviral vectors. The human sodium channel cDNAs are known to be difficult to maintain in high copy vectors. Although several attempts were made to insert *SCN1A* coding sequences into a lentiviral expression vector, it was not possible to produce full-length clones in this background (data not shown). Consequently, although this model has several advantages it was abandoned in the interest of time.

5.5 Discussion

5.5.1 SC-RT-PCR analysis of rat hippocampal cells

The majority of two-week cultured hippocampal cells, that expressed neuronal markers, up-regulated both inhibitory, GAD67 and excitatory SLC17A7 mRNAs. Classically, the hippocampus is thought to comprise of strictly defined neuronal types, with glutamatergic and GABAergic phenotypes segregated. However, data in the present study are in agreement with the few studies that have investigated the phenotype of hippocampal neurons in culture using SC-RT-PCR and shown less clearly defined expression profiles. For example, Gómez-Lira and colleagues (2005) showed that all cultured hippocampal granule cells from juvenile rats (P15) possessed a mixed excitatory/inhibitory phenotype. In similar hippocampal preparations to those in this study, neurons that evoked EPSPs also expressed an isoform of GAD67, GAD65 (Cao *et al.,* 1996). Lastly, 20% hippocampal neurons from two week old rats co-expressed GAD67 and SLC17A7. *In vivo*, certainly for granule cells, it is now recognized that glutamatergic cells are capable of synthesizing GABA (For reviews see Gutiérrez 2005 and Scharfman 2002).

Conversely, since neurons were grown in culture for two weeks it is possible that changes in the external environment may have changed the transcriptional regulation of a mainly inhibitory neuronal population, as 25% of cells were positive for GAD67. Further, since post-translational processes were not investigated it is impossible to decipher whether the mRNA transcribed for both excitatory and inhibitory markers was translated. There may be an RNA binding protein that suppresses translation of one marker and not the other, so although these cells may transcribe both mRNAs the proteins may be regulated at the level

287

of translation. Even if an mRNA is transcribed and translated, the proteins may be subjected to post-translational processing such as: phosphorylation, localization or degradation (Sucher *et al.,* 2000). To address this ambiguity in future, SC-RT-PCR should be coupled with electrophysiological recordings and, if possible, additional immunohistochemical or morphological data. This would allow a thorough examination of gene expression at transcriptional and functional levels combined with protein localization.

It is likely that inhibitory interneurons were aspirated as quarter of cells were solely inhibitory. Fewer SLC17A7 cells were harvested which is surprising as the main hippocampal projectory pyramidal neurons are excitatory. In the studies mentioned previously, no sole inhibitory or excitatory phenotypes were observed. Since the sample sizes were relatively small, typically 10 − 30 cells, it is unlikely a true phenotypic representation was covered in these studies. Additionally, the number of markers used was limited. There are at least three isoforms of SLC17A7 and GAD, each may be functionally similar but able to confer specific properties to different neuronal regions. Therefore, a neuron may have used glutamate as its principle neurotransmitter but its transporter may have been a different isoform to SLC17A7, that is, vGLUT2. In experiments by Danik *et al.* (2005) 60% of hippocampal neurons were positive for two isoforms of SLC17A7, vGLUT1 and 2 but no cell expressed exclusively one transporter, suggesting that the expression of one affects the regulation of the other. This interaction would not have been detected in this present study. One cell possessed a dual inhibitory and cholinergic phenotype. This has not been observed from hippocampal neuronal cultures in the literature. However, SC-RT-PCR involving brain slices suggests that fast spiking neurons within the medial septum-diagonal band complex release both GABA and acetylcholine

(Sotty *et al.,* 2003).

The main caveat to the SC-RT-PCR technique is contamination. It is estimated that each vertebrate neuron contains 1 pg of mRNA; consequently any DNA or RNA, derived from dead cells for instance, would severely affect the results. Originally random primers were used to generate cDNA and the PCR reaction contained specific primers for the amplification of any gene. However, there was a high level of GAPDH contamination within controls taken from the bath and intracellular solutions. Therefore the 'nested' primer technique was adopted as it was hypothesized the GAPDH may have share a high sequence similarity with several genes. Although low, contamination was still present. Another step was added, the mRNA was pre-treated with DNase, to degrade any DNA that may have contaminated the equipment or solutions. However, impurity levels were not greatly improved and data was frequently lost. In the present study, only experiments where GAPDH was absent in control reactions were used. The consistent absence of TH from hippocampal neurons, along with its presence in 197VMs, and in controls using whole brain mRNA, suggests that the detection of marker mRNAs was specific.

A drawback to using gene specific primers instead of random primers is that additional information about gene co-localizations, pathway crosstalk and other interactions cannot be investigated in these samples (Dixon 2000). This may be overcome by using 'three-prime-end amplification PCR'. This involves amplifying the 3' ends of all mRNAs in a single cell. This has allowed for 40 transcripts to be detected for one cell (Dixon *et al.,* 1998). A disadvantage is that this technique is not quantitative. There are quantitative techniques that use radioactively-labelled primers. Since the sample size is minute these methods are at

best likely to be semi-quantitative and could give informative on the relative differences of two markers rather than the quantity of mRNA transcribed (Sucher *et al.,* 2000).

5.5.2 Transcriptional and functional characterization of 197VMs

197VMs were originally developed to generate dopaminergic cells to be used in neuron replacement therapies to treat neurodegenerative disorders, for instance, Parkinson's disease. 197VMs are derived from progenitor cells dissected from the ventral mesencephalon, of a 10 week old foetus. Within this area three clusters of progenitor cells, A8-A10 give rise to a region of the red nucleus, the substantia nigra pars compacta and the ventral tegmental area, respectively. In the adult brain these regions are rich in dopaminergic neurons (Abeliovich & Hammond, 2007). It is not too surprising; therefore, that TH was expressed by a single undifferentiated 197VM cell. The ventral mesencephalon also gives rise to the tegmentum, where cholinergic neurons involved in wakefulness and arousal send their projections to the thalamus. The end phenotype of cells is dependent on local environment as well as their innate properties (Gage 2000). Since one cell also spontaneously differentiated to express ChAT, these cells could be directed to a cholinergic fate, possibly if grown in the presence of specific growth factors.

As previously discussed the for SC-RT-PCR analysis GAPDH was present in many control reactions. In the Donato *et al.* (2007) paper immunocytochemistry images showed that the differentiated 197VMs expressed a neuronal microtubule protein βIII tubulin. This change in marker was very successful and contamination vanished. Since electrophysiological studies were done in parallel, and demonstrated that differentiated cells did not produce active currents, it was decided that these cells would be not be use a model for the $Na_V1.1$

studies. This analysis, however, did confirm the findings from Donato *et al.* these multipotent cells when differentiated did express βIII tubulin and a proportion also expressed TH.

In this study, the 197VMs differentiated for 2-6 weeks did not develop into functional neurons. In the Donato *et al.* study, similar cells differentiated for 10 days generated action potentials and had TTX-sensitive sodium currents and potassium currents. Although the culture conditions were followed exactly, there may have been other variables; for example, different 197VM batches, unstable growth factors, laminin from different strains of mice, variations in exposure times to growth factors, or different cryogenic techniques may all have altered the expression profile of these cells.

197VMs were immortalized using a human oncogene, V-MYC. Gage (2005) hypothesizes that cell lines immortalized with this gene undergo subsequent mutations that may render them tumorigenic or disrupt their normal cell homeostasis. Mutations within the chicken homolog C-MYC changes its transforming capacity to a lesser or greater extent (Frykberg *et al.,* 1987). In the Donato *et al.* study a cortical stem cell was differentiated in the same manner but also did not produce voltage-gated channels. This cell line was created using the 'less potent' C-MYC and may have been the crucial determinate in cell fate rather than the differentiation protocol. Within the literature, laboratories using the similar cell lines receive varying results (Cho *et al.,* 2002; Donato *et al.,* 2007). Suggesting that stem cell research still relies on unknown factors that greatly influence cell fate.

5.5.3 Exon 5N is lost in Guinea Pig SCN1A but not chicken SCN1A

While splicing is conserved in six VGSCs (Raymond *et al.,* 2004), exon 5N has been lost in

Rodentia including rat, mouse and guinea pig *SCN1A* (Raymond *et al.,* 2004). However, the D>N switch in exon 5 is conserved in chicken *SCN1A*. As previously discussed, one aim of the study was to determine whether the upregulation of $Na_V1.1$-5N leads to changes in neuronal excitability that are correlated with epileptic behaviour and/or drug dosage. Determining what effect a shift in splicing of *SCN1A* has on the behaviour of neurons would have been the most direct way to address this goal. To achieve this aim, transducing chick neurons with $Na_V1.1$-5N and $Na_V1.1$-5A clones would have been a promising electrophysiological preparation. Indeed, biophysical investigations into the neuronal networks and ion channels of the avian auditory system frequently employ cultured embryonic chick neurons (Kuenzel *et al.,* 2007; Wirth *et al.,* 2008; Kuenzel *et al.,* 2009).

The pCDH1-copGFP lentivector (System Biosciences, CA) has been used successfully to transduce $K_V1.1$ channels into cultured hippocampal neurons in the lab (Heeroma *et al.,* 2009). However, cloning human *SCN1A* into the same vector proved unfeasible for technical reasons. Frequently during subcloning, fragments of *SCN1A* sequence were deleted, duplicated and often rearranged, and the effort was stopped because material and DNA sequencing costs were escalating and HEK experiments were a necessary compromise.

These results show that E14 immature chick telencephalon neurons only expressed TTX sensitive VGSCs. If inserting human *SCN1A* into the lentivector were successful, currents mediated by the splice variants would be isolated by generating TTX-resistant variants by introducing a single amino acid change, E945Q, into the construct (Kontis & Goldin, 1993). In the presence of TTX, the currents from each $Na_V1.1$ isoform could be isolated

from all other TTX sensitive VGSCs in the neuronal cells. Using a Cs-Aspartate-based intracellular and TEA-Cl-containing extracellular solutions $Na_V1.1$ splice variant currents in chicken neurons could be isolated from endogenous sodium and potassium currents. The intracellular solution would contain ATP and GTP, to preserve downstream signalling pathways.

Electrophysiological characterization of transduced neurons could be coupled with SC-RT-PCR analysis to determine if $Na_V1.1$ splice variants behave differently in different cell backgrounds. The chick genome is yet to be fully sequenced. One caveat of this analysis is that many of the oligonucleotides used to amplify chick VGSC genes (and therefore those that would be used to amplify genetic cell marker genes) were designed using predicted DNA sequences. Therefore, the VGSC gene expression profile of E14 chick neurons may be inaccurate. Ensembl are continuing to update the chicken DNA sequence database so future gene expression profiling may be more reliable (Last updated May 2010; http://www.Ensembl.org/Gallus_gallus/Info/StatsTable). Moreover, one report documented that between E7 to E20 two voltage-gated potassium channel isoforms were up-regulated in hindbrain auditory chick neurons. Expression of one isoform gradually increased and transcription of another was switched on at E14 (Kuenzel *et al.,* 2009). Computer modelling showed that this switch would *in vivo* dramatically alter the firing properties of these immature neurons (Kuenzel *et al.,* 2009). From the electrophysiological results in this study and the literature it is possible to record from dissociated chick neurons between E6.5 – E14 (Kuenzel *et al.,* 2007). Therefore this model would be ideal to examine the effects of neuronal development on the behaviour of wild-type and mutant $Na_V1.1$ splice variants. Chick $Na_V1.1$-5N or $Na_V1.1$-5A could be selectively knocked-down and/or GEFS+

mutations could be introduced.

Not only could voltage clamp protocols, similar to those described in this study be performed but also current clamp protocols could assess differences in firing properties of neurons expressing wild-type or mutant $Na_V1.1$-5N or $Na_V1.1$-5A channels in dissociated cultures. These experiments could be used in conjunction with immunocytochemistry (Chapter 7) and would give an indication if firstly, if the subcellular localization of each splice variant varies and if so, their relative contributions to spike development, especially with regards to inhibitory interneurons. Neurons could be cultured in the presence of GABA receptor antagonists, NMDA receptor activators or low magnesium conditions, which can induce SE-like neuronal firing discharges (Sombati & Delorenzo, 1995; Pitkänen *et al.,* 2005, p330). Pharmacology experiments could determine whether healthy or 'epileptic' neurons of different sub-types fire differently in response to AEDs depending on their *SCN1A* exon 5 identity.

Additionally the neuronal RMP, input resistance and capacitance could be calculated and single action potential parameters could be assessed with a brief, 1 ms, current clamp protocol. Here, action potential threshold, amplitude, spike width, AHP and rise time could be calculated and would determine how significantly each $Na_V1.1$ splice variant contributes to neuronal spike-phenotypes (Bean 2007). In a neuronal context these types of experiments may help to answer what is the real functional impact of splicing on $Na_V1.1$ properties, the role of $Na_V1.1$ isoforms in epileptic neurons, or if individual $Na_V1.1$ splice variants should be specifically targeted by future AEDs.

Chapter 6: Lack of G-protein effects on $I\text{Na}_P$ at physiological temperatures

6.1 Hypothesis and aim:

Hypothesis: $\text{Na}_V1.1$ splice variants are differentially modulated by G-protein receptor signalling pathways and more specifically by G-protein βγ subunits.

Background and experimental aims: When heterologously expressed in HEK cells, $\text{Na}_V1.1$ channels exhibit extremely variable levels of persistent or non-inactivating current. An examination into the factors that supported this current indicated that activation of G-protein βγ subunits was sufficient to increase the current from these channels (Mantegazza *et al.,* 2005). In preliminary experiments (carried out with Stephanie Schorge) it was demonstrated that $\text{Na}_V1.15A$ derived $I\text{Na}_P$ in HEK cells was inhibited by Pertussis toxin, a Gαi/o inhibitor, suggesting the presence of endogenous G-proteins in these cells were capable of modulating $I\text{Na}_P$. The aim of this section was to determine whether G-proteins, particularly βγ subunits exert splice variant specific effects on the $I\text{Na}_P$ of $\text{Na}_V1.1-5N$.

In an effort to determine what contributes to $I\text{Na}_P$ and to control the expression of this current in recordings in HEKs a series of experiments were carried out to identify and control G-protein βγ subunits that are active in HEK 293 cells. Molecular and pharmacological tools were constructed, verified and used, including: the GRKs, which bind to and inactivate different subsets of G-protein βγ subunits; and the α subunit of transducin the retinal G-protein, which has a high affinity for all βγ subunits, and can be used to disrupt all βγ-dependent G-protein signalling; finally GTPγS which is a non-

hydrolysable analogue of GTP that binds G-protein α subunits and locks them in the 'active' form, and releases the βγ subunits. GTPγS is a non-specific activator of G-proteins while the other reagents are more specific inactivators of subsets of βγ subunits only. These data show that at physiological temperatures none of the molecular or pharmacological manipulations of G-protein signalling alter INa$_P$, although several other parameters of Na$_V$1.1 macroscopic currents are altered. G-protein dependent modulation of INa$_P$ was only present in RT recordings.

6.2 Establishing tools 1: Which G-proteins are expressed in HEK 293 cells?

One aim of this study was to determine which G-proteins interact with Na$_V$1.1 variants. Heterotrimeric G-proteins are extremely diverse. There are 16 genes that code for α subunits, some are alternatively spliced, producing a total of 20 gene products. There are 5 β subtypes and at least 12 γ isoforms. The potential Gαβγ and more importantly βγ combinations are numerous. *In vivo*, however, not all possible arrangements exist. For instance, there is β1γ2 but not β2γ1 and β1γ1 is solely expressed by photoreceptors (Gomperts *et al.*, 2003). Indeed, the latter did not induce INa$_P$ derived from Na$_V$1.2 (Ma *et al.,* 1997) but Gβ2γ3, Gβ1γ3 and Gβ5γ3 all produced Na$_V$1.2 cells with slowly inactivating currents.

Using PCR, 22 G-protein subunit expression profiles of three consecutive passages of HEK 293 cells (cultured in 2007) were assessed, to determine which specific subunits were potentially modulating Na$_V$1.1. Bands corresponding to amplified subunit mRNAs were rated for relative brightness: a saturated band, 1, denoted abundant expression, a visible band, 0.5, moderate expression and no band detection was given 0.

296

In each passage all but two Gα subunits were moderately to abundantly expressed. GNAO was absent in all but one passage and GNAZ was not detected. Both genes are thought to exclusively neuronal (Wettschureck & Offermanns, 2006). All Gβ subunits were highly expressed in the three samples. The expression profiles of Gγ were more variable. In general, the majority of Gγ subunits were moderately to abundantly expressed. However, two subunits, GNG8 and GNG13 were not detected. This is expected since the former is detected only in the olfactory epithelium and the latter in taste buds (Wettschureck & Offermanns, 2006). In summary, this cell line expresses a wide range of G-protein subunits (Figure 6.1); the expression is also relatively consistent over multiple passages (Figure 6.2).
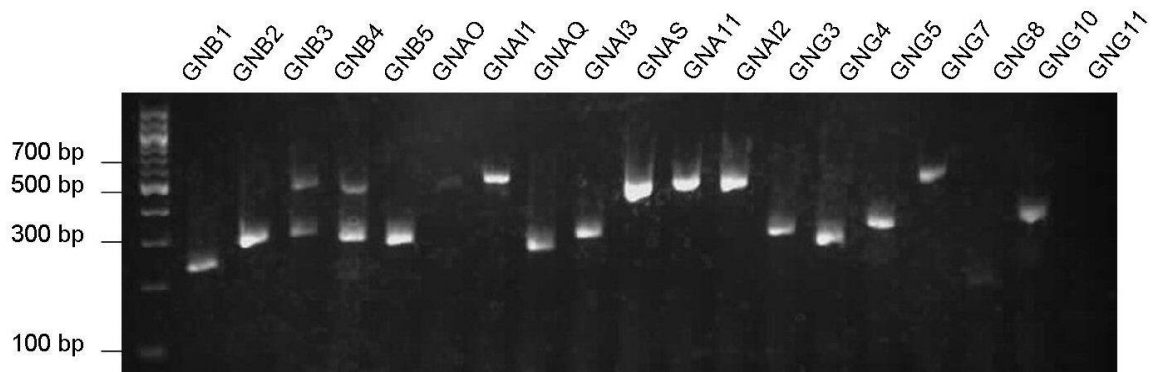
Figure 6.1: A typical image showing the PCR products from one HEK 293 passage.

Passage 1

α subunits | β subunits | γ subunits

Passage 2

α subunits | β subunits | γ subunits
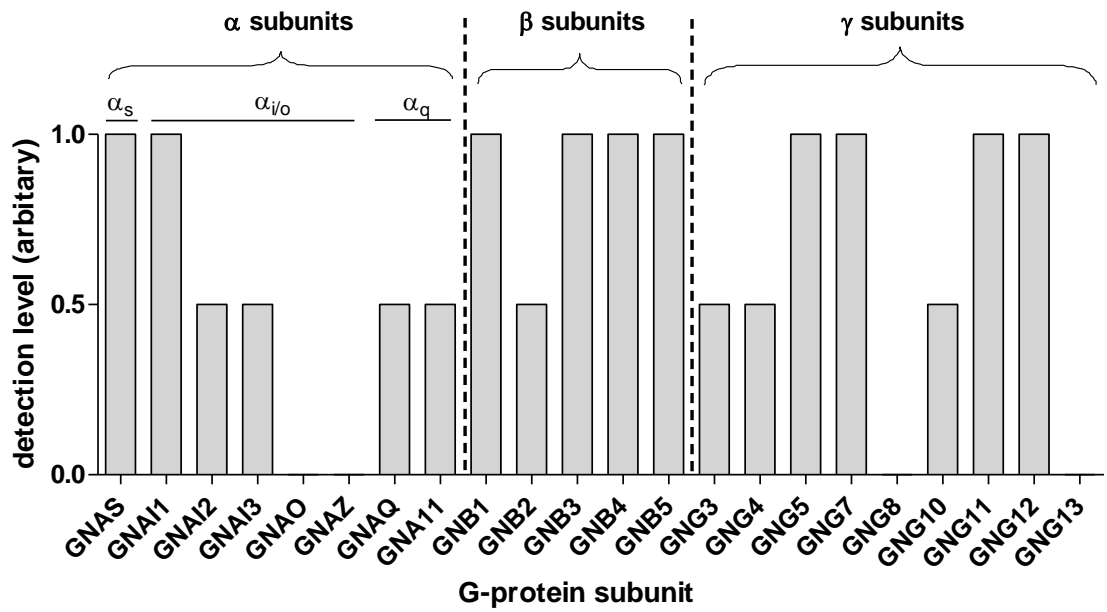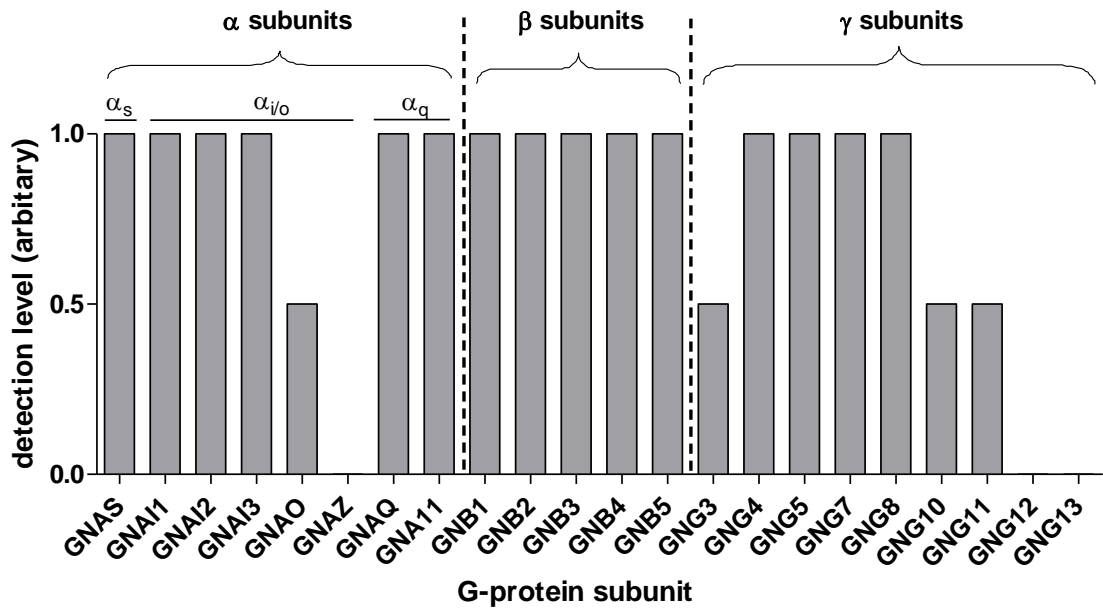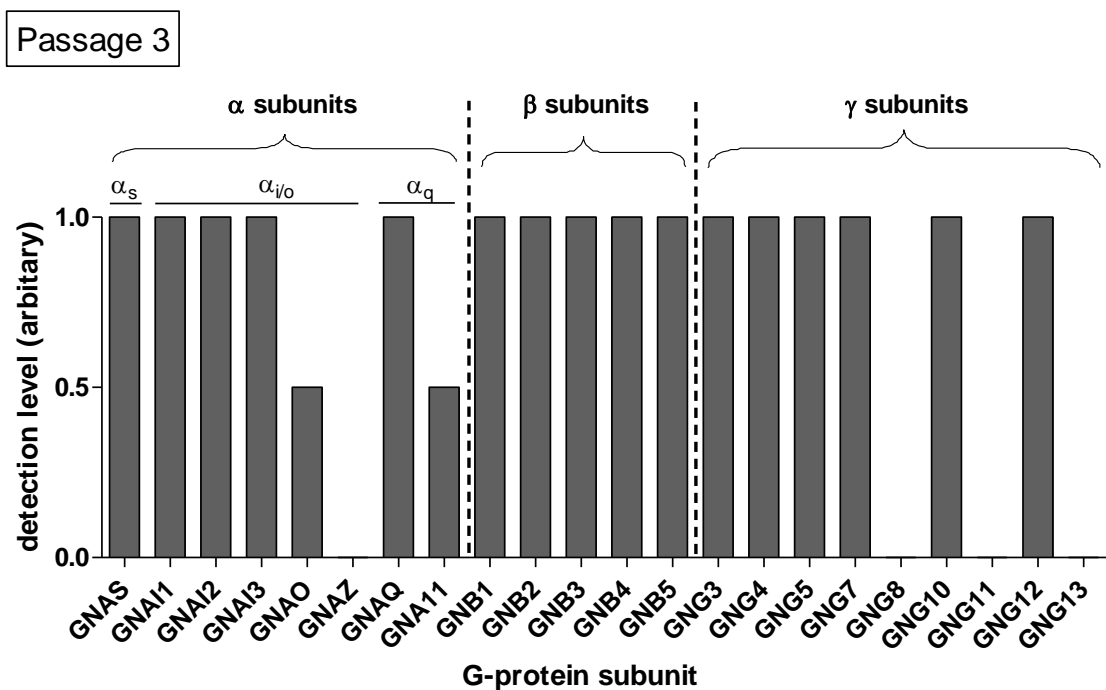
Figure 6.2: The G-protein expression profile of three passages of HEK 293 cells.
Expression levels of genes denoted were rated using band signal: 1 = abundant; 0.5 =
moderate and no expression = 0. Each chart shows data from a single experiment.

6.2 Establishing tools 2: Verification of the effectiveness of molecular sequestration tools

Given the wide range of G-protein subunits present in HEK cells, multiple strategies for
sequestering subsets of endogenous subunits were necessary. Molecular sequestration tools
(see Figures 6.3 & 6.4), were cloned and heterologously expressed. To test the
effectiveness of each clone at suppressing G-protein modulation, the effects of each
sequestrant was measured on channels with well-known G-protein modulation, the GIRKs.

GIRK 1,4 is an heterotetrameric inwardly rectifying potassium channel that is activated by
Gβγ proteins (Figure 6.3 A). It is well established that heterologous expressed GIRK 1,4
currents are inhibited by proteins that sequester intrinsic Gβγ subunits (Figure 6.3 A; Lei *et*

al., 2000). These proteins were subcloned into the pIRES-DsRed2 vector and fluoresced after transfection into HEK 293 cells. However, the control 'empty' vector did not fluoresce (data not shown). Therefore, it was necessary to verify that the sequesterants were translated when subcloned into pIRES-DsRed2,

Whole cell currents were elicited from HEK 293 cells transiently co-transfected with GIRK 1,4 with the sequesterant or reporter constructs indicated (Figure 6.3, B), by using a voltage ramp command (change in -90mV; 0.1V/s) applied at 0.1Hz, from holding potential of -50mV (replicated from Lei *et al.,* 2000). Conductance was calculated from a linear regression fit to the slope of the current-voltage data from -100 to -120mV. The ramp protocol evoked inwardly rectifying potassium currents with a mean conductance ($\pm$SEM) of 35 $\pm$ 9.0 pS (n=5; Figure 6.3 B) in cells transfected with GIRK 1,4 channels that were not present in untransfected cells 3.4 $\pm$ 1.0 nS (n=5; P<0.01; one-way ANOVA; Bonferroni's post-test; Figure 6.3, B). GIRK currents were significantly attenuated by both sequesterants, Gαt (mean pS $\pm$SEM: 11.1 $\pm$ 4.1 nS, n=6, P<0.05; one-way ANOVA; Bonferroni's post-test; Figure 6.3 B) and GRK2ct (mean nS $\pm$SEM: 10.8 $\pm$ 2.8 pS, n=7, P<0.05; one-way ANOVA; Bonferroni's post-test; Figure 6.3 B). The c-terminal of GRK5, which does not bind to G$\beta\gamma$, did not significantly inhibit GIRK 1,4 currents (mean nS $\pm$SEM: 20.1 $\pm$ 2.6 nS, n=3, P>0.05; one-way ANOVA; Bonferroni's post-test; Figure 6.3 B). Collectively these data suggest that the constructs were functional and specific. Based on these results it was assumed that pIRES-DsRED2-GRK3ct was also functional.
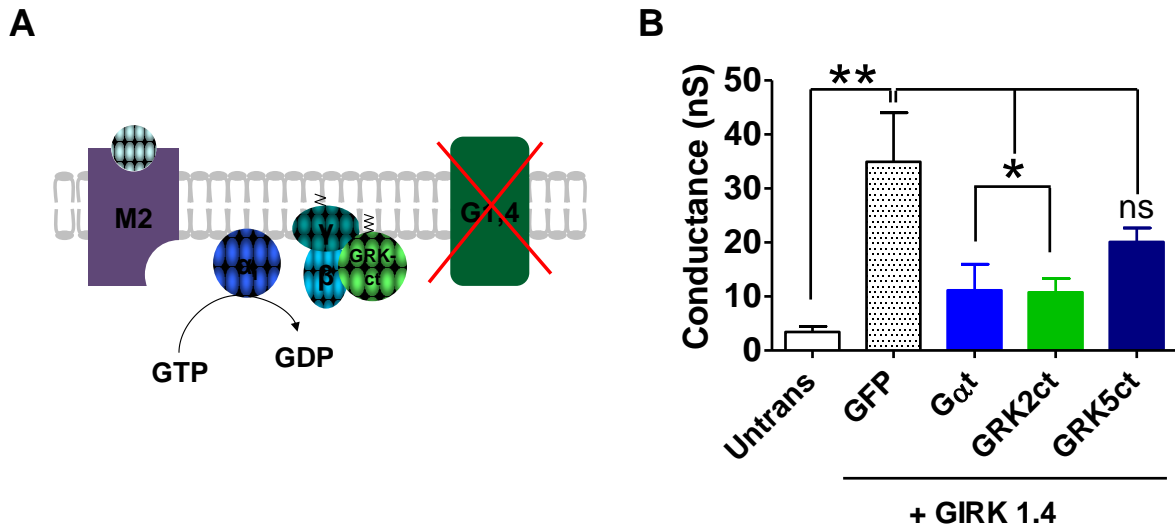
Figure 6.3 Verification of Gβγ sequesterants function when subcloned in pIRES-DsRED2 *A.* Gβγ subunits activate GIRK 1,4, a inwardly rectifying potassium channel; via activation, for example, of cardiac muscarinic receptors (M2). Previous reports suggest that channel activity is inhibited when Gβγ is sequestered by c-terminals of GRKs or Gαt (Lei *et al.,* 2000). This paradigm was used to test the function of inserts subcloned in to pIRES-DsRED2. *B.* The potassium conductance of GIRK 1,4 currents recorded from HEK 293 cells transiently transfected with the channel and denoted constructs. Cells were held at a holding potential of -50 mV and currents were elicited using a ramp protocol described in the text. Conductance was calculated from the slope of current-voltage curve between -100 and 120 mV; mean ±SEM. Currents evoked in cells transfected with GIRK 1,4 alone (and GFP) were not active in untransfected cells, and were inhibited by Gαt and the c-terminal of GRK2. Currents were unaffected by the c-terminal of GRK5 - a protein fragment that does not bind to Gβγ. Significant differences from GIRK 1,4 are indicated by *and** (P<0.05 and P<0.01 respectively, by one-way ANOVA, with Bonferroni's post-test).

6.3 The persistent current of Na$_V$1.1-5A is distinctly modulated by different subsets of

Gβγ proteins

To assess the impact of subsets of G-protein βγ subunits on INa$_P$ from Na$_V$1.1 variants,

individual sequestrants were co-expressed with each variant and the amount of INa$_P$ was

assessed by measuring the amount of persistent current as a proportion of the peak,

transient current. All experiments were carried out in average temperatures ranging from

35-37°C and used CsCl intracellular solutions. To assess the consequences of sequestering

different G-protein subunits, HEK 293 cells were co-transfected with individual channel isoforms and Gβγ binding proteins at a 3:1 ratio, to minimise the toxicity of the IRES vector (higher ratios caused cell death, data not shown).

Figure 6.4 shows families of sodium currents from both splice variants (5A, left; 5N, right) whole-cell recordings in the presence of denoted constructs (left figure panel). As demonstrated in chapter 3 persistent current is substantially reduced at higher temperatures. At physiological temperatures, in the absence of sequestrants, both splice variant channels demonstrated erratic persistent currents, which had similar means (Figure 6.5). The distribution of INa$_P$ as a percent of INa$_T$ from Na$_V$1.1-5A had a slightly larger range (3% - 30%; n=15) compared to that from Na$_V$1.1-5N (0%-11%; n=11; Figure 6.5). This variability may be an indicator of differential Gβγ modulation in different cells.
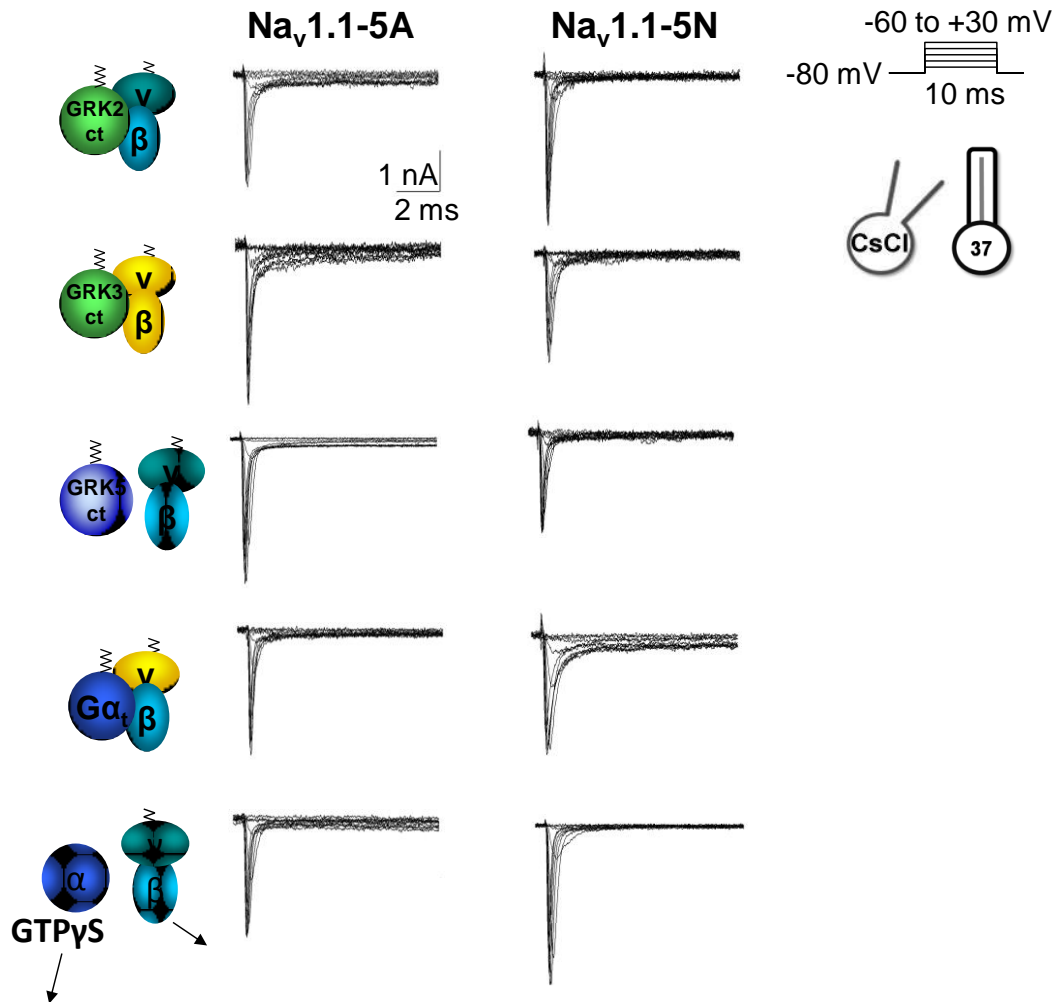
Figure 6.4 Raw traces of sodium currents derived from either Na$_V$1.1-5A (left panel) Na$_V$1.1-5N (right panel) channels when co-expressed with indicated Gβγ sequesterant proteins. Currents were evoked with the current protocol depicted in the inset. C-terminal tails of GRK2 and GRK3 (green) bind to different and overlapping Gβγ pairs, (shown in blues and yellow). GRK5ct (light blue) does not bind to Gβγ proteins unlike Gαt (dark blue) that binds to all Gβγ subunits. GTPγS activates all Gα and in turn Gβγ subunits (Bottom). All recordings were performed at physiological temperatures using CsCl-based solutions.

On consideration of whether both splicing and G-protein regulation affected Na$_V$1.1 persistent current, only GRK2ct significantly reduced the %INa$_P$ in cells co-transfected with Na$_V$1.1-5A. (5A: 8.6 ± 1.6 %, n= 15 versus 5A + GRK2: 3.6 ± 1.3 %, n= 9; P<0.05;

two-way ANOVA, Bonferroni's post-test; Figure 6.5). In contrast, sequestration of subsets of Gβγ by GRK2ct did not affect %INa$_P$ derived Na$_V$1.1-5N (5N: 5.2 ± 1.1 %, n=11 versus 5N + GRK2: 5.4 ± 1.1 %, n=9; P>0.05; Bonferroni's post-tests; Figure 6.5). The binding of a different subset of Gβγ subunits by GRK3ct had no affect on the mean %INa$_P$ recorded for each splice variant, nor the presence of GRK5ct (two-way ANOVA, Bonferroni's post-test; Figure 6.5). These data indicate that the subset of Gβγ subunits sequestered by GRK2ct may specifically activate the persistent current from the Na$_V$1.1-5A variant. While those Gβγ subunits that are sequestered by GRK3ct do not interact with either splice variant. In a final test, complete Gβγ sequestration was carried out by co-expression of Gαt. Interestingly, there was no attenuation of %INa$_P$ from either splice variant (P>0.05, two-way ANOVA, Bonferroni's post-test; Figure 6.5).

All the previous experiments relied on suppressing endogenously active G-proteins in HEK cells. A complementary strategy is to activate G-proteins pharmacologically. Unlike the sequestrants described above, GTPγS is broadly active, and not thought to distinguish between subsets of Gα subunits.

A significant reduction in Na$_V$1.1-5A derived persistent current was observed after complete dissociation of all βγ upon activation of Gα subunits by 0.5 mM of GTPγS (5A: 8.6 ± 1.6 %, n=15 versus 5A + GTPγS: 4.6 ± 0.9, n=9, P<0.05, two-way ANOVA, Bonferroni's post-test; Figure 6.5). This reduction was qualitatively similar to that seen in the presence of GRK2ct, and also was specific to Na$_V$1.1-5A variants (Figure 6.6). This suggests that the reduction of %INa$_P$ induced by the sequestration of Gβγ subunits associated with GRK2ct, could be overridden by extensive, non-specific loss of Gβγ

subunit activity (as with Gαt), and restored by complete activation of Gαβγ subunits (as with GTPγS), and indicates there may be competing regulation of INaP by different subsets of G proteins.

Together these data suggest that a subset of specific Gβγ subunits, and potentially Gα subunits, differentially modulate Na$_V$1.1-5A persistent currents.
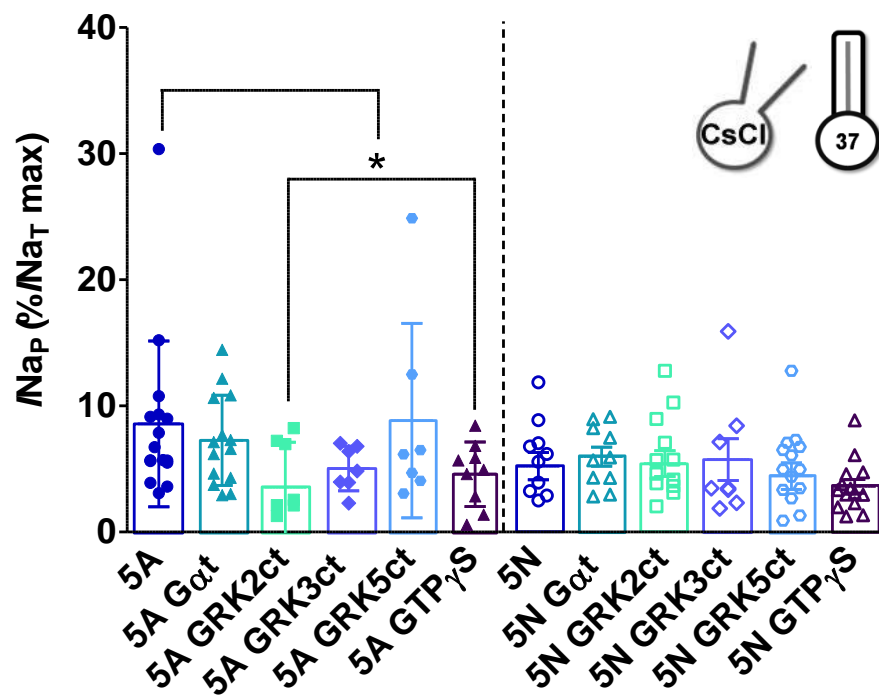
Figure 6.5 Na$_V$1.1 splice variant mean percentage persistent currents in the presence of G-protein modulators. Na$_V$1.1-5N persistent currents were unaffected by G-protein subunit modulation (right). Sequestration of subsets of Gβγ by GRK2ct and complete Gβγ activation by GTPγS significantly reduced Na$_V$1.1-5A persistent currents. In the presence of Gαt these effects were eradicated implying that a subset of specific G protein subunits differentially regulate Na$_V$1.1-5A derived persistent currents. *P<0.05, two-way ANOVA, Bonferroni's post test.

6.4 Other effects of Gβγ subunit sequestrants on macroscopic Na$_V$1.1 currents.

The original hypothesis, supported by preliminary experiments and work from other groups suggested a role for G-protein βγ subunits in regulating the amount of persistent currents produced by heterologously expressed Na$_V$1.1 channels. Only a small change was observed, induced by a single sequestrant, however, in the course of experiments several other effects of G-protein sequestrants were seen, and as these have not been described elsewhere they are briefly summarised here. The previous constructs were designed to analyse INa$_P$ and no earlier reports indicate that Gβγ subunits modify transient Na$_V$1.1 gating. Only parameters that were affected will be discussed for conciseness. Specific changes due to GTPγS are considered separately in section 6.5.

6.4 Other effects 1: GRK3ct and GRK5ct shift Na$_V$1.1-5A voltage dependence of activation to more depolarized potentials

To examine if attenuating the levels of intrinsic Gβγ subunits Na$_V$1.1 splice variant channel activation, current protocols and analyses previously described were applied. Unless otherwise stated statistical tests accounted for both the affect of splicing and Gβγ modulation on Na$_V$1.1 activation. As shown in Figure 6.6 A, GRK5ct caused a significant 5.1 ± 0.4 mV depolarizing shift in Na$_V$1.1-5A mean (±SEM) half-maximal activation (V$_{50act}$ 5A: -18.8 ± 0.9 mV, n=15; 5A + GRK5: -13.4 ± 1.3 mV, n=8; P<0.05, two-way ANOVA, Bonferroni's post-test; Figure 6.6 A). GRK5ct had little effect on 5N-containing channels, demonstrating a comparable midpoint to α subunits expressed alone: -18.7 ± 1.6 mV (n=10; 5N: -18.8 ± 0.8 mV, n=18), suggesting the effect of GRK5ct was specific to Na$_V$1.1-5A

activation (5A + GRK5ct versus 5N + GRK5ct P <0.05; Bonferroni's post-test; Figure 6.6

C).

GRK3ct caused a significant mean (±SEM) 3.7 ± 0.7 mV rightward shift in $Na_V1.1$-5A

half-maximal activation (5A + GRK3ct: -14.8 ± 1.6 mV, n=7; P<0.05, Bonferroni's post-

test; Figure 6.6B). GRK3ct caused a similar mean (±SEM) 2.6 ± 0.0 mV non-significant

shift in $Na_V1.1$-5N activation (5N + GRK3ct: -16.2 ± 0.8 mV; n=10), implying that

GRK3ct may have a general effect on $Na_V1.1$ activation. In support, the mean V_{50} values of

each variant with GRK3ct were not statistically different (Bonferroni's post-test; Figure 6.6

B). Since GRK5ct effected activation but does not interact with Gβγ, changes in INa$_T$

gating caused by GRK3ct and GRK2ct could not be attributed to G-protein interactions.
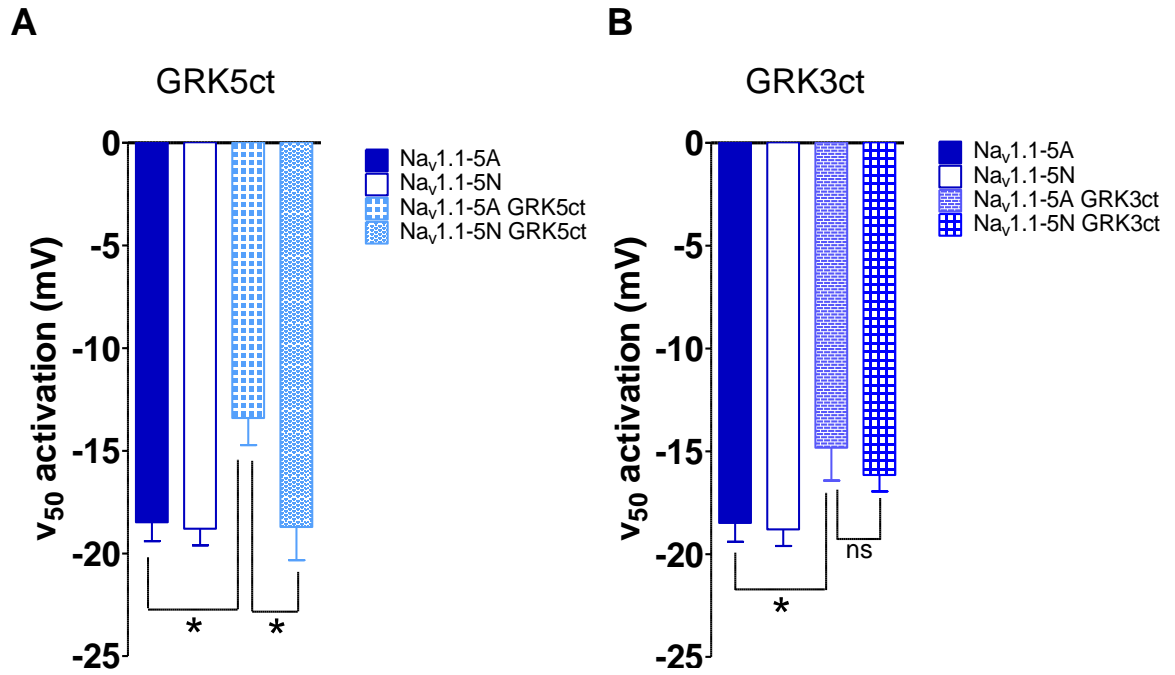
Figure 6.6 GRK3ct and GRK5ct shift Na$_V$1.1-5A voltage dependence of activation in a rightward direction. *A.* Mean (±SEM) V$_{50}$ of activation of Na$_V$1.1-5A + GRK5ct activation was shifted to more depolarized potentials compared to Na$_V$1.1-5A and Na$_V$1.1-5N + GRK5ct. *B.* Mean (±SEM) midpoint of Na$_V$1.1-5A activation was shifted in a rightward direction in the presence of GRK3ct. *P<0.05, two-way ANOVA, Bonferroni's post-tests.

6.4 Other effects 2: The voltage-dependence of inactivation for both Na$_V$1.1 splice variants is altered in the presence of GRK2ct

Unless otherwise stated statistical analyses considered both the affect of splicing and Gβγ modulation on Na$_V$1.1 inactivation. Applying a two-way ANOVA with Bonferroni's post-tests reveals that only GRK2ct affected Na$_V$1.1 channel inactivation. As shown in Figures 6.7 A&C, in the presence of GRK2ct Na$_V$1.1-5N demonstrated a significant -5.5 ± 0.8 mV hyperpolarizing shift in mean (±SEM) V$_{50}$ inactivation (5N: -53.1 ± 1.3 mV, *n*=11 versus 5N + GRK2ct: -58.7 ± 2.1 mV, *n*=9; P<0.05). 5A-containing channels demonstrated a

similar, lesser ~3 mV, midpoint shift (5A: -54.2 ± 1.1 mV, n=14 versus 5A + GRK2ct: -56.8 ± 1.9 mV, n=9; Figure 6.7 B&C); whereby significantly fewer channels were available at -70 mV (P<0.001; two-way ANOVA; Bonferroni's post-test; Figure 6.7 B&C). Compared to control cells GRK2ct significantly increased the slope factor of $Na_V1.1$-5A, but not $Na_V1.1$-5N channel inactivation by 2.6 ± 0.2 mV/e-fold change (5A versus 5A + GRK2ct P<0.01, two-way ANOVA, Bonferroni's post-test). Using the same mathematical analysis, however, slope factors of both α subunits in the presence of GRK2ct were not significantly different (Figure 6.7 C), suggesting that the reduction in voltage sensitivity of inactivation may not be specific to $Na_V1.1$-5A.
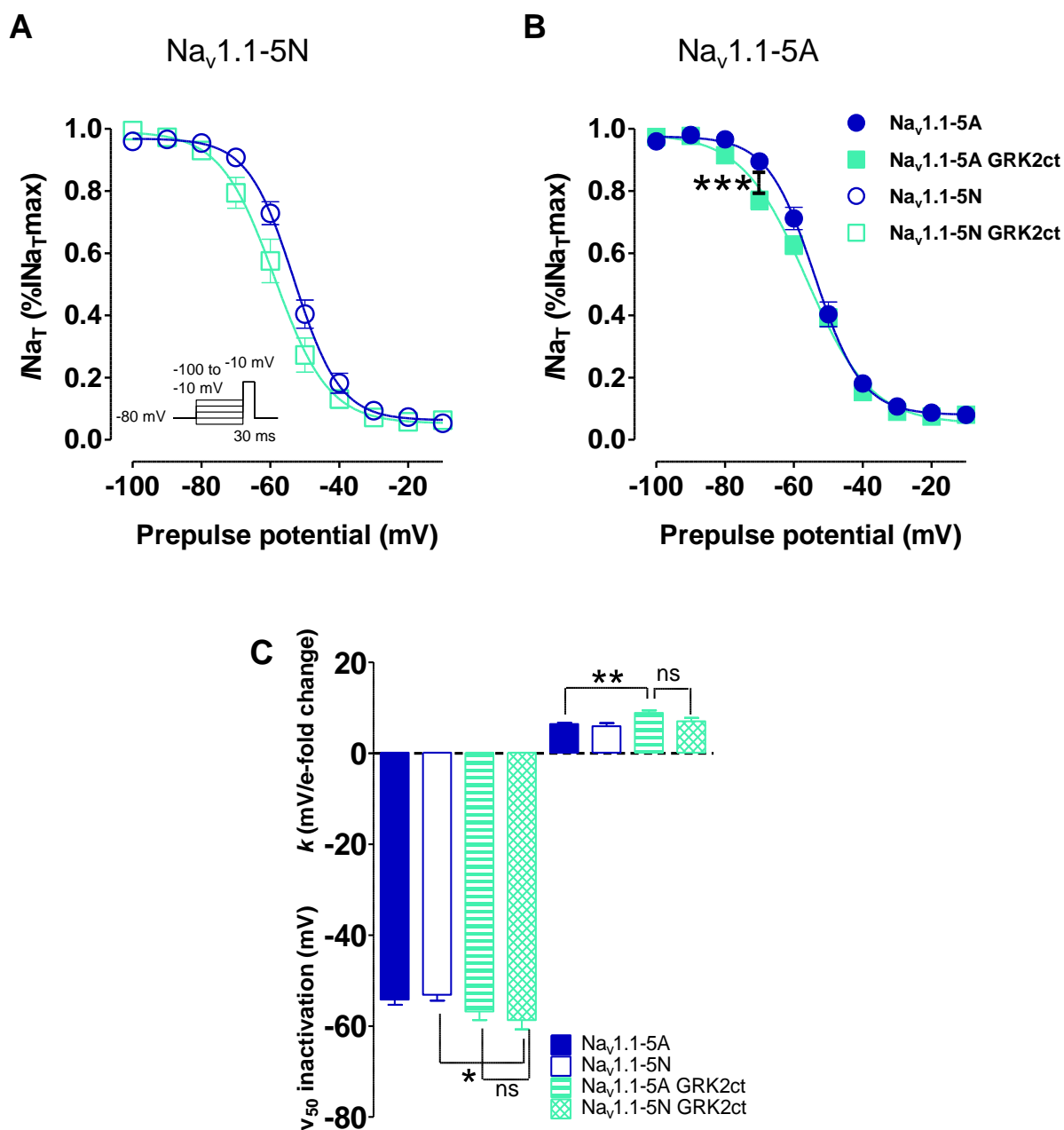
Figure 6.7 GRK2ct altered the voltage dependence of Na$_V$1.1 splice variant inactivation *A.* Shows that GRK2ct shifts Na$_V$1.1-5N activation curve to the left. Voltage protocol as in inset *B.* Significantly fewer channels were available at -70 mV in cells cotransfected Na$_V$1.1-5A and GRK2ct. ***P<0.0001, two-way ANOVA, Bonferroni's post test *C.* The average V$_{50}$ for activation for Na$_V$1.1-5N+GRK2ct was shifted to more hyperpolarized potentials compared to Na$_V$1.1-5N but not Na$_V$1.1-5A+GRK2ct. Compared to control cells GRK2ct significantly increased the mean slope factor of Na$_V$1.1-5A. **P<0.01, *P<0.05, two-way ANOVA, Bonferroni's post test.

6.4 Other effects 3: C-terminal fragments of GRK3 and GRK5 slow $Na_V1.1$ splice variant recovery from inactivation

GRK5ct introduced a significant overall variation in $Na_V1.1$-5N recovery from inactivation (P=0.02, two-way ANOVA; Figure 6.8 A); consequently, experiments using GRK2ct and GRK3ct were uninformative. However, through an unknown mechanism the recovery of inactivation over a range of time intervals was significantly slowed for both channel isoforms in the presence of GRK3ct (5A versus 5A GRK3ct, *n*=5; P=0.04; 5N versus 5N GRK3ct, *n*=7, P=0.04; two-way ANOVA). $Na_V1.1$-5A was particularly sensitive to GRK3ct action, as its time-course of recovery from inactivation was significantly slowed compared to $Na_V1.1$-5N channels in the same condition (5A GRK3ct versus 5N GRK3ct, P=0.0009; two-way ANOVA; Figure 6.8 B).
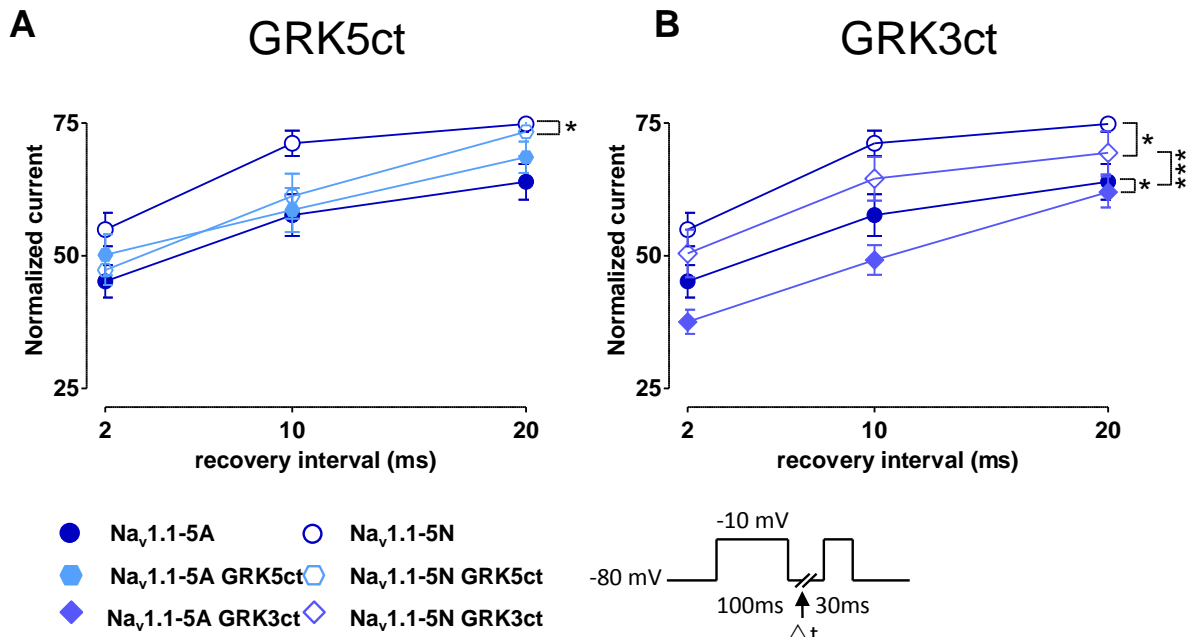
Figure 6.8 (previous page) GRK c-terminal fragments slow the recovery from inactivation of Na$_V$1.1 splice variants. ***A.*** Na$_V$1.1-5N channels were more available for activation than Na$_V$1.1-5N+GRK5ct channels for time points between 2 and 20 ms after prolonged depolarisations**.** *P<0.02, two-way ANOVA. ***B.*** Both splice variant channels recovery from inactivation were slowed in the presence of GRK3ct. Na$_V$1.1-5A in the presence of GRK3ct were more gradual to recover compared to Na$_V$1.15N channels in the same conditions.. *P=0.4, ***P=0.0009, two-way ANOVA. Currents were evoked using the protocol depicted at the bottom.

In summary, the sequestration of distinct subsets of G$\beta\gamma$, by GRK2ct differentially affected the persistent current derived from Na$_V$1.1-5A and Na$_V$1.1-5N. Sequestering all G$\beta\gamma$ subunits via Gαt had no affect on any parameter (INa$_P$ or INa$_T$) for either variant. The c-terminals of GRK proteins also modulated gating and recovery from inactivation but through unknown mechanisms. Channel current densities, the kinetics of activation and inactivation of Na$_V$1.1 splice variants were largely unaffected.

6.5 Stimulation of G-proteins

In the following sections GTPγS was used to probe the effects of global activation of G-proteins on macroscopic currents produced by Na$_V$1.1 splice variants. As shown in section 6.3 GTPγS had a similar effect on persistent currents as GRK2ct, these sections summarise the effects of GTPγS on other parameters.

6.5 GTPγS 1: The effect of GTPγS Gα subunit activation on Na$_V$1.1 splice variant transient currents

G-protein stimulation did not change Na$_V$1.1-5A INa$_T$ gating at higher temperatures. Experiments were performed in average temperatures ranging from $34 - 37^{\circ}$C and cells were dialyzed with 0.5 mM GTPγS. There were no significant changes in the mean

($\pm$SEM) V_{50} of *activation* or *inactivation* or steepness of the Boltzmann curves fitted for both parameters, in cells transfected with $Na_V1.1$-5A, in the presence or absence of GTPγS (5A versus 5A + GTPγS, P>0.05, two-way ANOVA, Bonferroni post test; Figure 6.9 A). In contrast, GTPγS subtly affected both the voltage dependence of $Na_V1.1$-5N activation and inactivation. For example, compared to control cells transfected with $Na_V1.1$-5N the mean ($\pm$SEM) V_{50} activation was shifted 2.8 $\pm$ 0.0 mV in a hyperpolarizing direction, with significantly more channels opened at -20 mV (P<0.001) and -10 mV (5N, n=15 versus 5N + GTPγS, n=13; P<0.01, two way ANOVA with Bonferroni's post test, Figures 6.9 A&B). At physiological temperatures, G-protein activation increased the voltage sensitivity of $Na_V1.1$-5N but not $Na_V1.1$-5A channels (mean $\pm$SEM k: 5N versus 5N + GTPγS P<0.05, two way ANOVA with Bonferroni's post test; Figure 6.9 B). GTPγS did not effect the rise time to peak over the voltage range (5A versus 5A + GTPγS, P=0.8; 5N versus 5N + GTPγS, P=0.9, two way ANOVA with Bonferroni's post test).

In cells dialyzed with GTPγS the mean ($\pm$SEM) $Na_V1.1$-5N V_{50} inactivation was shifted 3.2 $\pm$ 0.2 mV in a negative direction compared to control cells. Significantly fewer number of channels were available at -50 mV (P<0.001) and -40 mV (5N, n=11 versus 5N + GTPγS, n=14; P<0.05, two way ANOVA Bonferroni's post test, Figure 6.9 C). There was no change, however, in the voltage sensitivity of $Na_V1.1$-5N inactivation (mean $\pm$SEM k: 5N versus 5N + GTPγS, P>0.05, two way ANOVA, with Bonferroni's post test). Over the voltage range shown in Figure 6.9 D, the stimulation of G-proteins did significantly increase the rate of inactivation for both channels (5A, n=14 versus 5A + GTPγS, n=11, P= 0.0006; 5N, n=18 versus 5N + GTPγS, n=13, P<0.0001, two-way ANOVA), which was not

altered by splicing (5A + GTPγS versus 5N + GTPγS, P=0.4, two-way ANOVA). Lastly, G-protein activation did not alter either splice variants recovery from inactivation compared to control conditions at any time interval (±SEM normalized current: 5A versus 5A + GTPγS, *n*=5, P=0.8; 5N versus 5N + GTPγS, *n*=6, P=0.9, two-way ANOVA).
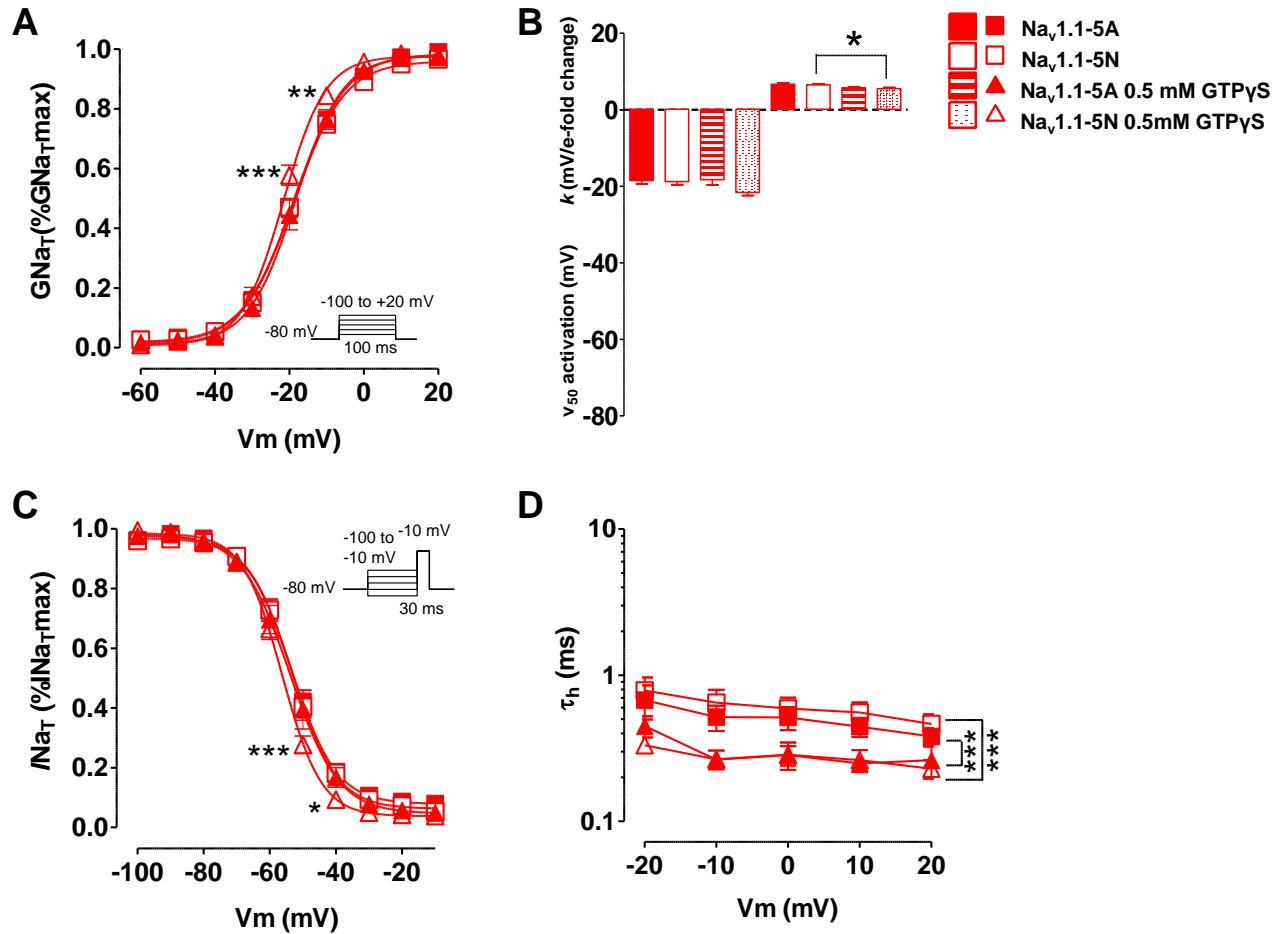
Figure 6.9 GTPγS regulation of Na$_V$1.1 splice variant gating at physiological temperatures. *A.* At -20 mV and -10 mV the voltage dependence of Na$_V$1.1-5N activation was shifted to more hyperpolarized potentials in cells dialyzed with GTPγS. ***P=0.001, **P=0.01, two way ANOVA, Bonferroni's post test. ***B.*** GTPγS did not alter the mean midpoint of Na$_V$1.1 splice activation but increased the voltage sensitivity of Na$_V$1.1-5N channels. *P<0.05, two way ANOVA, Bonferroni's post test. ***C.*** GTPγS exerted subtle effects on Na$_V$1.1-5N inactivation, and shifted the voltage dependence at -50 mV and -40 mV in a leftward direction. ***P<0.001, *P<0.05, two-way ANOVA, Bonferroni's post test ***D.*** In the presence of GTPγS the rate of inactivation (decay) was significantly

accelerated for a range of test potentials for both splice variants. ***P<0.0001, two-way ANOVA, Bonferroni's post test.

6 .5 GTP*γ*S 2: GTP*γ*S upregulated Na$_V$1.1 persistent currents at RT

Previous reports of GTPγS regulation of VGSCs have shown effects on INa$_P$ (Ostman *et al.*, 2008). However no change was seen here and this may be due to elevated temperatures, as previous reports used RT recordings. To confirm whether GTPγS exerted effects on INa$_P$ from either splice variant at lower temperatures, experiments were repeated at RT.

As shown in Figure 6.10 A, GTPγS dramatically upregulated persistent currents from both Na$_V$1.1 splice variants at RT. This effect was seen for both splice variants and was significantly greater than the increase produced at physiological temperatures. %INa$_P$ from Na$_V$1.1-5A channels was greater at RT compared to physiological temperatures (37 versus RT, 5A + GTPγS: 4.6 ± 0.9 %, n= 9; 16.2 ± 3.8 %, n=11, P<0.05 two way ANOVA). INa$_P$ from Na$_V$1.1-5N had a slightly larger increase at RT compared to physiological temperatures (37 versus RT, 5N + GTPγS: 3.6 ± 0.5 %, n=14; 29.0 ± 6.0, n=6, P<0.001; two way ANOVA with Bonferroni's post test, Figure 6.10). At RT, in cells dialyzed with GTPγS Na$_V$1.1-5A exhibited a large range of %INa$_P$: approximately 20% cells producing over 30% INa$_P$; a percentage not seen in untreated cells, but another ~40 % possessed less than 5% INa$_P$. Consequently, on comparison of both splice variants in the presence of GTPγS Na$_V$1.1-5N demonstrated a non-significant increase in proportional persistent current compared to Na$_V$1.1-5A (P>0.05, Mann-Whitney).

As expected in the presence of GTPγS the increase in stability of the non-inactivating current was reflected in the significant decrease in the rate of current decay over the voltage

range for both 5A and 5N-containing channels at RT (RT versus 37, P<0.001; two –way

ANOVA, Bonferroni's post-tests, Figure 6.10 C).
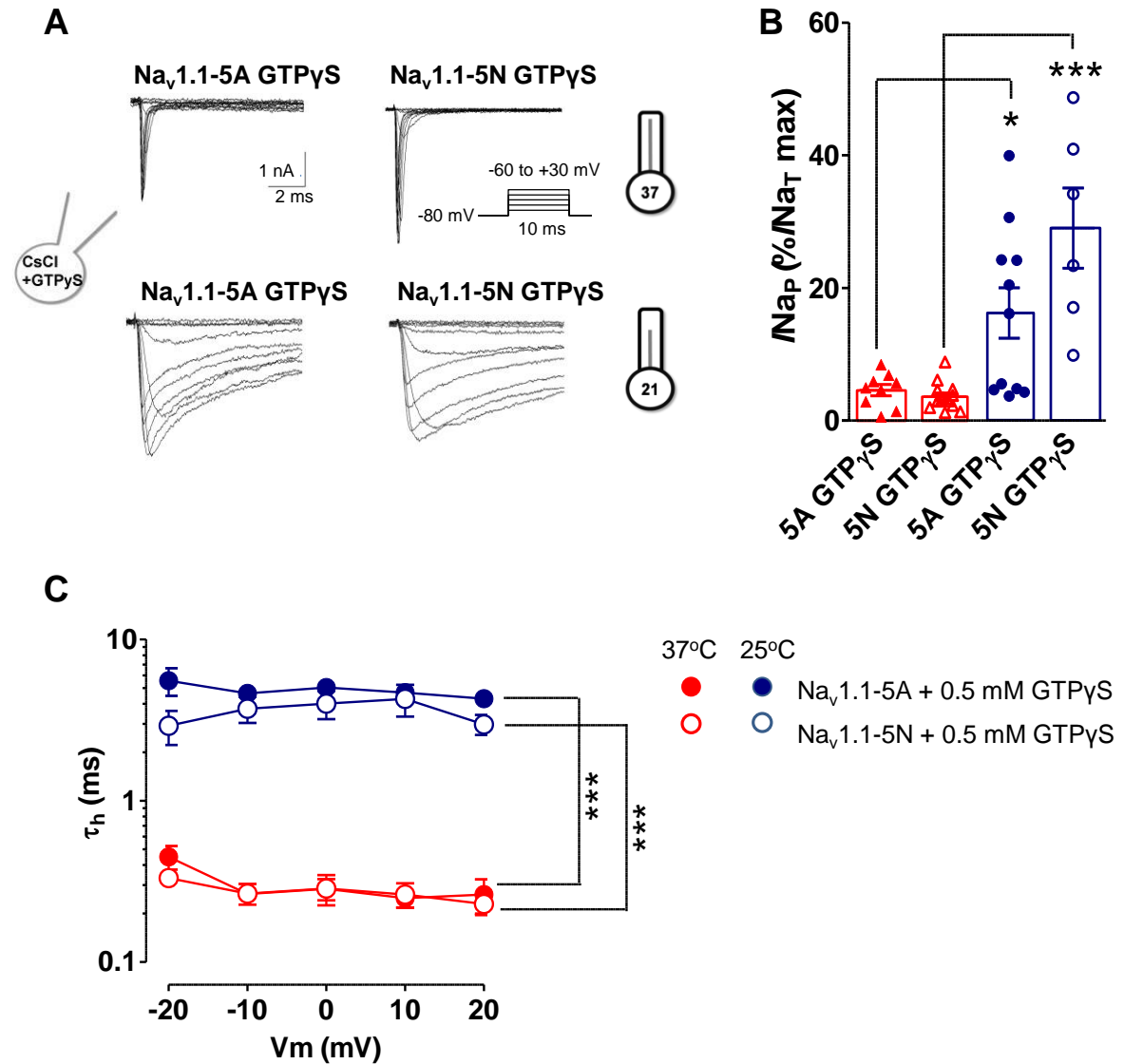
Figure 6.10 GTPγS significantly upregulated Na$_V$1.1 splice variant persistent currents
A. Raw traces demonstrating the dramatic increase in persistent currents at RT (bottom) compared to recordings at 37°C (top) of both channels isoforms in the presence of GTPγS. *B.* Mean ±SEM %*I*Na$_P$ Na$_V$1.1 currents were significantly increased in cells dialyzed with GTPγS compared to control conditions. *P<0.05, **P=0.001, two-way ANOVA, Bonferroni's post-test. **C.** The rate of current decay was significantly slowed at lower temperatures for both splice variants in the presence of GTPγS over a voltage range. ***P=0.0001, two-way ANOVA, Bonferroni's post-test.

316

6.5 GTPγS 3: GTPγS does not activate endogenous voltage or ligand gated ion channels

in HEK 293 cells

Since there was a dramatic increase in persistent currents it was important to establish that GTPγS did not stimulate intrinsic HEK 293 voltage and/or ligand-gated ion channels at lower temperatures. Endogenous currents were evoked and normalized using methods previously described in the methods. Recordings were performed using CsCl-based internal solutions containing 0.5 mM GTPγS at RT. In the presence of GTPγS negligible inward and outward currents peaking at +60 mV were observed (mean ±SEM = -4.3 ± 8.8 pA/pF; n = 5; Figure 6.11). At -10 mV GTPγS did not activate any substantial currents that would affect the calculation of %INa$_P$; for example, mean (±SEM) current density was 0.6 ± 5.0 pA/pF (n=5). This implies that persistent currents were derived from transfected sodium channels.
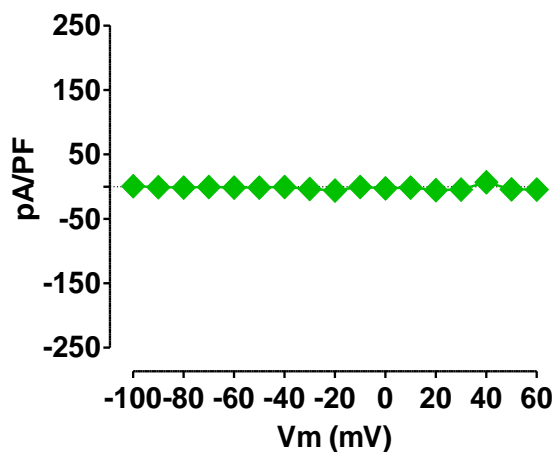
Figure 6.11. At RT negligible currents were observed from whole-cell patch clamp recordings of untransfected HEK 293 cells in the presence of GTPγS.

317

6.5 GTPγS 4: Na$_V$1.1-5N is sensitive to changes in temperature under GTPγS modulation

Na$_V$1.1 current density was not affected by splicing in G-protein activated conditions indiscriminate of temperature (interaction of all factors, P=0.2; two-way ANOVA). At biological temperatures significantly more Na$_V$1.1-5N channels were available at voltages between -20 mV and 0 mV (P<0.01, for noted voltages, two–way ANOVA, Bonferroni's post-tests). When considering both splicing and temperature, mean (±SEM) Na$_V$1.1-5N half maximal activation at ~ 37^{o}C is significantly 5.8 ± 0.4 mV more hyperpolarized compared to channels recorded at RT (P<0.05, two–way ANOVA, Bonferroni's post-tests, Figure 6.12 A). Allowing for the same conditions, temperature did not significantly change the mean (±SEM) steepness of the conductance curves for either Na$_V$1.1-5A or Na$_V$1.1-5N (Two–way ANOVA, Bonferroni's post-tests, Figure 6.12 B).

As expected the time-course of activation, was accelerated for both channels at higher temperatures and the activation kinetics of Na$_V$1.1-5N displaying a greater sensitivity to temperature in the presence of GTPγS. For example, between voltages -20 mV and + 20 mV, mean (±SEM) rise time is significantly reduced at higher temperatures (P<0.001 for each voltage step; two–way ANOVA, Bonferroni's post-tests, Figure 6.12 C). Na$_V$1.1-5A was less affected by the increase of temperature under the same conditions. Its time-course of activation was significantly accelerated at more hyperpolarized potentials, that is, -20 mV to 0 mV, but not significantly effected at more depolarized potentials (P <0.05, for all three noted voltages; two–way ANOVA, Bonferroni's post-tests, Figure 6.12 C).
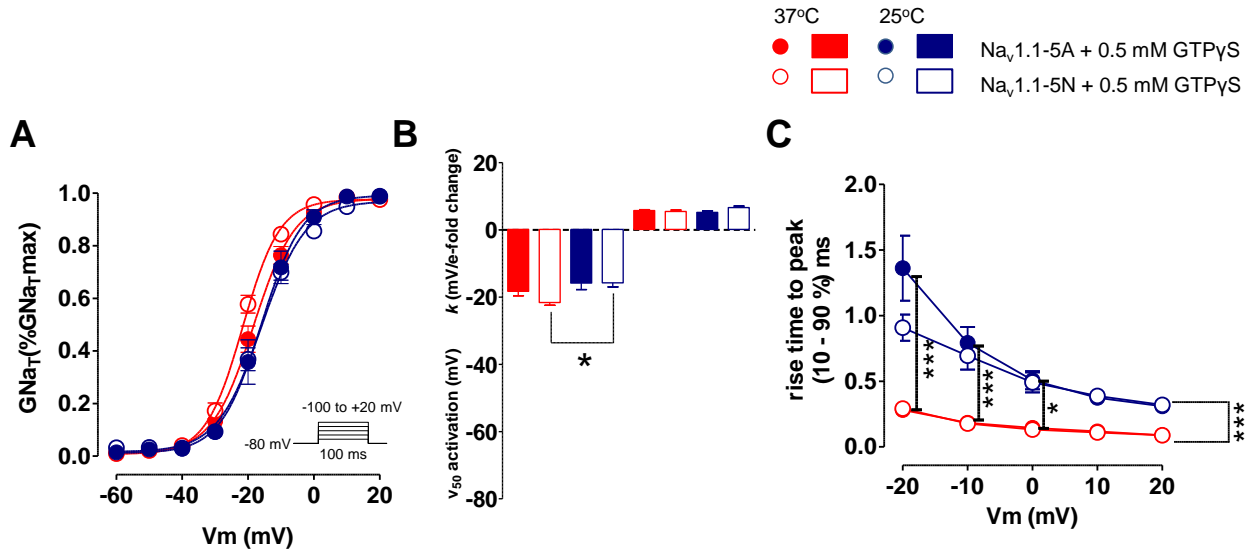
Figure 6.12 The effect of lower temperatures on the activation of $Na_V1.1$ splice variants *A.* Shows the activation of $Na_V1.1$-5N in the presence of GTPγS at higher temperatures is shifted to the left. *B.* Gα stimulation at higher temperatures shifts the average ±SEM V_{50} activation of $Na_V1.1$-5N to more hyperpolarized potentials compared to RT recordings. *C.* Over a voltage range the kinetics of $Na_V1.1$-5N activation was significantly slowed at RT in cells dialyzed with GTPγS. Bonferroni's post-tests revealed that only at more hyperpolarised potentials the kinetics of $Na_V1.1$-5A activation was affected by temperature in the presence of GTPγS. *P<0.05, ***P<0.001, two-way ANOVA Bonferroni's post-test.

6.5 GTPγS 5: At elevated temperatures GTPγS shifts the voltage dependence of inactivation in a leftward direction

The voltage dependence of inactivation for both splice variants was shifted in a hyperpolarized direction at biological temperatures. For both splice variants significantly more channels were unavailable between -50 mV and -30 mV at 37°C (P<0.01, for the voltage range, significant differences are not shown on Figure 6.13 A but notable voltages are marked by an asterisk for clarity). When considering individual channels, an increase in temperature caused a significant leftward shift 6.2 ± 0.7 mV in the mean V_{50} inactivation of $Na_V1.1$-5A (P= 0.04, 2-tailed *t*-test; whereas when considering both variants using a two-

319

way ANOVA this was not significant; Figure 6.13 B). The voltage-sensitivity of $Na_V1.1$-5A to inactivation was not significantly effected by temperature (mean ±SEM k; P= 0.10, 2-tailed t-test; Figure 6.13 B).   Although as previously mentioned temperature did change $Na_V1.1$-5N inactivation properties at less negative potentials but this did not significantly shift the mean (±SEM) V_{50} of inactivation (P=0.08, 2-tailed t-test). However higher temperatures did significantly decrease the slope factor by 6.6 ± 2.8 mV/e-fold change (P= 0.01, 2-tailed t-test; Figure 6.13 B).
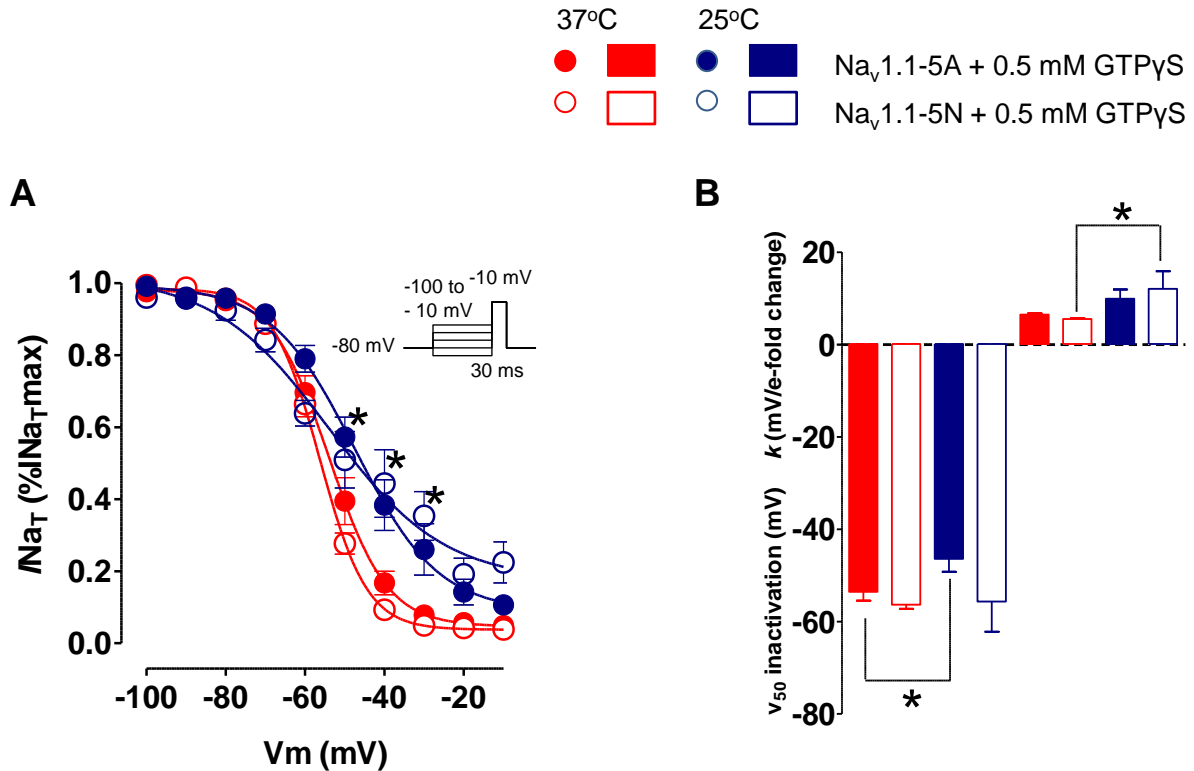
Figure 6.13   GTPγS changes the voltage dependence of $Na_V1.1$ splice variant inactivation at RT *A.* Conductance curves show that for both splice variants significantly more channels were available between -50 mV and -30 mV at RT *P<0.01, two-way ANOVA, Bonferroni's post test *B.* The mean ±SEM V_{50} inactivation of $Na_V1.1$-5A was shifted to more depolarized potentials by GTPγS at RT. The mean ±SEM slope factors of $Na_V1.1$-5N was increased in the presence of GTPγS at lower temperatures. P<0.05, two-way ANOVA, Bonferroni's post test.

320

At 37°C using CsCl based internal solutions the macroscopic currents from both variants were largely indistinguishable in the presence of GTPγS. Simply lowering the temperature had a distinct effect on the two variants, mainly stabilizing the non-inactivated states of both channels, which supports similar reports involving other VGSCs (Ostman *et al.,* 2008). In summary, these data reveal that $Na_V1.1$ splice variants are differentially modulated by different Gαβγ subunits and their response to G-protein activation is dependent on temperature. Therefore investigating what second-messenger cascades target these channel variants may be a new path to understanding regulation of these channels and possibly the seizures associated with them.

6.6 Discussion

The positive findings of this chapter were:

1. HEK 293 cells express a wide range of G-protein subunit genes.

2. The persistent current of $Na_V1.1$-5A is differentiately regulated by distinct subsets of Gβγ proteins.

3. Temperature markedly alters the properties of $Na_V1.1$ splice variant behaviour after GTPγS stimulation.

6.6.1 HEK 293 cells express a diverse range of G-protein subunit genes

The HEK 293 cells used in the present study were shown to express a wide range of G-protein subunits that are coupled to a variety of GPCRs (Shaw *et al.*, 2002). Although preliminary, this study aimed to provide a 'snapshot' expression profile rather than a

detailed examination. Two neuronal specific G-protein α subunits, GNAO and GNAZ were not found. All β subunits were highly expressed but two olfactory and gustatory γ subunits were undetected.

6.6.2 Na$_V$1.1 splice variant persistent currents are differentially modulated by βγ subunits

This study is the first to show that a subset of specific Gβγ subunits, and possibly Gα subunits, differentially modulate INa$_P$ from VGSC splice variants, specifically Na$_V$1.1-5A. It is unknown which Gβγ subunits GRK2ct selectively sequesters, and in turn, which Gβγ specifically reduce Na$_V$1.1-5A persistent currents. Since Gβγ subunits bind to the intracellular side of the channel and the amino acid differences between the splice variants are extracellular, the Gβγ may be interacting with different conformations of Na$_V$1.1. *In vivo*, this sub-set of Gβγ subunits would act to attenuate GABAergic neuron excitability. Compared to their voltage-gated calcium and potassium channel counterparts there is surprisingly little known about the GPCR regulation of VGSCs. INa$_T$ and INa$_P$ derived from a mixed population of Na$_V$1.1 and Na$_V$1.6 channels in striatal-cholinergic interneurons were attenuated after administration of a D$_2$ dopamine receptor agonist (Maurice *et al.,* 2004). D$_2$ receptors are coupled to Gαo and dialysis of purified GRK2ct, and therefore sequestration of Gβγ, also attenuated INa$_T$. The authors determined that PKC inhibition reduced transient currents and therefore continued to investigate kinase regulation of %INa$_P$. Unfortunately, the affects of GRK2ct on persistent currents were not determined. However, a reduction in sodium currents via D$_2$ receptors, and possibly Gαo associated Gβγ subunits, diminished these cells autonomous discharge and consequently their pacemaker activity (Maurice *et al.,* 2004). It is possible that this mechanism also exists in cells that

predominantly express $Na_V1.1$ (Yu *et al.,* 2006).

There are few reports demonstrating the differential modulation of G-proteins on ion channel splice variants. However, research suggests that this G-protein selective regulation on N-type calcium channels may have therapeutic implications for pain suffers. Neurotransmitter release from several neuronal types is reduced by inhibitory $G\beta\gamma$ subunits acting directly on N-type calcium channels (Gray *et al.,* 2007). *In vivo* c-terminal N-type calcium channel exon 37 splice variants, e37a and e37b, are differentially modulated by two mechanisms, which result from divergent pathways downstream of PTX sensitive G-proteins (Raingo *et al.,* 2007). Exon 37a and e37b containing channels are regulated by a $G\beta\gamma$ subunit, in a voltage dependant but tyrosine kinase *in*dependent mechanism. $Ca_V2.2$-e37b, however, can also be modulated by a mechanism that is *in*dependent of $G\beta\gamma$ subunits and voltage but is regulated by a tyrosine kinase activated downstream of G-protein stimulation (Gray *et al.,* 2007). An N-type calcium subtype, $Ca_V2.2$ containing e37a channels are upregulated on the presynaptic nerve terminals of C-fiber nociceptors. $Ca_V2.2$ channels containing the alternative exon, e37b are universally expressed in nervous system. Andrade *et al.* (2010) engineered a mouse whereby e37b replaced e37a in $Ca_V2.2$ channels expressed by DRG nociceptors. Morphine binds to μ-opioid-Gi/o coupled receptors and by comparing the behavioural responses to noxious stimuli of wild-type and $Ca_V2.2$ exon 37 mutant mice the authors discovered that morphine exerts its selective analgesia effects by indirectly inhibiting $Ca_V2.2$[e37a] and not $Ca_V2.2$[e37b] channels. Similar modulatory mechanisms could exist to control $Na_V1.1$ activity; for example, particular $Na_V1.1$ isoforms may be upregulated in inhibitory interneurons sub-types. This may be possible because

several *SCN1A* exons are alternatively spliced. If these splice variants do differentially respond to AEDs *in vivo*, cell-specific responses to drugs could be exploited for epilepsy treatment.

6.6.3 Future studies to determine the true effects of G-protein acting on Na$_V$1.1 splice variants

To prevent co-transfecting HEK 293 cells with numerous G-protein subunit combinations, Gβγ sequesterants were used. Although a significant decrease in Na$_V$1.1-5A %INa$_P$ was observed in the presence of GRK2ct, INa$_P$ throughout the study was very variable this may result may have been a false positive. Moreover, although control experiments confirmed that GRKct fragments did sequester Gβγ the non-specific effects of the control fragment, GRK5ct on INa$_T$ raises questions about whether the effects of GRK2ct on INa$_P$ were due to selectively sequestering Gβγ subunits. Additionally, since Gβγ subunits have dramatic effects on both potassium and calcium channels if there was a strong interaction between Na$_V$1.1 and Gβγ it would be predicted to be obvious; especially as the research tools used in this study are the gold standard for revealing G-protein interactions. In the Mantegazza *et al.* (2005) report, co-expression of Gβ2γ3 produced substantial persistent currents compared to this study, but that work was carried out at RT. In addition it may be that constitutively active G-proteins did not yield high concentrations of Gβγ to exert equal effects. This may be reflected by GTPγS shifting the equilibrium to full G-protein dissociation, causing the same reduction in INa$_P$ by perhaps increasing the number of free cytosolic Gβγ. Unfortunately it cannot be concluded that GTPγS acted via Gβγ or via other G-protein cascades. In future, both Na$_V$1.1 splice variants would be co-expressed with

Gβ2γ3 to determine INa$_P$ is differentially modulated by Gβγ and whether this interaction is conserved at physiological temperatures.

GPCRs that are likely to be expressed in inhibitory interneurons, for instance, GABA$_B$, cannabinoid, dopaminergic receptors (Stephens 2009), could be co-expressed with Na$_V$1.1 in HEK cells. The responses of each Na$_V$1.1 splice variant to GPCR agonists could be assessed using whole-cell voltage patch clamp. To test if the effect of the neurotransmitter results from Gβγ direct interactions Gβγ dimers known to associate with specific GPCRs could be purified using affinity chromatography (Dascal *et al.,* 2001). The purified proteins would be applied to the bath solution and using the 'inside out' configuration the effects of Gβγ on sodium currents could be assessed. If the latter mimicked the effects of macroscopic currents responding to agonist administration this would imply a direct interaction between Gβγ and Na$_V$1.1, rather an indirect downstream protein interaction. Investigations could be moved into chicken neurons, whereby preliminary experiments would give some insights into which GPCRs to manipulate. In addition, siRNA could be used to knock down specific Gα genes and Na$_V$1.1 splice variants to determine their potential synergistic effect on neuronal excitability.

6.6.4 Non-specific effects of GRKct may be due to modulation of the Gαq pathway

The non-specific effects of GRK5ct, and therefore possibly GRK2ct and GRK3ct, acting on INa$_T$ are hard to explain. One possibility is that the amino acid chains could fold into a tertiary structure that mimics a region of an endogenous protein that interacts with VGSCs. Alternatively the c-terminal tails of GRKs interact with a variety of proteins. For instance, both GRK5ct and GRK2ct bind to calmodulin but not GRK3ct. Since GRK3ct and GRK5ct

modulated two biophysical parameters of $Na_V1.1$ splice variants in a comparable manner this could mean that they are acting through a similar mechanism compared to GRK2ct. Therefore, non-specific effects may not be due to changes in calmodulin channel regulation. However, all three c-terminal fragments do contain lipid binding domains. GRK2ct, GR3ct and GRK5ct interact with Phosphatidylinositol 4,5-bisphosphate (PIP_2) PIP_2 acts as a second messenger within the Gq activation pathway (Penela *et al.,* 2003). PIP_2 modulates numerous ion channels, including inward rectifier potassium channels, non-voltage-gated sodium channels, purinergic receptors, AMPA and NMDA receptors (Logothetis *et al.,* 2010). These protein fragments may be manipulating a different GPCR pathway. However, one review states that VGSCs are insensitive to PIP_2 but fails to cite any references (Hilgemann *et al.,* 2001). Thus, there may be a disruption in the availability of PIP_2 within the pathway. This may lead to knock-on effects downstream altering $Na_V1.1$ behaviour. Attempts were made to investigate the effects of Gαq signalling on $Na_V1.1$ splice variants. As previously described, preliminary experiments involving PTX were going to be repeated with the Gαq inhibitor YM-254890. However, Asellas Pharmaceuticals has stopped supplying this bacterial toxin (Takasaki *et al.,* 2004). Alternatively the Gαq 'selective' activator, Pasteurella multocida toxin (Calbiochem) could have been used but these experiments were abandoned because this agent also activates Gαi subunits (Orth *et al.,* 2008)

6.6.5 The effects of GTPγS is dependant on temperature

The inactivation properties of both $Na_V1.1$ splice variants in G-protein activated conditions were dramatically different at varying temperatures. CsCl-GTPγS up-regulation of sodium

persistent currents at RT has been observed for endogenous rat DRG $Na_V1.9$ channels and enteric neurons (Baker *et al.,* 2003; Rugiero *et al.,* 2003; Ostman *et al.,* 2008). However, using same concentration of GTPγS in this study, Ma and colleagues showed no increase in $Na_V1.2$-6A INa$_P$ expressed in either in CHO or HEK cells. The intracellular solutions in these studies were fluoride free (Ma *et al.,* 1994, Ma *et al.,* 1997). These conflicting results may be due to differences in VGSC sub-type and/or cell backgrounds. In this study at RT the rate of current decay for both $Na_V1.1$ isoforms was significantly slowed compared to control conditions but at elevated temperatures this was reversed. Thus, perhaps *in vitro* after G-protein activation, channels undergo a complex conformation change. At RT, during a slowed kinetic state, G-protein activation stabilizes inactivation and therefore recordings reflect an intermediate state. During this intermediate state the voltage sensitivity of $Na_V1.1$-5N and $Na_V1.1$-5A channels decrease although $Na_V1.1$-5A channels to a lesser extent. Interestingly, in experiments performed at RT involving rat superior cervical ganglion neurons, the gating charges of TTX-sensitive VGSCs were disrupted by GTPγS; although this was not predicted to increase INa$_P$ (Hernández-Ochoa *et al.,* 2007). Nonetheless, at elevated temperatures, the kinetics of the conformational change might be accelerated and macroscopic currents may mirror the true physiological effect of G-protein modulation on $Na_V1.1$.

In the HEK cells used in this study, which as demonstrated by the mRNA data have a wide-ranging G-protein subunit background, GTPγS activated G-protein signalling pathways selectively increased the voltage sensitivity of $Na_V1.1$-5N activation. Subtle effects were also observed in the voltage dependency of $Na_V1.1$-5N gating. Therefore, it is possible that

global G-protein regulation of VGSCs may finely tune the excitability of neurons through changing the biophysical properties of splice variants of VGSCs. Concerning $Na_V1.1$ splice variants this may be developmentally co-ordinated with changes in GPCR expression. For instance; Nova2 may also control the splicing of several GPCRs expressed in GABAergic neurons, including $GABA_B$ receptors (Li *et al.,* 2007). GPCRs manipulation of $Na_V1.1$ activity may be disrupted during epilepsy, thus future treatments that influence these regulatory pathways could be developed. However, because of the flaws in experimental tools, these data only hint that $Na_V1.1$ splice variants are differentially modulated by G-proteins. Further studies are needed to untangle the true biological effect of Gαβγ on $Na_V1.1$.

Chapter 7: An investigation into the VGSC β subunit regulation of $Na_V1.1$ splice variants

7.1 Hypothesis and aims

Hypothesis: VGSC β subunits proteins have been shown to be important for regulating sodium channel properties in various heterologous systems. It was hypothesized that distinctive pairs of β subunits will differentially modify $Na_V1.1$ splice variant channel behaviour.

Background and experimental aims: Early in development, when alternative splicing is thought to favour exon 5N, a large proportion of sodium channel α subunits are not associated with β subunits (Scheinman *et al.,* 1989). In adult brain, however, α subunits are associated with two β subunits, including one of either β1- or β3- and one of either β2 or β4 (Isom 2001; Ulbricht 2005). Moreover, in experimental epilepsy models and/or following seizures, when exon 5N is upregulated, several sodium channel genes including those that code for $Na_V1.1$, β1, β2, and β3 are transiently down-regulated (Ellerkmann *et al.,* 2003; Gastaldi *et al.,* 1998; Gorter *et al.,* 2006). It is possible that β subunits may modulate each splice variant α subunit differently. Moreover, β subunits have been shown not only to alter channel gating but also to change channel localization. The aim of this section was to investigate whether β subunits had similar effects on the biophysical properties and trafficking of both splice variants of *SCN1A*.

7.2 Biophysics 1: β1b, β2 subunits attenuate the peak current densities of Na$_V$1.1 splice variants

To determine the functional impact of β subunits on the splice variants, Na$_V$1.1-5N and Na$_V$1.1-5A were co-expressed with β2 paired with one of three related β subunits: β1, its splice variant β1b or β3. All experiments in these sections were carried out in average temperatures ranging from 35-37^{o}C and used CsCl solutions. Figure 7.1 A shows raw traces of sodium currents from both splice variants co-expressed with β1,β2 (top panel) or β1b,β2 (bottom panel). No currents were recorded from Na$_V$1.1 channels co-transfected with β3,β2 (data not shown).
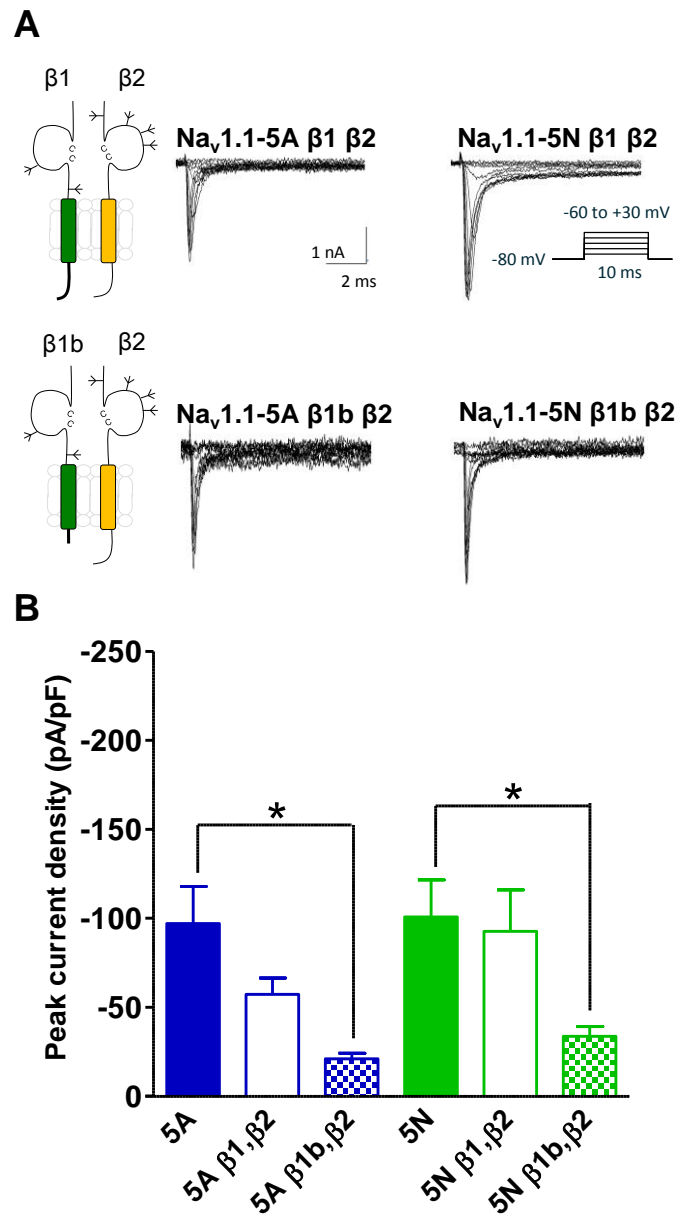
Figure 7.1 Peak current densities of splice variants is reduced in the presence of β1b, β2 *A.* Raw traces of Na$_V$1.1 splice variants co-expressed with β1,β2 (top) and β1b, β2 (bottom). Sweeps were elicited by the protocol in the inset. *B.* Mean peak (±SEM) current densities of splice variants co-expressed with denoted β subunits. Co-expression of β1b, β2 significantly reduced the peak current density of Na$_V$1.1 splice variants. *P<0.05, two-way ANOVA, Bonferroni's post-test. β1,β2 subunits had no significant effect on this parameter. P=>0.05, two-way ANOVA, Bonferroni's post-test.

In the presence of β1, β2 the mean peak current densities of 5A and 5N-containing channels

were not significantly altered (Figure 7.1 B; 5A: -97.1 ± 20.9 pA/pF, *n*=14 versus 5A +

β1,β2: -57.4 ± 9.2 pA/pF, n=12, 5N: -100.9 ± 20.8 pA/pF, n=18 versus 5N + β1,β2 : -92.8 ± 23.3 pA/pF; n=7; two-way ANOVA, Bonferroni's post-test). However, co-expression of β1b, β2 significantly reduced the mean peak current density of both Na_V1.1-5A and Na_V1.1-5N (by 75.9 ± 17.8 pA/pF n=7 and 67.1 ± 15.3 pA/pF n=10 respectively), compared to those observed for α subunits alone (P<0.05; two-way ANOVA, Bonferroni's post test, Figure 7.1 B). This indicates that these specific pairs of β subunits do not differentially regulate the Na_V1.1 α subunit splice variants.

Individual comparisons of Na_V1.1-5A or Na_V1.1-5N co-expressed with either β subunit pair, show that β1b,β2 significantly attenuates mean peak current densities compared to β1,β2. For instance, β1b,β2 caused a decrease in mean Na_V1.1-5A current density of 36.2 ± 6.1 pA/pF compared to values obtained with β1,β2 (P<0.01, Mann-Whitney). A similar mean (±SEM) reduction was observed for Na_V1.1-5N under the same conditions (59.0 ± 17.8 pA/pF; P<0.05; Mann-Whitney). These data indicate that the two β1 splice variants have different effects on Na_V1.1 current densities when matched with β2.

7.2 Electrophysiology 2: The gating of Na_V1.1 splice variants was largely unaffected by β subunit pairs

When conductances were normalised to compare voltage dependence of macroscopic gating, multiple two-way ANOVA with Bonferroni's post-tests revealed no significant differences between the cells transfected with Na_V1.1-5A, in the absence/presence of β subunit pairs, at any voltage step (5A vs 5A β1,β2, n=12, P=0.5; 5A vs 5A β1b,β2, n=7, P=0.06; two-way ANOVA, Figure 7.2 A). Moreover, the different α subunit splice variants also showed similar voltage dependence of activation in the presence of β subunits (5A

β1,β2 vs 5N β1,β2, $n=7$, P=0.07; 5A β1b,β2 vs 5N β1b,β2, $n=10$, P=0.2; two-way ANOVA, Figure 7.2 A).

In the presence of β1,β2 subunits some subtle variations in activation were observed for Na_V1.1-5N channels ($n=7$, P=0.01, two-way ANOVA). Whereas β1b splice variant had little effect on this parameter compared to currents mediated by Na_V1.1-5N α subunits with or without β1,β2 subunits (5N vs 5N β1b,β2, $n=10$, P=0.2; 5N β1,β2 vs 5N β1b,β2, P=0.6; two-way ANOVA). Finally, in all conditions, depicted in Figure 7.2 B there were no significant differences the mean (±SEM) inactivation V_{50} values and slope factors (V_{50act} and k: P=>0.05 two-way ANOVA, Bonferroni's post-tests). The rate of Na_V1.1-5A current decay was significantly slowed in the presence of β1b,β2 not β1,β2 subunits (5A vs 5A β1,β2, $n=12$, P=0.8; 5A vs 5A β1b,β2, $n=7$, P<0.0001; two-way ANOVA, Figure 7.2 A). Moreover this slowing was specific to 5A-containing channels (5N β1b,β2 vs 5A β1b,β2, P=0.0005, two-way ANOVA; Figure 7.2 C).
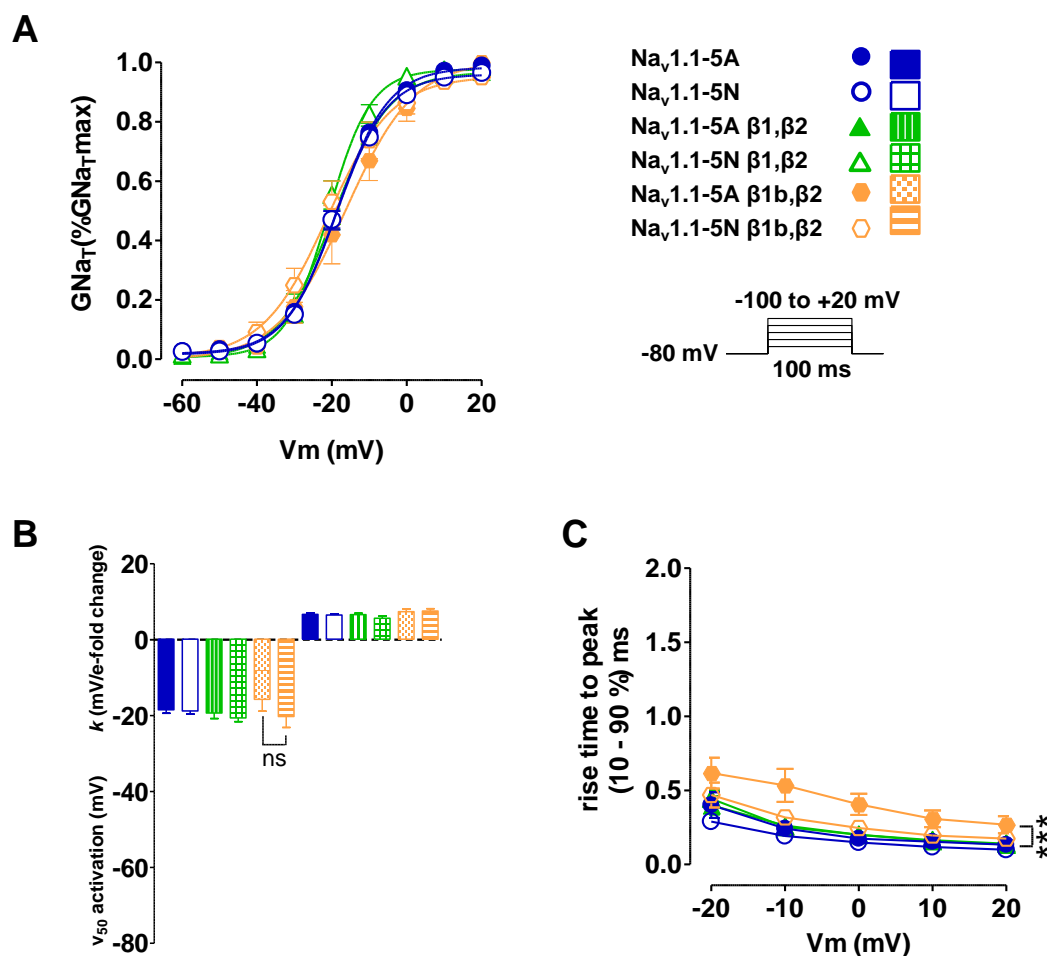
Figure 7.2 The effect of β1 splice variants paired with β2 on $Na_V1.1$-5A and $Na_V1.1$-5N gating *A.* Conductance curves of both splice variants in the presence and absence of denoted β subunits. Currents were evoked from the protocol in the inset. Deviations in the voltage dependence of inactivation of $Na_V1.1$-5N but not $Na_V1.1$-5A channels were introduced by β subunits. *B.* No significant changes the mean ± SEM midpoints and slope factors were detected for either variant in all conditions. *C.* The rate of current decay of $Na_V1.1$ channels isoforms over depolarizing steps in the presence and absence of indicated β subunits. $Na_V1.1$-5A kinetics of activation was significantly slowed in the presence of β1bβ2 compared to 5A α subunit currents. ***$P<0.0001$, two-way ANOVA.

Figure 7.3 A shows the relationship between prepulse potential and current available at the

test pulse for 5A and 5N-containing channels co-expressed with the denoted β subunits.

There was no difference in the fraction of current available at each voltage step for $Na_V1.1$-

5A channels in the absence or presence of β subunits (5A versus 5A β1,β2, $n=8$, P=0.1; 5A versus 5A β1b,β2, $n=3$, P=0.5, two-way ANOVAs). However, in the presence of β subunits there were significant variations in the steady-state inactivation for Na$_V$1.1-5N (5N versus 5N β1,β2, $n=8$, P=0.03; 5N versus 5N β1b,β2, $n=4$, P=0.04, two-way ANOVA), although these subtle changes were not affected by splicing (5A β1,β2 versus 5N β1,β2, P=0.2; 5A β1b,β2 versus 5N β1b,β2, P=0.5, two-way ANOVA). Although in all conditions, depicted in Figure 7.3 B there were no significant differences the mean (±SEM) inactivation V$_{50}$ values and slope factors, (V$_{50inact}$ and k: P>0.05 two-way ANOVA, Bonferroni's post-tests).

Collectively these data suggest that neither β1 nor β1b when paired with β2 significantly alters the voltage dependence of Na$_V$1.1 splice variant activation and inactivation.

A

B
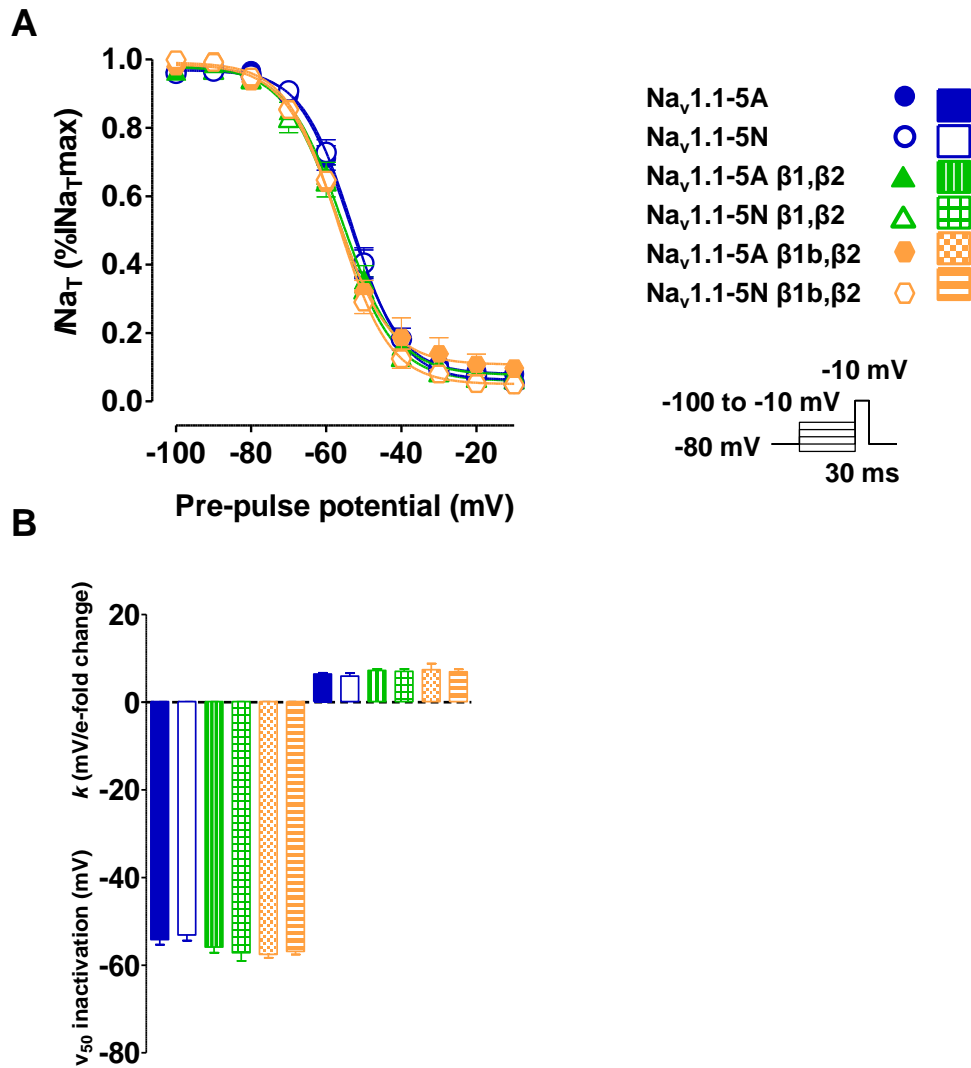
Figure 7.3 β subunits do not regulate the voltage dependence of Na$_V$1.1 splice variant inactivation The voltage dependence of inactivation of maximal peak transient currents show subtle variations in Na$_V$1.1-5N inactivation in the presence of β subunits (*A*) but no significant differences were detected between the mean (±SEM) slope factor for both variants in all conditions (*B*). Currents were evoked by the protocol depicted in the inset.

7.2 Electrophysiology 3: The rate of Na$_V$1.1-5A and 5N fast inactivation is slowed in the

presence of β1b, β2

In all conditions the non-inactivating, persistent component of transient Na$_V$1.1 splice

variant sodium currents were comparable (%INa$_P$ P>0.05, two-way ANOVA with

Bonferroni's post-test). β1b,β2 significantly slowed tau of $Na_V1.1$-5A and $Na_V1.1$-5N inactivation compared to channels in the presense or absence of β1,β2 subunits over a range of potentials (5A β1b,β2 versus 5A or 5A β1,β2 P<0.0001; 5N β1b,β2 versus 5N or 5N β1,β2 P<0.05 two-way ANOVA; Figures 7.4 A&B). In the presence of β1,β2 the rate of current decay was similar to rates calculated for $Na_V1.1$ α subunits alone (5A versus 5A β1,β2, P=0.2; 5N versus 5N β1,β2, P=0.7; two-way ANOVA; Figures 7.4 A&B) This implies that slowing of $Na_V1.1$ current decay is specific to β1b,β2.

In the presence of β1,β2 $Na_V1.1$-5N current decay was significantly slowed compared to $Na_V1.1$-5A channels (5A β1,β2 versus 5N β1,β2, P=0.02, two-way ANOVA; Figure 7.4 C). In contrast β1b,β2 did not differently modify the rate of fast inactivation from the two splice variants (5A βb1,β2 versus 5N β1b,β2, P=0.6, two-way ANOVA; Figure 7.4 D). The similarity between the splice variants is emphasized by the divergent slowing of $Na_V1.1$ α subunit inactivation at 0mV – a potential likely to evoke maximal current activation (Figure 7.4 D).
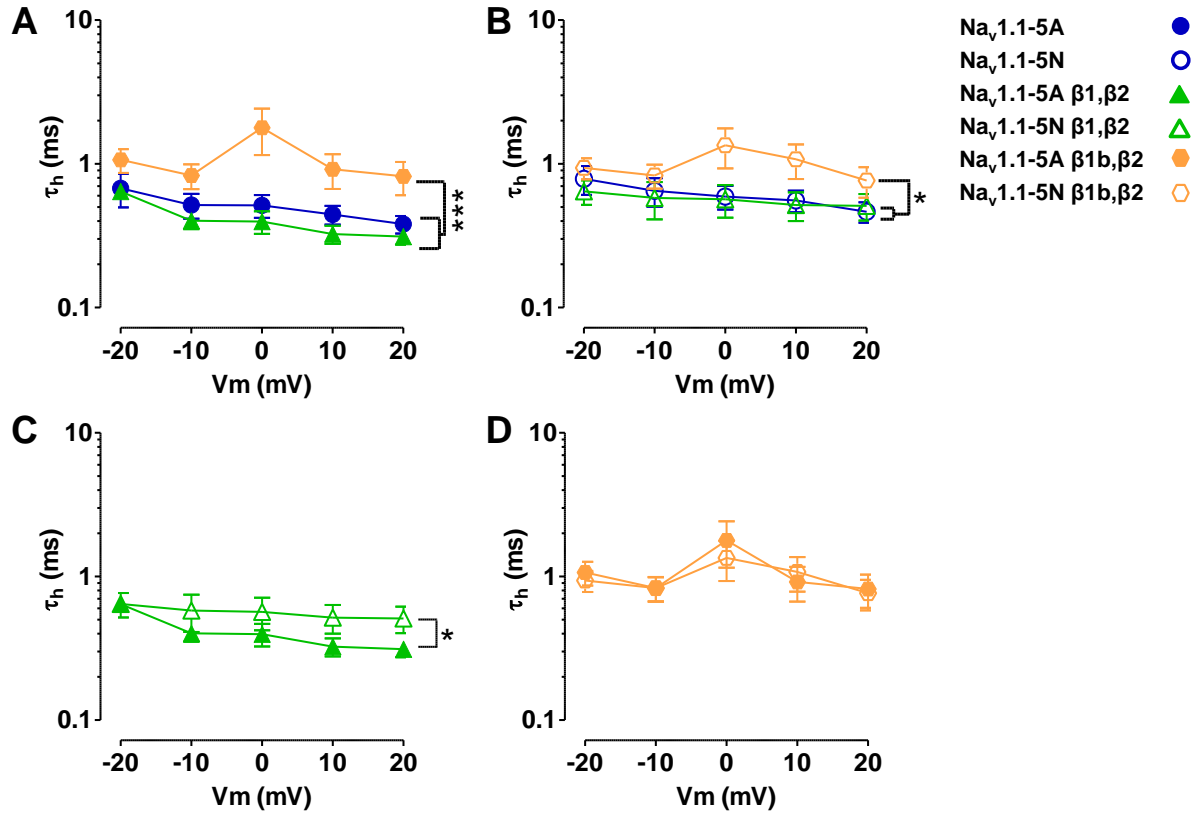
Figure 7.4 β subunit modulation of Na$_V$1.1 splice variant rate of current decay. β1b,β2 significantly slows the Na$_V$1.1 splice variant rate of inactivation at maximal current activation for Na$_V$1.1-5A channels in the presence or absence of β1,β2 subunits (*A*) and compared to Na$_V$1.1-5N channels expressed alone (*B*) ***$P<0.001$; *$P<0.05$, two-way ANOVA. β1,β2 differentially modulates Na$_V$1.1 splice variants rate of decay Semilogarithmic plot of the fast time constants derived from fits of one exponential to the decay of the current over a range of test potentials show that in the presence of β1,β2 (*C*) but not β1b,β2 (*D*) Na$_V$1.1-5N rate of current decay is significantly slowed compared to Na$_V$1.1-5A channels. *$P=0.02$, two-way ANOVA.

7.3 Immunocytochemistry: β subunits do not retain Na$_V$1.1 splice variant α subunits within the secretory pathway

The most striking effect of β subunit regulation on the biophysics of heterologously-expressed sodium channels was a pronounced reduction in current density. There are two possible mechanisms behind this effect: firstly, β subunits could directly interact with the

channels at the cell surface attenuating their conductance. The second possibility is that the β subunits may sequester the α subunits within the secretory pathway preventing them from reaching the cell surface. It has been well established that accessory subunits can act as a chaperone protein for α subunits (Cusdin *et al.,* 2007). To determine whether the β subunit pairs altered the subcellular localisation of $Na_V1.1$ α subunits, HEK 293 cells were transfected with the appropriate DNAs and fixed in 4% PFA and stained with anti-$Na_V1.1$ antibodies followed by TRITC conjugated secondary antibody. This sodium channel primary antibody is raised against amino acids within the first intracellular loop of the α subunit. However, a high level of background staining was detected in untransfected HEK cells using this antibody (Figure 7.5). This may represent unspecific binding of the antibody to non-VGSC proteins expressed by HEKs or, less likely, the expression of endogenous VGSCs in the HEKs, which did not produce currents. Therefore, in following immunocytochemisty experiments CHO cells were used. Subsequent imaging was performed by Elin Reeves, an MSc student under my supervision.
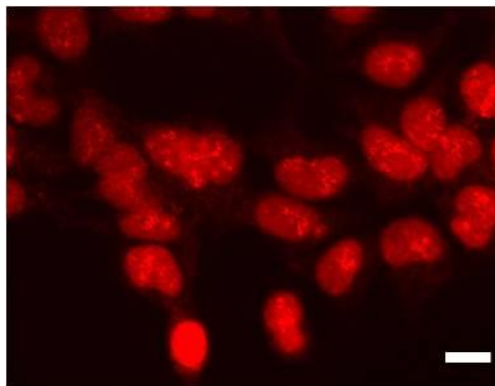
Figure 7.5 HEK 293 cells were unsuitable for immunocytochemistry studies Untransfected HEK 293 cells were fixed in 4% PFA and labelled with anti-$Na_V1.1$ antibodies raised in rabbit (against amino acids with the first intracellular loop) and detected with TRITC conjugated secondary antibodies. Cells were visualised at x40 magnification. A high level of background staining was detected. Scale bar: 20 μM.

To assess the background fluorescence of CHO cells untransfected cells were fixed and stained with TRITC conjugated secondary antibodies, with or without prior labelling with of anti-$Na_V1.1$ antibodies raised against amino acids within the third intracellular loop. Different primary antibodies were used to prevent potential unspecific binding detected by the previous antibody. No signal was detected in either condition (Figure 7.6 A). Cells were transfected with $Na_V1.1$ splice variants and α subunits were detected using the same indirect immunofluorescence microscopy method. $Na_V1.1$ α subunits were present in the plasma membrane indicated by a faint rim of fluorescence circling the perimeter of each cell (Figure 7.6 B). Positive staining also validated this primary antibody.
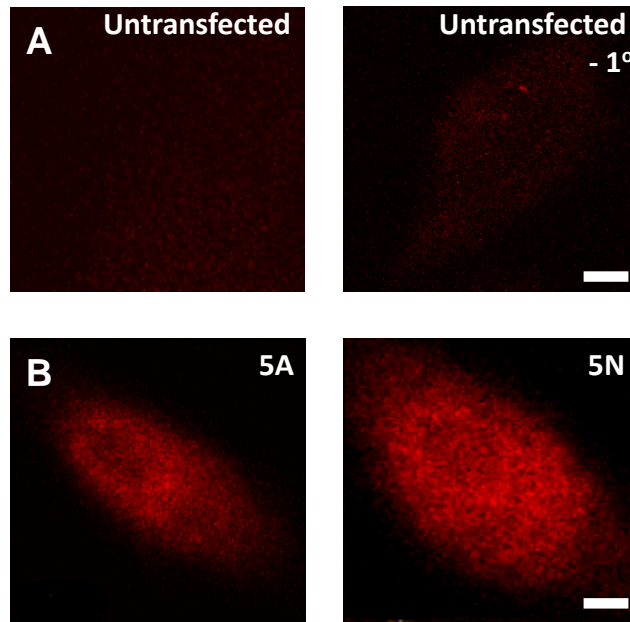
Figure 7.6 *A.* Untransfected CHO cells were fixed in 4% PFA and labelled with (left) or without (right) anti-$Na_V1.1$ antibody raised in rabbit and detected with TRITC conjugated secondary antibodies. Primary (left) and secondary (right, -1°) antibodies demonstrated no unspecific binding ***B.*** CHO cells were co-transfected with $Na_V1.1$ splice variants as indicated and fixed in 4% PFA. Cells were stained with anti-$Na_V1.1$ antibody raised in rabbit followed by TRITC conjugated secondary antibodies. Primary antibodies were raised

against amino acids within the third intracellular loop. Both Na$_V$1.1 splice variants were detected at the cell membrane (right & left). Cells were visualised at x63 magnification. Scale bar: 5 µM.

To test whether β subunits altered trafficking CHO cells were co-transfected with Na$_V$1.1 splice variants and with either β1,β2; β1b,β2 or β3,β2 subunit pairs. Immunocyctochemistry was performed as described previously. GFP indicates the presence *not the localization* of β subunits (Figure 7.7 right panels). In all conditions, staining showed Na$_V$1.1 splice variants were transported to the cell membrane (Figures 7.7 A – F). In the presence of β1b,β2 Na$_V$.1-5N appeared to have accumulated in endosomes and lysosomes, as numerous stained vesicles surrounded the perinuclear region (Figure 7.7 D), but this pattern of staining was inconsistent in these conditions. These results suggest that the reduction in current density by β1b,β2 and possibly β2,β3, was through subunit interactions at the cell surface rather than persistent retention within intracellular organelles.
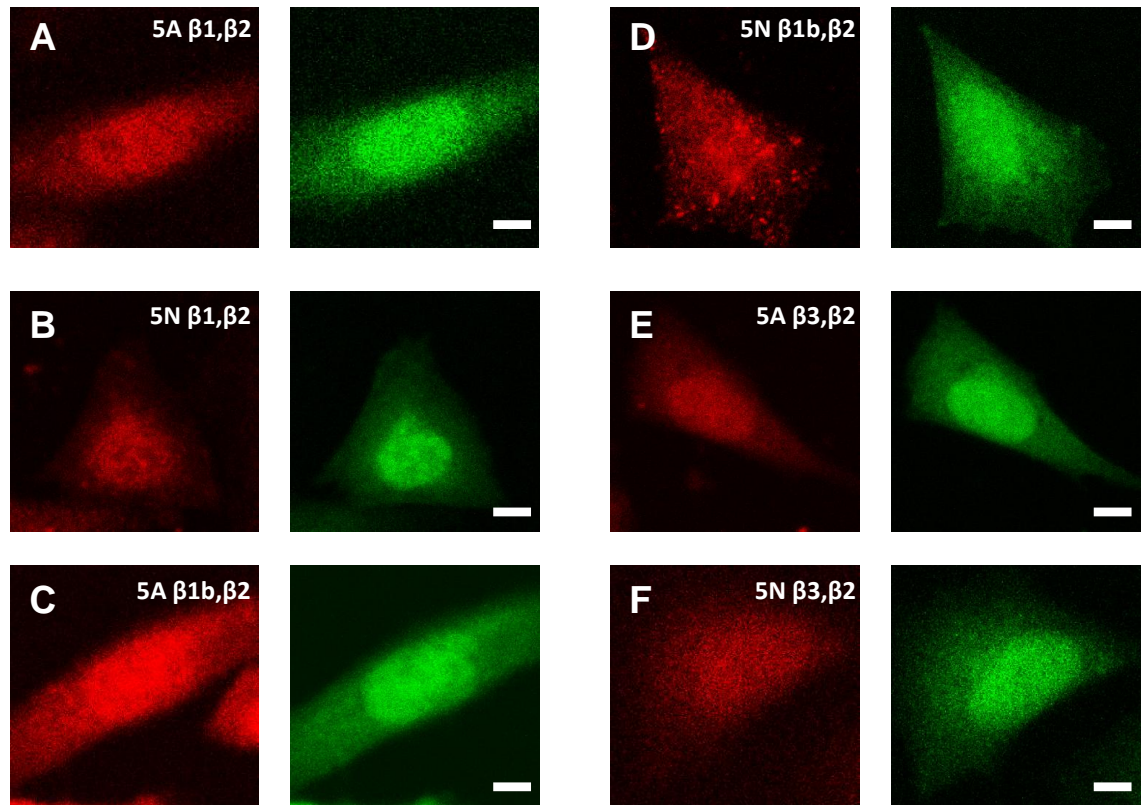
Figure 7.7 β subunit pairs do not prevent the trafficking of α subunits to the cell membrane *A-F*. CHO cells were co-transfected with Na$_V$1.1 splice variants and indicated subunits. Cells were fixed in 4% PFA and labelled with anti-Na$_V$1.1 antibody raised in rabbit and detected with TRITC conjugated secondary antibodies. GFP (green fluorescence) indicates successful co-transfection with β subunits, but not their localization (right panels). Trafficking to the cell surface is confirmed by faint red fluoresce at the cell periphery in all images. Cells were visualised at x63 magnification. Scale bar: 5 µM.

7.4 Discussion

The main findings of this chapter were:

1. β1b,β2 and possibily β3,β2 decreases the current density of Na$_V$1.1 splice variants.

2. Current density is not reduced by β subunit retention of Na$_V$1.1 splice variant α

subunits.

7.4.1 β1b, β2 reduced current density and slowed the kinetics of Na$_V$1.1 splice variants

The presence of both β1 splice variants and β2 did not alter the voltage dependency of Na$_V$1.1 gating. However β1b,β2 and β3,β2 did reduce the current density of Na$_V$1.1 sodium currents. The immunocytochemistry data implies that this was not due to β subunit-dependent intracellular retention of α subunits, and therefore β subunit pairs may inhibit Na$_V$1.1 conduction at the cell surface. No currents were recorded from cells expressing Na$_V$1.1 and β3,β2 subunits. Within 48 hours of Na$_V$1.1 with β3,β2 transfection the cells started to necrose and lift from the coverslips. Consequently the cells may have not had sufficient time to manufacture Na$_V$1.1 channels, particularly if the metabolism of the cells was impaired. The IRES vector may have been toxic to the cells as the transfection efficiency of the vector during immunocytochemistry experiments was poor ~5 % (personal estimation). Indeed, in preliminary experiments the same outcome was observed for cells transfected with β1b,β2, but a reduction in plasmid DNA concentration improved cell viability. Nevertheless, indirect immunofluorescence did detect Na$_V$1.1-5A and Na$_V$1.1-5N expression in the presence of β3,β2 48 hours after transfection. The toxicity of the β3,β2 IRES vector could be tested by transfecting *SCN2B* and *SCN3B* in separate plasmids. IRES vectors have been developed to ensure that reporter and experimental genes are co-transfected within the same cells. However, there is strong evidence that separate plasmids transfected together are incorporated into the same cells (Groot-Kormelink *et al.,* 2002).

The few functional studies investigating the effects of β1b on VGSCs are in contrast to these data and showed that β1b increased the current density of both Na$_V$1.2 and Na$_V$1.5

channels (Qin *et al.,* 2003; Watanabe *et al.,* 2008). However, in both studies β2 was not present and suggests that β2 may exert a dominant effect over β1b. This could be investigating by transfecting different ratios of β1b vs β2 with $Na_V1.1$ splice variants to determine if a sequential increase of β2 subunits correlated with a decrease $Na_V1.1$ current density. β1b may interact uniquely with β2 and α subunits through its c-terminal region because the extracellular Ig domains of β1 and β1b are identical but their c-terminal regions are less than 17% conserved.

It is surprising that β subunit expression did not decrease $Na_V1.1$ currents by retaining α subunits within the secretory pathway. Mutation of an intracellular β1 polar tyrosine residue 181 to a glutamate reduced $Na_V1.2$ channel expression in a heterologous cell line (McEwen *et al.,* 2004), and plasma membrane expression of sodium channels was decreased in *SCN2B* null mice (Chen *et al.,* 2002). The analogous residue at 181 in β1b is a non-polar proline; it would be interesting to mutagenize this residue to a tyrosine to analyze whether α subunit expression increased.

β1b,β2 also slowed the rate of current decay of both $Na_V1.1$ isoforms in the presence and absence of β1,β2. This was not observed for $Na_V1.2$ or $Na_V1.5$ channels (Qin *et al.,* 2003; Watanabe *et al.,* 2008). However, $Na_V1.5$ channels were co-expressed with β1b in CHO cells and the internal solution used was CsF (Watanabe *et al.,* 2008); two variables that alter the inactivation of VGSCs (Watanabe *et al.,* 2008). Similarly for $Na_V1.2$, β1b channels were expressed in *Xenopus* oocytes (Qin *et al.,* 2003). β1b,β2 specifically slowed the kinetics of activation of $Na_V1.1$-5A but because the currents were small, the signal-to-noise ratio was high, and this may have affected curve fitting and data analysis. Therefore, a

greater number of experiments would have to be performed to verify this result. In the presence of $\beta1,\beta2$ the rate of inactivation of $Na_V1.1$-5N channels was significantly slowed and therefore the up-regulation of one $Na_V1.1$ splice variant may help to finely tune the excitability of neurons.

7.4.2 β subunits may change AED efficacy

These data suggest that while different β subunit pairs do have different effects on $Na_V1.1$ currents they do not dramatically distinguish between *SCN1A* exon 5 splice variants. However, β subunit modulation of channel recovery from inactivation was not assessed. Further experiments would reveal if this parameter is changed by the presence of specific β subunits, including pairs containing $\beta4$ subunits. Additionally, these experiments could measure whether the actions of AEDs on $Na_V1.1$ splice variant currents may be sensitive to changes in β subunit pairs. A recent study involving *SCN1B* null mice demonstrated that β subunits can selectively change the responses of AEDs. Compared to control neurons carbamazepine significantly shifted the voltage dependency INa$_P$ derived from mutant dentate granule cells in a hyperpolarized direction. The authors concluded that in a $\beta1$ absent background carbamazepine would paradoxically encourage neuronal firing (Uebachs *et al.,* 2010). However, Scheinmann *et al.* (1989) were the first to report that CNS VGSCs without β subunits are present in the developing rodent brain. The authors surmised that these were intracellular intermediates in the assembly of mature VGSCs and β subunits may help to stabilize the pore at the cell membrane (Alcaraz *et al.,* 1997). There is no direct evidence to suggest that $Na_V1.1$ α-only channels, *in vivo*, serve as functional channels. However, it is a strong possibility because β subunits, not $Na_V1.1$ α subunits, are

persistently down-regulated in experimental models of epilepsy. Although β subunit data is conflicting and may rely on brain region and animal model (Ellerkmann *et al.,* Gastaldi *et al.,* Gorter *et al.,* 2006). There are no reports to suggest that β1b,β2 subunits are subjected to the same down-regulation or even if this pair exists *in vivo*. However, if β1b,β2 subunits are sequestered during ictal activity this may act as a protective mechanism because an increased $Na_V1.1$ α subunit only current would enhance inhibition. This may explain why some AEDs can exacerbate seizures in GEFS+ patients. Future immunoblotting analysis and could help ascertain the relative changes in membrane β subunit and $Na_V1.1$ splice variant α subunit expression and in chicken models of epilepsy. Selectively knocking down $Na_V1.1$ splice variants and β subunits genes in neurons may reveal important but previously unrecognized targets and accidental modulators for AEDs.

7.4.3 Overall conclusion and directions for future research

The main aim of this work was to try and provide a mechanistic explanation for the association between rs3812718 and AED dosage found in the Tate *et al.,* studies (2005, 2006). Combining molecular information with genotyping may improve patient drug selection, predict side effects and avoid seizure aggravation. However, from these results the initial assumption, that epilepsy patients with a greater percentage of exon 5N require lowered drug dosages, may be inaccurate. Based on these data a reasonable hypothesis is that patients that favour the inclusion of exon 5N may experience a greater perturbation in inhibition after AED administration. Therefore a lower dosage requirement may simply reflect drug intolerance. Additionally, as demonstrated by the $Na_V1.1$-R1648H family and the biophysical data presented in this study (Chapter 4), a change in splicing and a mutation

in *SCN1A* does not predict patient phenotype or drug responsiveness. One may ask how effective is genotyping in treating GEFS+ syndromes? Future association studies are needed whereby a genetic causality has to be confirmed and if positive these patients would be separated from individuals with non-genetic etiologies. Concerning GEFS+, in patients with a genetic epilepsy all known GEFS+ genes would have to be screened to assess possible multiple-genetic inheritance and cohorts would be needed to be selected whereby individuals suffered with GEFS+ rather than including individuals other epilepsy syndromes. Lastly precise clinical notes are essential as drug intolerance could be easily eliminated. Moreover, the hypothesis that a loss/dysfunction of $Na_V1.1$ is the causality of GEFS+ may be inaccurate as findings in rodents may not translate to humans. This would be of importance to determine for further study.

This study highlights the difficulties of heterologous expression studies and the need for more consistent methodologies to be used in the field with regards to solutions and cell models. This was especially important with regards to G-protein regulation of these channels. These results hints of a possible Gβγ differential regulation of $Na_V1.1$ splice variant derived $I$$Na_P$, but further characterization of this modulation would be relevant. The selected β subunit pairs affected the gating of each splice variant similarly; however the recovery from inactivation was not assessed and future studies are needed to determine their affect on this parameter. Co-expression with additional β subunit pairs would be of importance to assess the broader impact of auxiliary subunit regulation.

References

Abe T, Seo T, Ishitsu T, Nakagawa T, Hori M, Nakagawa K. 2008. Association between SCN1A polymorphism and carbamazepine-resistant epilepsy. *Br J Clin Pharmacol* 66:304-7

Abeliovich A, Hammond R. 2007. Midbrain dopamine neuron differentiation: factors and fates. *Dev Biol* 304:447-54

Adams DJ, Oxford GS. 1983. Interaction of internal anions with potassium channels of the squid giant axon. *J Gen Physiol* 82:429-48

Adelman WJ, Jr., Dyron FM, Senft JP. 1966. Internally perfused axons: effects of two different anions on ionic conductance. *Science* 151:1392-4

Agrawal N, Hamam BN, Magistretti J, Alonso A, Ragsdale DS. 2001. Persistent sodium channel activity mediates subthreshold membrane potential oscillations and low-threshold spikes in rat entorhinal cortex layer V neurons. *Neuroscience* 102:53-64

Alberts, B. et al.; Molecular biology of the cell; Garland Science; New York and London, c2002

Albrieux M, Platel JC, Dupuis A, Villaz M, Moody WJ. 2004. Early expression of sodium channel transcripts and sodium current by cajal-retzius cells in the preplate of the embryonic mouse neocortex. *J Neurosci* 24:1719-25

Alcaraz G, Sampo B, Tricaud N, Giraud P, Martin-Eauclaire MF, et al. 1997. Down-regulation of voltage-dependent sodium channels coincides with a low expression of alphabeta1 subunit complexes. *Brain Res Mol Brain Res* 51:143-53

Alekov AK, Rahman MM, Mitrovic N, Lehmann-Horn F, Lerche H. 2001. Enhanced inactivation and acceleration of activation of the sodium channel associated with epilepsy in man. *Eur J Neurosci* 13:2171-6

Altshuler D, Daly MJ, Lander ES. 2008. Genetic mapping in human disease. *Science* 322:881-8

Alzheimer C, Schwindt PC, Crill WE. 1993. Modal gating of Na+ channels as a mechanism of persistent Na+ current in pyramidal neurons from rat and cat sensorimotor cortex. *J Neurosci* 13:660-73

Aman TK, Grieco-Calub TM, Chen C, Rusconi R, Slat EA, et al. 2009. Regulation of persistent Na current by interactions between beta subunits of voltage-gated Na channels. *J Neurosci* 29:2027-42

Amara SG, Jonas V, Rosenfeld MG, Ong ES, Evans RM. 1982. Alternative RNA

processing in calcitonin gene expression generates mRNAs encoding different polypeptide products. *Nature* 298:240-4

Andersen P, Moser EI. 1995. Brain temperature and hippocampal function. *Hippocampus* 5:491-8

Andrade A, Denome S, Jiang YQ, Marangoudakis S, Lipscombe D. 2010. Opioid inhibition of N-type Ca(2+) channels and spinal analgesia couple to alternative splicing. *Nat Neurosci* 13:1249-56

Aram JA, Lodge D. 1987. Epileptiform activity induced by alkalosis in rat neocortical slices: block by antagonists of N-methyl-D-aspartate. *Neurosci Lett* 83:345-50

Aronica E, Yankaya B, Troost D, van Vliet EA, Lopes da Silva FH, Gorter JA. 2001. Induction of neonatal sodium channel II and III alpha-isoform mRNAs in neurons and microglia after status epilepticus in the rat hippocampus. *Eur J Neurosci* 13:1261-6

Ashcroft, F., Ion Channels and Disease: Channelopathies., Academic Press, International, 2000.

Astman N, Gutnick MJ, Fleidervish IA. 2006. Persistent sodium current in layer 5 neocortical neurons is primarily generated in the proximal axon. *J Neurosci* 26:3465-73

Audenaert D, Claes L, Claeys KG, Deprez L, Van Dyck T, et al. 2005. A novel susceptibility locus at 2p24 for generalised epilepsy with febrile seizures plus. *J Med Genet* 42:947-52

Avanzini G, Franceschetti S, Mantegazza M. 2007. Epileptogenic channelopathies: experimental models of human pathologies. *Epilepsia* 48 Suppl 2:51-64

Avila G, Sandoval A, Felix R. 2004. Intramembrane charge movement associated with endogenous K+ channel activity in HEK-293 cells. *Cell Mol Neurobiol* 24:317-30

Azmanov DN, Zhelyazkova S, Dimova PS, Radionova M, Bojinova V, et al. 2010. Mosaicism of a missense SCN1A mutation and Dravet syndrome in a Roma/Gypsy family. *Epileptic Disord* 12:117-24

Baker MD, Chandra SY, Ding Y, Waxman SG, Wood JN. 2003. GTP-induced tetrodotoxin-resistant Na+ current regulates excitability in mouse and rat small diameter sensory neurones. *J Physiol* 548:373-82

Barren B, Natochin M, Artemyev NO. 2006. Mutation R238E in transducin-alpha yields a GTPase and effector-deficient, but not dominant-negative, G-protein alpha-subunit. *Mol Vis* 12:492-8

Bartschat DK, Rhodes TE. 1995. Protein kinase C modulates calcium channels in isolated presynaptic nerve terminals of rat hippocampus. *J Neurochem* 64:2064-72

Baulac S, Gourfinkel-An I, Couarch P, Depienne C, Kaminska A, et al. 2008. A novel locus for generalized epilepsy with febrile seizures plus in French families. *Arch Neurol* 65:943-51

Baulac S, Gourfinkel-An I, Picard F, Rosenberg-Bourgin M, Prud'homme JF, et al. 1999. A second locus for familial generalized epilepsy with febrile seizures plus maps to chromosome 2q21-q33. *Am J Hum Genet* 65:1078-85

Baulac S, Huberfeld G, Gourfinkel-An I, Mitropoulou G, Beranger A, et al. 2001. First genetic evidence of GABA(A) receptor dysfunction in epilepsy: a mutation in the gamma2-subunit gene. *Nat Genet* 28:46-8

Bean BP. 2005. The molecular machinery of resurgent sodium current revealed. *Neuron* 45:185-7

Bean BP. 2007. The action potential in mammalian central neurons. *Nat Rev Neurosci* 8:451-65

Beckh S, Noda M, Lubbert H, Numa S. 1989. Differential regulation of three sodium channel messenger RNAs in the rat central nervous system during development. *EMBO J* 8:3611-6

Belcher SM, Zerillo CA, Levenson R, Ritchie JM, Howe JR. 1995. Cloning of a sodium channel alpha subunit from rabbit Schwann cells. *Proc Natl Acad Sci U S A* 92:11034-8

Bell TJ, Thaler C, Castiglioni AJ, Helton TD, Lipscombe D. 2004. Cell-specific alternative splicing increases calcium channel current density in the pain pathway. *Neuron* 41:127-38

Belleau ML, Warren RA. 2000. Postnatal development of electrophysiological properties of nucleus accumbens neurons. *J Neurophysiol* 84:2204-16

Ben-Ari Y. 2006. Seizures beget seizures: the quest for GABA as a key player. *Crit Rev Neurobiol* 18:135-44

Berendt FJ, Park KS, Trimmer JS. 2010. Multisite phosphorylation of voltage-gated sodium channel alpha subunits from rat brain. *J Proteome Res* 9:1976-84

Berg AT, Berkovic SF, Brodie MJ, Buchhalter J, Cross JH, et al. 2010. Revised terminology and concepts for organization of seizures and epilepsies: report of the ILAE Commission on Classification and Terminology, 2005-2009. *Epilepsia* 51:676-85

Bergren SK, Rutter ED, Kearney JA. 2009. Fine mapping of an epilepsy modifier gene on mouse Chromosome 19. *Mamm Genome* 20:359-66

Berjukow S, Doring F, Froschmayr M, Grabner M, Glossmann H, Hering S. 1996. Endogenous calcium channels in human embryonic kidney (HEK293) cells. *Br J Pharmacol* 118:748-54

Berkovic SF, Scheffer IE. 1998. Febrile seizures: genetics and relationship to other epilepsy syndromes. *Curr Opin Neurol* 11:129-34

Bianchi MT, Song L, Zhang H, Macdonald RL. 2002. Two different mechanisms of disinhibition produced by GABAA receptor mutations linked to epilepsy in humans. *J Neurosci* 22:5321-7

Bigay J, Deterre P, Pfister C, Chabre M. 1987. Fluoride complexes of aluminium or beryllium act on G-proteins as reversibly bound analogues of the gamma phosphate of GTP. *EMBO J* 6:2907-13

Blencowe BJ. 2006. Alternative splicing: new insights from global analyses. *Cell* 126:37-47

Bolivar F, Rodriguez RL, Greene PJ, Betlach MC, Heyneker HL, et al. 1977. Construction and characterization of new cloning vehicles. II. A multipurpose cloning system. *Gene* 2:95-113

Bowser DN, Wagner DA, Czajkowski C, Cromer BA, Parker MW, et al. 2002. Altered kinetics and benzodiazepine sensitivity of a GABAA receptor subunit mutation [gamma 2(R43Q)] found in human epilepsy. *Proc Natl Acad Sci U S A* 99:15170-5

Brackenbury WJ, Davis TH, Chen C, Slat EA, Detrow MJ, et al. 2008. Voltage-gated Na+ channel beta1 subunit-mediated neurite outgrowth requires Fyn kinase and contributes to postnatal CNS development in vivo. *J Neurosci* 28:3246-56

Brackenbury WJ, Djamgoz MB. 2006. Activity-dependent regulation of voltage-gated Na+ channel expression in Mat-LyLu rat prostate cancer cell line. *J Physiol* 573:343-56

Brodie MJ, Dichter MA. 1997. Established antiepileptic drugs. *Seizure* 6:159-74

Brodie MJ, French JA. 2000. Management of epilepsy in adolescents and adults. *Lancet* 356:323-9

Brooks-Kayal AR, Shumate MD, Jin H, Rikhter TY, Coulter DA. 1998. Selective changes in single cell GABA(A) receptor subunit expression and function in temporal lobe epilepsy. *Nat Med* 4:1166-72

Bromfield, E., et al., An Introduction to Epilepsy., American Epilepsy Society, USA, 2006

Cannon SC. 2006. Pathomechanisms in channelopathies of skeletal muscle and brain. *Annu Rev Neurosci* 29:387-415

Canti C, Dolphin AC. 2003. CaVbeta subunit-mediated up-regulation of CaV2.2 currents triggered by D2 dopamine receptor activation. *Neuropharmacology* 45:814-27

Cantrell AR, Catterall WA. 2001. Neuromodulation of Na+ channels: an unexpected form of cellular plasticity. *Nat Rev Neurosci* 2:397-407

Cao Y, Wilcox KS, Martin CE, Rachinsky TL, Eberwine J, Dichter MA. 1996. Presence of mRNA for glutamic acid decarboxylase in both excitatory and inhibitory neurons. *Proc Natl Acad Sci U S A* 93:9844-9

Carle T, Fournier E, Sternberg D, Fontaine B, Tabti N. 2009. Cold-induced disruption of Na+ channel slow inactivation underlies paralysis in highly thermosensitive paramyotonia. *J Physiol* 587:1705-14

Carr DB, Day M, Cantrell AR, Held J, Scheuer T, et al. 2003. Transmitter modulation of slow, activity-dependent alterations in sodium channel availability endows neurons with a novel form of cellular plasticity. *Neuron* 39:793-806

Catterall WA. 1995. Structure and function of voltage-gated ion channels. *Annu Rev Biochem* 64:493-531

Catterall WA. 2000. From ionic currents to molecular mechanisms: the structure and function of voltage-gated sodium channels. *Neuron* 26:13-25

Catterall WA, Goldin AL, Waxman SG. 2005. International Union of Pharmacology. XLVII. Nomenclature and structure-function relationships of voltage-gated sodium channels. *Pharmacol Rev* 57:397-409

Catterall WA, Kalume F, Oakley JC. 2010. NaV1.1 channels and epilepsy. *J Physiol* 588:1849-59

Chahine M, Ziane R, Vijayaragavan K, Okamura Y. 2005. Regulation of Na v channels in sensory neurons. *Trends Pharmacol Sci* 26:496-502

Chatelier A, Dahllund L, Eriksson A, Krupp J, Chahine M. 2008. Biophysical properties of human NaV1.7 splice variants and their regulation by protein kinase A. *J Neurophysiol* 99:2241-50

Chandler WK, Meves H. 1970. Rate constants associated with changes in sodium conductance in axons perfused with sodium fluoride. *J Physiol* 211:679-705

Chao TI, Alzheimer C. 1995. Effects of phenytoin on the persistent Na+ current of mammalian CNS neurones. *Neuroreport* 6:1778-80

Chen C, Bharucha V, Chen Y, Westenbroek RE, Brown A, et al. 2002. Reduced sodium channel density, altered voltage dependence of inactivation, and increased susceptibility to seizures in mice lacking sodium channel beta 2-subunits. *Proc Natl Acad Sci U S A* 99:17072-7

Chen C, Westenbroek RE, Xu X, Edwards CA, Sorenson DR, et al. 2004. Mice lacking sodium channel beta1 subunits display defects in neuronal excitability, sodium channel expression, and nodal architecture. *J Neurosci* 24:4030-42

Chen LQ, Santarelli V, Horn R, Kallen RG. 1996. A unique role for the S4 segment of domain 4 in the inactivation of sodium channels. *J Gen Physiol* 108:549-56

Chen TC, Law B, Kondratyuk T, Rossie S. 1995. Identification of soluble protein phosphatases that dephosphorylate voltage-sensitive sodium channels in rat brain. *J Biol Chem* 270:7750-6

Chen Y, Yu FH, Surmeier DJ, Scheuer T, Catterall WA. 2006. Neuromodulation of Na+ channel slow inactivation via cAMP-dependent protein kinase and protein kinase C. *Neuron* 49:409-20

Chih B, Gollan L, Scheiffele P. 2006. Alternative splicing controls selective trans-synaptic interactions of the neuroligin-neurexin complex. *Neuron* 51:171-8

Chioni AM, Fraser SP, Pani F, Foran P, Wilkin GP, et al. 2005. A novel polyclonal antibody specific for the Na(v)1.5 voltage-gated Na(+) channel 'neonatal' splice form. *J Neurosci Methods* 147:88-98

Chiu C, Reid CA, Tan HO, Davies PJ, Single FN, et al. 2008. Developmental impact of a familial GABAA receptor epilepsy mutation. *Ann Neurol* 64:284-93

Cho T, Bae JH, Choi HB, Kim SS, McLarnon JG, et al. 2002. Human neural stem cells: electrophysiological properties of voltage-gated ion channels. *Neuroreport* 13:1447-52

Choi JS, Cheng X, Foster E, Leffler A, Tyrrell L, et al. 2010. Alternative splicing may contribute to time-dependent manifestation of inherited erythromelalgia. *Brain* 133:1823-35

Chou IC, Peng CT, Huang CC, Tsai JJ, Tsai FJ, Tsai CH. 2003. Association analysis of gamma 2 subunit of gamma- aminobutyric acid type A receptor polymorphisms with febrile seizures. *Pediatr Res* 54:26-9

Claes L, Ceulemans B, Audenaert D, Smets K, Lofgren A, et al. 2003. De novo SCN1A

mutations are a major cause of severe myoclonic epilepsy of infancy. *Hum Mutat* 21:615-21

Clay JR. 2003. On the persistent sodium current in squid giant axons. *J Neurophysiol* 89:640-4

Cooper DC, Chung S, Spruston N. 2005. Output-mode transitions are controlled by prolonged inactivation of sodium channels in pyramidal neurons of subiculum. *PLoS Biol* 3:e175

Copley RR. 2004. Evolutionary convergence of alternative splicing in ion channels. *Trends Genet* 20:171-6

Coste B, Osorio N, Padilla F, Crest M, Delmas P. 2004. Gating and modulation of presumptive NaV1.9 channels in enteric and spinal sensory neurons. *Mol Cell Neurosci* 26:123-34

Crill WE. 1996. Persistent sodium current in mammalian central neurons. *Annu Rev Physiol* 58:349-62

Cummins TR, Xia Y, Haddad GG. 1994. Functional properties of rat and human neocortical voltage-sensitive sodium currents. *J Neurophysiol* 71:1052-64

Cummins TR, Zhou J, Sigworth FJ, Ukomadu C, Stephan M, et al. 1993. Functional consequences of a Na+ channel mutation causing hyperkalemic periodic paralysis. *Neuron* 10:667-78

Cusdin FS, Clare JJ, Jackson AP. 2008. Trafficking and cellular distribution of voltage-gated sodium channels. *Traffic* 9:17-26

Daaka Y, Pitcher JA, Richardson M, Stoffel RH, Robishaw JD, Lefkowitz RJ. 1997. Receptor and G betagamma isoform-specific interactions with G protein-coupled receptor kinases. *Proc Natl Acad Sci U S A* 94:2180-5

Dai A, Temporal S, Schulz DJ. 2010. Cell-specific patterns of alternative splicing of voltage-gated ion channels in single identified neurons. *Neuroscience* 168:118-29

Danik M, Cassoly E, Manseau F, Sotty F, Mouginot D, Williams S. 2005. Frequent coexpression of the vesicular glutamate transporter 1 and 2 genes, as well as coexpression with genes for choline acetyltransferase or glutamic acid decarboxylase in neurons of rat brain. *J Neurosci Res* 81:506-21

Dascal N. 2001. Ion-channel regulation by G proteins. *Trends Endocrinol Metab* 12:391-8

Denson DD, Li J, Wang X, Eaton DC. 2005. Activation of BK channels in GH3 cells by a c-PLA2-dependent G-protein signaling pathway. *J Neurophysiol* 93:3146-56

Depienne C, Arzimanoglou A, Trouillard O, Fedirko E, Baulac S, et al. 2006. Parental mosaicism can cause recurrent transmission of SCN1A mutations associated with severe myoclonic epilepsy of infancy. *Hum Mutat* 27:389

Depienne C, Bouteiller D, Keren B, Cheuret E, Poirier K, et al. 2009. Sporadic infantile epileptic encephalopathy caused by mutations in PCDH19 resembles Dravet syndrome but mainly affects females. *PLoS Genet* 5:e1000381

Dhaka A, Viswanath V, Patapoutian A. 2006. Trp ion channels and temperature sensation. *Annu Rev Neurosci* 29:135-61

Dibbens LM, Feng HJ, Richards MC, Harkin LA, Hodgson BL, et al. 2004. GABRD encoding a protein for extra- or peri-synaptic GABAA receptors is a susceptibility locus for generalized epilepsies. *Hum Mol Genet* 13:1315-9

Dibbens LM, Reid CA, Hodgson B, Thomas EA, Phillips AM, et al. 2010. Augmented currents of an HCN2 variant in patients with febrile seizure syndromes. *Ann Neurol* 67:542-6

Dibbens LM, Tarpey PS, Hynes K, Bayly MA, Scheffer IE, et al. 2008. X-linked protocadherin 19 mutations cause female-limited epilepsy and cognitive impairment. *Nat Genet* 40:776-81

Dichgans M, Freilinger T, Eckstein G, Babini E, Lorenz-Depiereux B, et al. 2005. Mutation in the neuronal voltage-gated sodium channel SCN1A in familial hemiplegic migraine. *Lancet* 366:371-7

Dietrich PS, McGivern JG, Delgado SG, Koch BD, Eglen RM, et al. 1998. Functional analysis of a voltage-gated sodium channel and its splice variant from rat dorsal root ganglia. *J Neurochem* 70:2262-72

Diss JK, Archer SN, Hirano J, Fraser SP, Djamgoz MB. 2001. Expression profiles of voltage-gated Na(+) channel alpha-subunit genes in rat and human prostate cancer cell lines. *Prostate* 48:165-78

Diss JK, Fraser SP, Djamgoz MB. 2004. Voltage-gated Na+ channels: multiplicity of expression, plasticity, functional implications and pathophysiological aspects. *Eur Biophys J* 33:180-93

Dixon AK, Richardson PJ, Lee K, Carter NP, Freeman TC. 1998. Expression profiling of single cells using 3 prime end amplification (TPEA) PCR. *Nucleic Acids Res* 26:4426-31

Dixon AK, Richardson PJ, Pinnock RD, Lee K. 2000. Gene-expression analysis at the single-cell level. *Trends Pharmacol Sci* 21:65-70

Database of Single Nucleotide Polymorphisms (dbSNP). Bethesda (MD): National Center for Biotechnology Information, National Library of Medicine. dbSNP accession: rs3812718. Available from: http://www.ncbi.nlm.nih.gov/SNP/

Donato R, Miljan EA, Hines SJ, Aouabdi S, Pollock K, et al. 2007. Differential development of neuronal physiological responsiveness in two human neural stem cell lines. *BMC Neurosci* 8:36

Dube C, Chen K, Eghbal-Ahmadi M, Brunson K, Soltesz I, Baram TZ. 2000. Prolonged febrile seizures in the immature rat model enhance hippocampal excitability long term. *Ann Neurol* 47:336-44

Dube C, Vezzani A, Behrens M, Bartfai T, Baram TZ. 2005. Interleukin-1beta contributes to the generation of experimental febrile seizures. *Ann Neurol* 57:152-5

Dube CM, Brewster AL, Baram TZ. 2009. Febrile seizures: mechanisms and relationship to epilepsy. *Brain Dev* 31:366-71

Dube CM, Brewster AL, Richichi C, Zha Q, Baram TZ. 2007. Fever, febrile seizures and epilepsy. *Trends Neurosci* 30:490-6

Duflocq A, Le Bras B, Bullier E, Couraud F, Davenne M. 2008. Nav1.1 is predominantly expressed in nodes of Ranvier and axon initial segments. *Mol Cell Neurosci* 39:180-92

Dzhala VI, Talos DM, Sdrulla DA, Brumback AC, Mathews GC, et al. 2005. NKCC1 transporter facilitates seizures in the developing brain. *Nat Med* 11:1205-13

Ellerkmann RK, Remy S, Chen J, Sochivko D, Elger CE, et al. 2003. Molecular and functional changes in voltage-dependent Na(+) channels following pilocarpine-induced status epilepticus in rat dentate granule cells. *Neuroscience* 119:323-33

Engelman DM, Steitz TA, Goldman A. 1986. Identifying nonpolar transbilayer helices in amino acid sequences of membrane proteins. *Annu Rev Biophys Biophys Chem* 15:321-53

Escayg A, Goldin AL. 2010. Sodium channel SCN1A and epilepsy: Mutations and mechanisms. *Epilepsia*

Escayg A, MacDonald BT, Meisler MH, Baulac S, Huberfeld G, et al. 2000. Mutations of SCN1A, encoding a neuronal sodium channel, in two families with GEFS+2. *Nat Genet* 24:343-5

Eugene E, Depienne C, Baulac S, Baulac M, Fritschy JM, et al. 2007. GABA(A) receptor gamma 2 subunit mutations linked to human epileptic syndromes differentially affect phasic and tonic inhibition. *J Neurosci* 27:14108-16

Faivre S, Regnauld K, Bruyneel E, Nguyen QD, Mareel M, et al. 2001. Suppression of cellular invasion by activated G-protein subunits Galphao, Galphai1, Galphai2, and Galphai3 and sequestration of Gbetagamma. *Mol Pharmacol* 60:363-72

Fan S, Stewart M, Wong RK. 1994. Differences in voltage-dependent sodium currents exhibited by superficial and deep layer neurons of guinea pig entorhinal cortex. *J Neurophysiol* 71:1986-91

Federman AD, Conklin BR, Schrader KA, Reed RR, Bourne HR. 1992. Hormonal stimulation of adenylyl cyclase through Gi-protein beta gamma subunits. *Nature* 356:159-61

Felts PA, Yokoyama S, Dib-Hajj S, Black JA, Waxman SG. 1997. Sodium channel alpha-subunit mRNAs I, II, III, NaG, Na6 and hNE (PN1): different expression patterns in developing rat nervous system. *Brain Res Mol Brain Res* 45:71-82

Feng HJ, Kang JQ, Song L, Dibbens L, Mulley J, Macdonald RL. 2006. Delta subunit susceptibility variants E177A and R220H associated with complex epilepsy alter channel gating and surface expression of alpha4beta2delta GABAA receptors. *J Neurosci* 26:1499-506

Fernandez-Fernandez JM, Abogadie FC, Milligan G, Delmas P, Brown DA. 2001. Multiple pertussis toxin-sensitive G-proteins can couple receptors to GIRK channels in rat sympathetic neurons when expressed heterologously, but only native G(i)-proteins do so in situ. *Eur J Neurosci* 14:283-92

Fertleman CR, Baker MD, Parker KA, Moffatt S, Elmslie FV, et al. 2006. SCN9A mutations in paroxysmal extreme pain disorder: allelic variants underlie distinct channel defects and phenotypes. *Neuron* 52:767-74

Filippov AK, Fernandez-Fernandez JM, Marsh SJ, Simon J, Barnard EA, Brown DA. 2004. Activation and inhibition of neuronal G protein-gated inwardly rectifying K(+) channels by P2Y nucleotide receptors. *Mol Pharmacol* 66:468-77

Fisher RS, van Emde Boas W, Blume W, Elger C, Genton P, et al. 2005. Epileptic seizures and epilepsy: definitions proposed by the International League Against Epilepsy (ILAE) and the International Bureau for Epilepsy (IBE). *Epilepsia* 46:470-2

Fotia AB, Ekberg J, Adams DJ, Cook DI, Poronnik P, Kumar S. 2004. Regulation of neuronal voltage-gated sodium channels by the ubiquitin-protein ligases Nedd4 and Nedd4-2. *J Biol Chem* 279:28930-5

Frustaci A, Priori SG, Pieroni M, Chimenti C, Napolitano C, et al. 2005. Cardiac histological substrate in patients with clinical phenotype of Brugada syndrome. *Circulation* 112:3680-7

Frykberg L, Graf T, Vennstrom B. 1987. The transforming activity of the chicken c-myc gene can be potentiated by mutations. *Oncogene* 1:415-22

Fujiwara T, Sugawara T, Mazaki-Miyazaki E, Takahashi Y, Fukushima K, et al. 2003. Mutations of sodium channel alpha subunit type 1 (SCN1A) in intractable childhood epilepsies with frequent generalized tonic-clonic seizures. *Brain* 126:531-46

Fukuda M, Morimoto T, Nagao H, Kida K. 1997. Clinical study of epilepsy with severe febrile seizures and seizures induced by hot water bath. *Brain Dev* 19:212-6

Gage FH. 2000. Mammalian neural stem cells. *Science* 287:1433-8

Garrido JJ, Fernandes F, Moussif A, Fache MP, Giraud P, Dargent B. 2003. Dynamic compartmentalization of the voltage-gated sodium channels in axons. *Biol Cell* 95:437-45

Gastaldi M, Bartolomei F, Massacrier A, Planells R, Robaglia-Schlupp A, Cau P. 1997. Increase in mRNAs encoding neonatal II and III sodium channel alpha-isoforms during kainate-induced seizures in adult rat hippocampus. *Brain Res Mol Brain Res* 44:179-90

Gastaldi M, Robaglia-Schlupp A, Massacrier A, Planells R, Cau P. 1998. mRNA coding for voltage-gated sodium channel beta2 subunit in rat central nervous system: cellular distribution and changes following kainate-induced seizures. *Neurosci Lett* 249:53-6

Gazina EV, Richards KL, Mokhtar MB, Thomas EA, Reid CA, Petrou S. 2010. Differential expression of exon 5 splice variants of sodium channel alpha subunit mRNAs in the developing mouse brain. *Neuroscience* 166:195-200

Gebhardt C, Breustedt JM, Noldner M, Chatterjee SS, Heinemann U. 2001. The antiepileptic drug losigamone decreases the persistent Na+ current in rat hippocampal neurons. *Brain Res* 920:27-31

Gennaro E, Santorelli FM, Bertini E, Buti D, Gaggero R, et al. 2006. Somatic and germline mosaicisms in severe myoclonic epilepsy of infancy. *Biochem Biophys Res Commun* 341:489-93

Genton P. 2000. When antiepileptic drugs aggravate epilepsy. *Brain Dev* 22:75-80

Goldin AL. 2001. Resurgence of sodium channel research. *Annu Rev Physiol* 63:871-94

Goldin AL, Snutch T, Lubbert H, Dowsett A, Marshall J, et al. 1986. Messenger RNA coding for only the alpha subunit of the rat brain Na channel is sufficient for expression of functional channels in Xenopus oocytes. *Proc Natl Acad Sci U S A*

83:7503-7

Gomez-Lira G, Lamas M, Romo-Parra H, Gutierrez R. 2005. Programmed and induced phenotype of the hippocampal granule cells. *J Neurosci* 25:6939-46

Gomperts, B., et al., Signal Transduction., Academic Press, USA, 2003

Gong B, Rhodes KJ, Bekele-Arcuri Z, Trimmer JS. 1999. Type I and type II Na(+) channel alpha-subunit polypeptides exhibit distinct spatial and temporal patterning, and association with auxiliary subunits in rat brain. *J Comp Neurol* 412:342-52

Gorter JA, van Vliet EA, Aronica E, Breit T, Rauwerda H, et al. 2006. Potential new antiepileptogenic targets indicated by microarray analysis in a rat model for temporal lobe epilepsy. *J Neurosci* 26:11083-110

Graham FL, Smiley J, Russell WC, Nairn R. 1977. Characteristics of a human cell line transformed by DNA from human adenovirus type 5. *J Gen Virol* 36:59-74

Gray AC, Raingo J, Lipscombe D. 2007. Neuronal calcium channels: splicing for optimal performance. *Cell Calcium* 42:409-17

Greenberg DA, Pal DK. 2007. The state of the art in the genetic analysis of the epilepsies. *Curr Neurol Neurosci Rep* 7:320-8

Greer S, Honeywell R, Geletu M, Arulanandam R, Raptis L. 2010. Housekeeping genes; expression levels may change with density of cultured cells. *J Immunol Methods* 355:76-9

Grieco TM, Malhotra JD, Chen C, Isom LL, Raman IM. 2005. Open-channel block by the cytoplasmic tail of sodium channel beta4 as a mechanism for resurgent sodium current. *Neuron* 45:233-44

Groot-Kormelink PJ, Beato M, Finotti C, Harvey RJ, Sivilotti LG. 2002. Achieving optimal expression for single channel recording: a plasmid ratio approach to the expression of alpha 1 glycine receptors in HEK293 cells. *J Neurosci Methods* 113:207-14

Guatteo E, Chung KK, Bowala TK, Bernardi G, Mercuri NB, Lipski J. 2005. Temperature sensitivity of dopaminergic neurons of the substantia nigra pars compacta: involvement of transient receptor potential channels. *J Neurophysiol* 94:3069-80

Guerrini R, Belmonte A, Genton P. 1998. Antiepileptic drug-induced worsening of seizures in children. *Epilepsia* 39 Suppl 3:S2-10

Guo J, Schofield GG. 2002. Activation of a PTX-insensitive G protein is involved in histamine-induced recombinant M-channel modulation. *J Physiol* 545:767-81

Gustafson TA, Clevinger EC, O'Neill TJ, Yarowsky PJ, Krueger BK. 1993. Mutually exclusive exon splicing of type III brain sodium channel alpha subunit RNA generates developmentally regulated isoforms in rat brain. *J Biol Chem* 268:18648-53

Gutierrez R. 2005. The dual glutamatergic-GABAergic phenotype of hippocampal granule cells. *Trends Neurosci* 28:297-303

Hakim P, Brice N, Thresher R, Lawrence J, Zhang Y, et al. 2010. Scn3b knockout mice exhibit abnormal sino-atrial and cardiac conduction properties. *Acta Physiol (Oxf)* 198:47-59

Hales TG, Tang H, Bollan KA, Johnson SJ, King DP, et al. 2005. The epilepsy mutation, gamma2(R43Q) disrupts a highly conserved inter-subunit contact site, perturbing the biogenesis of GABAA receptors. *Mol Cell Neurosci* 29:120-7

Harkin LA, Bowser DN, Dibbens LM, Singh R, Phillips F, et al. 2002. Truncation of the GABA(A)-receptor gamma2 subunit in a family with generalized epilepsy with febrile seizures plus. *Am J Hum Genet* 70:530-6

Harkin LA, McMahon JM, Iona X, Dibbens L, Pelekanos JT, et al. 2007. The spectrum of SCN1A-related infantile epileptic encephalopathies. *Brain* 130:843-52

Hart MJ, Jiang X, Kozasa T, Roscoe W, Singer WD, et al. 1998. Direct stimulation of the guanine nucleotide exchange activity of p115 RhoGEF by Galpha13. *Science* 280:2112-4

Hartshorne RP, Catterall WA. 1981. Purification of the saxitoxin receptor of the sodium channel from rat brain. *Proc Natl Acad Sci U S A* 78:4620-4

Hartshorne RP, Catterall WA. 1984. The sodium channel from rat brain. Purification and subunit composition. *J Biol Chem* 259:1667-75

Harwood JP, Low H, Rodbell M. 1973. Stimulatory and inhibitory effects of guanyl nucleotides on fat cell adenylate cyclase. *J Biol Chem* 248:6239-45

Harwood JP, Rodbell M. 1973. Inhibition by fluoride ion of hormonal activation of fat cell adenylate cyclase. *J Biol Chem* 248:4901-4

Haspolat S, Mihci E, Coskun M, Gumuslu S, Ozben T, Yegin O. 2002. Interleukin-1beta, tumor necrosis factor-alpha, and nitrite levels in febrile seizures. *J Child Neurol* 17:749-51

Hausser M, Clark BA. 1997. Tonic synaptic inhibition modulates neuronal output pattern and spatiotemporal synaptic integration. *Neuron* 19:665-78

Heeroma JH, Henneberger C, Rajakulendran S, Hanna MG, Schorge S, Kullmann DM. 2009. Episodic ataxia type 1 mutations differentially affect neuronal excitability and transmitter release. *Dis Model Mech* 2:612-9

Heinemann SH, Terlau H, Stuhmer W, Imoto K, Numa S. 1992. Calcium channel characteristics conferred on the sodium channel by single mutations. *Nature* 356:441-3

Heinzen EL, Yoon W, Tate SK, Sen A, Wood NW, et al. 2007. Nova2 interacts with a cis-acting polymorphism to influence the proportions of drug-responsive splice variants of SCN1A. *Am J Hum Genet* 80:876-83

Hermann B. 2010. 100 years of Epilepsia: landmark papers and their influence in neuropsychology and neuropsychiatry. *Epilepsia* 51:1107-19

Hernandez-Ochoa EO, Garcia-Ferreiro RE, Garcia DE. 2007. G protein activation inhibits gating charge movement in rat sympathetic neurons. *Am J Physiol Cell Physiol* 292:C2226-38

Heron SE, Scheffer IE, Iona X, Zuberi SM, Birch R, et al. 2010. De novo SCN1A mutations in Dravet syndrome and related epileptic encephalopathies are largely of paternal origin. *J Med Genet* 47:137-41

Herrmann A, Braathen GJ, Russell MB. 2005. [Episodic ataxias]. *Tidsskr Nor Laegeforen* 125:2005-7

Herzig S, Neumann J. 2000. Effects of serine/threonine protein phosphatases on ion channels in excitable membranes. *Physiol Rev* 80:173-210

Herzog RI, Liu C, Waxman SG, Cummins TR. 2003. Calmodulin binds to the C terminus of sodium channels Nav1.4 and Nav1.6 and differentially modulates their functional properties. *J Neurosci* 23:8261-70

Hickman-Davis JM, Davis IC. 2006. Transgenic mice. *Paediatr Respir Rev* 7:49-53

Hilgemann DW, Feng S, Nasuhoglu C. 2001. The complex and intriguing lives of PIP2 with ion channels and transporters. *Sci STKE* 2001:re19

Hille, B., (2001) 3rd Ed. Ion Channels of Excitable Membranes, Sinauer Associates Inc.,U.S.

Holtzman D, Obana K, Olson J. 1981. Hyperthermia-induced seizures in the rat pup: a model for febrile convulsions in children. *Science* 213:1034-6

Horn R, Vandenberg CA. 1984. Statistical properties of single sodium channels. *J Gen Physiol* 84:505-34

Huang B, El-Sherif T, Gidh-Jain M, Qin D, El-Sherif N. 2001. Alterations of sodium channel kinetics and gene expression in the postinfarction remodeled myocardium. *J Cardiovasc Electrophysiol* 12:218-25

Hughes P, Marshall D, Reid Y, Parkes H, Gelber C. 2007. The costs of using unauthenticated, over-passaged cell lines: how much more data do we need? *Biotechniques* 43:575, 7-8, 81-2 passim

Inoue M, Imanaga I. 1995. Phosphatase is responsible for run down, and probably G protein-mediated inhibition of inwardly rectifying K+ currents in guinea pig chromaffin cells. *J Gen Physiol* 105:249-66

Isom LL. 2001. Sodium channel beta subunits: anything but auxiliary. *Neuroscientist* 7:42-54

Isom LL, Ragsdale DS, De Jongh KS, Westenbroek RE, Reber BF, et al. 1995a. Structure and function of the beta 2 subunit of brain sodium channels, a transmembrane glycoprotein with a CAM motif. *Cell* 83:433-42

Isom LL, Scheuer T, Brownstein AB, Ragsdale DS, Murphy BJ, Catterall WA. 1995b. Functional co-expression of the beta 1 and type IIA alpha subunits of sodium channels in a mammalian cell line. *J Biol Chem* 270:3306-12

Ito H, Vereecke J, Carmeliet E. 1994. Mode of regulation by G protein of the ATP-sensitive K+ channel in guinea-pig ventricular cell membrane. *J Physiol* 478 (Pt 1):101-7

Ito M, Yamakawa K, Sugawara T, Hirose S, Fukuma G, Kaneko S. 2006. Phenotypes and genotypes in epilepsy with febrile seizures plus. *Epilepsy Res* 70 Suppl 1:S199-205

Jahnsen H, Llinas R. 1984. Electrophysiological properties of guinea-pig thalamic neurones: an in vitro study. *J Physiol* 349:205-26

Jamal SM, Basran RK, Newton S, Wang Z, Milunsky JM. 2010. Novel de novo PCDH19 mutations in three unrelated females with epilepsy female restricted mental retardation syndrome. *Am J Med Genet A* 152A:2475-81

Jansen FE, Sadleir LG, Harkin LA, Vadlamudi L, McMahon JM, et al. 2006. Severe myoclonic epilepsy of infancy (Dravet syndrome): recognition and diagnosis in adults. *Neurology* 67:2224-6

Jarecki BW, Sheets PL, Xiao Y, Jackson JO, 2nd, Cummins TR. 2009. Alternative splicing of Na(V)1.7 exon 5 increases the impact of the painful PEPD mutant channel I1461T. *Channels* (Austin) 3:259-67

Jenkins SM, Bennett V. 2001. Ankyrin-G coordinates assembly of the spectrin-based membrane skeleton, voltage-gated sodium channels, and L1 CAMs at Purkinje neuron initial segments. *J Cell Biol* 155:739-46

Jeong SY, Goto J, Hashida H, Suzuki T, Ogata K, et al. 2000. Identification of a novel human voltage-gated sodium channel alpha subunit gene, SCN12A. *Biochem Biophys Res Commun* 267:262-70

Johnson D, Montpetit ML, Stocker PJ, Bennett ES. 2004. The sialic acid component of the beta1 subunit modulates voltage-gated sodium channel function. *J Biol Chem* 279:44303-10

Johnson DD, Crawford KD, Crawford RD. 1983. Febrile seizures in epileptic chicks: the effects of phenobarbital, phenytoin and valproate. *Can J Neurol Sci* 10:96-9

Kahlig KM, Misra SN, George AL, Jr. 2006. Impaired inactivation gate stabilization predicts increased persistent current for an epilepsy-associated SCN1A mutation. *J Neurosci* 26:10958-66

Kammermeier PJ, Ruiz-Velasco V, Ikeda SR. 2000. A voltage-independent calcium current inhibitory pathway activated by muscarinic agonists in rat sympathetic neurons requires both Galpha q/11 and Gbeta gamma. *J Neurosci* 20:5623-9

Kamouchi M, Van Den Bremt K, Eggermont J, Droogmans G, Nilius B. 1997. Modulation of inwardly rectifying potassium channels in cultured bovine pulmonary artery endothelial cells. *J Physiol* 504 (Pt 3):545-56

Kananura C, Haug K, Sander T, Runge U, Gu W, et al. 2002. A splice-site mutation in GABRG2 associated with childhood absence epilepsy and febrile convulsions. *Arch Neurol* 59:1137-41

Kang JQ, Macdonald RL. 2009. Making sense of nonsense GABA(A) receptor mutations associated with genetic epilepsies. *Trends Mol Med* 15:430-8

Kang JQ, Shen W, Macdonald RL. 2006. Why does fever trigger febrile seizures? GABAA receptor gamma2 subunit mutations associated with idiopathic generalized epilepsies have temperature-dependent trafficking deficiencies. *J Neurosci* 26:2590-7

Kearney JA, Wiste AK, Stephani U, Trudeau MM, Siegel A, et al. 2006. Recurrent de novo mutations of SCN1A in severe myoclonic epilepsy of infancy. *Pediatr Neurol* 34:116-20

Keiser MJ, Setola V, Irwin JJ, Laggner C, Abbas AI, et al. 2009. Predicting new molecular targets for known drugs. *Nature* 462:175-81

Kerb R, Aynacioglu AS, Brockmoller J, Schlagenhaufer R, Bauer S, et al. 2001. The predictive value of MDR1, CYP2C9, and CYP2C19 polymorphisms for phenytoin plasma levels. *Pharmacogenomics J* 1:204-10

Kerr NC, Holmes FE, Wynick D. 2004. Novel isoforms of the sodium channels Nav1.8 and Nav1.5 are produced by a conserved mechanism in mouse and rat. *J Biol Chem* 279:24826-33

Kerr NC, Holmes FE, Wynick D. 2008. Novel mRNA isoforms of the sodium channels Na(v)1.2, Na(v)1.3 and Na(v)1.7 encode predicted two-domain, truncated proteins. *Neuroscience* 155:797-808

Kim DY, Carey BW, Wang H, Ingano LA, Binshtok AM, et al. 2007. BACE1 regulates voltage-gated sodium channels and neuronal activity. *Nat Cell Biol* 9:755-64

Kim JA, Gibson HE, Kauer JA, Connors BW. TRPV1 channels enhance susceptibility to febrile seizures. Annual meeting of the Society for Neuroscience; November 15–19; Washington DC. 2008. Abstr Soc Neurosci # 628.1.

Klugbauer N, Lacinova L, Flockerzi V, Hofmann F. 1995. Structure and functional expression of a new member of the tetrodotoxin-sensitive voltage-activated sodium channel family from human neuroendocrine cells. *EMBO J* 14:1084-90

Kohling R. 2002. Voltage-gated sodium channels in epilepsy. *Epilepsia* 43:1278-95

Kohrman DC, Smith MR, Goldin AL, Harris J, Meisler MH. 1996. A missense mutation in the sodium channel Scn8a is responsible for cerebellar ataxia in the mouse mutant jolting. *J Neurosci* 16:5993-9

Krikova EV, Val'dman EA, Avakian GN, Andreev Ia A, Denisov EV, et al. 2009. [Association study of the SCN1 gene polymorphism and effective dose of lamotrigine]. *Zh Nevrol Psikhiatr Im S S Korsakova* 109:57-62

Kucken AM, Teissere JA, Seffinga-Clark J, Wagner DA, Czajkowski C. 2003. Structural requirements for imidazobenzodiazepine binding to GABA(A) receptors. *Mol Pharmacol* 63:289-96

Kuenzel T, Monig B, Wagner H, Mey J, Luksch H. 2007. Neuronal differentiation of the early embryonic auditory hindbrain of the chicken in primary culture. *Eur J Neurosci* 25:974-84

Kuenzel T, Wirth MJ, Luksch H, Wagner H, Mey J. 2009. Increase of Kv3.1b expression in avian auditory brainstem neurons correlates with synaptogenesis in vivo and in vitro. *Brain Res* 1302:64-75

Kuhn FJ, Greeff NG. 1999. Movement of voltage sensor S4 in domain 4 is tightly coupled to sodium channel fast inactivation and gating charge immobilization. *J Gen Physiol* 114:167-83

Kullmann DM. 2002. The neuronal channelopathies. *Brain* 125:1177-95

Kuo CC, Bean BP. 1994. Slow binding of phenytoin to inactivated sodium channels in rat hippocampal neurons. *Mol Pharmacol* 46:716-25

Kwan P, Poon WS, Ng HK, Kang DE, Wong V, et al. 2008. Multidrug resistance in epilepsy and polymorphisms in the voltage-gated sodium channel genes SCN1A, SCN2A, and SCN3A: correlation among phenotype, genotype, and mRNA expression. *Pharmacogenet Genomics* 18:989-98

Lakhan R, Kumari R, Misra UK, Kalita J, Pradhan S, Mittal B. 2009. Differential role of sodium channels SCN1A and SCN2A gene polymorphisms with epilepsy and multiple drug resistance in the north Indian population. *Br J Clin Pharmacol* 68:214-20

Lee CJ, Irizarry K. 2003. Alternative splicing in the nervous system: an emerging source of diversity and regulation. *Biol Psychiatry* 54:771-6

Lei Q, Jones MB, Talley EM, Schrier AD, McIntire WE, et al. 2000. Activation and inhibition of G protein-coupled inwardly rectifying potassium (Kir3) channels by G protein beta gamma subunits. *Proc Natl Acad Sci U S A* 97:9771-6

Lenkowski PW, Stevens EB, Yusaf SP, Patel MK. (2004). G-protein β1γ2 subunits bind directly to the C-terminus of Nav1.3 and modulate channel properties. Biophysical Journal, 86: (1): 881 Part 2.

Lenz RA, Pitler TA, Alger BE. 1997. High intracellular Cl- concentrations depress G-protein-modulated ionic conductances. *J Neurosci* 17:6133-41

Lerche H, Peter W, Fleischhauer R, Pika-Hartlaub U, Malina T, et al. 1997. Role in fast inactivation of the IV/S4-S5 loop of the human muscle Na+ channel probed by cysteine mutagenesis. *J Physiol* 505 (Pt 2):345-52

Li Q, Lee JA, Black DL. 2007. Neuronal regulation of alternative pre-mRNA splicing. *Nat Rev Neurosci* 8:819-31

Liao Y, Deprez L, Maljevic S, Pitsch J, Claes L, et al. 2010. Molecular correlates of age-dependent seizures in an inherited neonatal-infantile epilepsy. *Brain* 133:1403-14

Logothetis DE, Petrou VI, Adney SK, Mahajan R. 2010. Channelopathies linked to plasma membrane phosphoinositides. *Pflugers Arch* 460:321-41

Lohberger B, Groschner K, Tritthart H, Schreibmayer W. 2000. IK.ACh activation by arachidonic acid occurs via a G-protein-independent pathway mediated by the GIRK1 subunit. *Pflugers Arch* 441:251-6

Loscher W, Cramer S, Ebert U. 1998. Selection of phenytoin responders and nonresponders in male and female amygdala-kindled Sprague-Dawley rats. *Epilepsia* 39:1138-47

Loscher W, Klotz U, Zimprich F, Schmidt D. 2009. The clinical impact of pharmacogenetics on the treatment of epilepsy. *Epilepsia* 50:1-23

Lossin C. 2009. A catalog of SCN1A variants. *Brain Dev* 31:114-30

Lossin C, Rhodes TH, Desai RR, Vanoye CG, Wang D, et al. 2003. Epilepsy-associated dysfunction in the voltage-gated neuronal sodium channel SCN1A. *J Neurosci* 23:11289-95

Lu CM, Brown GB. 1998. Isolation of a human-brain sodium-channel gene encoding two isoforms of the subtype III alpha-subunit. *J Mol Neurosci* 10:67-70

Luthi A, McCormick DA. 1998. H-current: properties of a neuronal and network pacemaker. *Neuron* 21:9-12

Ma JY, Catterall WA, Scheuer T. 1997. Persistent sodium currents through brain sodium channels induced by G protein betagamma subunits. *Neuron* 19:443-52

Ma JY, Li M, Catterall WA, Scheuer T. 1994. Modulation of brain Na+ channels by a G-protein-coupled pathway. *Proc Natl Acad Sci U S A* 91:12351-5

Maingret F, Coste B, Padilla F, Clerc N, Crest M, et al. 2008. Inflammatory mediators increase Nav1.9 current and excitability in nociceptors through a coincident detection mechanism. *J Gen Physiol* 131:211-25

Makita N, Bennett PB, Jr., George AL, Jr. 1996. Multiple domains contribute to the distinct inactivation properties of human heart and skeletal muscle Na+ channels. *Circ Res* 78:244-52

Malhotra JD, Thyagarajan V, Chen C, Isom LL. 2004. Tyrosine-phosphorylated and nonphosphorylated sodium channel beta1 subunits are differentially localized in cardiac myocytes. *J Biol Chem* 279:40748-54

Mancardi MM, Striano P, Gennaro E, Madia F, Paravidino R, et al. 2006. Familial occurrence of febrile seizures and epilepsy in severe myoclonic epilepsy of infancy (SMEI) patients with SCN1A mutations. *Epilepsia* 47:1629-35

Mantegazza M, Curia G, Biagini G, Ragsdale DS, Avoli M. 2010. Voltage-gated sodium channels as therapeutic targets in epilepsy and other neurological disorders. *Lancet*

Neurol 9:413-24

Mantegazza M, Yu FH, Powell AJ, Clare JJ, Catterall WA, Scheuer T. 2005. Molecular determinants for modulation of persistent sodium current by G-protein betagamma subunits. *J Neurosci* 25:3341-9

Marin P, Fagni L, Torrens Y, Alcaraz G, Couraud F, et al. 2001. AMPA receptor activation induces association of G-beta protein with the alpha subunit of the sodium channel in neurons. *Eur J Neurosci* 14:1953-60

Marini C, Mei D, Temudo T, Ferrari AR, Buti D, et al. 2007. Idiopathic epilepsies with seizures precipitated by fever and SCN1A abnormalities. *Epilepsia* 48:1678-85

Marini C, Scheffer IE, Nabbout R, Mei D, Cox K, et al. 2009. SCN1A duplications and deletions detected in Dravet syndrome: Implications for molecular diagnosis. *Epilepsia*

Martin MS, Dutt K, Papale LA, Dube CM, Dutton SB, et al. 2010. Altered function of the SCN1A voltage-gated sodium channel leads to gamma-aminobutyric acid-ergic (GABAergic) interneuron abnormalities. *J Biol Chem* 285:9823-34

Matsuki N, Quandt FN, Ten Eick RE, Yeh JZ. 1984. Characterization of the block of sodium channels by phenytoin in mouse neuroblastoma cells. *J Pharmacol Exp Ther* 228:523-30

Matthews E, Labrum R, Sweeney MG, Sud R, Haworth A, et al. 2009. Voltage sensor charge loss accounts for most cases of hypokalemic periodic paralysis. *Neurology* 72:1544-7

Maurice N, Mercer J, Chan CS, Hernandez-Lopez S, Held J, et al. 2004. D2 dopamine receptor-mediated modulation of voltage-dependent Na+ channels reduces autonomous activity in striatal cholinergic interneurons. *J Neurosci* 24:10289-301

McCloskey MA, Cahalan MD. 1990. G protein control of potassium channel activity in a mast cell line. *J Gen Physiol* 95:205-27

McCormick DA, Contreras D. 2001. On the cellular and network bases of epileptic seizures. *Annu Rev Physiol* 63:815-46

McCormick KA, Isom LL, Ragsdale D, Smith D, Scheuer T, Catterall WA. 1998. Molecular determinants of Na+ channel function in the extracellular domain of the beta1 subunit. *J Biol Chem* 273:3954-62

McEwen DP, Meadows LS, Chen C, Thyagarajan V, Isom LL. 2004. Sodium channel beta1 subunit-mediated modulation of Nav1.2 currents and cell surface density is dependent on interactions with contactin and ankyrin. *J Biol Chem* 279:16044-9

McLean MJ, Macdonald RL. 1983. Multiple actions of phenytoin on mouse spinal cord neurons in cell culture. *J Pharmacol Exp Ther* 227:779-89

McPhee JC, Ragsdale DS, Scheuer T, Catterall WA. 1998. A critical role for the S4-S5 intracellular loop in domain IV of the sodium channel alpha-subunit in fast inactivation. *J Biol Chem* 273:1121-9

Meadows LS, Chen YH, Powell AJ, Clare JJ, Ragsdale DS. 2002a. Functional modulation of human brain Nav1.3 sodium channels, expressed in mammalian cells, by auxiliary beta 1, beta 2 and beta 3 subunits. *Neuroscience* 114:745-53

Meadows LS, Malhotra J, Loukas A, Thyagarajan V, Kazen-Gillespie KA, et al. 2002b. Functional and biochemical analysis of a sodium channel beta1 subunit mutation responsible for generalized epilepsy with febrile seizures plus type 1. *J Neurosci* 22:10699-709

Mechaly I, Scamps F, Chabbert C, Sans A, Valmier J. 2005. Molecular diversity of voltage-gated sodium channel alpha subunits expressed in neuronal and non-neuronal excitable cells. *Neuroscience* 130:389-96

Melliti K, Meza U, Adams BA. 2001. RGS2 blocks slow muscarinic inhibition of N-type Ca(2+) channels reconstituted in a human cell line. *J Physiol* 532:337-47

Merrick EC, Kalmar CL, Snyder SL, Cusdin FS, Yu EJ, et al. 2010. The importance of serine 161 in the sodium channel beta3 subunit for modulation of Na(V)1.2 gating. *Pflugers Arch* 460:743-53

Merritt HH, Putnam TJ. 1984. Landmark article Sept 17, 1938: Sodium diphenyl hydantoinate in the treatment of convulsive disorders. By H. Houston Merritt and Tracy J. Putnam. *JAMA* 251:1062-7

Messner DJ, Catterall WA. 1985. The sodium channel from rat brain. Separation and characterization of subunits. *J Biol Chem* 260:10597-604

Meza U, Thapliyal A, Bannister RA, Adams BA. 2007. Neurokinin 1 receptors trigger overlapping stimulation and inhibition of CaV2.3 (R-type) calcium channels. *Mol Pharmacol* 71:284-93

Miyazaki H, Oyama F, Wong HK, Kaneko K, Sakurai T, et al. 2007. BACE1 modulates filopodia-like protrusions induced by sodium channel beta4 subunit. *Biochem Biophys Res Commun* 361:43-8

Modrek B, Lee C. 2002. A genomic view of alternative splicing. *Nat Genet* 30:13-9

Moody WJ, Bosma MM. 2005. Ion channel development, spontaneous activity, and

activity-dependent development in nerve and muscle cells. *Physiol Rev* 85:883-941

Morgan K, Stevens EB, Shah B, Cox PJ, Dixon AK, et al. 2000. beta 3: an additional auxiliary subunit of the voltage-sensitive sodium channel that modulates channel gating with distinct kinetics. *Proc Natl Acad Sci U S A* 97:2308-13

Morimoto M, Mazaki E, Nishimura A, Chiyonobu T, Sawai Y, et al. 2006. SCN1A mutation mosaicism in a family with severe myoclonic epilepsy in infancy. *Epilepsia* 47:1732-6

Motoike HK, Liu H, Glaaser IW, Yang AS, Tateyama M, Kass RS. 2004. The Na+ channel inactivation gate is a molecular complex: a novel role of the COOH-terminal domain. *J Gen Physiol* 123:155-65

Molleman, A; Patch Clamping: An Introductory Guide to Patch Clamp Electrophysiology; WileyBlackwell; 2003

Mu Y, Otsuka T, Horton AC, Scott DB, Ehlers MD. 2003. Activity-dependent mRNA splicing controls ER export and synaptic delivery of NMDA receptors. *Neuron* 40:581-94

Mulley JC, Scheffer IE, Petrou S, Dibbens LM, Berkovic SF, Harkin LA. 2005. SCN1A mutations and epilepsy. *Hum Mutat* 25:535-42

Murray KT, Anno T, Bennett PB, Hondeghem LM. 1990. Voltage clamp of the cardiac sodium current at 37 degrees C in physiologic solutions. *Biophys J* 57:607-13

Nabbout R, Gennaro E, Dalla Bernardina B, Dulac O, Madia F, et al. 2003. Spectrum of SCN1A mutations in severe myoclonic epilepsy of infancy. *Neurology* 60:1961-7

Nam SC, Hockberger PE. 1997. Analysis of spontaneous electrical activity in cerebellar Purkinje cells acutely isolated from postnatal rats. *J Neurobiol* 33:18-32

Nishimura T, Schwarzer C, Gasser E, Kato N, Vezzani A, Sperk G. 2005. Altered expression of GABA(A) and GABA(B) receptor subunit mRNAs in the hippocampus after kindling and electrically induced status epilepticus. *Neuroscience* 134:691-704

Noda M. 2006. The subfornical organ, a specialized sodium channel, and the sensing of sodium levels in the brain. *Neuroscientist* 12:80-91

O'Reilly JP, Wang SY, Kallen RG, Wang GK. 1999. Comparison of slow inactivation in human heart and rat skeletal muscle Na+ channel chimaeras. *J Physiol* 515 (Pt 1):61-73

Oakley JC, Kalume F, Yu FH, Scheuer T, Catterall WA. 2009. Temperature- and age-

dependent seizures in a mouse model of severe myoclonic epilepsy in infancy. *Proc Natl Acad Sci U S A* 106:3994-9

Ogiwara I, Miyamoto H, Morita N, Atapour N, Mazaki E, et al. 2007. Na(v)1.1 localizes to axons of parvalbumin-positive inhibitory interneurons: a circuit basis for epileptic seizures in mice carrying an Scn1a gene mutation. *J Neurosci* 27:5903-14

Oh Y, Waxman SG. 1998. Novel splice variants of the voltage-sensitive sodium channel alpha subunit. *Neuroreport* 9:1267-72

Ohmori I, Ouchida M, Miki T, Mimaki N, Kiyonaka S, et al. 2008. A CACNB4 mutation shows that altered Ca(v)2.1 function may be a genetic modifier of severe myoclonic epilepsy in infancy. *Neurobiol Dis* 32:349-54

Ohmori I, Ouchida M, Ohtsuka Y, Oka E, Shimizu K. 2002. Significant correlation of the SCN1A mutations and severe myoclonic epilepsy in infancy. *Biochem Biophys Res Commun* 295:17-23

Ohno Y, Ishihara S, Mashimo T, Sofue N, Shimizu S, et al. 2010. Scn1a missense mutation causes limbic hyperexcitability and vulnerability to experimental febrile seizures. *Neurobiol Dis*

Ong BH, Tomaselli GF, Balser JR. 2000. A structural rearrangement in the sodium channel pore linked to slow inactivation and use dependence. *J Gen Physiol* 116:653-62

Onkal R, Mattis JH, Fraser SP, Diss JK, Shao D, et al. 2008. Alternative splicing of Nav1.5: an electrophysiological comparison of 'neonatal' and 'adult' isoforms and critical involvement of a lysine residue. *J Cell Physiol* 216:716-26

Orrico A, Galli L, Grosso S, Buoni S, Pianigiani R, et al. 2009. Mutational analysis of the SCN1A, *SCN1B* and GABRG2 genes in 150 Italian patients with idiopathic childhood epilepsies. *Clin Genet* 75:579-81

Orth JH, Fester I, Preuss I, Agnoletto L, Wilson BA, Aktories K. 2008. Activation of Galpha (i) and subsequent uncoupling of receptor-Galpha(i) signaling by Pasteurella multocida toxin. *J Biol Chem* 283:23288-94

Ostman JA, Nassar MA, Wood JN, Baker MD. 2008. GTP up-regulated persistent Na+ current and enhanced nociceptor excitability require NaV1.9. *J Physiol* 586:1077-87

Owens DF, Kriegstein AR. 2002. Is there more to GABA than synaptic inhibition? *Nat Rev Neurosci* 3:715-27

Pal DK, Pong AW, Chung WK. 2010. Genetic evaluation and counseling for epilepsy. *Nat Rev Neurol*

Panayiotopoulos CP. 2005. Idiopathic generalized epilepsies: a review and modern approach. *Epilepsia* 46 Suppl 9:1-6

Patino GA, Claes LR, Lopez-Santiago LF, Slat EA, Dondeti RS, et al. 2009. A functional null mutation of *SCN1B* in a patient with Dravet syndrome. *J Neurosci* 29:10764-78

Patton DE, Isom LL, Catterall WA, Goldin AL. 1994. The adult rat brain beta 1 subunit modifies activation and inactivation gating of multiple sodium channel alpha subunits. *J Biol Chem* 269:17649-55

Pearce JM. 2002. Bromide, the first effective antiepileptic agent. *J Neurol Neurosurg Psychiatry* 72:412

Penela P, Ribas C, Mayor F, Jr. 2003. Mechanisms of regulation of the expression and function of G protein-coupled receptor kinases. *Cell Signal* 15:973-81

Petrovski S, Scheffer IE, Sisodiya SM, O'Brien TJ, Berkovic SF. 2009. Lack of replication of association between scn1a SNP and febrile seizures. *Neurology* 73:1928-30

Pinkse MW, Merkx M, Averill BA. 1999. Fluoride inhibition of bovine spleen purple acid phosphatase: characterization of a ternary enzyme-phosphate-fluoride complex as a model for the active enzyme-substrate-hydroxide complex. *Biochemistry* 38:9926-36

Pitcher JA, Freedman NJ, Lefkowitz RJ. 1998. G protein-coupled receptor kinases. *Annu Rev Biochem* 67:653-92

Pitkänen A, Schwartzkroin PA, Moshé SL., Models of Seizures and Epilepsy, Academic Press, USA, 2005

Planells-Cases R, Caprini M, Zhang J, Rockenstein EM, Rivera RR, et al. 2000. Neuronal death and perinatal lethality in voltage-gated sodium channel alpha(II)-deficient mice. *Biophys J* 78:2878-91

Plummer NW, McBurney MW, Meisler MH. 1997. Alternative splicing of the sodium channel SCN8A predicts a truncated two-domain protein in fetal brain and non-neuronal cells. *J Biol Chem* 272:24008-15

Powell KL, Ng C, O'Brien TJ, Xu SH, Williams DA, et al. 2008. Decreases in HCN mRNA expression in the hippocampus after kindling and status epilepticus in adult rats. *Epilepsia* 49:1686-95

Probstle T, Rudel R, Ruppersberg JP. 1988. Hodgkin-Huxley parameters of the sodium channels in human myoballs. *Pflugers Arch* 412:264-9

Ptak K, Zummo GG, Alheid GF, Tkatch T, Surmeier DJ, McCrimmon DR. 2005. Sodium currents in medullary neurons isolated from the pre-Botzinger complex region. *J*

Neurosci 25:5159-70

Pugliatti M, Beghi E, Forsgren L, Ekman M, Sobocki P. 2007. Estimating the cost of epilepsy in Europe: a review with economic modeling. *Epilepsia* 48:2224-33

Pusch M, Noda M, Stuhmer W, Numa S, Conti F. 1991. Single point mutations of the sodium channel drastically reduce the pore permeability without preventing its gating. *Eur Biophys J* 20:127-33

Qin N, D'Andrea MR, Lubin ML, Shafaee N, Codd EE, Correa AM. 2003. Molecular cloning and functional expression of the human sodium channel beta1B subunit, a novel splicing variant of the beta1 subunit. *Eur J Biochem* 270:4762-70

Qu Y, Curtis R, Lawson D, Gilbride K, Ge P, et al. 2001. Differential modulation of sodium channel gating and persistent sodium currents by the beta1, beta2, and beta3 subunits. *Mol Cell Neurosci* 18:570-80

Radnikow G, Feldmeyer D, Lubke J. 2002. Axonal projection, input and output synapses, and synaptic physiology of Cajal-Retzius cells in the developing rat neocortex. *J Neurosci* 22:6908-19

Ragsdale DS. 2008. How do mutant Nav1.1 sodium channels cause epilepsy? *Brain Res Rev* 58:149-59

Ragsdale DS, Avoli M. 1998. Sodium channels as molecular targets for antiepileptic drugs. *Brain Res Brain Res Rev* 26:16-28

Ragsdale DS, Scheuer T, Catterall WA. 1991. Frequency and voltage-dependent inhibition of type IIA Na+ channels, expressed in a mammalian cell line, by local anesthetic, antiarrhythmic, and anticonvulsant drugs. *Mol Pharmacol* 40:756-65

Raingo J, Castiglioni AJ, Lipscombe D. 2007. Alternative splicing controls G protein-dependent inhibition of N-type calcium channels in nociceptors. *Nat Neurosci* 10:285-92

Raman IM, Sprunger LK, Meisler MH, Bean BP. 1997. Altered subthreshold sodium currents and disrupted firing patterns in Purkinje neurons of Scn8a mutant mice. *Neuron* 19:881-91

Rangel A, Sanchez-Armass S, Meza U. 2010. Protein kinase C-mediated inhibition of recombinant T-type Cav3.2 channels by neurokinin 1 receptors. *Mol Pharmacol* 77:202-10

Raymond CK, Castle J, Garrett-Engele P, Armour CD, Kan Z, et al. 2004. Expression of alternatively spliced sodium channel alpha-subunit genes. Unique splicing patterns are observed in dorsal root ganglia. *J Biol Chem* 279:46234-41

Reid CA, Berkovic SF, Petrou S. 2009. Mechanisms of human inherited epilepsies. *Prog Neurobiol* 87:41-57

Remy S, Beck H. 2006. Molecular and cellular mechanisms of pharmacoresistance in epilepsy. *Brain* 129:18-35

Richardson PJ, Dixon AK, Lee K, Bell MI, Cox PJ, et al. 2000. Correlating physiology with gene expression in striatal cholinergic neurones. *J Neurochem* 74:839-46

Richerson GB. 2004. Looking for GABA in all the wrong places: the relevance of extrasynaptic GABA(A) receptors to epilepsy. *Epilepsy Curr* 4:239-42

Rodin E, Constantino T, Rampp S, Wong PK. 2009. Spikes and epilepsy. *Clin EEG Neurosci* 40:288-99

Rogawski MA, Loscher W. 2004. The neurobiology of antiepileptic drugs. *Nat Rev Neurosci* 5:553-64

Ruff RL. 1999. Effects of temperature on slow and fast inactivation of rat skeletal muscle Na(+) channels. *Am J Physiol* 277:C937-47

Rugiero F, Mistry M, Sage D, Black JA, Waxman SG, et al. 2003. Selective expression of a persistent tetrodotoxin-resistant Na+ current and NaV1.9 subunit in myenteric sensory neurons. *J Neurosci* 23:2715-25

Rundfeldt C, Loscher W. 1993. Anticonvulsant efficacy and adverse effects of phenytoin during chronic treatment in amygdala-kindled rats. *J Pharmacol Exp Ther* 266:216-23

Rusconi R, Combi R, Cestele S, Grioni D, Franceschetti S, et al. 2009. A rescuable folding defective Nav1.1 (SCN1A) sodium channel mutant causes GEFS+: common mechanism in Nav1.1 related epilepsies? *Hum Mutat* 30:E747-60

Rusconi R, Scalmani P, Cassulini RR, Giunti G, Gambardella A, et al. 2007. Modulatory proteins can rescue a trafficking defective epileptogenic Nav1.1 Na+ channel mutant. *J Neurosci* 27:11037-46

Rush AM, Cummins TR, Waxman SG. 2007. Multiple sodium channels and their roles in electrogenesis within dorsal root ganglion neurons. *J Physiol* 579:1-14

Saab CY, Cummins TR, Waxman SG. 2003. GTP gamma S increases Nav1.8 current in small-diameter dorsal root ganglia neurons. *Exp Brain Res* 152:415-9

Sancar F, Czajkowski C. 2004. A GABAA receptor mutation linked to human epilepsy (gamma2R43Q) impairs cell surface expression of alphabetagamma receptors. *J*

Biol Chem 279:47034-9

Sands Z, Grottesi A, Sansom MS. 2005. Voltage-gated ion channels. *Curr Biol* 15:R44-7

Sangameswaran L, Fish LM, Koch BD, Rabert DK, Delgado SG, et al. 1997. A novel tetrodotoxin-sensitive, voltage-gated sodium channel expressed in rat and human dorsal root ganglia. *J Biol Chem* 272:14805-9

Sarao R, Gupta SK, Auld VJ, Dunn RJ. 1991. Developmentally regulated alternative RNA splicing of rat brain sodium channel mRNAs. *Nucleic Acids Res* 19:5673-9

Sato C, Ueno Y, Asai K, Takahashi K, Sato M, et al. 2001. The voltage-sensitive sodium channel is a bell-shaped molecule with several cavities. *Nature* 409:1047-51

Schaller KL, Krzemien DM, McKenna NM, Caldwell JH. 1992. Alternatively spliced sodium channel transcripts in brain and muscle. *J Neurosci* 12:1370-81

Scharfman HE. 2002. Does the Development of a GABAergic Phenotype by Hippocampal Dentate Gyrus Granule Cells Contribute to Epileptogenesis. *Epilepsy Curr* 2:63

Scharfman HE. 2007. The neurobiology of epilepsy. *Curr Neurol Neurosci Rep* 7:348-54

Schaub C, Uebachs M, Beck H. 2007. Diminished response of CA1 neurons to antiepileptic drugs in chronic epilepsy. *Epilepsia* 48:1339-50

Scheffer IE, Harkin LA, Dibbens LM, Mulley JC, Berkovic SF. 2005. Neonatal epilepsy syndromes and generalized epilepsy with febrile seizures plus (GEFS+). *Epilepsia* 46 Suppl 10:41-7

Scheffer IE, Harkin LA, Grinton BE, Dibbens LM, Turner SJ, et al. 2007. Temporal lobe epilepsy and GEFS+ phenotypes associated with *SCN1B* mutations. *Brain* 130:100-9

Scheffer IE, Zhang YH, Jansen FE, Dibbens L. 2009. Dravet syndrome or genetic (generalized) epilepsy with febrile seizures plus? *Brain Dev* 31:394-400

Scheinman RI, Auld VJ, Goldin AL, Davidson N, Dunn RJ, Catterall WA. 1989. Developmental regulation of sodium channel expression in the rat forebrain. *J Biol Chem* 264:10660-6

Scheyer RD, During MJ, Hochholzer JM, Spencer DD, Cramer JA, Mattson RH. 1994. Phenytoin concentrations in the human brain: an in vivo microdialysis study. *Epilepsy Res* 18:227-32

Schirmeyer J, Szafranski K, Leipold E, Mawrin C, Platzer M, Heinemann SH. 2010. A subtle alternative splicing event of the Na(V)1.8 voltage-gated sodium channel is

conserved in human, rat, and mouse. *J Mol Neurosci* 41:310-4

Schlachter K, Gruber-Sedlmayr U, Stogmann E, Lausecker M, Hotzy C, et al. 2009. A splice site variant in the sodium channel gene SCN1A confers risk of febrile seizures. *Neurology* 72:974-8

Schmidt J, Rossie S, Catterall WA. 1985. A large intracellular pool of inactive Na channel alpha subunits in developing rat brain. *Proc Natl Acad Sci U S A* 82:4847-51

Schmutz M, Klein M, Klebs K, Bernasconi R, Bittiger H, Baltzer V. 1985. Pharmacological and neurochemical aspects of kindling. *J Neural Transm* 63:143-55

Schouten JP, McElgunn CJ, Waaijer R, Zwijnenburg D, Diepvens F, Pals G. 2002. Relative quantification of 40 nucleic acid sequences by multiplex ligation-dependent probe amplification. *Nucleic Acids Res* 30:e57

Schroeter A, Walzik S, Blechschmidt S, Haufe V, Benndorf K, Zimmer T. 2010. Structure and function of splice variants of the cardiac voltage-gated sodium channel Na(v)1.5. *J Mol Cell Cardiol* 49:16-24

Schwarz JR. 1986. The effect of temperature on Na currents in rat myelinated nerve fibres. *Pflugers Arch* 406:397-404

Selyanko AA, Hadley JK, Brown DA. 2001. Properties of single M-type KCNQ2/KCNQ3 potassium channels expressed in mammalian cells. *J Physiol* 534:15-24

Shao D, Okuse K, Djamgoz MB. 2009. Protein-protein interactions involving voltage-gated sodium channels: Post-translational regulation, intracellular trafficking and functional expression. *Int J Biochem Cell Biol* 41:1471-81

Shaw G, Morse S, Ararat M, Graham FL. 2002. Preferential transformation of human neuronal cells by human adenoviruses and the origin of HEK 293 cells. *FASEB J* 16:869-71

Shibasaki K, Suzuki M, Mizuno A, Tominaga M. 2007. Effects of body temperature on neural activity in the hippocampus: regulation of resting membrane potentials by transient receptor potential vanilloid 4. *J Neurosci* 27:1566-75

Shoffner JM, Lott MT, Lezza AM, Seibel P, Ballinger SW, Wallace DC. 1990. Myoclonic epilepsy and ragged-red fiber disease (MERRF) is associated with a mitochondrial DNA tRNA(Lys) mutation. *Cell* 61:931-7

Simon C, Stieger B, Kullak-Ublick GA, Fried M, Mueller S, et al. 2007. Intestinal expression of cytochrome P450 enzymes and ABC transporters and carbamazepine and phenytoin disposition. *Acta Neurol Scand* 115:232-42

Singh NA, Pappas C, Dahle EJ, Claes LR, Pruess TH, et al. 2009. A role of SCN9A in human epilepsies, as a cause of febrile seizures and as a potential modifier of Dravet syndrome. *PLoS Genet* 5:e1000649

Smith, M.R. and A.L. Goldin. 1999. A mutation that causes ataxia shifts the voltage-dependence of the scn8a sodium channel. *NeuroReport* 10:3027-3031.

Sombati S, Delorenzo RJ. 1995. Recurrent spontaneous seizure activity in hippocampal neuronal networks in culture. *J Neurophysiol* 73:1706-11

Sotty F, Danik M, Manseau F, Laplante F, Quirion R, Williams S. 2003. Distinct electrophysiological properties of glutamatergic, cholinergic and GABAergic rat septohippocampal neurons: novel implications for hippocampal rhythmicity. *J Physiol* 551:927-43

Spampanato J, Aradi I, Soltesz I, Goldin AL. 2004. Increased neuronal firing in computer simulations of sodium channel mutations that cause generalized epilepsy with febrile seizures plus. *J Neurophysiol* 91:2040-50

Spampanato J, Escayg A, Meisler MH, Goldin AL. 2001. Functional effects of two voltage-gated sodium channel mutations that cause generalized epilepsy with febrile seizures plus type 2. *J Neurosci* 21:7481-90

Spampanato J, Escayg A, Meisler MH, Goldin AL. 2003. Generalized epilepsy with febrile seizures plus type 2 mutation W1204R alters voltage-dependent gating of Na(v)1.1 sodium channels. *Neuroscience* 116:37-48

Sperk G, Schwarzer C, Tsunashima K, Kandlhofer S. 1998. Expression of GABA(A) receptor subunits in the hippocampus of the rat after kainic acid-induced seizures. *Epilepsy Res* 32:129-39

Srinivasan J, Schachner M, Catterall WA. 1998. Interaction of voltage-gated sodium channels with the extracellular matrix molecules tenascin-C and tenascin-R. *Proc Natl Acad Sci U S A* 95:15753-7

Stafstrom CE. 2007. Persistent sodium current and its role in epilepsy. *Epilepsy Curr* 7:15-22

Stafstrom CE. 2009. Severe epilepsy syndromes of early childhood: the link between genetics and pathophysiology with a focus on SCN1A mutations. *J Child Neurol* 24:15S-23S

Stevens EB, Cox PJ, Shah BS, Dixon AK, Richardson PJ, et al. 2001. Tissue distribution and functional expression of the human voltage-gated sodium channel beta3 subunit. *Pflugers Arch* 441:481-8

Struyk AF, Cannon SC. 2002. Slow inactivation does not block the aqueous accessibility to the outer pore of voltage-gated Na channels. *J Gen Physiol* 120:509-16

Strachan & Read 1999 (2nd edition) Human Molecular Genetics 2; Bios Scientific Publishers Ltd; Oxford, UK

Strichartz G, Zimmermann M. Selective conduction blockade among different fiber types in mammalian nerves by lidocaine combined with low temperature [abstracts] Soc Neurosci. 1983;9:675.

Sucher NJ, Deitcher DL, Baro DJ, Warrick RM, Guenther E. 2000. Genes and channels: patch/voltage-clamp analysis and single-cell RT-PCR. *Cell Tissue Res* 302:295-307

Sugawara T, Mazaki-Miyazaki E, Fukushima K, Shimomura J, Fujiwara T, et al. 2002. Frequent mutations of SCN1A in severe myoclonic epilepsy in infancy. *Neurology* 58:1122-4

Sugawara T, Tsurubuchi Y, Agarwala KL, Ito M, Fukuma G, et al. 2001. A missense mutation of the Na+ channel alpha II subunit gene Na(v)1.2 in a patient with febrile and afebrile seizures causes channel dysfunction. *Proc Natl Acad Sci U S A* 98:6384-9

Sugawara T, Tsurubuchi Y, Fujiwara T, Mazaki-Miyazaki E, Nagata K, et al. 2003. Nav1.1 channels with mutations of severe myoclonic epilepsy in infancy display attenuated currents. *Epilepsy Res* 54:201-7

Sugiura Y, Makita N, Li L, Noble PJ, Kimura J, et al. 2003. Cold induces shifts of voltage dependence in mutant SCN4A, causing hypokalemic periodic paralysis. *Neurology* 61:914-8

Sun GC, Werkman TR, Battefeld A, Clare JJ, Wadman WJ. 2007. Carbamazepine and topiramate modulation of transient and persistent sodium currents studied in HEK293 cells expressing the Na(v)1.3 alpha-subunit. *Epilepsia* 48:774-82

Taddese A, Bean BP. 2002. Subthreshold sodium current from rapidly inactivating sodium channels drives spontaneous firing of tuberomammillary neurons. *Neuron* 33:587-600

Takasaki J, Saito T, Taniguchi M, Kawasaki T, Moritani Y, et al. 2004. A novel Galphaq/11-selective inhibitor. *J Biol Chem* 279:47438-45

Tan HO, Reid CA, Single FN, Davies PJ, Chiu C, et al. 2007. Reduced cortical inhibition in a mouse model of familial childhood absence epilepsy. *Proc Natl Acad Sci U S A* 104:17536-41

Tan J, Liu Z, Nomura Y, Goldin AL, Dong K. 2002. Alternative splicing of an insect

sodium channel gene generates pharmacologically distinct sodium channels. *J Neurosci* 22:5300-9

Tang B, Dutt K, Papale L, Rusconi R, Shankar A, et al. 2009. A BAC transgenic mouse model reveals neuron subtype-specific effects of a Generalized Epilepsy with Febrile Seizures Plus (GEFS+) mutation. *Neurobiol Dis* 35:91-102

Tasaki I, Singer I, Takenaka T. 1965. Effects of internal and external ionic environment on excitability of squid giant axon. A macromolecular approach. *J Gen Physiol* 48:1095-123

Tate SK, Depondt C, Sisodiya SM, Cavalleri GL, Schorge S, et al. 2005. Genetic predictors of the maximum doses patients receive during clinical use of the anti-epileptic drugs carbamazepine and phenytoin. *Proc Natl Acad Sci U S A* 102:5507-12

Tate SK, Singh R, Hung CC, Tai JJ, Depondt C, et al. 2006. A common polymorphism in the SCN1A gene associates with phenytoin serum levels at maintenance dose. *Pharmacogenet Genomics* 16:721-6

Tateyama M, Kurokawa J, Terrenoire C, Rivolta I, Kass RS. 2003. Stimulation of protein kinase C inhibits bursting in disease-linked mutant human cardiac sodium channels. *Circulation* 107:3216-22

Terlau H, Heinemann SH, Stuhmer W, Pusch M, Conti F, et al. 1991. Mapping the site of block by tetrodotoxin and saxitoxin of sodium channel II. *FEBS Lett* 293:93-6

Terzic A, Tung RT, Inanobe A, Katada T, Kurachi Y. 1994. G proteins activate ATP-sensitive K+ channels by antagonizing ATP-dependent gating. *Neuron* 12:885-93

Thapliyal A, Bannister RA, Hanks C, Adams BA. 2008. The monomeric G proteins AGS1 and Rhes selectively influence Galphai-dependent signaling to modulate N-type (CaV2.2) calcium channels. *Am J Physiol Cell Physiol* 295:C1417-26

Thomas EA, Hawkins RJ, Richards KL, Xu R, Gazina EV, Petrou S. 2009. Heat opens axon initial segment sodium channels: a febrile seizure mechanism? *Ann Neurol* 66:219-26

Tibbs VC, Gray PC, Catterall WA, Murphy BJ. 1998. AKAP15 anchors cAMP-dependent protein kinase to brain sodium channels. *J Biol Chem* 273:25783-8

Toby G, Law SF, Golemis EA. 1998. Vectors to target protein domains to different cellular compartments. *Biotechniques* 24:637-40

Toib A, Lyakhov V, Marom S. 1998. Interaction between duration of activity and time course of recovery from slow inactivation in mammalian brain Na+ channels. *J Neurosci* 18:1893-903

Toledo-Aral JJ, Moss BL, He ZJ, Koszowski AG, Whisenand T, et al. 1997. Identification of PN1, a predominant voltage-dependent sodium channel expressed principally in peripheral neurons. *Proc Natl Acad Sci U S A* 94:1527-32

Toth Z, Yan XX, Haftoglou S, Ribak CE, Baram TZ. 1998. Seizure-induced neuronal injury: vulnerability to febrile seizures in an immature rat model. *J Neurosci* 18:4285-94

Tutuncuoglu S, Kutukculer N, Kepe L, Coker C, Berdeli A, Tekgul H. 2001. Proinflammatory cytokines, prostaglandins and zinc in febrile convulsions. *Pediatr Int* 43:235-9

Uebachs M, Opitz T, Royeck M, Dickhof G, Horstmann MT, et al. 2010. Efficacy loss of the anticonvulsant carbamazepine in mice lacking sodium channel beta subunits via paradoxical effects on persistent sodium currents. *J Neurosci* 30:8489-501

Ukomadu C, Zhou J, Sigworth FJ, Agnew WS. 1992. muI Na+ channels expressed transiently in human embryonic kidney cells: biochemical and biophysical properties. *Neuron* 8:663-76

Ulbricht W. 2005. Sodium channel inactivation: molecular determinants and modulation. *Physiol Rev* 85:1271-301

Ule J, Ule A, Spencer J, Williams A, Hu JS, et al. 2005. Nova regulates brain-specific splicing to shape the synapse. *Nat Genet* 37:844-52

Vandenberg CA, Bezanilla F. 1991. A sodium channel gating model based on single channel, macroscopic ionic, and gating currents in the squid giant axon. *Biophys J* 60:1511-33

Vanoye CG, Lossin C, Rhodes TH, George AL, Jr. 2006. Single-channel properties of human NaV1.1 and mechanism of channel dysfunction in SCN1A-associated epilepsy. *J Gen Physiol* 127:1-14

Vervaeke K, Hu H, Graham LJ, Storm JF. 2006. Contrasting effects of the persistent Na+ current on neuronal excitability and spike timing. *Neuron* 49:257-70

Vezzani A, Granata T. 2005. Brain inflammation in epilepsy: experimental and clinical evidence. *Epilepsia* 46:1724-43

Volgushev M, Vidyasagar TR, Chistiakova M, Yousef T, Eysel UT. 2000. Membrane properties and spike generation in rat visual cortical cells during reversible cooling. *J Physiol* 522 Pt 1:59-76

Wakai S, Ito N, Sueoka H, Kawamoto Y, Hayasaka H, Chiba S. 1996. Severe myoclonic

epilepsy in infancy and carbamazepine. *Eur J Pediatr* 155:724

Wallace RH, Hodgson BL, Grinton BE, Gardiner RM, Robinson R, et al. 2003. Sodium channel alpha1-subunit mutations in severe myoclonic epilepsy of infancy and infantile spasms. *Neurology* 61:765-9

Wallace RH, Marini C, Petrou S, Harkin LA, Bowser DN, et al. 2001a. Mutant GABA(A) receptor gamma2-subunit in childhood absence epilepsy and febrile seizures. *Nat Genet* 28:49-52

Wallace RH, Scheffer IE, Barnett S, Richards M, Dibbens L, et al. 2001b. Neuronal sodium-channel alpha1-subunit mutations in generalized epilepsy with febrile seizures plus. *Am J Hum Genet* 68:859-65

Wallace RH, Scheffer IE, Parasivam G, Barnett S, Wallace GB, et al. 2002. Generalized epilepsy with febrile seizures plus: mutation of the sodium channel subunit *SCN1B*. *Neurology* 58:1426-9

Wallace RH, Wang DW, Singh R, Scheffer IE, George AL, Jr., et al. 1998. Febrile seizures and generalized epilepsy associated with a mutation in the Na+-channel beta1 subunit gene *SCN1B*. *Nat Genet* 19:366-70

Walsh KB, Wilson SP, Long KJ, Lemon SC. 1996. Stimulatory regulation of the large-conductance, calcium-activated potassium channel by G proteins in bovine adrenal chromaffin cells. *Mol Pharmacol* 49:379-86

Wang JW, Kurahashi H, Ishii A, Kojima T, Ohfu M, et al. 2008. Microchromosomal deletions involving SCN1A and adjacent genes in severe myoclonic epilepsy in infancy. *Epilepsia* 49:1528-34

Watanabe H, Koopmann TT, Le Scouarnec S, Yang T, Ingram CR, et al. 2008. Sodium channel beta1 subunit mutations associated with Brugada syndrome and cardiac conduction disease in humans. *J Clin Invest* 118:2260-8

Weale ME, Depondt C, Macdonald SJ, Smith A, Lai PS, et al. 2003. Selection and evaluation of tagging SNPs in the neuronal-sodium-channel gene SCN1A: implications for linkage-disequilibrium gene mapping. *Am J Hum Genet* 73:551-65

Webb J, Cannon SC. 2008. Cold-induced defects of sodium channel gating in atypical periodic paralysis plus myotonia. *Neurology* 70:755-61

West JW, Patton DE, Scheuer T, Wang Y, Goldin AL, Catterall WA. 1992. A cluster of hydrophobic amino acid residues required for fast Na(+)-channel inactivation. *Proc Natl Acad Sci U S A* 89:10910-4

Westenbroek RE, Noebels JL, Catterall WA. 1992. Elevated expression of type II Na+

channels in hypomyelinated axons of shiverer mouse brain. *J Neurosci* 12:2259-67

Wettschureck N, Offermanns S. 2005. Mammalian G proteins and their cell type specific functions. *Physiol Rev* 85:1159-204

Wickman KD, Iniguez-Lluhl JA, Davenport PA, Taussig R, Krapivinsky GB, et al. 1994. Recombinant G-protein beta gamma-subunits activate the muscarinic-gated atrial potassium channel. *Nature* 368:255-7

Wirth MJ, Kuenzel T, Luksch H, Wagner H. 2008. Identification of auditory neurons by retrograde labelling for patch-clamp recordings in a mixed culture of chick brainstem. *J Neurosci Methods* 169:55-64

Wu J, Javedan SP, Ellsworth K, Smith K, Fisher RS. 2001. Gamma oscillation underlies hyperthermia-induced epileptiform-like spikes in immature rat hippocampal slices. *BMC Neurosci* 2:18

Wu N, Enomoto A, Tanaka S, Hsiao CF, Nykamp DQ, et al. 2005. Persistent sodium currents in mesencephalic v neurons participate in burst generation and control of membrane excitability. *J Neurophysiol* 93:2710-22

Xu J, Clancy CE. 2008. Ionic mechanisms of endogenous bursting in CA3 hippocampal pyramidal neurons: a model study. *PLoS One* 3:e2056

Xu Q, Modrek B, Lee C. 2002. Genome-wide detection of tissue-specific alternative splicing in the human transcriptome. *Nucleic Acids Res* 30:3754-66

Xu R, Thomas EA, Gazina EV, Richards KL, Quick M, et al. 2007a. Generalized epilepsy with febrile seizures plus-associated sodium channel beta1 subunit mutations severely reduce beta subunit-mediated modulation of sodium channel function. *Neuroscience* 148:164-74

Xu R, Thomas EA, Jenkins M, Gazina EV, Chiu C, et al. 2007b. A childhood epilepsy mutation reveals a role for developmentally regulated splicing of a sodium channel. *Mol Cell Neurosci* 35:292-301

Yu FH, Mantegazza M, Westenbroek RE, Robbins CA, Kalume F, et al. 2006. Reduced sodium current in GABAergic interneurons in a mouse model of severe myoclonic epilepsy in infancy. *Nat Neurosci* 9:1142-9

Yu FH, Westenbroek RE, Silos-Santiago I, McCormick KA, Lawson D, et al. 2003. Sodium channel beta4, a new disulfide-linked auxiliary subunit with similarity to beta2. *J Neurosci* 23:7577-85

Zeng J, Powers RK, Newkirk G, Yonkers M, Binder MD. 2005. Contribution of persistent sodium currents to spike-frequency adaptation in rat hypoglossal motoneurons. *J*

Neurophysiol 93:1035-41

Zhang MQ. 1998. Statistical features of human exons and their flanking regions. *Hum Mol Genet* 7:919-32

Zhang ZN, Li Q, Liu C, Wang HB, Wang Q, Bao L. 2008. The voltage-gated Na+ channel Nav1.8 contains an ER-retention/retrieval signal antagonized by the beta3 subunit. *J Cell Sci* 121:3243-52

Zhu G, Zhang Y, Xu H, Jiang C. 1998. Identification of endogenous outward currents in the human embryonic kidney (HEK 293) cell line. *J Neurosci Methods* 81:73-83

Zhuang Y, Weiner AM. 1986. A compensatory base change in U1 snRNA suppresses a 5' splice site mutation. *Cell* 46:827-35

Zimmer T, Bollensdorff C, Haufe V, Birch-Hirschfeld E, Benndorf K. 2002. Mouse heart Na+ channels: primary structure and function of two isoforms and alternatively spliced variants. *Am J Physiol Heart Circ Physiol* 282:H1007-17

Zimprich F, Stogmann E, Bonelli S, Baumgartner C, Mueller JC, et al. 2008. A functional polymorphism in the SCN1A gene is not associated with carbamazepine dosages in Austrian patients with epilepsy. *Epilepsia* 49:1108-9

Zucca C, Redaelli F, Epifanio R, Zanotta N, Romeo A, et al. 2008. Cryptogenic epileptic syndromes related to SCN1A: twelve novel mutations identified. *Arch Neurol* 65:489-94